# Preparation of $^{11}$C-Carbonyl Compounds and Radiotracer Validation for Cardiac PET Imaging

Braeden Mair

A thesis submitted to the University of Ottawa in partial fulfillment
of the requirements for the degree of

**Doctorate in Philosophy in Chemistry**

Department of Chemistry and Biomolecular Sciences,
Faculty of Science
University of Ottawa


Supervisor: Benjamin H. Rotstein, PhD

## Abstract

Molecular imaging techniques serve an integral role in clinical practice for the diagnosis and prognosis of various morbidities. Positron emission tomography (PET) is an imaging modality employing radiolabelled probes to visualize biochemical processes. Radiochemical synthesis is used to incorporate radioactive isotopes into small molecules or peptides targeting a protein of interest. Access to radiotracers is therefore dependent on the availability of radiochemical methods for the addition of radionuclides. This thesis describes the key steps in the process of developing a new radiotracer, from designing methodologies for their synthesis, to the production and evaluation of a novel probe, and finally the analysis of tracer kinetics in PET imaging. Beginning with Chapter 1, PET and radiochemistry will be introduced.

Chapter 2 is focused on a general methodology to access $^{11}$C-amides, using transition metal-catalyzed additions of organozinc iodides to $^{11}$C-isocyanates. In the chapter's central article, [$^{11}$C]$CO_2$ produced directly from the cyclotron was captured and converted to reactive $^{11}$C-isocyanate electrophiles before being derivatized by aryl and alkyl organozinc iodides. Additional work on the development of alternative $^{11}$C-carbonyl compounds is also described.

Chapter 3 presents the radiolabelling of one such $^{11}$C-carbonyl, describing the development of a radiotracer based on the selective Rev-erb inhibitor SR9009. Given recently elucidated potential for therapeutic applications of Rev-erb inhibitors like SR9009 in the management of cardiovascular disease, (*R*)- and (*S*)-[$^{11}$C]SR9009 were synthesized for cardiac investigation of circadian biology.

Chapter 4 explores a novel approach to prepare $^{11}$C-amino acids with [$^{11}$C]$CO_2$ *via* carbon isotope exchange. In this chapter, α-amino acids are condensed to Schiff bases using aldehydes; this intermediate can then undergo a carboxylation/decarboxylation cycle in which isotopically-labelled carbon ($^{11}$C, $^{13}$C, $^{14}$C) is incorporated. The key paper details the optimization of carbon-11 labelling to prepare enantiopure L- and D-$^{11}$C-amino acids for imaging.

Chapter 5 discusses the pharmacokinetic and metabolic evaluation of [$^{18}$F]flubrobenguane (FBBG) in clinical imaging populations to determine radiotracer kinetics. Patients underwent FBBG PET scans to evaluate cardiac denervation. Blood samples were collected and processed to derive vital parameters for image analysis and interpretation. Patient cohorts were statistically compared to evaluate disease-specific differences in the pharmacokinetics of FBBG.

## Acknowledgements

**To my collaborators:** It's been a privilege to work with so many talented people, from those at the institute like Dr. Robert DeKemp and Dr. Jason Zelt, to Katie Dinelle down the street at the Royal, to others in Ontario like Dr. Tami Martino, and those in other provinces like Dr. Rylan Lundgren and Mike Doyle. I am also forever fortunate to have worked with international teams, including Sanofi in Franfkurt, and Dr. Marius Ozenil from Vienna, Austria. I wish to thank you all for your assistance and contributions. It's been a joy learning from each and every one of you.

**To those at the UOHI Radiochemistry Core:** I have so much gratitude for all your support over the years. To Christian, Elmi, Hussein, and Hugo, thanks for keeping the cyclotron alive despite its best efforts to not be, and for giving me a second home away from the lab. I've spent many long hours in the rad room with you all, and I have had such a great time.

**To current and past members of the Rotstein Lab:** I thank you all for helping to create such a positive environment. For 8 years I've been a part of this lab, and we've spent those 8 years enjoying every single one of our lunches, all our "Oopsies", and each memory we've made. I'd like to specifically take the chance to thank Maxime, Uzair, and Ariel; each of you have truly set the standard of what it means to be colleagues and coworkers, but you've gone even further in being the epitome of what it means to be friends. None of this would have been as enjoyable without your ongoing presence and the laughs we've shared, and I can never thank each of you enough for your impact on my life.

**To my family:** I would like to take the chance to thank my family for their continued support and love. To Mum, Dad, and Kelsey, to Kyle and Mason, and to Sarah, Hongchang and Davina: thank you for being there whenever I need you. You have all helped me become who and what I am today, and none of my accomplishments would be worth it without your love and support.

**To Elayna:** I would not have made it here without you and your constant support. You have been the greatest partner, my best friend, and I am beyond fortunate to have you in my life. I look forward to the future we create together.

**Finally, to Ben:** Thank you for the incredible time you've provided me in your lab for all these years. For all the training, for your support, and for your constant advice, I thank you, but for your kindness, your empathy, your patience, and for our conversations through the years, I can't even begin to thank you enough. You have been the dream supervisor in what has been over a quarter of my life now, and I am forever grateful that you gave me a chance to experience the world of radiochemistry and to learn from you. I will fondly look back on my time on your team and I hope it's been even half as fun having me around as it's been for me to be here.

## Table of Contents

## List of Figures

## Nomenclature and Abbreviations

| Abbreviation | Meaning |
|---|---|
| $^{11}C$ | carbon-11 |
| $[^{11}C]CH_3I$ | carbon-11-labelled methyl iodide |
| $[^{11}C]CH_3OTf$ | carbon-11-labelled methyl triflate |
| $[^{11}C]CO_2$ | carbon-11-labelled carbon dioxide |
| $^{nat}C$ | naturally-occurring carbon isotope |
| $^{18}F$ | fluorine-18 |
| $[^{18}F]$FBBG | fluorine-18-labelled flubrobenguane |
| AY | activity yield |
| $A_M$ | molar activity |
| BEMP | 2-*tert*-butylimino-2-diethylamino-1,3-dimethyl-perhydro-1,3,2-diazaphosphorine |
| Bq | becquerels |
| Ci | curie |
| CIE | carbon isotope exchange |
| DBU | diazabicyclo[5.4.0]undec-7-ene |
| MPI | myocardial perfusion imaging |
| PET | positron emission tomography |
| RCC | radiochemical conversion |
| RCY | radiochemical yield |
| TE | trapping efficiency |

# Chapter 1: Existing Knowledge

## 1.1. Positron Emission Tomography

### 1.1.1. Medical Imaging

Due to the invasive nature of surgical interventions and clinical practices like tissue biopsies in patient diagnosis and care, medical imaging has been increasingly relied upon to monitor and evaluate patient condition commencing with the discovery of x-rays around the cusp of the 20th century.[1] In the 130 years since, imaging technologies have become an invaluable medical tool for disease diagnosis and management, enabling clinicians to gather insights into the inner workings of the human body while foregoing the need for intrusive medical procedures. In their place, medical imaging techniques can be used to visualize internal structures underneath layers of skin, tissue and bones, as well as to monitor and diagnose abnormalities that may be pathological.

Many forms of imaging technologies exist in regular clinical practice.[2] This involves the identification and subsequent evaluation of internal pathology, providing information about the stage of disease and potentially the best course for treatment. Functional measurement techniques such as electroencephalography (EEG) and electrocardiograms (ECG), used to compute electrical signals in the brain and heart respectively, do not themselves produce images but provide invaluable data that can be translated to maps or other visual interpretations.[3] Their readings can substantiate diagnosis of clinical morbidities all while avoiding intensive examinations and imposing diagnostic procedures.[4]

More advanced imaging techniques like computed tomography (CT), magnetic resonance imaging (MRI), and ultrasound (US) allow for anatomical and morphological imaging, supplying physiological mapping of the body's inner structures and tissues. Nuclear techniques like single-photon emission computed tomography (SPECT) and positron emission tomography (PET) on the other hand can provide essential biological information via molecular imaging of the body's processes.[5] While technologies like MRI and US can still be used for functional imaging, as with functional MRI to monitor blood flow or using echocardiography US to visualize the heart, they are lacking in the biochemical information provided by a molecular technique.

Each imaging modality can serve a vital role in diagnostic practice, although few offer as much potential for enriched biochemical understanding as PET. The downside comes with poor spatial resolution; multimodality imaging systems like PET/CT and PET/MRI aim to address the

variances in imaging characteristics, pairing the high-resolution imaging and anatomical data of CT or MRI with the molecular data provided by PET.

Nuclear imaging modalities rely on the fact that the body contains negligible levels of endogenous radioactive biomolecules, allowing for rapid and simple distinguishing of injected radioactivity.[6] These radiopharmaceuticals are chemical compounds (most often small molecules, peptides and large bioconjugates) in which one (and in some situations, more than one) atom has been replaced by a radioisotope. They are most frequently used for imaging purposes, as well as medical radioligand therapy in certain cases wherein these injected radiopharmaceuticals deliver targeted therapeutic radiation within the body.[7]

### 1.1.2. PET Imaging

Radionuclides refer to atomic nuclei unstable due to their excess of nuclear energy.[8] The release of this energy is known as radioactive decay, occurring either via γ-, α- and β-decay. The first method of decay, γ-emission, occurs through the release of a gamma photon, those of which can be detected by gamma cameras employed in SPECT imaging.[9] The most used isotope for this is technetium-99m.[10] In comparison, α-decay is the process of decay from one atomic nucleus to another through the emission of an α-particle, like with actinium-225 eventually decaying to stable thallium-205.[11] Alpha emitters can be employed in medicine, like in cancer treatment, with targeted therapy effectively killing cancer cells.[12] Finally, β-decay is the process of emitting an electron ($\beta^-$) or a positron ($\beta^+$); the latter is used for positron emission tomography.[13]

PET imaging employs probes containing radioisotopes that undergo $\beta^+$ decay. Radioisotopes are typically produced using a medical cyclotron, a particle accelerator harnessing magnetic centripetal acceleration to bombard a target material with positively charged hydrogen nuclei.[14] Upon production, these isotopes begin to undergo decay, emitting a positron ($\beta^+$) and a neutrino ($\nu_e$) in the process.[15] When administered (usually via intravenous injection) to a subject, like pre-clinical animal models or humans in clinical patient cohorts, a radiotracer accumulates in target tissues dependent on its pharmaceutical properties and distribution, as well as on target characteristics.

The radioisotope undergoes radioactive degradation; each nuclide has a half-life ($t_{1/2}$), the time in which half of the sample decays. The amount of radioactivity that remains after a given amount of time can be calculated with the decay equation:

$$A = A_0 e^{-\lambda t}$$

where,

$$A = radioactivity\ at\ time\ t$$

$$A_0 = radioactivity\ at\ time\ 0$$

$$\lambda = \frac{ln(2)}{t_{1/2}}$$

Subsequent the decay of the radioactive isotope, the emitted positron will travel through tissue until it spontaneously collides with an electron. Since positrons are anti-particles of electrons this causes a matter-antimatter reaction defined as an "annihilation event", which leads to the release of two gamma photons in opposite, antiparallel directions (Figure 1.1).

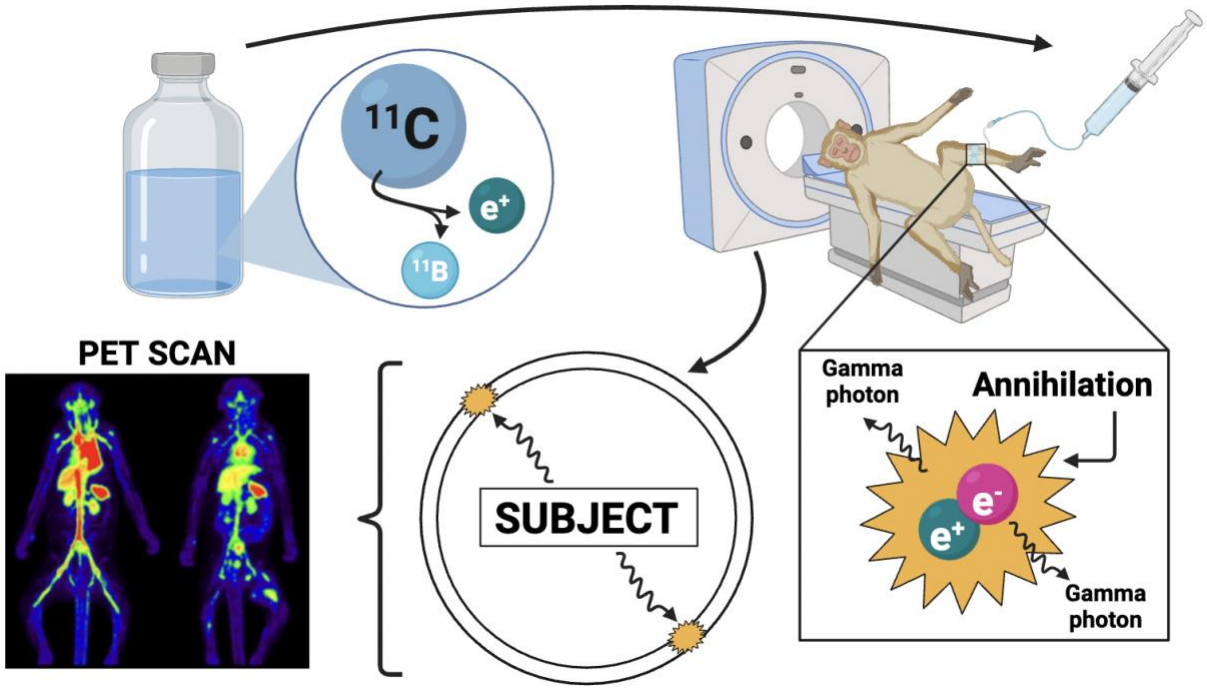


**Figure 1.1.** Positron emission tomography. The process in which PET imaging operates; following decay and emission of positron, "annihilation events" occur and release antiparallel gamma photons. These can be detected using rings of scintillators surrounding a subject administered the radioactive probe; event hits are then assembled into accumulated heat maps. Created with BioRender.

To capture visual representation of this decay, the imaging subject is placed on a bed surrounded by a PET scanner, a series of rings made of scintillators or semi-conductor-based detectors.[16] The energy of a gamma photon is absorbed by scintillation, then converted to an electrical signal to be processed and registered as a photon detection. Due to the presence of the antiparallel photon, a simultaneous detection by scintillators in the array allows for the drawing of a line of response between two hits. Throughout the scan, this occurs several thousands of times and with sufficient instances of coincidence, positron annihilation events can be localized. The series of near-simultaneous detections of coincidence are corrected for photon scattering and random events, and using iterative reconstruction algorithms, an image is generated to provide distribution heat maps of annihilation events.

While the spatial resolution of PET remains one of its biggest limitations, the development of dual imaging technologies like PET/CT and PET/MR has assisted in the co-registration of functional imaging with clearer structural scans.[17]

### 1.1.3. Applications

PET imaging can play a vital role in a wide variety of clinical and research-oriented cases. These are largely divided into three core purposes: medical-, biochemical-, and drug development-related investigations. In each of these applications, trace quantities are injected in which biological effects are not triggered.

Perhaps the most frequent indication for PET imaging is in clinical practice, wherein it can be used to inform on diagnosis and prognosis of disease in patients that arrive at medical care facilities. Provided there is either access to a production cyclotron and radiochemistry unit on-site or to an off-site production facility capable of shipping and distributing radiotracer product, patients can undergo PET scans to evaluate disease pathology. This information is invaluable, as it can provide conclusive evidence of the presence and/or progression of disease state. One of the most frequently used clinical radiotracers is [$^{18}$F]fluorodeoxyglucose ([$^{18}$F]FDG), a glucose analogue containing a radioactive isotope of fluorine-18 that accumulates in sites with high metabolic activity. While [$^{18}$F]FDG has many applications in the clinic, its primary usage is in oncological diagnostics for localization of tumours within the body due to elevated uptake into malignant tissue.[18]

Beyond medical diagnostics, PET imaging can be used in research settings to further ameliorate the understanding of biological and biochemical processes. Due to the functional information that can be derived from images, researchers can gain insight on target behaviour and characteristics. For example, a research group from the National Institutes of Health in Bethesda, Maryland explored rates of cerebral protein synthesis using L-[$^{11}$C]-leucine, a carbon-11-labelled radiotracer of the branched-chain amino acid. By monitoring its brain uptake and using compartmental modelling, rates of incorporation into proteins within the brain were derived.[19,20]

Molecular imaging with PET further addresses questions for drug development and pharmacology. Developing a drug to market takes years and can cost billions of dollars, and so it is best to be confident in the drug's ability to "go the distance". PET imaging can provide valuable reassurance in the drug's binding, tissue uptake, as well as its overall ability to be delivered to the target (like, for example, across the blood brain barrier). Furthermore, from studying the target's binding potential, pharmaceutical companies can determine a sufficient and optimal dosing range that can be well-tolerated by patients.

These applications each reinforce the strength and value of PET, but none would be possible without the immense amount of work that goes into the development of radiopharmaceuticals.

## 1.2. Radiochemistry

### 1.2.1. Considerations

The development of PET radiotracers requires expertise from several diverse fields of scientific research, from organic chemistry to pharmacology, biochemistry to physics, and clinical medicine to image analysis and quantification. The radiotracer development process first begins with radiochemistry. Whereas in synthetic chemistry reaction optimization aims to exclusively maximize chemical yield, radiochemical synthesis is instead focused on the relationship between the maximum yield within the confines of the radioisotopic half-life. While reaction yield tends to increase over time, the amount of radioactivity decreases over time. This balancing act is a primary focus in radiochemistry, and ultimately radiotracer development.

Reaction success can be measured by different metrics, most commonly radiochemical conversion (RCC), radiochemical yield (RCY), radiochemical purity (RCP), activity yield (AY) and molar activity ($A_m$).

*Radiochemical conversion* is measured as the chromatographic ratio of desired product to all radioactive products in a crude or semi-crude mixture. This is most frequently determined via radioHPLC or radioTLC, in which a small aliquot of the reaction mixture is sampled. RCC alone is not a sufficient determination of radiochemical reaction success as it does not account for all process steps; RCY is a superior metric to depict product conversion through the process entirety.[21,22]

*Radiochemical yield* is a measure of the efficiency of the radioactive labelling procedure. This value accurately measures the yield of the process, from delivery of the radioisotope, through incorporation into the desired compound, and towards product formation. RCY is commonly calculated for products of gaseous or volatile precursors by multiplying the RCC with the trapping efficiency (TE), the measure of trapped radioactivity relative to untrapped radioactivity. This is especially important with [$^{11}$C]carbon dioxide, which will be discussed in more detail later.

*Radiochemical purity* is the isolated ratio of desired product to all radioactive products. It is important not to confuse RCC with RCP despite their similarities: RCP is specifically in reference to isolated products and is a quality control metric as opposed to a measurement of reaction efficiency like RCC.

*Activity yield* is defined as the amount of radioactive product at the end of synthesis but in which it is not decay corrected. This measurement is frequently used to assess the utility of the production process with a greater focus on reaction time. A reaction with a 50% RCY recorded 20 minutes after radioisotope delivery differs greatly from one recorded 2 hours post-delivery. This is especially important with shorter-lived isotopes undergoing multiple half-lives during synthesis.

*Molar activity* is the measured radioactivity per mole of the given compound. $A_m$ is an essential metric when considering image quality. Radioactive products are formed in incredibly low concentrations due to the nanomole levels of delivered radioisotope. To ensure non-competitive binding to target receptors, the amount of unlabelled, stable isotope-containing product should be minimized. This is especially critical when studying low-density receptors or toxic molecules, to avoid high mole loading in subject injections.

Before proceeding with development, it is important to consider certain criteria: this largely includes (1) the choice of biological target, whether it be informed by disease-implications or for enriched biochemical understanding, (2) the ligand, whether it be a drug-like small molecule or larger delivery methods like antibodies, (3) the radioisotope, and (4) the method for incorporation.

### 1.2.2. Molecular Target

Several important considerations exist when designing radiotracers, often beginning with selecting a target of interest. Choice of target can come from different reasonings, like its importance in disease pathology, a desire to probe its biochemical mechanism, or its role in a drug's effects on the body. All decisions first come from choosing a biomedical question to answer and identifying the biological target that can best provide that information. It is not only about determining what mysteries need to be elucidated, but also what mysteries *should* be elucidated to satisfy the interest and demands of clinicians. Most target selection therefore comes from trying to address unmet needs in medical research and practice.

Selecting a viable target involves identifying conditions most likely to lead to a successful hit, to avoid the high costs of development from particle accelerator to clinic. Promising radiotracers should have high specificity for the molecular target of interest and conversely have low non-specific uptake into other tissues. Specificity, in the context of radiopharmaceuticals, indicates the radiotracer's ability to bind to targets. Selectivity on the other hand is the preference to bind to its intended target compared to off-target sites. Having high affinity for and rapid uptake into the target tissue is also important to ensure image quality. Sufficient retention within the target tissue provides high contrast with the background. As such, the binding characteristics and function of the desired target as well as its distribution and localization in the body are instrumental in the development of a radiotracer.

An essential characteristic that radiochemists and radiopharmacists optimize is binding potential (BP). This measurement is made up of the total target density ($B_{max}$) and the binding affinity for said target, depicted through the radiotracer dissociation constant ($K_d$), and represents the interaction between the radiotracer and the target.[23]

Perhaps the most essential element in target selection comes from access to promising ligands for further investigation.

### 1.2.3. Ligand

With a biomedical question in mind and a target selected, the next major decision comes in choosing a selective and specific ligand that can form the basis of the radiotracer and the vehicle for the radiolabel.[24–26] Selection of a ligand can be done in one of two main ways: (1) identifying known ligands or therapeutics that can be radiolabelled or, (2) *de novo* synthesis of radiotracers.

The former is often a strong starting point – beginning with an already established ligand with known binding properties for the target of interest ensures enough activity to establish the effectiveness of the radiotracer without requiring significant synthesis or optimization. Many ligands are thus selected from an existing library of active candidates, often populated by known drugs from pharmaceutical literature and practice. While this approach can provide a route to more rapid translation into radiochemistry and beyond, it is limited by requiring a sufficiently appropriate chemical methodology for synthetic access, and a logical labelling site on the selected molecule.

Alternatively, radiotracers can be developed through *de novo* synthesis, frequently discovered as hits from high-throughput screening. Extensive libraries are constructed with potential compounds for a particular target, with the expectation that only a few would be viable for translation to radiochemistry. Improvements using structure activity relationship (SAR) studies can identify the perfect candidate to derive a successful radiotracer candidate.

Potential radiotracers must satisfy a few key conditions in order to be desirable and have clinical efficacy. They include, but are not limited to:

- A nanomolar or subnanomolar dissociation constant indicating affinity for the target, to achieve sufficiently low mass dose;
- High specificity and high selectivity, to differentiate from background and off-target binding;
- Metabolic stability and its ability to be quantified, to account for remaining parent compound;
- A site for radiolabelling.

Using these qualities, the challenge is to identify which candidates should be radiolabeled and tested using preclinical imaging in either animal models or cell studies. Much like medicinal chemistry, optimizing binding properties is essential.

Of the utmost importance is identifying a site for radiolabelling. In the process of radiolabelling a probe candidate, an element is substituted for a radioactive isotope. To not adjust the pharmacokinetic properties of the selected ligand(s), identifying a radioisotope already contained within the structure provides great value.

### 1.2.4. Radioisotope

Amongst the toolbox of radionuclides used for PET imaging, there are four non-metal isotopes most frequently used in the synthesis of small molecule radioactive ligands: three short-lived isotopes in carbon-11 ($^{11}C$, $t_{1/2}$ = 20.34 min), nitrogen-13 ($^{13}N$, $t_{1/2}$ = 9.97 min) and oxygen-15 ($^{15}O$, $t_{1/2}$ = 2.04 min), and a longer-lived isotope, fluorine-18 ($^{18}F$, $t_{1/2}$ = 109.8 min). Outside of the myocardial perfusion imaging (MPI) radiotracers [$^{13}N$]ammonia and [$^{15}O$]water, clinical radiopharmaceuticals are primarily labelled with carbon-11 and fluorine-18, and much of the radiosynthetic focus is on incorporation of these radionuclides into chemical compounds.[27]

Radiometals are an alternative for radiolabelling.[28] Some of the more frequently used radiometal isotopes are gallium-68, zirconium-89, and copper-64. Their incorporation into molecules is typically very simple in relation to $^{11}C$ and $^{18}F$ and they are therefore a strong option for production facilities. In most radiometal-based radiopharmaceuticals the metal is bound to a chelating agent possessing a linkage between itself and a ligand pharmacophore. An additional advantage in their use is the potential to exchange out a diagnostic isotope like the three aforementioned for a therapeutic alternative – this is explored by the field of theranostics (*therapy* and *diagnostics*).

However, carbon-11 and fluorine-18 are still the predominant isotopes in the radiolabelling of PET imaging agents. Due to the half-life of fluorine-18 being more convenient for widespread distribution and handling, it is often the desired isotope of the two. However, by virtue of carbon's presence as the backbone of organic molecules, fewer pharmaceutically relevant compounds contain native fluorine atoms than carbon atoms. As such, and in spite of the limitations (which will be discussed shortly), carbon-11 is an incredibly attractive radioisotope for radiotracer development. What remains to be seen is how these isotopes are incorporated into the chosen ligand.

### 1.2.4. Method of Incorporation

Discovering new ways to add radioactive isotopes into ligands of interest is at the core of the field of synthetic radiochemistry.[29] Radiochemists employ a diverse array of synthetic methodologies, from classical organic reactions that have been adapted to incorporate radioactive isotopes, to novel methodologies and approaches developed with radiosynthesis in mind. Much of the challenges are in line with organic chemistry, with a focus on improving product conversions

and reaction optimization. However, the unique difficulties posed by working with decaying materials puts a much larger focus on time constraints, and on technical challenges for handling radioactivity. Additionally, radiosyntheses typically produce trace amounts of product on the nanomole scale. As such, analytical techniques become of the utmost importance to assess reaction success. Radiochemists have nonetheless, for several decades, pioneered labelling strategies within the confines and constraints of radioactive decay and with reliable methods of product characterization.

Selecting a radiosynthetic approach depends on the radioisotope being incorporated and the radiochemical synthon being used – different reaction scaffolds exist for $[^{11}C]CO_2$ compared to $[^{11}C]CH_3I$, for example. The value in having a wider array of possible methodologies for incorporation and synthesis is to find the highest yielding approach that is compatible with the functionality included in the ligand precursor.

While methods can be completed manually, and often are for optimization purposes, radiosyntheses frequently employ automated synthesis modules and microfluidic systems to assist in handling, reproducibility, and in minimizing radiation exposure (Figure 1.2). These synthesis units can be operated remotely while shielded behind protective lead enclosures, and typically are made up of a reaction vessel, delivery valves, and an onboard preparative column chromatography system for product purification. Methods are programmed as lists of timed commands, ensuring consistent reaction conditions and reliability with reduced chance of human error.

The process begins with the synthesis of precursors for radiolabelling. In addition to precursors, radiochemists purchase or prepare standards for product identification – typically done with high performance liquid chromatography connected to a radiation detector.

Radiolabelling can be done in two different ways: direct or indirect labelling. The former refers to the incorporation of the radioisotope directly into the target molecule, often replacing a stable isotope of the same element without altering any biological properties. This is the case in most small molecules that are labelled, like having carbon-11 in place of what is typically a naturally abundant carbon isotope. Alternatively, indirect labelling focuses on the use of prosthetic groups to assist in labelling in cases where the ligand may be too complex. This tends to involve labelling a smaller molecule that can then be attached to a larger target molecule. Radiometals, for example, are bound to chelators attached to the target molecule.

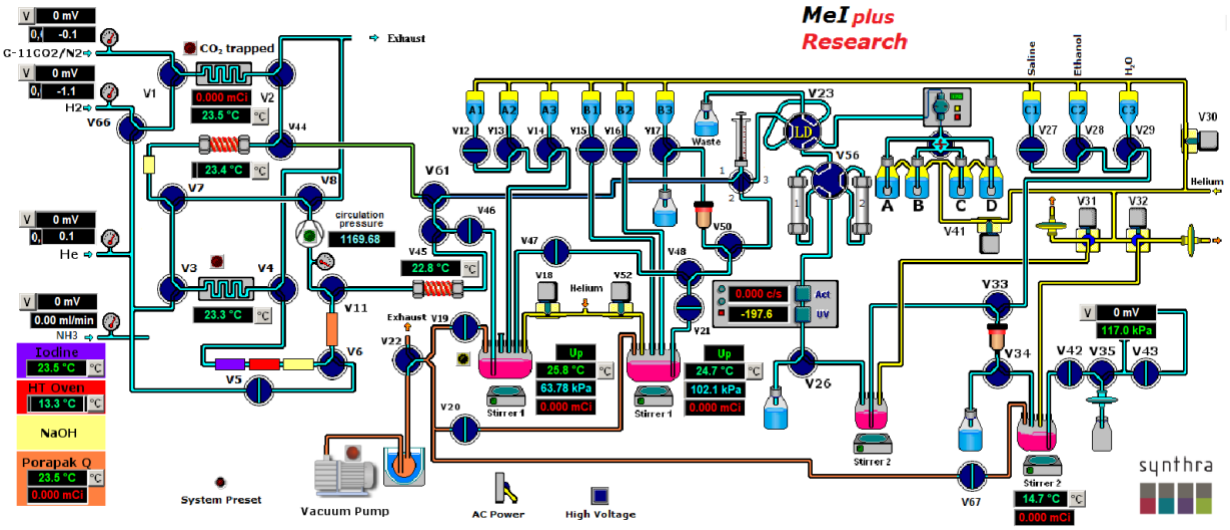


**Figure 1.2.** Automated synthesis module schematic. The layout of valves and lines for the Synthra MeIplus Research automated radiosynthesis unit.

Following radiosynthesis, the crude product is purified by chromatographic methods. The desired product is isolated, and then readied for animal or patient injection.

### 1.2.5. Formulation

The process of reformulation is essential for the preparation of radiotracers for preclinical and clinical applications. The main purposes are to (1) concentrate the radiotracer to achieve higher radioactivity concentrations in a smaller volume, (2) remove undesirable organic solvents, salts, and/or extreme pH solutions that are not biocompatible, and (3) subsequently formulate the tracer in a suitable solution for injection. Current synthetic methods tend to produce products in volumes far too large for preclinical applications, ensuring concentrations are too low to have suitable image quality.

Traditionally, the fraction collected from the HPLC has a high content of organic solvent and is therefore collected and diluted in large volumes of water. This is then passed slowly over a solid phase extraction cartridge, removing the solvent and trapping the radiotracer. It is then eluted with a minimal volume of ethanol, before being suspended in saline or other injection vehicles to be used in subsequent imaging studies.

## 1.3. Carbon-11

### 1.3.1. General Characteristics

Due to the ubiquitous presence of carbon in organic compounds, the radioactive isotope carbon-11 is an invaluable nuclide to perform isotopic radiolabelling for the purposes of PET imaging. Carbon's existence as the backbone for drug molecules offers the unique and important quality of accessing radiolabelled molecules of interest without requiring modification of their chemical structure, and their biological properties as a result. This isotopologue labelling, exchanging natural carbon for carbon-11, is solely reliant on a sufficient chemical methodology for access, whereas in the case of, say, fluorine-18, it is additionally dependent on the native presence of a fluorine-19 atom within the drug molecule.

The half-life of $^{11}C$ is simultaneously sufficiently long to allow for multistep syntheses, product purifications and dose reformulation, whilst being short enough to allow for consecutive studies on the same patient or subject in one day. This directly contrasts with $^{18}F$ with which the longer half-life prevents subsequent studies. However, it is limited in its ability to be distributed; the half-life poses significant challenges for carbon-11 radiotracers to be used outside of facilities with on-site cyclotrons.

Many radiotracers labelled with carbon-11 are used for applications in oncology, cardiology, and in neuropathies.

Detection and evaluation of cancer remains one of the most common clinical uses for PET imaging, and carbon-11 is a staple in its radiotracers. Tracers like [$^{11}C$]methionine and [$^{11}C$]choline are frequently employed in oncologic diagnosis for brain and prostate cancers, respectively.[30–35] Cancer PET imaging is frequently performed with [$^{18}F$]FDG, although investigation into alternatives labelled with carbon-11 continues.

Cardiovascular diseases can be rapidly diagnosed and evaluated using carbon-11-based PET radiotracers. A commonly used carbon-11 radiotracer is [$^{11}C$]*meta*-hydroxyephedrine ([$^{11}C$]HED), primarily used to assess cardiac sympathetic innervation as a norepinephrine analog taken up by sympathetic nerve terminals within the heart.[36–38] [$^{11}C$]Acetate is another, used in cardiac imaging to assess myocardial oxygen consumption. It can also be used for imaging certain types of tumours, like prostate cancer.[39]

Imaging the brain can provide vital information in the diagnosis of neuropathologies involving dementia and neurological decline, or psychiatric disorders. Pittsburgh Compound B

([$^{11}$C]PIB) is used for imaging beta-amyloid plaques in the brain and is therefore frequently used for disease research and diagnosis for Alzheimer's.[40–42] Alternatively, a radiotracer like [$^{11}$C]raclopride detects dopamine D2 receptors in the brain and can be used for studying disorders like Parkinson's disease, addiction, and schizophrenia.[43,44] Another example is [$^{11}$C]flumazenil, used to study neurological conditions like epilepsy by binding to GABA-benzodiazepine receptors in the brain.[45,46]

Radiochemistry with carbon-11 offers significant challenges due to its shorter half-life, restricting traditional synthetic methods and all but eliminating time-consuming processes. It's often essential to design protocols that introduce the carbon-11 radionuclide at the last step and to do so with a short reaction time. An important consideration before approaching synthesis is therefore *how* to deliver carbon-11, as this will affect the scope of reactions available as well as the resulting reaction time.

### 1.3.2. Production and Precursors

Carbon-11 is regularly produced in a cyclotron by proton bombardment of nitrogen-14 gas using the $^{14}N(p,\alpha)^{11}C$ nuclear reaction. The target is also enriched with either $O_2$ or $H_2$ gas, forming [$^{11}$C]carbon dioxide ([$^{11}$C]$CO_2$) or [$^{11}$C]methane ([$^{11}$C]$CH_4$) respectively. Most medical cyclotrons are loaded with gas containing trace amounts of oxygen in order to produce [$^{11}$C]$CO_2$ in-target, which can then be immediately reduced to [$^{11}$C]$CH_4$ as part of the radiosynthetic process.

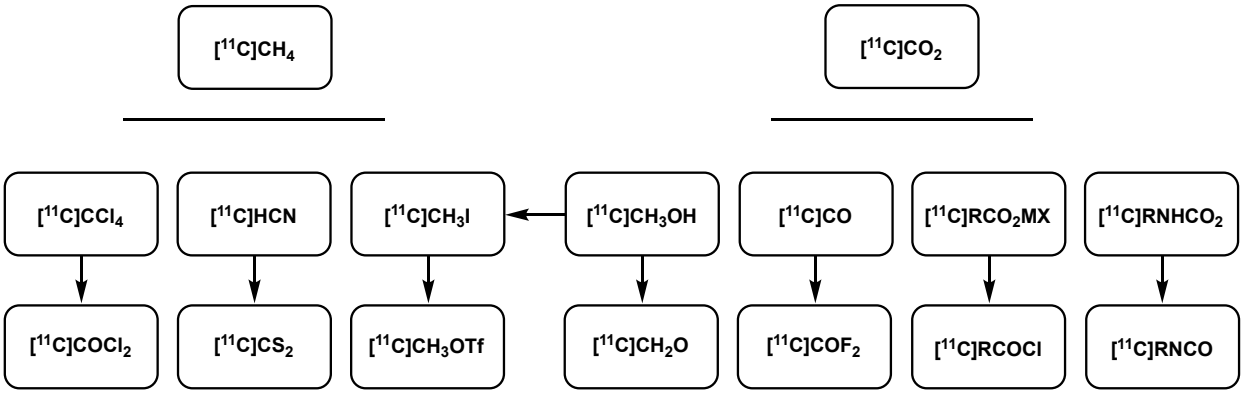


**Figure 1.3.** Primary and secondary $^{11}$C intermediates. [$^{11}$C]$CH_4$ and [$^{11}$C]$CO_2$ can be produced directly from the cyclotron and subsequently derivatized into secondary intermediates.

The focus of this thesis will largely be on the use of $[^{11}C]CO_2$ produced directly from the cyclotron, however, the less reactive $[^{11}C]CH_4$ and $[^{11}C]CO_2$ intermediates are often converted to more reactive reagents (Figure 1.3). Conversion is often dependent on specialized setups within radiosynthesis units, and so using the simplest intermediates direct from the cyclotron adds additional value.

### 1.3.3. Labelling Techniques

Several different techniques exist for labelling with carbon-11.[29,47–52]

#### *1.3.3.1. $^{11}$C-Methylation*

Most carbon-11 labelling techniques employ $^{11}$C-methylation of hydroxy, amino or thiol groups with either [$^{11}$C]methyl iodide ($[^{11}C]CH_3I$) or [$^{11}$C]methyl triflate ($[^{11}C]CH_3OTf$) prepared rapidly from $[^{11}C]CO_2$ or $[^{11}C]CH_4$. The reliability of this method has made it the primary source for $^{11}$C-radiolabelled compounds, with heteroatom methylations that proceed simply and do not often require complex optimizations.

Carbon-11-labelled methyl iodide is most frequently formed in a gas phase production scaffold following the reduction of $[^{11}C]CO_2$ to $[^{11}C]CH_4$ *via* a nickel catalyst and a final conversion to $[^{11}C]CH_3I$ using iodination with $I_2$. This can then be further converted to $[^{11}C]CH_3OTf$ by passage through a silver triflate column for substrates requiring superior reactivity. These $^{11}$C-methylation precursors have been used regularly in the production of clinical radiotracers, like L-[*methyl*-$^{11}$C]methionine, [$^{11}$C]Pittsburgh Compound B ([$^{11}$C]PiB), [*methoxy*-$^{11}$C]raclopride and [$^{11}$C]DASB.

However efforts to expand the arsenal of $^{11}$C-chemistry have been made in recent years due to inconsistent prevalence of these methyl groups in drug targets, potential metabolic demethylation, and the requirement for this post-production derivatization to these methylating agents from $[^{11}C]CO_2$ or $[^{11}C]CH_4$.

#### *1.3.3.2. $^{11}$C-Cyanation*

Cyanation using [$^{11}$C]hydrogen cyanide ([$^{11}$C]HCN) is an alternative approach for accessing product derivatization; it is obtained from $[^{11}C]CO_2$ after reduction to $[^{11}C]CH_4$ followed by a platinum-catalyzed reaction with ammonia. Due to requiring this additional catalytic step,

few automated radiosynthesis units are equipped to regularly produce [$^{11}$C]HCN and so there has been relatively limited exploration into its potential. Synthetic methodologies are also still quite restricted, however valuable approaches like the Strecker synthesis for access to α-amino acids (to be discussed later) and the synthesis of nitriles like in [$^{11}$C]LY2795050 demonstrate the potential strength of $^{11}$C-cyanation.

*1.3.3.3.$^{11}$C-Carbonylation*

Interest has been paid to the development of $^{11}$C-carbonylation chemistry, accessing $^{11}$C-carbonyl products *via* the secondary precursors [$^{11}$C]carbon monoxide ([$^{11}$C]CO), [$^{11}$C]phosgene ([$^{11}$C]$COCl_2$), and [$^{11}$C]carbonyl difluoride ([$^{11}$C]$COF_2$).

[$^{11}$C]CO is commonly produced from [$^{11}$C]$CO_2$ using columns packed with metal reductants (like zinc or molybdenum) maintained at temperatures beyond 400 °C. This setup requires a specific apparatus not commonly found in automated radiosynthesis units however, and has thusly limited the uptake of $^{11}$C-carbonylation chemistry using [$^{11}$C]CO. Additionally, implementation of [$^{11}$C]CO into radiotracer candidates typically uses transition-metal catalysts which can often be difficult to handle by production chemists and/or relatively expensive to use in regular, routine radiosynthesis. Palladium catalysis obviates this financial barrier, but does not overcome the additional challenges of handling [$^{11}$C]CO. Nonetheless, clinical radiotracer production using [$^{11}$C]CO can still be achieved, like in the case of [*carbonyl*-$^{11}$C]raclopride (which contrasts [*methoxy*-$^{11}$C]raclopride, wherein it is labelled at a more metabolically stable position).

[$^{11}$C]$COCl_2$ is most frequently produced through the conversion of [$^{11}$C]$CO_2$ to [$^{11}$C]$CH_4$, followed by chlorination to [$^{11}$C]$CCl_4$ and oxidation to [$^{11}$C]$COCl_2$. Until recent methods that will be covered later, $^{11}$C-ureas and $^{11}$C-carbamates were most commonly prepared using this synthetic precursor. The use of [$^{11}$C]$COCl_2$ has nonetheless remained limited to a small number of research programs in spite of its high reactivity due to concerns over traces of $Cl_2$ gas and the requirements for cumbersome and specialized production set ups. Its rapid formation of product is perhaps best demonstrated by the formation of [$^{11}$C]EMD-95885 for NMDA receptor imaging.

[$^{11}$C]$COF_2$ is a relatively new synthon with similar reactivity to [$^{11}$C]$COCl_2$ but with a far simpler production route using [$^{11}$C]$CO_2$ from the cyclotron, converting to [$^{11}$C]CO and followed by passage over a silver fluoride cartridge to yield the desired intermediate. While there is a lot of

promise thanks to its relatively simple means of preparation, there has been limited exploration into its capabilities at this time.

*1.3.3.4.$^{11}$C-Carboxylation*

[$^{11}$C]Carbon dioxide has traditionally been a difficult option for carbon-11-labelling due to moderate reactivities and the potential for isotopic dilution with atmospheric $CO_2$.[53,54] Reactivity is especially important as carbon dioxide frequently requires reactive nucleophiles or catalytic conditions for bond formation. Industrially, this is achieved using large excess of $CO_2$; this is not feasible in radiochemistry in which the amount of [$^{11}$C]$CO_2$ delivered is incredibly low (in the nmol range). These constraints limit the translation of several literature methods, requiring robust development to find what can work.

Isotopic dilution is also a significant problem due to molar activity. Due to low levels of carbon-11 produced, non-radioactive reagents are in extreme excess, and so any impurities can have a significant outcome on the reaction itself as well as eventual imaging characteristics. It's especially important with [$^{11}$C]$CO_2$ due to the abundant presence of atmospheric $CO_2$. A labelling pathway should therefore be designed to minimize the possible contamination with carbon-12.

Despite these limitations, [$^{11}$C]$CO_2$ labelling is of great interest as rapid synthesis may be achievable when delivered directly from the cyclotron to radiosynthesis units or reaction vessels handled manually. Additionally with the modularity of carbonyls and their ubiquitous presence in drug molecules, as well as general stability to metabolic outcomes that would prove to be a hinderance for $^{11}$C-methylated probes, methods to directly label this moiety would access a vast range of targets, including [$^{11}$C]carboxylic acids, [$^{11}$C]ureas, [$^{11}$C]carbamates, [$^{11}$C]thioureas, and [$^{11}$C]amides.

An important consideration to determine uptake of a tracer in clinical rotation is the complexity, or conversely, the ease of the radiosynthesis. Use of carbon-11 requires an on-site cyclotron, and thus needs an in-house radiosynthetic core unit capable of preparing radiotracers according to GMP standards for clinical use. The staff may be but are not always organic chemists, and thus the importance of straightforwardly prepared or easily sourced precursors, as well as simple synthetic procedures, is invaluable. Developing reproduceable methodologies is vital to ensure adaptability across various worldwide clinical infrastructures.

While direct labelling methods employing [$^{11}$C]$CO_2$ are promising, very few successful radiopharmaceuticals have been translated to the clinic. Radiotracers like the monoamine oxidase-B ligand [$^{11}$C]SL25.1188,[55–57] the fatty acid amide hydrolase ligand [$^{11}$C]CURB,[58,59] and the renal imaging tracer [$^{11}$C]PABA[60,61] represent the bulk of [$^{11}$C]$CO_2$-derived clinical probes.

## 1.4. Method Development

### 1.4.1. General Considerations

Radiopharmaceuticals would otherwise be inaccessible without the toolbox of methodologies developed by radiochemists. Determining novel ways to produce the desired functionality while incorporating the radioisotopic label carries much of the synthetic burden in developing PET radiotracers. Production chemists in cyclotron facilities do not always come with organic chemistry backgrounds, and as such, key syntheses need to be as simplistic, reproducible, and approachable as possible to ensure widespread adaptation of the method. With this in mind, developing a method has to ensure it accounts for reaction time, to respect radioactive decay, for product yield, to ensure sufficient radioactivity in the final product, and for the ease of the method, to ensure its likelihood of being taken up by clinical production facilities.

### 1.4.2. Approaches

There are different approaches to method development depending on the state of the pertaining chemical literature. Radiochemists can often "borrow" from organic chemistry, adapting currently known methodologies and adjusting as required to account for radiosynthetic limitations. However, when there is a general lack of research into the topic, radiosynthesis can also forge its own path and be borne from theory instead of adaptation.

The development of methods from theory is typically done by evaluating holes in the current availability of radiosyntheses and determining where to go next. It's often informed by gaps in the data and a need for new methodologies that address specific problems. This is often accompanied by significant development in the stable isotope space, harnessing the method to demonstrate its utility and effectiveness before translating to a radiosynthetic lens.

In chapter 2, the development of a methodology from the proposed reactivity of an organometallic nucleophile and a radiolabelled electrophile made from [$^{11}$C]$CO_2$ produced directly by the cyclotron will be discussed. In this method, reactivity with $^{11}$C-isocyanates was explored.

Organozinc halides were theorized to be sufficiently reactive when under control from transition metal catalysis but still tolerant of functionality in the scope of accessible substrates. A substrate scope using stable isotopes was conducted to demonstrate the utility of the method and to optimize the catalyst alongside reaction conditions. The method was then adapted to radiochemical synthesis to access $^{11}$C-amides.

On the other hand, many methods are inspired from current literature in organic synthesis or from reactions in nature. Radiochemistry tends to be a handful of years delayed from the discoveries in synthetic chemistry, requiring extra time in adapting its methodologies due to the technical challenges of reaction time, automated operation, and exposure to radiation. As such, methodologies are frequently developed in reference to stable isotope chemistry that has been established and proven in literature. This turns the problem into more of a technical challenge, attempting to adjust the conditions of the reaction to suit what is required in radiochemical synthesis.

In chapter 4, the development of a methodology adapted from the enzymatic decarboxylation of α-amino acids is described. This approach, inspired by the catalyzed extrusion of $CO_2$ by the aromatic amino acid decarboxylase, can derive labelled amino acids using isotopic exchange and following a carboxylation-decarboxylation cycle. In this method, we develop conditions tailored to fit the expectations of carbon-11 radiochemistry (reaction time, stoichiometry, automation, etc) in parallel with colleagues addressing carbon-13 and carbon-14 labelling.

### 1.5. Radiotracer Development

While developing a method focuses on maximizing yield, developing a radiotracer shifts to yielding *enough*. Further study only demands sufficient activity at the end of synthesis and doesn't necessarily require high percentage yields. The more important considerations are focused on rapid syntheses and high radiochemical purity. Additionally, molar activity is stressed in the production to ensure low amounts of mass loading.

Radiotracers undergo preclinical validation before being translated to the clinic. They often undergo extensive investigation with *in vitro* studies assessing binding affinity and specificity, cell studies to evaluate uptake and retention, and animal studies to determine distribution and pharmacokinetics. Promising candidates that pass preclinical testing can move on to clinical trials, beginning with development of standard operating procedures for reliable and reproducible

syntheses. What follows tends to be human studies to evaluate safety, dosimetry, and imaging performance.

Chapter 3 details the development of (*R*)- and (*S*)-[$^{11}$C]SR9009, a radiotracer candidate for imaging Rev-erb's role in circadian biology. While the pharmaceutical racemate is currently patented, potential enantiomeric differences in imaging characteristics indicates the importance of an approach to enantiopure radiotracers. As such, a synthesis conserving stereochemistry was developed to provide precursors for labelling and for optimization of carbon-11 radiosynthetic conditions.

### 1.6. Image Analysis

Proper analysis of PET images is essential in its interpretation. Scans are evaluated based on high uptake areas that appear as hot spots in the image; these indicate increased biochemical activity with the body's processes. Low uptake represents the opposite, suggesting reduced function in those tissues. It is often quantified in terms of standardized uptake value (SUV), a measure used to assess the concentration of radiotracer in regions of interest. SUV is calculated by dividing the concentration of radioactivity in the tissue by the injected dose per unit of body mass. This normalizes the uptake of the radiotracer for variations in injected dose and patient size, allowing for more standardized comparisons between scans and patients.

Chapter 5 will discuss the evaluation and analysis of [$^{18}$F]flubrobenguane in clinical cohorts. The radiotracer, used to image cardiac sympathetic innervation, was first injected into patients of different clinical indications to evaluate its effectiveness in comparison to the gold standard, [$^{11}$C]HED. Blood samples were collected from each patient in order to derive the input function for [$^{18}$F]flubrobenguane. Metabolic outcomes and pharmacokinetic parameters were measured to develop image corrections for data interpretation. This work details the process of analyzing a radiotracer and its images, and for making medical decisions with the data provided.

## 1.7. References


(1) Hussain, S.; Mubeen, I.; Ullah, N.; Shah, S. S. U. D.; Khan, B. A.; Zahoor, M.; Ullah, R.; Khan, F. A.; Sultan, M. A. Modern Diagnostic Imaging Technique Applications and Risk Factors in the Medical Field: A Review. *BioMed Research International* **2022**, *2022* (1), 5164970. https://doi.org/10.1155/2022/5164970.

(2) Massoud, T. F.; Gambhir, S. S. Molecular Imaging in Living Subjects: Seeing Fundamental Biological Processes in a New Light. *Genes Dev* **2003**, *17* (5), 545–580. https://doi.org/10.1101/gad.1047403.

(3) Reilly, R. B.; Lee, T. C. Electrograms (ECG, EEG, EMG, EOG). *Technology and Health Care* **2010**, *18* (6), 443–458. https://doi.org/10.3233/THC-2010-0604.

(4) Tong, S.; Thankor, N. V. *Quantitative EEG Analysis Methods and Clinical Applications*; Artech House, 2009.

(5) Ganguly, D.; Chakraborty, S.; Balitanas, M.; Kim, T. Medical Imaging: A Review. In *Security-Enriched Urban Computing and Smart Grid*; Kim, T., Stoica, A., Chang, R.-S., Eds.; Springer: Berlin, Heidelberg, 2010; pp 504–516. https://doi.org/10.1007/978-3-642-16444-6_63.

(6) Crișan, G.; Moldovean-Cioroianu, N. S.; Timaru, D.-G.; Andrieș, G.; Căinap, C.; Chiș, V. Radiopharmaceuticals for PET and SPECT Imaging: A Literature Review over the Last Decade. *International Journal of Molecular Sciences* **2022**, *23* (9), 5023. https://doi.org/10.3390/ijms23095023.

(7) Burkett, B. J.; Bartlett, D. J.; McGarrah, P. W.; Lewis, A. R.; Johnson, D. R.; Berberoğlu, K.; Pandey, M. K.; Packard, A. T.; Halfdanarson, T. R.; Hruska, C. B.; Johnson, G. B.; Kendi, A. T. A Review of Theranostics: Perspectives on Emerging Approaches and Clinical Advancements. *Radiology: Imaging Cancer* **2023**, *5* (4), e220157. https://doi.org/10.1148/rycan.220157.

(8) Loveland, Walter D; Morrissey, David J.; Seaborg, Glenn T. Nuclear Properties. In *Modern Nuclear Chemistry*; John Wiley & Sons, Ltd, 2017; pp 25–55. https://doi.org/10.1002/9781119348450.ch2.

(9) Khalil, M. M.; Tremoleda, J. L.; Bayomy, T. B.; Gsell, W. Molecular SPECT Imaging: An Overview. *International Journal of Molecular Imaging* **2011**, *2011* (1), 796025. https://doi.org/10.1155/2011/796025.

(10) Duatti, A. Review on 99mTc Radiopharmaceuticals with Emphasis on New Advancements. *Nuclear Medicine and Biology* **2021**, *92*, 202–216. https://doi.org/10.1016/j.nucmedbio.2020.05.005.

(11) Jalloul, W.; Ghizdovat, V.; Stolniceanu, C. R.; Ionescu, T.; Grierosu, I. C.; Pavaleanu, I.; Moscalu, M.; Stefanescu, C. Targeted Alpha Therapy: All We Need to Know about 225Ac's Physical Characteristics and Production as a Potential Theranostic Radionuclide. *Pharmaceuticals* **2023**, *16* (12), 1679. https://doi.org/10.3390/ph16121679.

(12) Poty, S.; Francesconi, L. C.; McDevitt, M. R.; Morris, M. J.; Lewis, J. S. α-Emitters for Radiotherapy: From Basic Radiochemistry to Clinical Studies—Part 1. *Journal of Nuclear Medicine* **2018**, *59* (6), 878–884. https://doi.org/10.2967/jnumed.116.186338.

(13) Conti, M.; Eriksson, L. Physics of Pure and Non-Pure Positron Emitters for PET: A Review and a Discussion. *EJNMMI Physics* **2016**, *3* (1), 8. https://doi.org/10.1186/s40658-016-0144-5.

(14) Internationale Atomenergie-Organisation. *Cyclotron Produced Radionuclides: Principles and Practice*; Technical reports series / International Atomic Energy Agency; Vienna, 2008.

(15) Konya, Jozsef; Nagy, Noemi M. *Nuclear and Radiochemistry*, 2nd ed.; 2018.

(16) Imaging, N. R. C. (US) and I. of M. (US) C. on the M. and P. of E. D. B. Positron Emission Tomography. In *Mathematics and Physics of Emerging Biomedical Imaging*; National Academies Press (US), 1996.

(17) Martí-Bonmatí, L.; Sopena, R.; Bartumeus, P.; Sopena, P. Multimodality Imaging Techniques. *Contrast Media & Molecular Imaging* **2010**, *5* (4), 180–189. https://doi.org/10.1002/cmmi.393.

(18) Kelloff, G. J.; Hoffman, J. M.; Johnson, B.; Scher, H. I.; Siegel, B. A.; Cheng, E. Y.; Cheson, B. D.; O'Shaughnessy, J.; Guyton, K. Z.; Mankoff, D. A.; Shankar, L.; Larson, S. M.; Sigman, C. C.; Schilsky, R. L.; Sullivan, D. C. Progress and Promise of FDG-PET Imaging for Cancer Patient Management and Oncologic Drug Development. *Clin Cancer Res* **2005**, *11* (8), 2785–2808. https://doi.org/10.1158/1078-0432.CCR-04-2626.

(19) Hawkins, R. A.; Huang, S. C.; Barrio, J. R.; Keen, R. E.; Feng, D.; Mazziotta, J. C.; Phelps, M. E. Estimation of Local Cerebral Protein Synthesis Rates with L-[1-$^{11}$C]Leucine and PET: Methods, Model, and Results in Animals and Humans. *J Cereb Blood Flow Metab* **1989**, *9* (4), 446–460. https://doi.org/10.1038/jcbfm.1989.68.

(20) Bishu, S.; Schmidt, K. C.; Burlin, T.; Channing, M.; Conant, S.; Huang, T.; Liu, Z.; Qin, M.; Unterman, A.; Xia, Z.; Zametkin, A.; Herscovitch, P.; Smith, C. B. Regional Rates of Cerebral Protein Synthesis Measured with L-[1-$^{11}$C]Leucine and PET in Conscious, Young Adult Men: Normal Values, Variability, and Reproducibility. *J Cereb Blood Flow Metab* **2008**, *28* (8), 1502–1513. https://doi.org/10.1038/jcbfm.2008.43.

(21) Coenen, H. H.; Gee, A. D.; Adam, M.; Antoni, G.; Cutler, C. S.; Fujibayashi, Y.; Jeong, J. M.; Mach, R. H.; Mindt, T. L.; Pike, V. W.; Windhorst, A. D. Consensus Nomenclature Rules for Radiopharmaceutical Chemistry — Setting the Record Straight. *Nuclear Medicine and Biology* **2017**, *55*, v–xi. https://doi.org/10.1016/j.nucmedbio.2017.09.004.

(22) Herth, M. M.; Ametamey, S.; Antuganov, D.; Bauman, A.; Berndt, M.; Brooks, A. F.; Bormans, G.; Choe, Y. S.; Gillings, N.; Häfeli, U. O.; James, M. L.; Kopka, K.; Kramer, V.; Krasikova, R.; Madsen, J.; Mu, L.; Neumaier, B.; Piel, M.; Rösch, F.; Ross, T.; Schibli, R.; Scott, P. J. H.; Shalgunov, V.; Vasdev, N.; Wadsak, W.; Zeglis, B. M. On the Consensus Nomenclature Rules for Radiopharmaceutical Chemistry – Reconsideration of Radiochemical Conversion. *Nuclear Medicine and Biology* **2021**, *93*, 19–21. https://doi.org/10.1016/j.nucmedbio.2020.11.003.

(23) Innis, R. B.; Cunningham, V. J.; Delforge, J.; Fujita, M.; Gjedde, A.; Gunn, R. N.; Holden, J.; Houle, S.; Huang, S.-C.; Ichise, M.; Iida, H.; Ito, H.; Kimura, Y.; Koeppe, R. A.; Knudsen, G. M.; Knuuti, J.; Lammertsma, A. A.; Laruelle, M.; Logan, J.; Maguire, R. P.; Mintun, M. A.; Morris, E. D.; Parsey, R.; Price, J. C.; Slifstein, M.; Sossi, V.; Suhara, T.; Votaw, J. R.; Wong, D. F.; Carson, R. E. Consensus Nomenclature for in Vivo Imaging of Reversibly Binding Radioligands. *J Cereb Blood Flow Metab* **2007**, *27* (9), 1533–1539. https://doi.org/10.1038/sj.jcbfm.9600493.

(24) Pike, V. W. PET Radiotracers: Crossing the Blood–Brain Barrier and Surviving Metabolism. *Trends in Pharmacological Sciences* **2009**, *30* (8), 431–440. https://doi.org/10.1016/j.tips.2009.05.005.

(25) Hooker, J. M. Modular Strategies for PET Imaging Agents. *Current Opinion in Chemical Biology* **2010**, *14* (1), 105–111. https://doi.org/10.1016/j.cbpa.2009.10.005.

(26) Lindberg, A.; Chassé, M.; Varlow, C.; Pees, A.; Vasdev, N. Strategies for Designing Novel Positron Emission Tomography (PET) Radiotracers to Cross the Blood–Brain Barrier. *Journal of Labelled Compounds and Radiopharmaceuticals* **2023**, *66* (9), 205–221. https://doi.org/10.1002/jlcr.4019.

(27) Pichler, V.; Berroterán-Infante, N.; Philippe, C.; Vraka, C.; Klebermass, E.-M.; Balber, T.; Pfaff, S.; Nics, L.; Mitterhauser, M.; Wadsak, W. An Overview of PET Radiochemistry, Part 1: The Covalent Labels $^{18}$F, $^{11}$C, and $^{13}$N. *Journal of Nuclear Medicine* **2018**, *59* (9), 1350–1354. https://doi.org/10.2967/jnumed.117.190793.

(28) Brandt, M.; Cardinale, J.; Aulsebrook, M. L.; Gasser, G.; Mindt, T. L. An Overview of PET Radiochemistry, Part 2: Radiometals. *Journal of Nuclear Medicine* **2018**, *59* (10), 1500–1506. https://doi.org/10.2967/jnumed.117.190801.

(29) Rong, J.; Haider, A.; Jeppesen, T. E.; Josephson, L.; Liang, S. H. Radiochemistry for Positron Emission Tomography. *Nat Commun* **2023**, *14*, 3257. https://doi.org/10.1038/s41467-023-36377-4.

(30) Leskinen-Kallio, S.; Någren, K.; Lehikoinen, P.; Ruotsalainen, U.; Teräs, M.; Joensuu, H. Carbon-11-Methionine and PET Is an Effective Method To Image Head and Neck Cancer. *Journal of Nuclear Medicine* **1992**, *33* (5), 691–695.

(31) Glaudemans, A. W. J. M.; Enting, R. H.; Heesters, M. A. A. M.; Dierckx, R. A. J. O.; van Rheenen, R. W. J.; Walenkamp, A. M. E.; Slart, R. H. J. A. Value of $^{11}$C-Methionine PET in Imaging Brain Tumours and Metastases. *Eur J Nucl Med Mol Imaging* **2013**, *40* (4), 615–635. https://doi.org/10.1007/s00259-012-2295-5.

(32) Hotta, M.; Minamimoto, R.; Miwa, K. $^{11}$C-Methionine-PET for Differentiating Recurrent Brain Tumor from Radiation Necrosis: Radiomics Approach with Random Forest Classifier. *Sci Rep* **2019**, *9* (1), 15666. https://doi.org/10.1038/s41598-019-52279-2.

(33) Reske, S. N.; Blumstein, N. M.; Neumaier, B.; Gottfried, H.-W.; Finsterbusch, F.; Kocot, D.; Möller, P.; Glatting, G.; Perner, S. Imaging Prostate Cancer with $^{11}$C-Choline PET/CT. *Journal of Nuclear Medicine* **2006**, *47* (8), 1249–1254.

(34) Welle, C. L.; Cullen, E. L.; Peller, P. J.; Lowe, V. J.; Murphy, R. C.; Johnson, G. B.; Binkovitz, L. A. $^{11}$C-Choline PET/CT in Recurrent Prostate Cancer and Nonprostatic Neoplastic Processes. *RadioGraphics* **2016**, *36* (1), 279–292. https://doi.org/10.1148/rg.2016150135.

(35) Michaud, L.; Touijer, K. A.; Mauguen, A.; Zelefsky, M. J.; Morris, M. J.; Lyashschenko, S. K.; Durack, J. C.; Humm, J. L.; Weber, W. A.; Schöder, H. $^{11}$C-Choline PET/CT in Recurrent Prostate Cancer: Retrospective Analysis in a Large U.S. Patient Series. *Journal of Nuclear Medicine* **2020**, *61* (6), 827. https://doi.org/10.2967/jnumed.119.233098.

(36) Rosenspire, K. C.; Haka, M. S.; Van Dort, M. E.; Jewett, D. M.; Gildersleeve, D. L.; Schwaiger, M.; Wieland, D. M. Synthesis and Preliminary Evaluation of Carbon-11-Meta-Hydroxyephedrine: A False Transmitter Agent for Heart Neuronal Imaging. *J Nucl Med* **1990**, *31* (8), 1328–1334.

(37) Franzius, C.; Hermann, K.; Weckesser, M.; Kopka, K.; Juergens, K. U.; Vormoor, J.; Schober, O. Whole-Body PET/CT with $^{11}$C-Meta-Hydroxyephedrine in Tumors of the Sympathetic Nervous System: Feasibility Study and Comparison with $^{123}$I-MIBG SPECT/CT. *J Nucl Med* **2006**, *47* (10), 1635–1642.

(38) Thackeray, J. T.; Beanlands, R. S.; DaSilva, J. N. Presence of Specific $^{11}$C-Meta-Hydroxyephedrine Retention in Heart, Lung, Pancreas, and Brown Adipose Tissue. *Journal of Nuclear Medicine* **2007**, *48* (10), 1733–1740. https://doi.org/10.2967/jnumed.107.043570.

(39) Grassi, I.; Nanni, C.; Allegri, V.; Morigi, J. J.; Montini, G. C.; Castellucci, P.; Fanti, S. The Clinical Use of PET with $^{11}$C-Acetate. *American Journal of Nuclear Medicine and Molecular Imaging* **2011**, *2* (1), 33.

(40) Landau, S. M.; Breault, C.; Joshi, A. D.; Pontecorvo, M.; Mathis, C. A.; Jagust, W. J.; Mintun, M. A. Amyloid-β Imaging with Pittsburgh Compound B and Florbetapir: Comparing Radiotracers and Quantification Methods. *Journal of Nuclear Medicine* **2013**, *54* (1), 70–77. https://doi.org/10.2967/jnumed.112.109009.

(41) Leuzy, A.; Chiotis, K.; Hasselbalch, S. G.; Rinne, J. O.; de Mendonça, A.; Otto, M.; Lleó, A.; Castelo-Branco, M.; Santana, I.; Johansson, J.; Anderl-Straub, S.; von Arnim, C. A. F.; Beer, A.; Blesa, R.; Fortea, J.; Herukka, S.-K.; Portelius, E.; Pannee, J.; Zetterberg, H.; Blennow, K.; Nordberg, A. Pittsburgh Compound B Imaging and Cerebrospinal Fluid Amyloid-β in a Multicentre European Memory Clinic Study. *Brain* **2016**, *139* (9), 2540–2553. https://doi.org/10.1093/brain/aww160.

(42) Yamin, G.; Teplow, D. B. Pittsburgh Compound-B (PiB) Binds Amyloid β-Protein Protofibrils. *Journal of Neurochemistry* **2017**, *140* (2), 210–215. https://doi.org/10.1111/jnc.13887.

(43) Antonini, A.; Schwarz, J.; Oertel, W. H.; Beer, H. F.; Madeja, U. D.; Leenders, K. L. [$^{11}$C]Raclopride and Positron Emission Tomography in Previously Untreated Patients with Parkinson's Disease. *Neurology* **1994**, *44* (7), 1325–1325. https://doi.org/10.1212/WNL.44.7.1325.

(44) Slifstein, M.; Hwang, D.-R.; Martinez, D.; Ekelund, J.; Huang, Y.; Hackett, E.; Abi-Dargham, A.; Laruelle, M. Biodistribution and Radiation Dosimetry of the Dopamine D2 Ligand $^{11}$C-Raclopride Determined from Human Whole-Body PET. *Journal of Nuclear Medicine* **2006**, *47* (2), 313–319.

(45) Richardson, M. P.; Koepp, M. J.; Brooks, D. J.; Duncan, J. S. $^{11}$C-Flumazenil PET in Neocortical Epilepsy. *Neurology* **1998**, *51* (2), 485–492. https://doi.org/10.1212/WNL.51.2.485.

(46) Salmi, E.; Aalto, S.; Hirvonen, J.; Långsjö, J. W.; Maksimow, A. T.; Oikonen, V.; Metsähonkala, L.; Virkkala, J.; Någren, K.; Scheinin, H. Measurement of GABAA Receptor Binding *in Vivo* with [$^{11}$C]Flumazenil: A Test–Retest Study in Healthy Subjects. *NeuroImage* **2008**, *41* (2), 260–269. https://doi.org/10.1016/j.neuroimage.2008.02.035.

(47) Dahl, K.; Halldin, C.; Schou, M. New Methodologies for the Preparation of Carbon-11 Labeled Radiopharmaceuticals. *Clinical and Translational Imaging* **2017**, *5* (3), 275. https://doi.org/10.1007/s40336-017-0223-1.

(48) Taddei, C.; Gee, A. D. Recent Progress in [$^{11}$C]Carbon Dioxide ([$^{11}$C]$CO_2$) and [$^{11}$C]Carbon Monoxide ([$^{11}$C]CO) Chemistry. *J Labelled Comp Radiopharm* **2018**, *61* (3), 237–251. https://doi.org/10.1002/jlcr.3596.

(49) Taddei, C.; Pike, V. W. [$^{11}$C]Carbon Monoxide: Advances in Production and Application to PET Radiotracer Development over the Past 15 Years. *EJNMMI Radiopharmacy and Chemistry* **2019**, *4* (1), 25. https://doi.org/10.1186/s41181-019-0073-4.

(50) Goud, N. S.; Bhattacharya, A.; Joshi, R. K.; Nagaraj, C.; Bharath, R. D.; Kumar, P. Carbon-11: Radiochemistry and Target-Based PET Molecular Imaging Applications in Oncology, Cardiology, and Neurology. *J. Med. Chem.* **2021**, *64* (3), 1223–1259. https://doi.org/10.1021/acs.jmedchem.0c01053.

(51) Shegani, A.; Kealey, S.; Luzi, F.; Basagni, F.; Machado, J. do M.; Ekici, S. D.; Ferocino, A.; Gee, A. D.; Bongarzone, S. Radiosynthesis, Preclinical, and Clinical Positron Emission Tomography Studies of Carbon-11 Labeled Endogenous and Natural Exogenous Compounds. *Chem. Rev.* **2023**, *123* (1), 105–229. https://doi.org/10.1021/acs.chemrev.2c00398.

(52) Pees, A.; Chassé, M.; Lindberg, A.; Vasdev, N. Recent Developments in Carbon-11 Chemistry and Applications for First-In-Human PET Studies. *Molecules* **2023**, *28* (3), 931. https://doi.org/10.3390/molecules28030931.

(53) Rotstein, B. H.; Liang, S. H.; Holland, J. P.; Collier, T. L.; Hooker, J. M.; Wilson, A. A.; Vasdev, N. $^{11}CO_2$ Fixation: A Renaissance in PET Radiochemistry. *Chemical Communications* **2013**, *49* (50), 5621. https://doi.org/10.1039/c3cc42236d.

(54) Rotstein, B. H.; Liang, S. H.; Placzek, M. S.; Hooker, J. M.; Gee, A. D.; Dollé, F.; Wilson, A. A.; Vasdev, N. $^{11}C$=O Bonds Made Easily for Positron Emission Tomography Radiopharmaceuticals. *Chemical Society Reviews* **2016**, *45* (17), 4708–4726. https://doi.org/10.1039/C6CS00310A.

(55) Saba, W.; Valette, H.; Peyronneau, M.-A.; Bramoullé, Y.; Coulon, C.; Curet, O.; George, P.; Dollé, F.; Bottlaender, M. [$^{11}C$]SL25.1188, a New Reversible Radioligand to Study the Monoamine Oxidase Type B with PET: Preclinical Characterisation in Nonhuman Primate. *Synapse* **2010**, *64* (1), 61–69. https://doi.org/10.1002/syn.20703.

(56) Vasdev, N.; Sadovski, O.; Garcia, A.; Dollé, F.; Meyer, J. H.; Houle, S.; Wilson, A. A. Radiosynthesis of [$^{11}C$]SL25.1188 via [$^{11}C$]$CO_2$ Fixation for Imaging Monoamine Oxidase B. *Journal of Labelled Compounds and Radiopharmaceuticals* **2011**, *54* (10), 678–680. https://doi.org/10.1002/jlcr.1908.

(57) Rusjan, P. M.; Wilson, A. A.; Miler, L.; Fan, I.; Mizrahi, R.; Houle, S.; Vasdev, N.; Meyer, J. H. Kinetic Modeling of the Monoamine Oxidase B Radioligand [$^{11}C$]SL25.1188 in Human Brain with High-Resolution Positron Emission Tomography. *J Cereb Blood Flow Metab* **2014**, *34* (5), 883–889. https://doi.org/10.1038/jcbfm.2014.34.

(58) Wilson, A. A.; Hicks, J. W.; Sadovski, O.; Parkes, J.; Tong, J.; Houle, S.; Fowler, C. J.; Vasdev, N. Radiosynthesis and Evaluation of [$^{11}C$-Carbonyl]-Labeled Carbamates as Fatty Acid Amide Hydrolase Radiotracers for Positron Emission Tomography. *J. Med. Chem.* **2013**, *56* (1), 201–209. https://doi.org/10.1021/jm301492y.

(59) Boileau, I.; Tyndale, R. F.; Williams, B.; Mansouri, E.; Westwood, D. J.; Foll, B. L.; Rusjan, P. M.; Mizrahi, R.; De Luca, V.; Zhou, Q.; Wilson, A. A.; Houle, S.; Kish, S. J.; Tong, J. The Fatty Acid Amide Hydrolase C385A Variant Affects Brain Binding of the Positron Emission Tomography Tracer [$^{11}$C]CURB. *J Cereb Blood Flow Metab* **2015**, *35* (8), 1237–1240. https://doi.org/10.1038/jcbfm.2015.119.

(60) Holt, D. P.; Kalinda, A. S.; Bambarger, L. E.; Jain, S. K.; Dannals, R. F. Radiosynthesis and Validation of [Carboxy-$^{11}$C]4-Aminobenzoic Acid ([$^{11}$C]PABA), a PET Radiotracer for Imaging Bacterial Infections. *Journal of Labelled Compounds and Radiopharmaceuticals* **2019**, *62* (1), 28–33. https://doi.org/10.1002/jlcr.3674.

(61) Ruiz-Bedoya, C. A.; Ordonez, A. A.; Werner, R. A.; Plyku, D.; Klunk, M. H.; Leal, J.; Lesniak, W. G.; Holt, D. P.; Dannals, R. F.; Higuchi, T.; Rowe, S. P.; Jain, S. K. $^{11}$C-PABA as a PET Radiotracer for Functional Renal Imaging: Preclinical and First-in-Human Study. *Journal of Nuclear Medicine* **2020**, *61* (11), 1665–1671. https://doi.org/10.2967/jnumed.119.239806.

# Chapter 2: $^{11}CO_2$-Fixation to Access $^{11}C$-Carbonyls
## Novel Method Development

This chapter and discussion contains information from multiple published studies.

- **FOCUS:** Mair et al. "Rhodium-Catalyzed Addition of Organozinc Iodides to Carbon-11 Isocyanates" *Org. Lett.* **2020**, 22 (7), 2746–2750. doi: 10.1021/acs.orglett.0c00729.
    - Contributions: Project lead, completed experiments, wrote manuscript.
- Ismailani, Munch, Mair et al. "Interrupted aza-Wittig reactions using iminophosphoranes to synthesize $^{11}C$-carbonyls" *Chem. Commun.* **2021**, 57, 5266–5269. doi: 10.1039/D1CC01016F.
    - Contributions: Assisted with $^{11}C$ translation and performed $^{11}C$ experiments.
- Ozenil, Kogler, Mair et al. "Intramolecular Friedel-Crafts Acylation of [$^{11}C$]Isocyanates Enabling the Radiolabeling of [*carbonyl*-$^{11}C$]DPQ" *Chem. – Eur. J.* **2024**. doi: 10.1002/chem.202400581.
    - Contributions: Assisted with $^{11}C$ translation and experiments.

## 2.1. Context

### 2.1.1. [$^{11}$C]$CO_2$-Fixation

The low amounts of [$^{11}$C]$CO_2$ contained within the nitrogen carrier gas delivered from the cyclotron, as well as its gaseous state, call for efficient capturing of [$^{11}$C]$CO_2$ in solution. However, [$^{11}$C]$CO_2$ possesses poor solubility in polar organic solvents and thus necessitates reliable trapping techniques and/or methods.[1] This can be accomplished technically, like with cryogenic trapping or molecular sieves, or through chemical fixation. Many chemical approaches have been developed since the 1940s, ranging from harnessing organometallics to form a more soluble and non-gaseous intermediate, to the use of superbases in order to improve [$^{11}$C]$CO_2$ solubility and to increase trapped radioactivity in solution.

Grignard reagents have been employed in the fixation of [$^{11}$C]$CO_2$, most notably in the preparation of $^{11}$C-carboxylic acids and $^{11}$C-amides.[2–4] While these methods work efficiently, the high reactivity of Grignard reagents limits the scope of applications and requires strict handling that may not be compatible with automated radiosynthesis units. Due to rapid absorption of atmospheric $CO_2$ and the moisture sensitivity of Grignard reagents, it is important to carefully prepare and store them pending radiochemical synthesis to avoid magnesium salt precipitation and reaction poisoning, and to ensure higher molar activities.

Methyllithium has also been shown to readily accept [$^{11}$C]$CO_2$ to form a dilithium salt of acetone acetal.[5] This can be further converted to [$^{11}$C]acetone following hydrolysis, and can be used as a secondary precursor.[6,7] Silylated amines were shown by Ram et al. to produce *O*-silyl carbamates when exposed to [$^{11}$C]$CO_2$ at elevated temperatures, which could then be reduced to tertiary methylamines.[8] However, the use of these unstable species poses severe obstacles for radiochemical automation to mitigate side reactivity and the presence of moisture.

In order to access more structurally diverse and pharmaceutically-relevant products, base-mediated [$^{11}$C]$CO_2$-fixation was explored thanks in part to inspiration from industrial-focused "green" processes of a similar nature.[9] Triethylamine was first relied upon in dichloromethane for the $^{11}$C-carboxylation of aniline and aliphatic amines.[10] These then undergo dehydration with phosphoryl chloride ($POCl_3$) to yield $^{11}$C-isocyanates.

### 2.1.2. $^{11}$C-Isocyanates

Isocyanates are heterocumulenes made up of both C=O and C=N bonds. They can be used as highly reactive electrophiles and, dependent on the nucleophile involved, can generate carbonyl-based moieties. However, the elevated chemical reactivity of isocyanates is mirrored in its toxicity, in which they can be acutely toxic, and are one of the most common causes of occupational asthma.[11] Industrial handling of isocyanates is greatly concerned in minimizing the risks of exposure. This offers a uniquely valuable opportunity in radiochemistry wherein the incredibly low concentrations of radiolabelled product being formed negates the concerns of toxicity while still allowing for the harnessing of higher reactivities.

#### *2.1.2.1. Synthesis*

$^{11}$C-Isocyanates were first prepared with [$^{11}$C]phosgene in reaction with an amine,[12–15] but due to the limited availability of [$^{11}$C]phosgene production apparatuses, the method was limited in its use. More recent approaches use fixation bases like the amidine diazabicyclo[5.4.0]undec-7-ene (DBU)[16] and the phosphazene 2-*tert*-butylimino-2-diethylamino-1,3-dimethyl-perhydro-1,3,2-diazaphosphorine (BEMP)[17] to yield ionic carbamates, followed by conversion to $^{11}$C-isocyanates either through acid dehydration with phosphoryl chloride ($POCl_3$)[18] or through Mitsunobu chemistry with phosphines and azo compounds (Figure 2.1).[19,20]

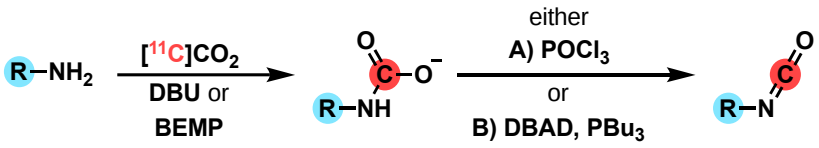


**Figure 2.1.** The common methods for preparation of $^{11}$C-isocyanates. Using amines, [$^{11}$C]$CO_2$ directly produced by the cyclotron, and trapping bases like DBU and BEMP, the two conversion techniques to access $^{11}$C-isocyanates are either (A) acid dehydration or (B) Mitsunobu chemistry.

Following their preparation, $^{11}$C-isocyanates can then be further derivatized by a nucleophile to access a series of $^{11}$C-carbonyl compounds.

### 2.1.3. $^{11}$C-Carbonyl Compounds

Carbonyl groups are commonly found throughout bioactive molecules and pharmaceutical candidates. While $^{11}$C-methylation is frequently reliant on *O*-, *N*-, and *S*-methylation (and in some rare cases, $^{nat}$*C*-methylation) that may not always be compatible with radiotracer candidates, $^{11}$C-carbonylation to access $^{11}$C-carbonyls offers a far more versatile approach. As has been previously discussed, [$^{11}$C]CO, [$^{11}$C]HCN and [$^{11}$C]$COCl_2$ are frequently harnessed to access labelled carbonyls, but none are as convenient as [$^{11}$C]$CO_2$. As such, the enrichment of methodologies to access $^{11}$C-carbonyls with [$^{11}$C]$CO_2$ is paramount to the development of radiotracer candidates.

Depending on the nucleophile used, various $^{11}$C-carbonyls can be made. These primarily include, but are not limited to: $^{11}$C-ureas, $^{11}$C-carbamates, $^{11}$C-carboxylic acids, and $^{11}$C-amides.

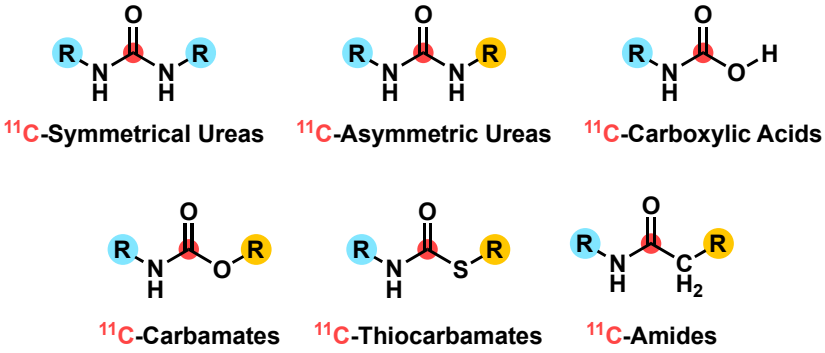


**Figure 2.2.** $^{11}$C-Carbonyl targets. Reliable labelling techniques to access $^{11}$C-carbonyls would provide many opportunities for PET radiotracer development.

#### *2.1.3.1. $^{11}$C-Ureas*

Urea functionalities are abundant in medicinal chemistry, thanks in part to their capability to form multiple stable hydrogen bonds with receptor targets.[21] Their modular nature is valuable for the development of large libraries of potential drug compounds, and by extension PET radiotracers. Methods for accessing $^{11}$C-ureas have traditionally been through [$^{11}$C]$COCl_2$, however its availability for radiosynthesis units remains a problem. As such, methodologies for synthesis with [$^{11}$C]$CO_2$ offers much easier implementation and more widespread access.

One of the first instances of preparing $^{11}$C-ureas with [$^{11}$C]$CO_2$ was from Chakraborty *et al.* in the 90s, in which they bubbled [$^{11}$C]$CO_2$ directly into a solution of LHMDS, followed by hydrolysis with ammonium chloride, then a condensation to [$^{11}$C]uracil (Figure 2.3).[22] This

method, however, is not widely applicable to a wide variety of derivatized ureas and is limited in the pharmaceutically relevant targets it can access. An alternative approach is to activate the intermediate ionic carbamate formed by conversion to an $^{11}$C-isocyanate – this strategy drastically improved access to urea-based radiotracers.[23]

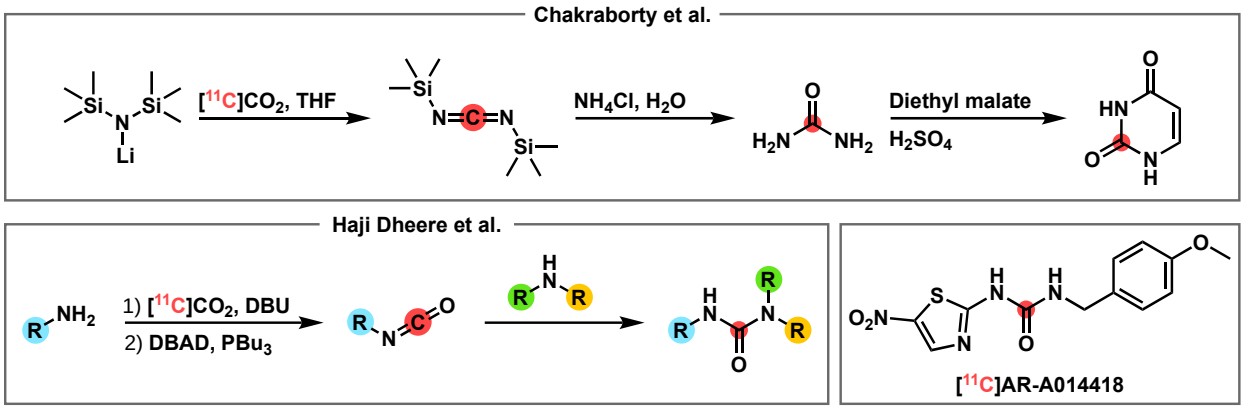


**Figure 2.3**. Radiosynthetic approaches to $^{11}$C-ureas. One of the first synthetic approaches to labelling $^{11}$C-ureas targeted [$^{11}$C]uracil. Further improvement of carbon-11 methodologies provided $^{11}$C-isocyanate intermediates that can be reacted with amines for a general synthesis to $^{11}$C-ureas like [$^{11}$C]AR-A014418.

An early adoption of [$^{11}$C]$CO_2$-fixation to form $^{11}$C-ureas targeted a glycogen synthase kinase-3 (GSK-3) inhibitor AR-A014418.[24] Following preparation of an $^{11}$C-isocyanate with 4-methoxybenzylamine and addition of 2-amino-5-nitrothiazole, [$^{11}$C]AR-A014418 was prepared in 8% uncorrected RCY. Similarly, the fatty acid amide hydrolase (FAAH) inhibitor [$^{11}$C]PF-04457845,[25] the beta-adrenoceptor ligand [$^{11}$C]CGP12177,[26] and a novel cholesterol 24-hydroxylase inhibitor[27] have been prepared with [$^{11}$C]$CO_2$-fixation techniques.

### *2.1.3.2. $^{11}$C-Carbamates*

Carbamate moieties play a critical role in modern drug discovery and development.[28] Their metabolic stability within the body is a key characteristic prescribing their use in pharmaceutical and medicinal chemistry. Similar to ureas they offer a modular opportunity for ligand development, allowing for rapid iteration of the *N*- and *O*-termini to derive a large catalogue. Also similar to ureas, traditional $^{11}$C-carbamate synthesis was achieved using [$^{11}$C]$COCl_2$ and with

[$^{11}$C]CO.[29] Expansion of radiochemical protocols for $^{11}$C-carbamate synthesis could improve the selection of radiotracers available to clinicians.

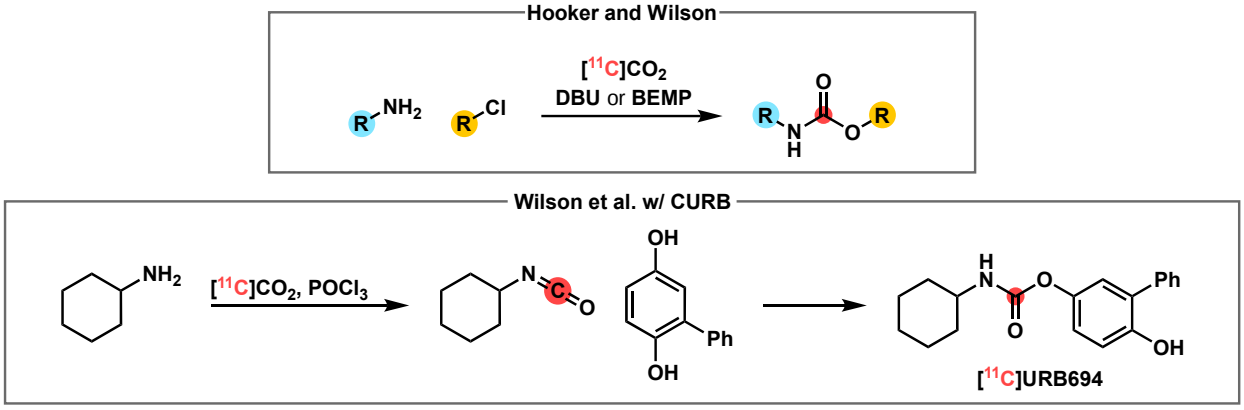


**Figure 2.4.** Radiosynthetic approaches to $^{11}$C-carbamates. Independent but simultaneous development of $^{11}$C-carbamate synthesis from Hooker and Wilson gained access to labelling strategies. Subsequent the enrichment of $^{11}$C-isocyanate techniques, additional $^{11}$C-carbamates could be accessed like the FAAH inhibitor [$^{11}$C]CURB.

Hooker *et al.* harnessed [$^{11}$C]$CO_2$-fixation with amines, alkyl chlorides, and DBU to provide $^{11}$C-carbamates in strong yields (Figure 2.4).[16] The synthesis of [$^{11}$C]metergoline, a ligand for serotonin and dopamine receptors, was performed in demonstration and proceeded in 32% decay-corrected RCY. Using the same method, they produced the histone deacetylase inhibitor [$^{11}$C]MS-275 in 25% decay-corrected RCY.[30] Following shortly after the DBU-mediated method, Wilson *et al.* shared a similar method using methylating agents and BEMP-mediation.[17] The synthesis of [$^{11}$C]GR103545, an agonist of the kappa opioid receptor, was completed in 13% non-decay corrected RCY.

Rather than direct reaction with alkyl electrophiles using the ionic carbamate formed following [$^{11}$C]$CO_2$-fixation, Wilson *et al*. explored conversion to $^{11}$C-isocyanates, as mentioned previously.[18] Using this method, they prepared the FAAH inhibitor [$^{11}$C]URB694 in 8% non-decay corrected RCY; this radiotracer has been investigated preclinically and translated to human use.[31,32] Cyclic carbamates and oxazolidinones could also be prepared, as demonstrated by the synthesis of [$^{11}$C]SL25.1188 in 12% non-decay corrected RCY and its subsequent human translation.[33–35]

*2.1.3.3. $^{11}$C-Carboxylic Acids*

Carboxylic acids are part of many pharmacophores of pharmaceuticals and therapeutic agents.[36] The capabilities for hydrogen bond formation impart vital importance in a large number of drugs and drug candidates. Approaches to radiolabelling this functionality have long been a focus, although limitations still exist. Targeting $^{11}$C-carboxylic acids, namely $^{11}$C-amino acids, is the focus of Chapter 4, and will therefore be discussed further in that context.

*2.1.3.4. $^{11}$C-Amides*

Amides are one of the most common functional groups found in drug molecules, while amide bond formation is amongst the most frequent reactions in synthetic and medicinal chemistry.[37] Developing a methodology to access $^{11}$C-amides would be one of the most valuable tools in the radiochemist's toolbox and unlock countless possibilities for PET imaging targets. The difficulty in their preparation comes from the limitations in precursors; carbon-11 can only be delivered in single carbon units, like [$^{11}$C]$CH_3I$ and [$^{11}$C]$CO_2$, and so methodologies for $^{11}$C-amides require both formation of a C–C bond, and activated intermediates that can readily form C–N bonds (Figure 2.5).

Traditional methods for the preparation of $^{11}$C-amides rely on the coupling of $^{11}$C-carboxylic acids and amines either at elevated temperatures[2] or through further activation of the $^{11}$C-carbonyl *via* conversion to $^{11}$C-acyl chlorides.[38] However, due to isotopic dilution with atmospheric $CO_2$, alternative methods are required to control reagent stoichiometry and to isolate the reaction's reagents from moisture and atmosphere.

A more recent approach harnesses the reactivity of $^{11}$C-isocyanates to begin with a pre-formed C–N bond and to rely on the former strategy of carbon-carbon bond formation by using Grignard reagents.[39] By forming a $^{11}$C-carbamate anion which is then converted to a $^{11}$C-isocyanate using Mitsunobu reagents *in situ*, the intermediate was further derivatized with methyl Grignard to yield [$^{11}$C]melatonin in sufficient yields and molar activity for continued investigation. However, very few products were found to be successful using $CO_2$, and only two products were tested with [$^{11}$C]$CO_2$. This is potentially due to the excessive reactivity of Grignard reagents, limiting its capacity to tolerate functionality and restricting its translation to simple compounds void of heteroatoms or other popular moieties in drug molecules. With that in mind, organometallics with more controlled reactivity become of interest.

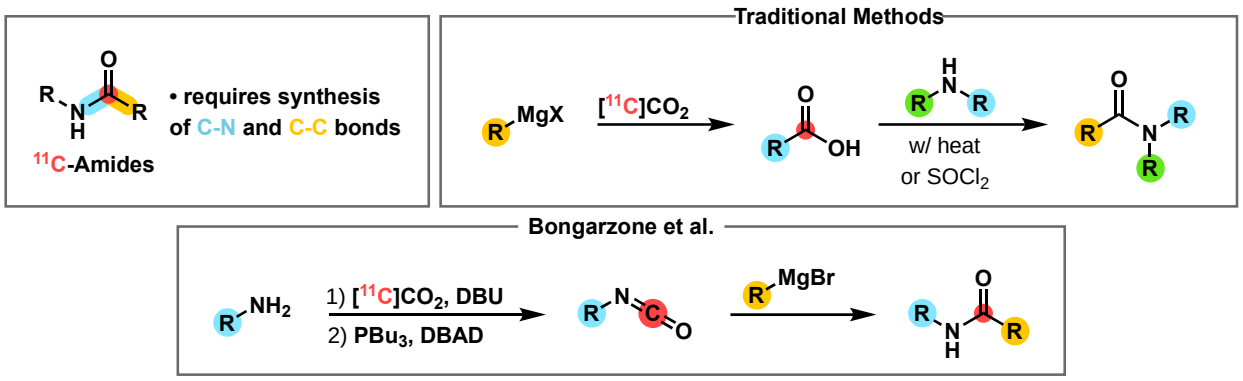


**Figure 2.5.** Radiosynthetic approaches to $^{11}$C-amides. Requiring both the C–C and C–N bond to be formed, $^{11}$C-amides necessitate intermediate synthesis that can satisfy both conditions. Approaches have typically gone through $^{11}$C-carboxylic acids or $^{11}$C-acyl chlorides along with condensation with an amine, but more recent work has explored $^{11}$C-isocyanates with reactive nucleophiles like Grignards.

### 2.1.4. Organozinc Halides and Transition Metal Catalysis

#### *2.1.4.1. Organozinc Halides*

Alternative organometallics to Grignard reagents with sufficiently lowered reactivity are organozinc halides. These reagents typically have tolerance and superior compatibility for functionality and complexity due to their relatively poor reactivity with most electrophiles.[40] As such, in theory we can access more pharmaceutically relevant products thanks to the robustness of a derivatizing nucleophile based on organozinc halides. They're frequently prepared by the direct insertion of zinc into organic halides,[41] although significant work has been done by Dr. Paul Knochel to improve access to diverse organozinc intermediates using a lithium chloride accelerant.[42]

Importantly, while organozinc halides have limited reactivity on their own, they are drastically improved under the addition of transition metal catalysts based from rhodium, palladium, nickel, copper, and others.[43] This elevated control satisfies the potential for greater stability towards functional groups while also ensuring sufficient reactivity with isocyanates and $^{11}$C-isocyanates prepared *in situ*.

#### *2.1.4.2. Transition Metal Catalysis*

Transition metals have been historically used sparingly in radiochemical methodologies for carbon-11, largely limited to $^{11}$C-carbonylations with [$^{11}$C]CO.[44] The proper handling and

addition of these reagents can often be a technical difficulty using automated radiosynthesis units, as they're frequently moisture and atmosphere sensitive and are quite expensive if used in routine productions. Isocyanates had been employed previously with palladium catalysts in which the palladium induced C–N bond formation.[45,46] On the other hand, C–C bond formation using palladium catalysts and isocyanates had been relatively unexplored.

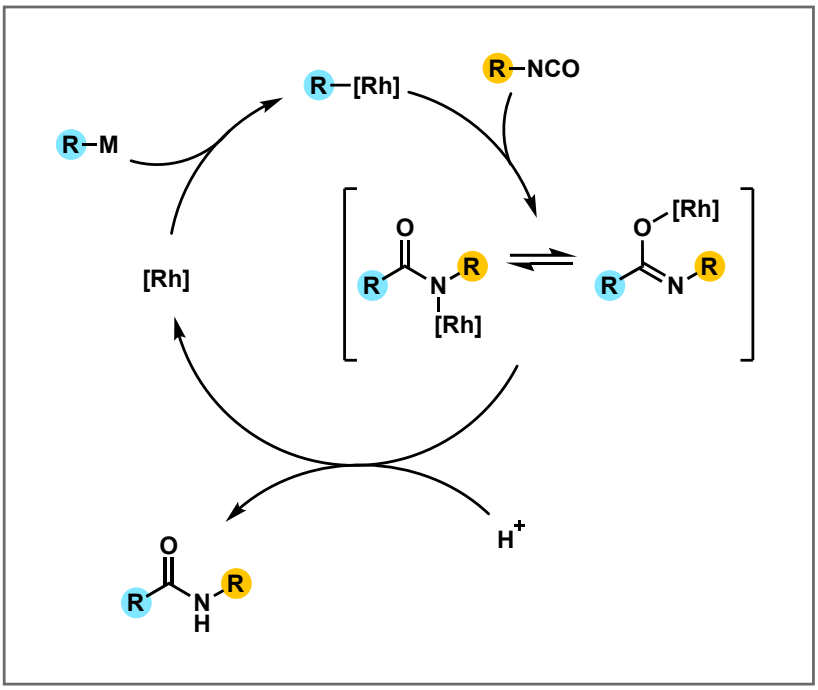


**Figure 2.6.** Possible catalytic cycle of rhodium-based catalysts. A suggested pathway for rhodium's addition to isocyanates, followed by its mediation of nucleophilic addition.

Nonetheless, rhodium catalysts had been found to catalyze the addition of aryl boronic acids to isocyanates, offering an interesting starting point for further investigation.[47] Following transmetallation with the boronic acid, the aryl rhodium species adds across the isocyanate's C=N or C=O bond to form rhodium(I) complexes that can undergo protonolysis to release the desired amide product (Figure 2.6). This methodology was similarly conducted using organostannanes,[48] and thus appeared like a promising avenue for exploration with organozinc halides and for translation to carbon-11 radiochemistry.

### 2.1.5. References


(1) Taddei, C.; Gee, A. D. Recent Progress in [$^{11}$C]Carbon Dioxide ([$^{11}$C]$CO_2$) and [$^{11}$C]Carbon Monoxide ([$^{11}$C]CO) Chemistry. *J Labelled Comp Radiopharm* **2018**, *61* (3), 237–251. https://doi.org/10.1002/jlcr.3596.

(2) Aubert, C.; Huard-Perrio, C.; Lasne, M.-C. Rapid Synthesis of Aliphatic Amides by Reaction of Carboxylic Acids, Grignard Reagent and Amines: Application to the Preparation of [$^{11}$C]Amides. *J. Chem. Soc., Perkin Trans. 1* **1997**, No. 19, 2837–2842. https://doi.org/10.1039/A702897K.

(3) Perrio-Huard, C.; Aubert, C.; Lasne, M.-C. Reductive Amination of Carboxylic Acids and [$^{11}$C]Magnesium Halide Carboxylates. *J. Chem. Soc., Perkin Trans. 1* **2000**, No. 3, 311–316. https://doi.org/10.1039/A908991H.

(4) Luthra, S. K.; Pike, V. W.; Brady, F. The Preparation of Carbon-11 Labelled Diprenorphine: A New Radioligand for the Study of the Opiate Receptor System in Vivo. *J. Chem. Soc., Chem. Commun.* **1985**, No. 20, 1423–1425. https://doi.org/10.1039/C39850001423.

(5) Berger, G.; Maziere, M.; Prenant, C.; Comar, D. Synthesis of Carbon-11-Labelled Acetone. *The International Journal of Applied Radiation and Isotopes* **1980**, *31* (9), 577–578. https://doi.org/10.1016/0020-708X(80)90102-7.

(6) Studenov, A. R.; Berridge, M. S.; Soloviev, D. V.; Matarrese, M.; Todde, S. High Yield Synthesis of [$^{11}$C]-Acetone through Selective Quenching of Methyl Lithium. *Nuclear Medicine and Biology* **1999**, *26* (4), 431–435. https://doi.org/10.1016/S0969-8051(99)00003-7.

(7) van der Meij, M.; Carruthers, N. I.; Herscheid, J. D. M.; Jablonowski, J. A.; Leysen, J. E.; Windhorst, A. D. Reductive N-Alkylation of Secondary Amines with [2-$^{11}$C]Acetone. *Journal of Labelled Compounds and Radiopharmaceuticals* **2003**, *46* (11), 1075–1085. https://doi.org/10.1002/jlcr.740.

(8) Ram, S.; Ehrenkaufer, R. E. Rapid Reductive-Carboxylation of Secondary Amines. One Pot Synthesis of Tertiary N-Methylated Amines. *Tetrahedron Letters* **1985**, *26* (44), 5367–5370. https://doi.org/10.1016/S0040-4039(00)98209-1.

(9) Sakakura, T.; Kohno, K. The Synthesis of Organic Carbonates from Carbon Dioxide. *Chemical Communications* **2009**, *0* (11), 1312–1330. https://doi.org/10.1039/B819997C.

(10) Schirbel, A.; Holschbach, M. H.; Coenen, H. H. N.C.A.[$^{11}$C]$CO_2$ as a Safe Substitute for Phosgene in the Carbonylation of Primary Amines. *Journal of Labelled Compounds and Radiopharmaceuticals* **1999**, *42* (6), 537–551. https://doi.org/10.1002/(SICI)1099-1344(199906)42:6<537::AID-JLCR215>3.0.CO;2-3.

(11) Lockey, J. E.; Redlich, C. A.; Streicher, R.; Pfahles-Hutchens, A.; Hakkinen, P. (Bert) J.; Ellison, G. L.; Harber, P.; Utell, M.; Holland, J.; Comai, A.; White, M. Isocyanates and Human Health: Multistakeholder Information Needs and Research Priorities. *Journal of Occupational and Environmental Medicine* **2015**, *57* (1), 44. https://doi.org/10.1097/JOM.0000000000000278.

(12) Crouzel, C.; Hinnen, F.; Maitre, E. Radiosynthesis of Methyl and Heptyl [$^{11}$C]Isocyanates from [$^{11}$C]Phosgene, Application to the Synthesis of Carbamates: [$^{11}$C]Physostygmine and [$^{11}$C]Heptylphysostigmine. *Applied Radiation and Isotopes* **1995**, *46* (3), 167–170. https://doi.org/10.1016/0969-8043(94)00126-K.

(13) Brown, G. D.; Henderson, D.; Steel, C.; Luthra, S.; Price, P. M.; Brady, F. Two Routes to [$^{11}$C-*Carbonyl*]Organo-Isocyanates Utilizing [$^{11}$C]Phosgene ([$^{11}$C]Organo-Isocyanates from [$^{11}$C]Phosgene). *Nuclear Medicine and Biology* **2001**, *28* (8), 991–998. https://doi.org/10.1016/S0969-8051(01)00263-3.

(14) Brown, G. D.; Luthra, S. K.; Brock, C. S.; Stevens, M. F. G.; Price, P. M.; Brady, F. Antitumor Imidazotetrazines. 40. Radiosyntheses of [4-$^{11}$C-*Carbonyl*]- and [3-N-$^{11}$C-*Methyl*]-8-Carbamoyl-3-Methylimidazo[5,1-*d*]-1,2,3,5-Tetrazin-4(3*H*)-One (Temozolomide) for Positron Emission Tomography (PET) Studies. *J. Med. Chem.* **2002**, *45* (25), 5448–5457. https://doi.org/10.1021/jm020921f.

(15) Lemoucheux, L.; Rouden, J.; Ibazizene, M.; Sobrio, F.; Lasne, M.-C. Debenzylation of Tertiary Amines Using Phosgene or Triphosgene: An Efficient and Rapid Procedure for the Preparation of Carbamoyl Chlorides and Unsymmetrical Ureas. Application of Carbon-11 Chemistry. *J. Org. Chem.* **2003**, *68* (22), 8742–8742. https://doi.org/10.1021/jo0335847.

(16) Hooker, J. M.; Reibel, A. T.; Hill, S. M.; Schueller, M. J.; Fowler, J. S. One-Pot, Direct Incorporation of [$^{11}$C]$CO_2$ into Carbamates. *Angewandte Chemie International Edition* **2009**, *48* (19), 3482–3485. https://doi.org/10.1002/anie.200900112.

(17) Wilson, A. A.; Garcia, A.; Houle, S.; Vasdev, N. Direct Fixation of [$^{11}$C]-$CO_2$ by Amines: Formation of [$^{11}$C-Carbonyl]-Methylcarbamates. *Org. Biomol. Chem.* **2009**, *8* (2), 428–432. https://doi.org/10.1039/B916419G.

(18) Wilson, A. A.; Garcia, A.; Houle, S.; Sadovski, O.; Vasdev, N. Synthesis and Application of Isocyanates Radiolabeled with Carbon-11. *Chemistry – A European Journal* **2011**, *17* (1), 259–264. https://doi.org/10.1002/chem.201002345.

(19) Horvath, M. J.; Saylik, D.; Elmes, P. S.; Jackson, W. R.; Lovel, C. G.; Moody, K. A Mitsunobu-Based Procedure for the Preparation of Alkyl and Hindered Aryl Isocyanates from Primary Amines and Carbon Dioxide under Mild Conditions. *Tetrahedron Letters* **1999**, *40* (2), 363–366. https://doi.org/10.1016/S0040-4039(98)02312-0.

(20) Saylik, D.; Horvath, M. J.; Elmes, P. S.; Jackson, W. R.; Lovel, C. G.; Moody, K. Preparation of Isocyanates from Primary Amines and Carbon Dioxide Using Mitsunobu Chemistry. *J. Org. Chem.* **1999**, *64* (11), 3940–3946. https://doi.org/10.1021/jo982362j.

(21) Ghosh, A. K.; Brindisi, M. Urea Derivatives in Modern Drug Discovery and Medicinal Chemistry. *J. Med. Chem.* **2020**, *63* (6), 2751–2788. https://doi.org/10.1021/acs.jmedchem.9b01541.

(22) Chakraborty, P. K.; Mangner, T. J.; Chugani, H. T. The Synthesis of No-Carrier-Added [$^{11}$C]Urea from [$^{11}$C]Carbon Dioxide and Application to [$^{11}$C]Uracil Synthesis. *Applied Radiation and Isotopes* **1997**, *48* (5), 619–621. https://doi.org/10.1016/S0969-8043(97)00007-9.

(23) Dheere, A. K. H.; Yusuf, N.; Gee, A. Rapid and Efficient Synthesis of [$^{11}$C]Ureas via the Incorporation of [$^{11}$C]$CO_2$ into Aliphatic and Aromatic Amines. *Chem. Commun.* **2013**, *49* (74), 8193–8195. https://doi.org/10.1039/C3CC44046J.

(24) Hicks, J. W.; Wilson, A. A.; Rubie, E. A.; Woodgett, J. R.; Houle, S.; Vasdev, N. Towards the Preparation of Radiolabeled 1-Aryl-3-Benzyl Ureas: Radiosynthesis of [$^{11}$C-*Carbonyl*] AR-A014418 by [$^{11}$C]$CO_2$ Fixation. *Bioorganic & Medicinal Chemistry Letters* **2012**, *22* (5), 2099–2101. https://doi.org/10.1016/j.bmcl.2011.12.139.

(25) Hicks, J. W.; Parkes, J.; Sadovski, O.; Tong, J.; Houle, S.; Vasdev, N.; Wilson, A. A. Synthesis and Preclinical Evaluation of [$^{11}$C-*Carbonyl*]PF-04457845 for Neuroimaging of Fatty Acid Amide Hydrolase. *Nuclear Medicine and Biology* **2013**, *40* (6), 740–746. https://doi.org/10.1016/j.nucmedbio.2013.04.008.

(26) Horkka, K.; Dahl, K.; Bergare, J.; Elmore, C. S.; Halldin, C.; Schou, M. Rapid and Efficient Synthesis of $^{11}$C-Labeled Benzimidazolones Using [$^{11}$C]Carbon Dioxide. *ChemistrySelect* **2019**, *4* (6), 1846–1849. https://doi.org/10.1002/slct.201803561.

(27) Chen, Z.; Chen, J.; Mast, N.; Rong, J.; Deng, X.; Shao, T.; Fu, H.; Yu, Q.; Sun, J.; Shao, Y.; Josephson, L.; Collier, T. L.; Pikuleva, I.; Liang, S. H. Synthesis and Pharmacokinetic Study of a $^{11}$C-Labeled Cholesterol 24-Hydroxylase Inhibitor Using 'in-Loop' [$^{11}$C]$CO_2$ Fixation Method. *Bioorganic & Medicinal Chemistry Letters* **2020**, *30* (9), 127068. https://doi.org/10.1016/j.bmcl.2020.127068.

(28) Ghosh, A. K.; Brindisi, M. Organic Carbamates in Drug Design and Medicinal Chemistry. *J. Med. Chem.* **2015**, *58* (7), 2895–2940. https://doi.org/10.1021/jm501371s.

(29) Roeda, D.; Dolle, F. [$^{11}$C]Phosgene: A Versatile Reagent for Radioactive Carbonyl Insertion Into Medicinal Radiotracers for Positron Emission Tomography. *Curr Top Med Chem*. **2010**, 10 (16), 1680–1700. https://doi.org/10.2174/156802610793176710.

(30) Hooker, J. M.; Kim, S. W.; Alexoff, D.; Xu, Y.; Shea, C.; Reid, A.; Volkow, N.; Fowler, J. S. Histone Deacetylase Inhibitor MS-275 Exhibits Poor Brain Penetration: Pharmacokinetic Studies of [$^{11}$C]MS-275 Using Positron Emission Tomography. *ACS Chem. Neurosci.* **2010**, *1* (1), 65–73. https://doi.org/10.1021/cn9000268.

(31) Wilson, A. A.; Garcia, A.; Parkes, J.; Houle, S.; Tong, J.; Vasdev, N. [$^{11}$C]CURB: Evaluation of a Novel Radiotracer for Imaging Fatty Acid Amide Hydrolase by Positron Emission Tomography. *Nuclear Medicine and Biology* **2011**, *38* (2), 247–253. https://doi.org/10.1016/j.nucmedbio.2010.08.001.

(32) Rusjan, P. M.; Wilson, A. A.; Mizrahi, R.; Boileau, I.; Chavez, S. E.; Lobaugh, N. J.; Kish, S. J.; Houle, S.; Tong, J. Mapping Human Brain Fatty Acid Amide Hydrolase Activity with PET. *J Cereb Blood Flow Metab* **2013**, *33* (3), 407–414. https://doi.org/10.1038/jcbfm.2012.180.

(33) Vasdev, N.; Sadovski, O.; Garcia, A.; Dollé, F.; Meyer, J. H.; Houle, S.; Wilson, A. A. Radiosynthesis of [$^{11}$C]SL25.1188 via [$^{11}$C]$CO_2$ Fixation for Imaging Monoamine Oxidase B. *Journal of Labelled Compounds and Radiopharmaceuticals* **2011**, *54* (10), 678–680. https://doi.org/10.1002/jlcr.1908.

(34) Koshimori, Y.; Cusimano, M. D.; Vieira, E. L.; Rusjan, P. M.; Kish, S. J.; Vasdev, N.; Moriguchi, S.; Boileau, I.; Chao, T.; Nasser, Z.; Ishrat Husain, M.; Faiz, K.; Braga, J.; Meyer, J. H. Astrogliosis Marker $^{11}$C-SL25.1188 PET in Traumatic Brain Injury with Persistent Symptoms. *Brain* **2023**, *146* (11), 4469–4475. https://doi.org/10.1093/brain/awad279.

(35) Braga, J.; Kuik, E. J. Y.; Lepra, M.; Rusjan, P. M.; Kish, S. J.; Vieira, E. L.; Nasser, Z.; Verhoeff, N.; Vasdev, N.; Chao, T.; Bagby, M.; Boileau, I.; Kloiber, S.; Ishrat Husain, M.; Kolla, N.; Koshimori, Y.; Faiz, K.; Wang, W.; Meyer, J. H. Astrogliosis Marker [$^{11}$C]SL25.1188 After COVID-19 With Ongoing Depressive and Cognitive Symptoms. *Biological Psychiatry* **2024**. https://doi.org/10.1016/j.biopsych.2024.09.027.

(36) Ballatore, C.; Huryn, D. M.; Smith, A. B. Carboxylic Acid (Bio)Isosteres in Drug Design. *ChemMedChem* **2013**, *8* (3), 385–395. https://doi.org/10.1002/cmdc.201200585.

(37) Brown, D. G.; Boström, J. Analysis of Past and Present Synthetic Methodologies on Medicinal Chemistry: Where Have All the New Reactions Gone? *J. Med. Chem.* **2016**, *59* (10), 4443–4458. https://doi.org/10.1021/acs.jmedchem.5b01409.

(38) Hwang, D.-R.; Kegeles, L. S.; Laruelle, M. (−)-N-[$^{11}$C]Propyl-Norapomorphine: A Positron-Labeled Dopamine Agonist for PET Imaging of D2 Receptors. *Nuclear Medicine and Biology* **2000**, *27* (6), 533–539. https://doi.org/10.1016/S0969-8051(00)00144-X.

(39) Bongarzone, S.; Runser, A.; Taddei, C.; Dheere, A. K. H.; Gee, A. D. From [$^{11}$C]$CO_2$ to [$^{11}$C]Amides: A Rapid One-Pot Synthesis via the Mitsunobu Reaction. *Chemical Communications* **2017**, *53* (38), 5334–5337. https://doi.org/10.1039/C7CC01407D.

(40) *Organozinc Reagents: A Practical Approach*; Knochel, E. by P., Jones, P., Eds.; The Practical Approach in Chemistry Series; Oxford University Press: Oxford, New York, 1999.

(41) Krasovskiy, A.; Malakhov, V.; Gavryushin, A.; Knochel, P. Efficient Synthesis of Functionalized Organozinc Compounds by the Direct Insertion of Zinc into Organic Iodides and Bromides. *Angewandte Chemie International Edition* **2006**, *45* (36), 6040–6044. https://doi.org/10.1002/anie.200601450.

(42) Piller, F. M.; Metzger, A.; Schade, M. A.; Haag, B. A.; Gavryushin, A.; Knochel, P. Preparation of Polyfunctional Arylmagnesium, Arylzinc, and Benzylic Zinc Reagents by Using Magnesium in the Presence of LiCl. *Chemistry - A European Journal* **2009**, *15* (29), 7192–7202. https://doi.org/10.1002/chem.200900575.

(43) Dilman, A. D.; Levin, V. V. Advances in the Chemistry of Organozinc Reagents. *Tetrahedron Letters* **2016**, *57* (36), 3986–3992. https://doi.org/10.1016/j.tetlet.2016.07.080.

(44) Kealey, S.; Gee, A.; Miller, P. W. Transition Metal Mediated [$^{11}$C]Carbonylation Reactions: Recent Advances and Applications. *Journal of Labelled Compounds and Radiopharmaceuticals* **2014**, *57* (4), 195–201. https://doi.org/10.1002/jlcr.3150.

(45) Larksarp, C.; Alper, H. Palladium-Catalyzed Cyclocarbonylation of *o*-Iodoanilines with Heterocumulenes: Regioselective Preparation of 4(3*H*)-Quinazolinone Derivatives. *J. Org. Chem.* **2000**, *65* (9), 2773–2777. https://doi.org/10.1021/jo991922r.

(46) Kamijo, S.; Yamamoto, Y. A Bimetallic Catalyst and Dual Role Catalyst: Synthesis of N-(Alkoxycarbonyl)Indoles from 2-(Alkynyl)Phenylisocyanates. *J. Org. Chem.* **2003**, *68* (12), 4764–4771. https://doi.org/10.1021/jo034254p.

(47) Miura, T.; Takahashi, Y.; Murakami, M. Rhodium-Catalysed Addition Reaction of Aryl- and Alkenylboronic Acids to Isocyanates. *Chemical Communications* **2007**, No. 34, 3577. https://doi.org/10.1039/b709203b.

(48) Koike, T.; Takahashi, M.; Arai, N.; Mori, A. Addition of Organostannanes to Isocyanate Catalyzed by a Rhodium Complex. *Chemistry Letters* **2004**, *33* (10), 1364–1365. https://doi.org/10.1246/cl.2004.1364.

## 2.2. Rhodium-Catalyzed Addition of Organozinc Iodides to Carbon-11 Isocyanates

Braeden A. Mair,[1,2] Moustafa H. Fouad,[3] Uzair S. Ismailani,[2,3] Maxime Munch,[2,3] Benjamin H. Rotstein*[1,2,3]

[1] Department of Chemistry and Biomolecular Sciences, University of Ottawa, Ottawa, Canada K1H 8M5

[2] University of Ottawa Heart Institute, Ottawa, Canada K1Y 4W7

[3] Department of Biochemistry, Microbiology and Immunology, University of Ottawa, Ottawa, Canada K1H 8M5

Mair et al. *Org Lett*. **2020**, 22, 2746–2750.

### 2.2.1. Statement of the manuscript

The manuscript "Rhodium-Catalyzed Addition of Organozinc Iodides to Carbon-11 Isocyanates" was accepted into *Organic Letters* and published on March 24, 2020. This paper details the development of a methodology to access $^{11}$C-amides using rhodium catalysis and organozinc iodides.

I conducted the development of the methodology and optimization with alkyl and aryl zinc iodides, with assistance from Moustafa Fouad (BSc Candidate) on the aryl scope. I synthesized organozinc iodides, with assistance from Moustafa Fouad. I performed the radiochemical translation, optimization, and scope, with technical collaboration from Uzair Ismailani (MSc/PhD Candidate) and Dr. Maxime Munch (PDF) for the automation of the method. I isolated a representative radiotracer and performed all product and precursor characterization. I wrote the manuscript with editing from Dr. Benjamin Rotstein. All authors approved the final version.

### 2.2.2. Abstract

Amides were prepared using rhodium-catalyzed coupling of organozinc iodides and carbon-11 ($^{11}$C, $t_{1/2}$ = 20.4 min) isocyanates. Non-radioactive isocyanates and $sp^3$ or $sp^2$ organozinc iodides generated amides in 13–87% yields. Incorporation of cyclotron-produced [$^{11}$C]$CO_2$ into $^{11}$C-amide products proceeded in 5–99% yields. The synthetic utility of the methodology was demonstrated through the isolation of [$^{11}$C]*N*-(4-fluorophenyl)-4-methoxybenzamide ([$^{11}$C]**6g**) with a molar activity of 267 GBq·μmol$^{-1}$ and 12% radiochemical yield in 21 minutes from beginning of synthesis.

### 2.2.3. Introduction

Positron emission tomography (PET) is a non-invasive nuclear medicine technology used for *in vivo* molecular imaging. Carbon-11 ($^{11}$C, $t_{1/2}$ = 20.4 min), a short-lived PET isotope, is commonly used for labeling small molecules and peptide radiotracer candidates, though its utility is limited by the availability of chemical methodologies suitable for its incorporation.[1,2] The abundance and diversity of organic frameworks in radiopharmaceuticals therefore calls for continued development of novel $^{11}$C-labeling techniques to satisfy imaging needs.

Amides are a prodigious functional group in synthetic and biological molecules and amide bond formation is among the most commonly used and important reactions in drug discovery.[3,4] However, many powerful synthetic strategies using stable isotopes prove wasteful, impractical and/or ineffective when applied to carbon-11 radiochemistry. Conventional approaches to amide synthesis focus on acylation of an amine, and indeed the same can be accomplished using low molecular weight $^{11}$C-acid chlorides.[5] Still, $^{11}$C can only be produced in single carbon units, most frequently as [$^{11}$C]$CO_2$, and therefore more general methods directed at rapid formation of both the C–N and the C–C bonds of amides are needed to leverage existing medicinal chemistry approaches for radiotracer development.

Established methods for the preparation of $^{11}$C-amides use amines and $^{11}$C-carboxylic acids, the latter prepared from organolithium or Grignard reagents and [$^{11}$C]$CO_2$. These syntheses require great care due to the use of reagents that can readily react with atmospheric $CO_2$ resulting in lower molar activity products. Recent advances using less reactive organometallic precursors for [$^{11}$C]$CO_2$-fixation[6,7] overcome this obstacle, but still require multistep activation to intermediate acid chlorides, which themselves often require purification.[8–11] Alternative synthetic approaches have been developed for $^{11}$C-carbonylation with [$^{11}$C]carbon monoxide, using either preformed arylpalladium complexes[12] or alkyl iodide coupling mediated by nickel.[13] While these options are effective in synthesizing complex amide products, only a few laboratories prepare [$^{11}$C]CO.[14]

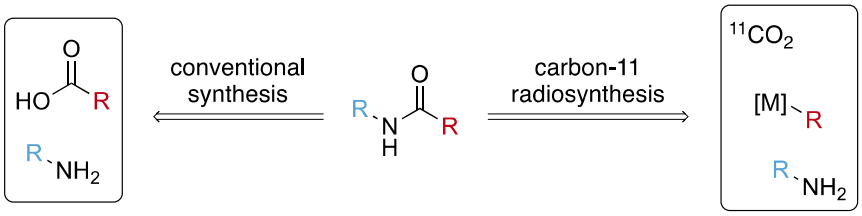


**Figure 2.7.** Strategies for stable isotope and carbon-11 amide synthesis.

An alternative strategy toward $^{11}$C-amides is to begin with $^{11}$C–N formation, for example through an $^{11}$C-isocyanate or $^{11}$C-carbamyl chloride intermediate (Figure 1), followed by derivatization with a carbon-based nucleophile. Indeed, Grignard reagents have recently been successfully deployed in such a context for preparing $^{11}$C-amides, although their elevated reactivity and limited functional group compatibility may restrict practical applications in radiopharmaceutical synthesis.[15] Organozinc halides represent another class of organometallics offering greater stability towards many chemical moieties. Previously, a limited scope of amides had been prepared from allyl and propargyl organozinc halides and aryl isocyanates.[16] Direct addition of alkyl and benzyl organozinc halides to isocyanates did not, however, yield amides, but rather carbamates and urea byproducts. Foreseeing a potential direct route to $^{11}$C-amides that could prove useful in PET radiochemistry, we set out to evaluate conditions redirecting organozinc halide reactivity with isocyanates towards selective C–N bond formation.

We herein report a transition metal-catalyzed coupling of organozinc iodides and isocyanates to produce a diverse scope of amides. This approach is effective with *in situ* prepared $^{11}$C-isocyanates to generate $^{11}$C-amides in suitable yields for radiotracer development.

### 2.2.4. Results and discussion

Arylzinc iodides were the initial target for reaction discovery. First, the addition of phenylzinc iodide (**1a**) to phenyl isocyanate (**2a**) to produce benzanilide (**3a**) was used to develop coupling conditions (Table 1). Only trace product was detected in the absence of a catalyst (Table 1, entry 1). While $Pd(OAc)_2$ proved ineffective for improvement of conversion, $[Rh(Cl)(cod)]_2$ successfully yielded **3a** in 71% yield (entries 2–3). $[Rh(OH)(cod)]_2$ also demonstrated strong selectivity and conversion with a yield of 74% (entry 4). The yields were not further improved by the use of heat, which led to a slight increase in symmetrical diphenyl urea formation (entry 5).

More polar solvents could also facilitate the reaction (entries 6–8), which would prove important for radiochemical applications. A significant drop in yield upon reversing the order of reactant addition indicated the importance of premixing the isocyanate with the catalyst before introducing organozinc iodides (entry 9).

**Figure 2.8.** Optimization of arylzinc iodide reaction conditions.

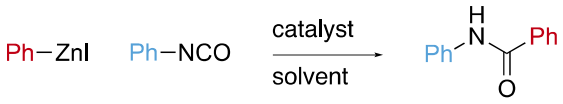


**1a** **2a** **3a** [a]

| Entry | Solvent | Catalyst | Yield **3a** [%][b] |
|---|---|---|---|
| 1 | THF | - | <5 |
| 2 | THF | $Pd(OAc)_2$ | <5 |
| 3 | THF | $[Rh(Cl)(cod)]_2$ | 75,[c] 71 |
| 4 | THF | $[Rh(OH)(cod)]_2$ | 78,[c] 74 |
| 5[d] | THF | $[Rh(OH)(cod)]_2$ | 68 |
| 6 | $Et_2O$ | $[Rh(OH)(cod)]_2$ | 30 |
| 7 | ACN | $[Rh(OH)(cod)]_2$ | 62 |
| 8 | DMSO | $[Rh(OH)(cod)]_2$ | 19 |
| 9[e] | THF | $[Rh(OH)(cod)]_2$ | 13 |

[a]Unless otherwise specified, reactions were carried out n=1 with **1a** (0.4 mmol), **2a** (0.2 mmol) and 2.5 mol% catalyst in solvent (2 mL) at room temperature. [b]Yields were calculated using calibrated HPLC-UV peak integration. [c]Isolated yields. [d]50 °C [e]Reversed order of addition.

The scope of the reaction was evaluated for arylzinc iodides under the optimized conditions with various isocyanates (Table 2). Electron-deficient aryl isocyanates reacted smoothly, affording the products **3b–3d** in good yields. Conversely, coupling with electron-rich 2-methoxyphenyl isocyanate (**2e**) was accompanied by a reduced isolated yield (**3e**). One or more *ortho*-methyl substituents were well-tolerated on isocyanates with only slightly decreased product yields (**3f–3g**). Benzyl, phenethyl, isopropyl and allyl isocyanates could also be used to form amides **3i–3l**. Functionalized electron-rich arylzinc iodides were superior in reactivity, improving nucleophilicity of the reagent, as with **3m** compared to those with electron-withdrawing groups such as products **3n** and **3o**.

**Figure 2.9.** Substrate scope with respect to arylzinc iodides.

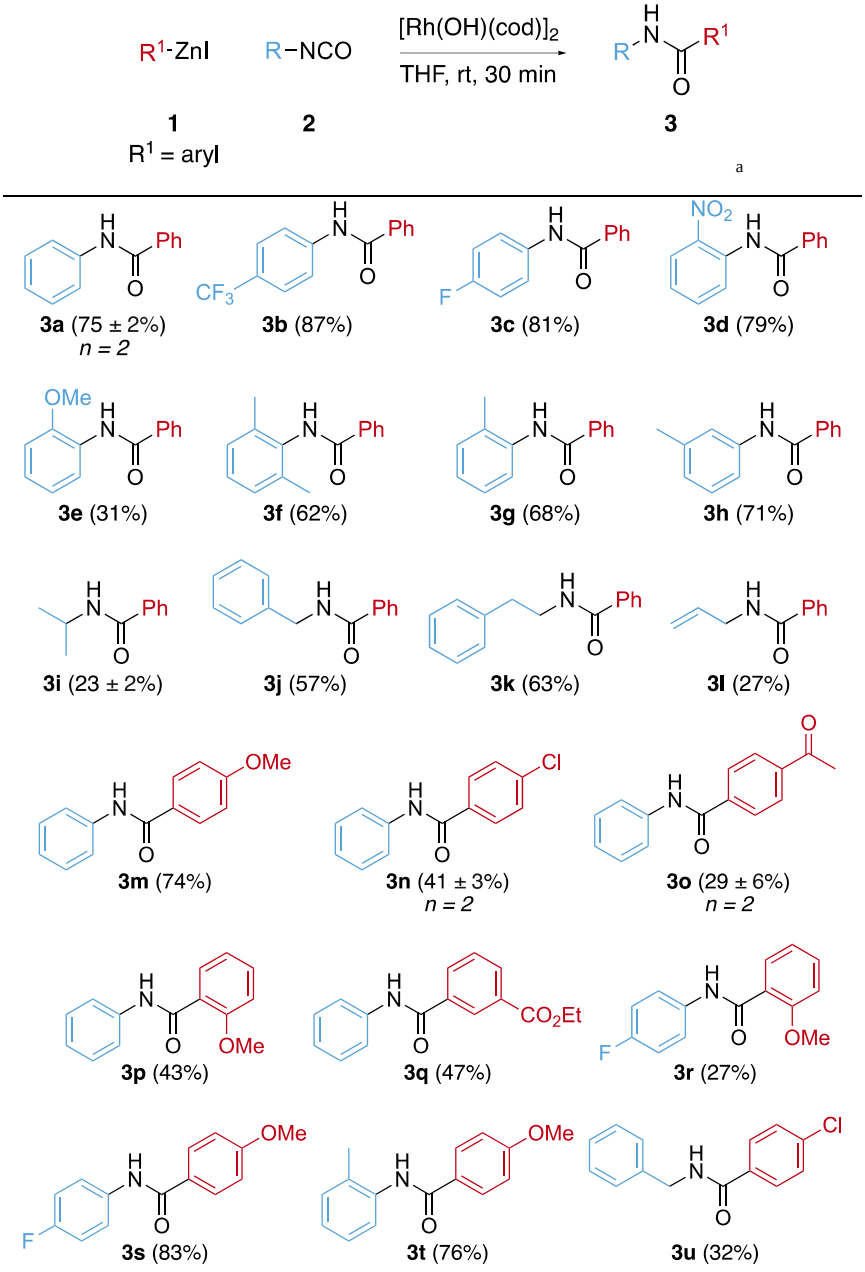


[a]Reaction conditions: **1** (2 equiv., 0.4 mmol), **2** (1 equiv., 0.2 mmol), $[Rh(OH)(cod)]_2$ (2.5 mol%, 0.005 mmol), THF (2 mL), rt, 30 min, under Ar.

Alkyl organozinc iodides were prepared[17] and successfully coupled with isocyanates under similar conditions to prepare *C*-alkyl amides, with longer reaction times required for complete conversion. Notably, addition of $[Rh(OH)(cod)]_2$ suppresses the previously reported carbamate formation.[16] Various additives were evaluated for their effect on reaction progress. Conversions

dropped with the addition of triethylamine,[18] while phenol,[19] DBU, and azo compounds were well tolerated (see ESI), suggesting the possibility of a one-pot $^{11}$C-amide synthesis from $CO_2$.

Similar steric and electronic trends could be observed with alkylzinc iodides as with arylzinc iodides (Table 3): more electron-poor isocyanates proceeded with useful product yields (**4b–4c**) and *ortho*-substituents were moderately tolerated (**4e–4g**), while electron-donating groups or alkyl isocyanates fared worse (**4e, 4i–4j**). In general, products of ethylzinc iodide were isolated in higher yields compared to those prepared from methylzinc iodide, though functionality trends were maintained throughout (for the full zinc iodide reaction scope, including additional compounds, see the supporting information).

**Figure 2.10.** Scope with respect to alkylzinc iodides.

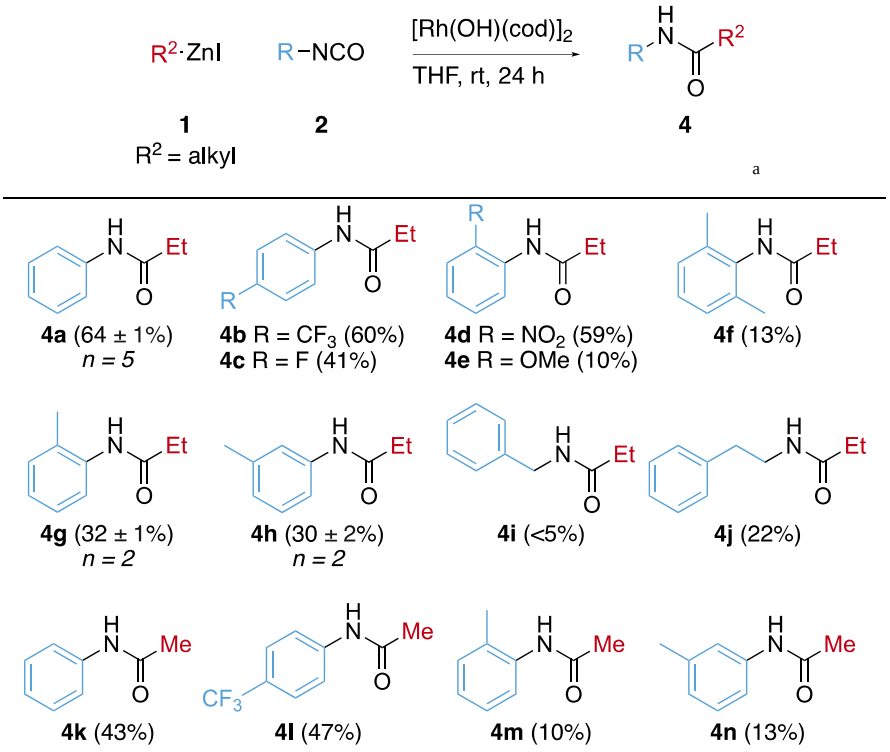


[a]Reaction conditions: **1** (3 equiv., 0.6 mmol), **2** (1 equiv., 0.2 mmol), $[Rh(OH)(cod)]_2$ (2.5 mol%, 0.005 mmol), THF (2 mL), rt, 24 h, under Ar.

Satisfied with this characterization of rhodium-catalyzed organozinc iodide coupling with stable isotope isocyanates, the findings provided a framework to develop a method for $^{11}$C-labelling. Less reactive methylzinc iodide was selected for optimization, aiming towards

[$^{11}$C]acetanilide due to its relevance as a parent compound to metabolic paracetamol, one of the most commonly used analgesics.[20]

**Figure 2.11.** Optimization for [$^{11}$C]acetanilide synthesis.

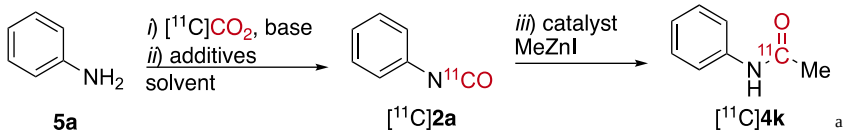


**5a** [$^{11}$C]**2a** [$^{11}$C]**4k** [a]

| Entry | Base | TE [%][b] | RCY [%][c] | TE x RCY [%] |
|---|---|---|---|---|
| 1 ($n$ = 2) | BEMP | 99 ± 1 | 15 ± 1 | 20 |
| 2[d] | BEMP | 75 | 5 | 4 |
| 3[e] | BEMP | 60 | 11 | 7 |
| 4[f] | DBU | >99 | 74 | 74 |
| 5[g] | DBU | 92 | 78 | 72 |
| 6 ($n$ = 4) | DBU | 95 ± 3 | 81 ± 2 | 77 |
| 7[h] | DBU | 68 | 40 | 27 |
| 8[i] | DBU | 68 | 12 | 8 |
| 9[j] | DBU | 90 | 81 | 73 |
| 10[k] | DBU | 89 | 80 | 71 |

[a]Reaction conditions: *i*) **5a** (22.90 μmol), base (35.50 μmol), ACN (500 μL), <2 min; *ii*) $PBu_3$ (45.80 μmol) and DBAD (45.80 μmol), ACN (100 μL), 1 min; *iii*) 15 min [b]Trapping efficiency [c]Radiochemical yield, calculated from integration of radioHPLC signal [d]DMSO [e]DMF [f]Coupling performed for 10 min [g]$[Rh(Cl)(cod)]_2$ used as catalyst [h]50 °C [i]0 °C [j]2.0 equiv. DBU [k]2.5 equiv. DBU

Initial trials using a $POCl_3$-induced dehydration procedure for the synthesis of $^{11}$C-isocyanates[21,22] proved incompatible with the coupling conditions. Dehydration using Mitsunobu reagents[23,24] (tributyl phosphine and di-*tert*-butyl azodicarboxylate, DBAD) in acetonitrile provided more reliable access to [$^{11}$C]phenyl isocyanate and was also compatible with the subsequent rhodium-catalyzed coupling with methylzinc iodide (Table 4, entries 1–3). DBU, a base more commonly used with Mitsunobu dehydration, provided a substantial increase to both the trapping efficiency and RCY (entries 4–6). Various amounts of DBU were used to evaluate stoichiometric effect on the reaction; 1.5 equivalents yielded the best results for trapping and conversion (entries 6, 9–10).

With an optimized procedure in hand, a series of biologically relevant compounds were labeled with $^{11}$C using this technique (Table 5). Isocyanates were prepared *in situ* using an automated $^{11}$C synthesis system before being routed to a secondary reactor containing the rhodium catalyst. The coupling reaction was commenced with the addition of organozinc iodide (0.3 mL,

3.3–9.8 equivalents), then reacted for 10–15 minutes before aqueous quenching and radioHPLC analysis. Peak integration was performed in order to derive radiochemical yields and product identities were confirmed by coinjection with nonradioactive standards of each compound. The method ensures reliable trapping conditions while also leading to moderate to strong radiochemical purity and yield. A number of compounds were prepared, including the biologically-relevant *tert*-butyl protected [$^{11}$C]*N*-acetyl glutamic acid ([$^{11}$C]**6d**), the agrochemical [$^{11}$C]propanil ([$^{11}$C]**6e**), and a pharmaceutically-relevant [$^{11}$C]acetanilide ([$^{11}$C]**4k**).

**Figure 2.12.** Carbon-11 substrate scope.

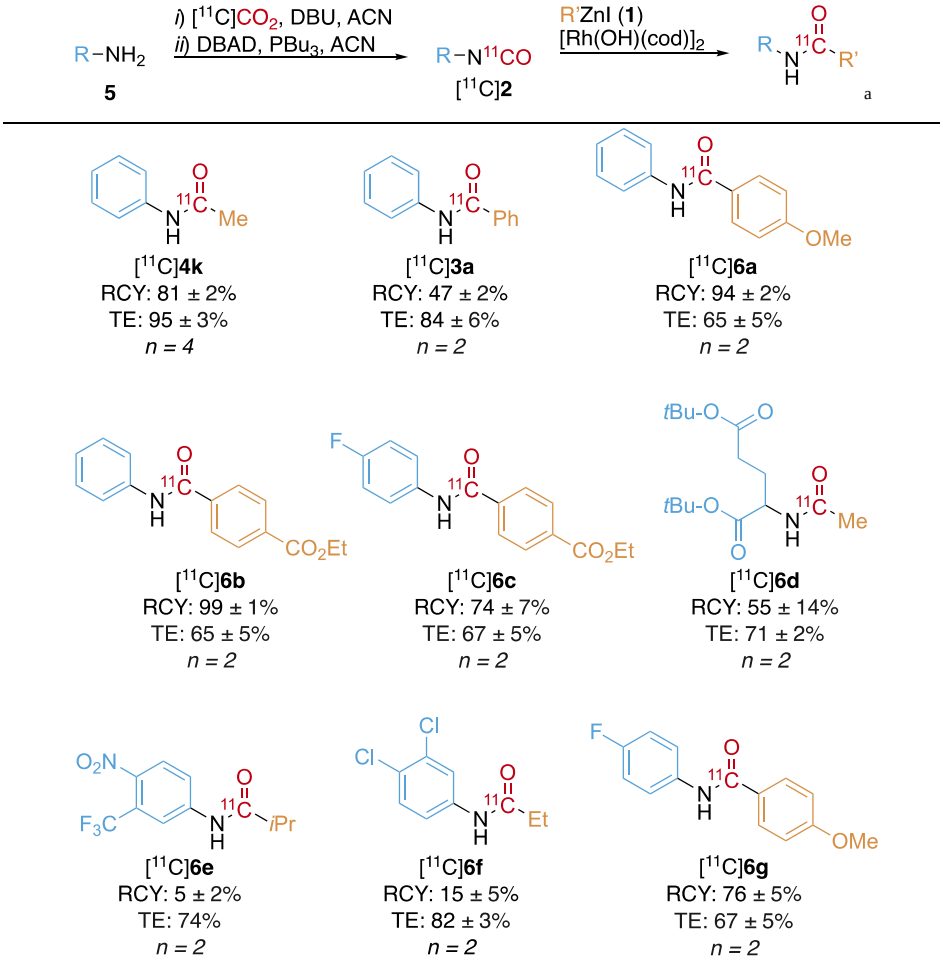


[a]See ESI for general procedure (P5). Standard error given for all reactions.

Amide [$^{11}$C]**6g** was selected for further isolation to demonstrate the utility of this labeling technique. A fully automated method was implemented (see ESI) with a total time of 21 minutes from delivery of [$^{11}$C]$CO_2$ to end of semi-preparative HPLC purification (C18, aqueous

acetonitrile mobile phase). The decay-corrected radiochemical yield was 12% from [$^{11}$C]$CO_2$ delivery with a molar activity of 267 GBq·μmol$^{-1}$ (Scheme 4).

**Figure 2.13.** Automated synthesis and isolation of amide [$^{11}$C]6g.

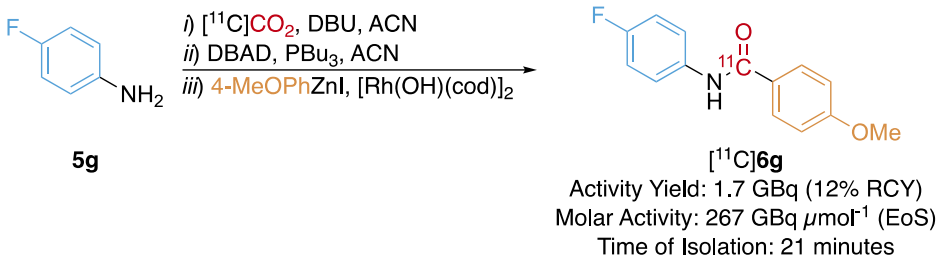


See ESI for details.

### 2.2.5. Conclusion

In conclusion, we have developed a transition metal-catalyzed synthesis of amides that can be translated for use with $^{11}$C. Organozinc iodides and isocyanates can be coupled using rhodium-catalysis to synthesize a wide array of amide products under mild reaction conditions and with fast synthesis times. $^{11}$C-Amide products can be derived in suitable yields and fully automated for practical radiotracer synthesis. This method will represent a new strategy for $^{11}$C-labeling of biologically relevant amides.

### 2.2.6. Acknowledgement

Financial and infrastructure support for this work were provided by the University of Ottawa Heart Institute (UOHI), and the Natural Sciences and Engineering Research Council of Canada (NSERC), the Canada Foundation for Innovation (CFI), and the Ontario Ministry for Research, Innovation and Science. B.A.M. was supported by the BioTalent Student Work-Integrated Learning Program. The authors are grateful to Dr. Tayebeh Hadizad and Daniel Duan (UOHI PET Radiochemistry Core) for isotope production, and Prof. André Beauchemin (University of Ottawa) for helpful discussions.

### 2.2.7. References


(1) Deng, X.; Rong, J.; Wang, L.; Vasdev, N.; Zhang, L.; Josephson, L.; Liang, S. H. Chemistry for Positron Emission Tomography: Recent Advances in $^{11}$C-, $^{18}$F-, $^{13}$N-, and $^{15}$O-Labeling Reactions. *Angew. Chem. Int. Ed.* **2019**, *58* (9), 2580–2605. https://doi.org/10.1002/anie.201805501.

(2) Miller, P. W.; Long, N. J.; Vilar, R.; Gee, A. D. Synthesis of $^{11}$C, $^{18}$F, $^{15}$O, and $^{13}$N Radiolabels for Positron Emission Tomography. *Angew. Chem. Int. Ed.* **2008**, *47* (47), 8998–9033. https://doi.org/10.1002/anie.200800222.

(3) Boström, J.; Brown, D. G.; Young, R. J.; Keserü, G. M. Expanding the Medicinal Chemistry Synthetic Toolbox. *Nat. Rev. Drug Discov.* **2018**. 17, 709–727. https://doi.org/10.1038/nrd.2018.116.

(4) Roughley, S. D.; Jordan, A. M. The Medicinal Chemist's Toolbox: An Analysis of Reactions Used in the Pursuit of Drug Candidates. *J. Med. Chem.* **2011**, *54* (10), 3451–3479. https://doi.org/10.1021/jm200187y.

(5) Luthra, S. K.; Pike, V. W.; Brady, F. Preparation of Some NCA [1-$^{11}$C]Acid Chlorides as Labelling Agents. *Int. J. Rad. Appl. Instrum. [A]* **1990**, *41* (5), 471–476. https://doi.org/10.1016/0883-2889(90)90007-4.

(6) Rotstein, B. H.; Liang, S. H.; Placzek, M. S.; Hooker, J. M.; Gee, A. D.; Dollé, F.; Wilson, A. A.; Vasdev, N. $^{11}$C=O Bonds Made Easily for Positron Emission Tomography Radiopharmaceuticals. *Chem. Soc. Rev.* **2016**, *45* (17), 4708–4726. https://doi.org/10.1039/C6CS00310A.

(7) Rotstein, B. H.; Liang, S. H.; Holland, J. P.; Collier, T. L.; Hooker, J. M.; Wilson, A. A.; Vasdev, N. $^{11}CO_2$ Fixation: A Renaissance in PET Radiochemistry. *Chem. Commun.* **2013**, *49* (50), 5621. https://doi.org/10.1039/c3cc42236d.

(8) Aubert, C.; Huard-Perrio, C.; Lasne, M.-C. Rapid Synthesis of Aliphatic Amides by Reaction of Carboxylic Acids, Grignard Reagent and Amines: Application to the Preparation of [$^{11}$C]Amides. *J. Chem. Soc. Perkin 1* **1997**, No. 19, 2837–2842. https://doi.org/10.1039/a702897k.

(9) McCarron, J. A.; Turton, D. R.; Pike, V. W.; Poole, K. G. Remotely-Controlled Production of the 5-HT1A Receptor Radioligand, [Carbonyl-$^{11}$C]WAY-100635, via $^{11}$C-Carboxylation of an Immobilized Grignard Reagent. *J. Labelled Compd. Radiopharm.* **1996**, *38* (10), 941–953. https://doi.org/10.1002/(SICI)1099-1344(199610)38:10<941::AID-JLCR906>3.0.CO;2-Y.

(10) Luthra, S. K.; Pike, V. W.; Brady, F. The Preparation of Carbon-11 Labelled Diprenorphine: A New Radioligand for the Study of the Opiate Receptor System in Vivo. *J. Chem. Soc. Chem. Commun.* **1985**, (20), 1423–1425. https://doi.org/10.1039/C39850001423.

(11) Riss, P. J.; Lu, S.; Telu, S.; Aigbirhio, F. I.; Pike, V. W. CuI-Catalyzed 11C Carboxylation of Boronic Acid Esters: A Rapid and Convenient Entry to $^{11}$C-Labeled Carboxylic Acids, Esters, and Amides. *Angew. Chem. Int. Ed.* **2012**, *51* (11), 2698–2702. https://doi.org/10.1002/anie.201107263.

(12) Andersen, T. L.; Friis, S. D.; Audrain, H.; Nordeman, P.; Antoni, G.; Skrydstrup, T. Efficient $^{11}$C-Carbonylation of Isolated Aryl Palladium Complexes for PET: Application to Challenging Radiopharmaceutical Synthesis. *J. Am. Chem. Soc.* **2015**, *137* (4), 1548–1555. https://doi.org/10.1021/ja511441u.

(13) Rahman, O.; Långström, B.; Halldin, C. Alkyl Iodides and [$^{11}$C]CO in Nickel-Mediated Cross-Coupling Reactions: Successful Use of Alkyl Electrophiles Containing a β Hydrogen Atom in Metal-Mediated [$^{11}$C]Carbonylation. *ChemistrySelect* **2016**, *1* (10), 2498–2501. https://doi.org/10.1002/slct.201600643.

(14) Taddei, C.; Pike, V. W. [$^{11}$C]Carbon Monoxide: Advances in Production and Application to PET Radiotracer Development over the Past 15 Years. *EJNMMI Radiopharm. Chem.* **2019**, *4* (1), 25. https://doi.org/10.1186/s41181-019-0073-4.

(15) Bongarzone, S.; Runser, A.; Taddei, C.; Dheere, A. K. H.; Gee, A. D. From [$^{11}$C]$CO_2$ to [$^{11}$C]Amides: A Rapid One-Pot Synthesis via the Mitsunobu Reaction. *Chem. Commun.* **2017**, *53* (38), 5334–5337. https://doi.org/10.1039/C7CC01407D.

(16) Yang, H.; Huang, D.; Wang, K.-H.; Xu, C.; Niu, T.; Hu, Y. Reaction of Organozinc Halides with Aryl Isocyanates. *Tetrahedron* **2013**, *69* (12), 2588–2593. https://doi.org/10.1016/j.tet.2013.01.053.

(17) Edeson, S. J.; Maduli, E. J. M.; Swanson, S.; Procopiou, P. A.; Harrity, J. P. A. Investigation of a Late-Stage Derivatization Approach to Isatogens: Discovery of New Reaction Pathways: Late-Stage Derivatization Approach to Isatogens. *Eur. J. Org. Chem.* **2016**, *2016* (1), 83–86. https://doi.org/10.1002/ejoc.201501372.

(18) Vinogradova, E. V.; Fors, B. P.; Buchwald, S. L. Palladium-Catalyzed Cross-Coupling of Aryl Chlorides and Triflates with Sodium Cyanate: A Practical Synthesis of Unsymmetrical Ureas. *J. Am. Chem. Soc.* **2012**, *134* (27), 11132–11135. https://doi.org/10.1021/ja305212v.

(19) Koike, T.; Takahashi, M.; Arai, N.; Mori, A. Addition of Organostannanes to Isocyanate Catalyzed by a Rhodium Complex. *Chem. Lett.* **2004**, *33* (10), 1364–1365. https://doi.org/10.1246/cl.2004.1364.

(20) Lester, D.; Greenberg, L. A.; Carroll, R. P. The Metabolic Fate of Acetanilid and Other Aniline Derivatives: Ii. Major Metabolites of Acetanilid Appearing in the Blood. *J. Pharmacol. Exp. Ther.* **1947**, *90* (1), 68–75.

(21) Schirbel, A.; Holschbach, M. H.; Coenen, H. H. N.C.A.[$^{11}$C]$CO_2$ as a Safe Substitute for Phosgene in the Carbonylation of Primary Amines. *J. Labelled Compd. Radiopharm.* **1999**, *42* (6), 537–551. https://doi.org/10.1002/(SICI)1099-1344(199906)42:6<537::AID-JLCR215>3.0.CO;2-3.

(22) Wilson, A. A.; Garcia, A.; Houle, S.; Sadovski, O.; Vasdev, N. Synthesis and Application of Isocyanates Radiolabeled with Carbon-11. *Chem. Eur. J.* **2011**, *17* (1), 259–264. https://doi.org/10.1002/chem.201002345.

(23) Dheere, A. K. H.; Yusuf, N.; Gee, A. Rapid and Efficient Synthesis of [$^{11}$C]Ureas via the Incorporation of [$^{11}$C]$CO_2$ into Aliphatic and Aromatic Amines. *Chem. Commun.* **2013**, *49* (74), 8193–8195. https://doi.org/10.1039/C3CC44046J.

(24) Horvath, M. J.; Saylik, D.; Elmes, P. S.; Jackson, W. R.; Lovel, C. G.; Moody, K. A Mitsunobu-Based Procedure for the Preparation of Alkyl and Hindered Aryl Isocyanates from Primary Amines and Carbon Dioxide under Mild Conditions. *Tetrahedron Lett.* **1999**, *40* (2), 363–366. https://doi.org/10.1016/S0040-4039(98)02312-0.

## 2.3. Supporting Information

### 2.3.1. General Information

All chemicals and solvents used were bought commercially and were not further purified unless indicated otherwise. All reactions were routinely carried out under inert (argon or nitrogen) atmosphere. All solvents used were anhydrous. 1,4-dioxane was distilled in the lab. All reaction products were confirmed using TLC, mass spectrometry, and $^{1}$H-NMR. Purification of reaction products was carried out by flash column chromatography using silica gel. Analytical thin layer chromatography (TLC) was performed on aluminum or glass backing. Visualization was accomplished with UV light. $^{1}$H-NMR spectra obtained using Magritek Spinsolve 80 Carbon, Bruker AVANCE 300 or Bruker AVANCE 400. Spectral data are reported in ppm using solvent as the reference ($CDCl_3$ at 7.26 ppm for $^{1}$H NMR). $^{1}$H NMR data was reported as: multiplicity (ap = apparent, br = broad, s = singlet, d = doublet, t = triplet, q = quartet, m = multiplet), integration, and coupling constant(s) in Hz. Mass spectrometry was performed using Waters Xevo TQD with an Acquity UPLC H-Class Plus system. Radiolabeled amides were synthesized using Synthra MeIplus Research module. All products generated were characterized in accordance to the literature.

Phenyl Isocyanate (≥ 98%), phenethyl isocyanate (96%), 4-(trifluoromethyl) phenyl isocyanate (98%), o-tolyl isocyanate (98%), m-tolyl Isocyanate (98%), and isopropyl isocyanate (98%+) were purchased from Alfa Aesar. 4-fluorophenyl isocyanate (99%), 2-methoxyphenyl isocyanate (99%), and phenethyl isocyanate (98%) were purchased from Oakwood Chemicals. 2,6-dimethylphenyl isocyanate (99%) and benzyl isocyanate (99%) were purchased from Thermo Fischer Scientific. Iodobenzene (98%), 4-methoxy iodobenzene (98%), ethyl 3-iodobenzoate (98%), 4′-iodoacetophenone (98%), 1-chloro-4-iodobenzene (99%) were purchased from sigma Aldrich. Anhydrous tetrahydrofuran (THF, ≥ 99%, distilled before use), ethyl acetate (EtOAc, ≥ 99.9%), anhydrous diethylene glycol dimethyl ether (diglyme ≥ 99.5%), acetonitrile (99.8%+), trichloromethylsilane (TMSCl, 99%), and 1,2-dibromoethane (98%+) were purchased from Sigma-Aldrich. Hydroxy(1,5-cyclooctadiene) rhodium(I) dimer (min. 97%), chloro(1,5-cyclooctadiene)rhodium(I) dimer (min. 97%), and palladium(II) acetate (min. 98%) and zinc powder (99.9%) were purchased from Strem Chemicals.

### 2.3.2. Synthetic Procedures

**P1 - Synthesis of alkylzinc iodides.**

Following literature methods, a flame dried flask (equipped with magnetic stir bar and reflux condenser) was charged with zinc dust (26.00 mmol) in THF (2.00 mL). 1,2-Dibromoethane (0.10 mL) was added and the mixture was heated to reflux with a heat gun. This was repeated a further two times, after which the reaction mixture was cooled to room temperature and TMSCl (0.10 mL) was added slowly followed by 10 minutes of vigorous stirring. Primary alkyl iodide (26.00 mmol) was added as a solution of THF (10.0 mmol) then stirred and heated at 50 °C for 18 hours. The concentration of alkylzinc iodide was determined using iodometric titration.

**P2 - Synthesis of phenyl zinc iodide.**

Following literature methods,[1] 10 mmol (654 mg) of zinc dust was added to a 10 mL oven-dried round bottom flask. The flask was heated by a heat gun for 10 minutes under vacuum. To the solid, 2.5 mL of diglyme, followed by 0.16 mmol (0.02 mL) of TMSCl, followed by 5 mmol (0.56 mL) of iodobenzene were added under inert atmosphere (argon). The reaction mixture was then stirred for 24 hours at 130 °C. The final mixture was centrifuged, and the supernatant was extracted. Concentration of the phenylzinc iodide solution was determined using an iodometric titration procedure. The final concentration of the phenylzinc iodide used for the reactions in Tables 1 and 2 was 1.03 M.

**P3 - Synthesis of functional arylzinc iodide-lithium chloride compounds**.

Following literature methods[2] and applying modifications, a dry and argon-flushed Schlenk-tube, equipped with a magnetic stirring bar and a rubber septum, was charged with LiCl (0.90 mmol) and heated to 250 °C for 5 min under high vacuum. After cooling to room temperature under vigorous stirring, $InCl_3$ (0.09 mmol) was added and the Schlenk-tube was again heated to 250 °C for 5 min under high vacuum. After cooling to room temperature, zinc powder (9.0 mmol, 3.0 equiv) and dry THF (4.5 mL) were added. The resulting suspension was treated with a few drops of trimethylsilyl chloride and heated briefly to reflux. Subsequently, the corresponding aryl iodide (3.0 mmol, 1.0 equiv) was added and the reaction mixture was heated under given conditions.[3] The reaction mixture was then centrifuged. The supernatant liquid was transferred via a syringe into an oven-dried test tube. The final concentration of the resulting arylzinc iodides were determined by iodometric titration.

**P4 - Synthesis of amides using organozinc iodides and isocyanates.**

To a 10 mL oven-dried round bottom flask, 0.005 mmol (2.3 mg) of $[Rh(OH)(cod)]_2$ is added. Then, 2 mL of THF and 0.2 mmol of isocyanate are added. The reaction mixture is stirred for 5 minutes before the addition of 0.4 mmol of arylzinc iodide or 0.6 mmol of alkylzinc iodide. The reaction is stirred for 30 minutes (24 hours for alkylzinc iodides) under inert atmosphere at room temperature. The reaction is then quenched with 2.0 mL saturated aqueous ammonium chloride ($NH_4^+Cl^-$) The mixture was extracted with EtOAc (3 x 10 mL); the organic phase was washed with brine (10 mL), dried over $MgSO_4$, concentrated under reduced pressure and purified by flash column chromatography (using silica gel, 0–25% ethyl acetate/hexane gradient).

*This procedure is better completed when scaled out rather than scaled up. In testing on a 1 mmol scale, the reactivity was not consistent from batch to batch; comparatively, multiple reaction set ups in parallel could reliably reproduce similar results.

**P5 - Synthesis of radiolabeled amides.**

Using Synthra MeIplus Research module, 22.90 μmol of the amine with 35.50 μmol of DBU in 500 μL ACN are added in Reactor 1. 45.80 μmol of DBAD with 45.80 μmol of $PBu_3$ in 200uL ACN are added in Vial 1. Carbon-11 $CO_2$ ($[^{11}C]CO_2$) — generated from bombardment of a gas target filled with a pressurized $N_2/O_2$ mixture using a Siemens 11 MeV cyclotron, typically 40–55 μA for 1–2 minutes — was trapped at -180 °C in a steel coil. $[^{11}C]CO_2$ is then bubbled into a 2 mL glass reactor vessel, after which the contents in vial 1 are immediately added into the reactor to convert the carbamate to the radiolabeled isocyanate. After reacting for 1 minute, the solution is transferred to a vial charged with 1.0 mg of $[Rh(OH)(cod)]_2$. 0.3 mL of organozinc iodide is then added and allowed to react for 15* minutes. The mixture is subsequently quenched with 1.0 mL of deionized water, followed by addition of ethyl acetate. The mixture is centrifuged to rapidly separate the layers. The organic phase is sampled and analyzed using radioHPLC. Trapping efficiency is calculated as the decay-corrected activity yield in the reactor relative to the steel coil using calibrated proximal radiation detectors. Product yield is determined according to relative peak integrations on radioHPLC, with decay-correction to time of injection. When needed, a sand bath was used to heat the reaction.

*Products $[^{11}C]$**6d** and $[^{11}C]$**6g** were reacted for 10 minutes.

**P6 – Automated synthesis of radiolabeled amides.**

Using Synthra MeIplus Research module, 22.90 µmol of the amine with 35.50 µmol of DBU in 500 µL ACN are added in Reactor 1. 45.80 µmol of DBAD with 45.80 µmol of $PBu_3$ in 200uL ACN are added in Vial A3. 1.0 mg of $[Rh(OH)(cod)]_2$ in 0.4 mL ACN was added in Vial A2. 0.3 mL of organozinc iodide was placed in Reactor 2 while 1.0 mL of 1 M HCl (aq) was added to Vial B1. Carbon-11 $CO_2$ ($[^{11}C]CO_2$) — generated from bombardment of a gas target filled with a pressurized $N_2/O_2$ mixture using a Siemens 11 MeV cyclotron, 55 µA for 20 minutes — was trapped at -180 °C in a steel coil. $[^{11}C]CO_2$ is then bubbled into a 2 mL glass reactor vessel, after which the contents in Vial A3 are immediately added into the reactor to convert the carbamate to the radiolabeled isocyanate, stirring for 1 minute. Vial A2 was added to the reaction mixture, then directed towards reactor 2. The solution was allowed to react for 10 minutes with the organozinc iodide. The mixture is subsequently quenched with the contents of B1. This solution was added to the HPLC injection loop and injected onto a Macherey-Nagel Nucleodur C18 HTec column (5 µm, 250x10 mm). It was purified using 45:55 acetonitrile to 0.1 M ammonium formate mobile phase at a flow rate of 5 mL/min. The isolated product was verified by analytical radioHPLC and molar activity was determined via a calibration curve. Trapping efficiency is calculated as the decay-corrected activity yield in the reactor relative to the steel coil using calibrated proximal radiation detectors.

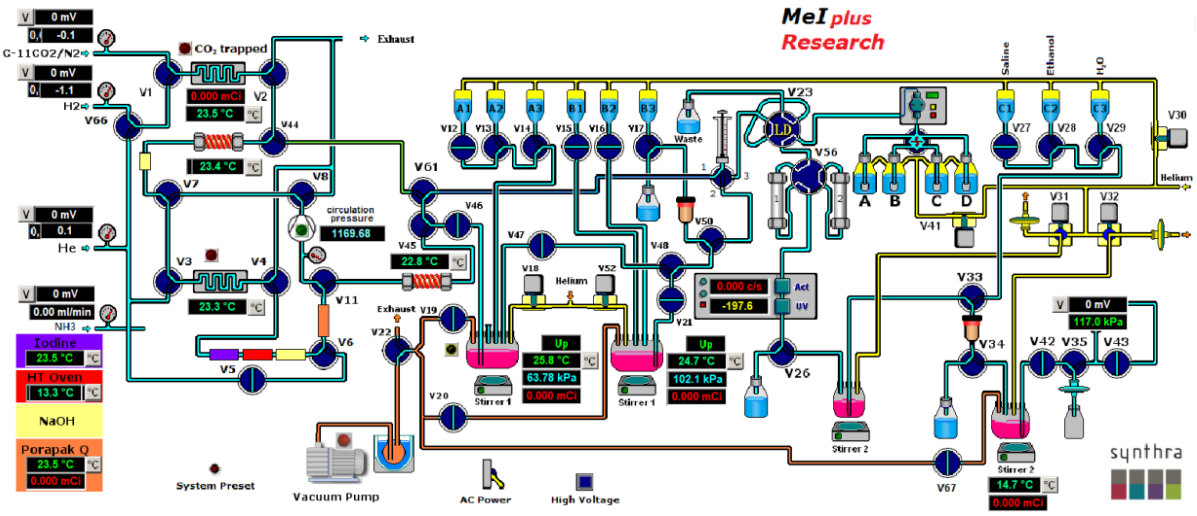


**Figure S2.1.** Synthra MeIplus Research apparatus scheme.

## 2.3.3. Experimental Data

**3a. *N*-phenyl benzamide**

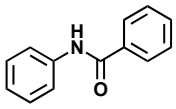

Followed the general procedure of amide synthesis (P4), product obtained as a white solid (31 mg, yield 78%). $^1$H-NMR (80 MHz, $CDCl_3$): d 7.87 (d, 2H), 7.83 (s, 1H), 7.63 (d, 2H), 7.57 (t, 1H), 7.50 (t, 2H), 7.39 (t, 2H), 7.17 (t, 1H). MS (ESI+): Calculated $C_{11}H_{13}NO$ as 197.08, [M+H] found as 198.22 *m/z*. Characterized in accordance to the literature.

**3b. *N*-4-trifluoromethylphenyl benzamide**

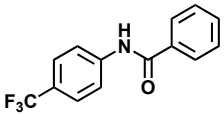

Followed the general procedure of amide synthesis (P4), product obtained as a white solid (45 mg, yield 87%), $^1$H-NMR (80 MHz, $CDCl_3$): d 7.91 (s, 1H), 7.89 (d, 2H), 7.79 (d, 2H), 7.65 (d, 2H), 7.60 (m, 1H), 7.53 (t, 2H). MS (ESI+): Calculated $C_{14}H_{10}F_3NO$ as 265.07, [M+H] found as 266.08 *m/z*. Characterized in accordance to the literature.[5]

**3c. *N*-4-fluorophenyl benzamide**

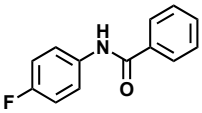

Followed the general procedure of amide synthesis (P4), product obtained as a white solid (35 mg, yield 81%), $^1$H-NMR (80 MHz, $CDCl_3$): δ 7.89 (m, 2H), 7.77 (s, 1H), 7.62 (d, 2H), 7.38 (t, 2H), 7.23 (m, 3H). MS (ESI+): Calculated $C_{13}H_{10}FNO$ as 215.07, [M+H] found 216.03 *m/z*. Characterized in accordance to the literature.[5]

**3d. *N*-2-nitrophenyl benzamide**

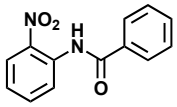

Followed the general procedure of amide synthesis (P4), product obtained as a yellow solid (38 mg, yield 79%). $^1$H-NMR (80 MHz, $CDCl_3$): δ 7.24 (t, 1H), 7.55 (m, 2H), 7.63 (t, 1H), 7.74 (t, 1H), 8.01 (m, 2H), 8.30 (dd, 1H), 9.03 (dd, 1H), 11.38 (s, 1H). MS (ESI+): Calculated $C_{13}H_{10}N_2O_3$ as 242.07 [M+H] found 243.07 *m/z*. Characterized in accordance to the literature.[6]

**3e. *N*-2-methoxyphenyl benzamide**

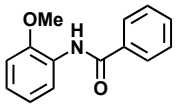

Followed the general procedure of amide synthesis (P4), product obtained as a white solid. (14 mg, yield 31%), $^1$H-NMR (80 MHz, $CDCl_3$): 8.55 (m, 2H), 7.91 (m, 2H), 7.50 (m, 3H), 6.94 (m, 3H) 3.96 (s, 3H). MS (ESI+): Calculated $C_{14}H_{13}NO_2$ as 227.09, [M+H] found 228.09 *m/z*. Characterized in accordance to the literature.[7]

**3f. *N*-2,6-dimethylphenyl benzamide**

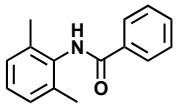

Followed the general procedure of amide synthesis (P4), product obtained as a white solid (28 mg, yield 62%), $^1$H-NMR (80 MHz, $CDCl_3$): δ 7.94 (m, 2H), 7.59 (m, 1H), 7.51 (m, 3H), 7.15 (m, 3H), 2.41 (s, 6H). MS (ESI+): Calculated $C_{15}H_{15}NO$ as 225.12, [M+H] found 226.13 *m/z*. Characterized in accordance to the literature.[8]

**3g. *N*-2-methylphenyl benzamide**

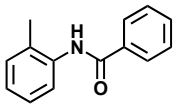

Followed the general procedure of amide synthesis (P4), product obtained as a white solid (17 mg, yield 68%), $^1$H-NMR (80 MHz, $CDCl_3$): δ 7.98 (d, 1H), 7.90 (d, 2H), 7.65 (s, 1H), 7.58 (m, 1H), 7.52 (m, 2H), 7.29 (m, 1H), 7.24 (m, 1H), 7.14 (m, 1H), 2.35 (s, 3H). MS (ESI+): Calculated $C_{14}H_{13}NO$ as 211.10, [M+H] found 212.13 *m/z*. Characterized in accordance to the literature.[4]

**3h. *N*-3-methylphenyl benzamide**

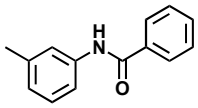

Followed the general procedure of amide synthesis (P4), product obtained as a white solid (18 mg, yield 71%), $^1$H-NMR (80 MHz, $CDCl_3$): δ 7.87 (d, 2H), 7.75 (s, 1H), 7.56 (m, 4H), 7.42 (d, 1H), 7.26 (m, 1H), 6.98 (m, 1H), 2.21 (s, 3H). MS (ESI+): Calculated $C_{14}H_{13}NO$ as 211.10, [M+H] found 212.10 *m/z*. Characterized in accordance to the literature.[4]

**3i. *N*-isopropyl benzamide**

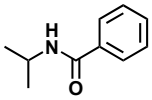

Followed the general procedure of amide synthesis (P4), product obtained as a white solid (8 mg, yield 25%). $^1$H-NMR (80 MHz, $CDCl_3$): δ 7.60 (dd, 2H), 7.25 (tt, 1H), 7.20 (dt, 2H), 5.75 (bs, 1H), 4.15 (sept, 1H), 1.15 (d, 6H). MS (ESI+): Calculated $C_{10}H_{13}NO$ as 163.10, [M+H] found 164.15 *m/z*. Characterized in accordance to the literature.[9]

**3j. *N*-benzyl benzamide**

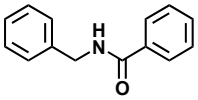

Followed the general procedure of amide synthesis (P4), product obtained as a white solid (24 mg, yield 57%), $^1$H-NMR (80 MHz, $CDCl_3$): δ 7.82 (d, 2H), 7.51 (t, 1H), 7.43 (t, 2H), 7.36 (m, 4H), 7.29 (m, 1H), 6.69 (s, 1H), 4.64 (d, 2H). MS (ESI+): Calculated $C_{14}H_{13}NO$ as 211.10, [M+H] found 212.04 *m/z*. Characterized in accordance to the literature.[10]

**3k. *N*-phenethyl benzamide**

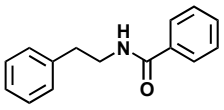

Followed the general procedure of amide synthesis (P4), product obtained as a white solid. (26mg, yield 63%), $^1$H-NMR (80 MHz, $CDCl_3$): δ 7.69 (d, 2H), 7.46 (t, 1H), 7.38 (t, 2H), 7.31 (t, 2H), 7.23 (t, 3H), 6.40 (s, 1H), 3.69 (q, 2H), 2.91 (t, 2H). MS (ESI+): Calculated $C_{15}H_{15}NO$ as 225.12, [M+H] found 226.21 *m/z*. Characterized in accordance to the literature.[11]

**3l. *N*-allyl benzamide**

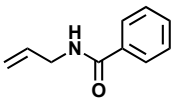

Followed the general procedure of amide synthesis (P4), product obtained as a white solid (9 mg, yield 27%). $^1$H-NMR (80 MHz, $CDCl_3$): δ 7.78 (dd, 2H), 7.45-7.50 (m, 1H), 7.25 (dt, 2H), 6.75 (bs, 1H), 5.85-5.95 (m, 1H), 5.20 (dd, 1H), 5.13 (ddd, 1H), 4.00-4.05 (m, 2H). MS (ESI+): Calculated $C_{10}H_{11}NO$ as 161.08, [M+H] found 162.08 *m/z*. Characterized in accordance to the literature.[9]

**3m. *N*-phenyl 4-methoxybenzamide**

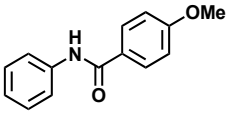

Followed the general procedure of amide synthesis (P4), product obtained as a white solid (34 mg, yield 74%). $^1$H-NMR (80 MHz, $CDCl_3$): δ 7.83 (m, 2H), 7.82 (m, 1H), 7.62 (m, 2H), 7.37 (m, 2H), 7.14 (m, 1H), 6.96 (m, 2H), 3.87 (s, 3H). MS (ESI+): Calculated $C_{14}H_{13}NO_2$ as 227.09, [M+H] found 228.27 *m/z*. Characterized in accordance to the literature.[12]

**3n. *N*-phenyl 4-chlorobenzamide**

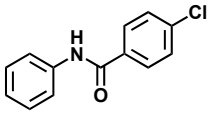

Followed the general procedure of amide synthesis (P4), product obtained as a white solid (14 mg, yield 44%), $^1$H-NMR (80 MHz, $CDCl_3$): δ 7.96 (d, 2H), 7.84 (d, 2H), 7.61 (t, 1H), 7.55 (t, 2H), 7.42 (d, 2H). MS (ESI+): Calculated $C_{13}H_{10}ClNO$ as 231.05, [M+H] found 232.07 *m/z*. Characterized in accordance to the literature.[12]

**3o. *N*-phenyl 4-acetylbenzamide**

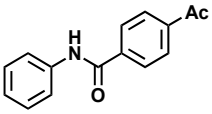

Followed the general procedure of amide synthesis (P4), product obtained as a light yellow solid (9mg, yield 34%), $^1$H-NMR (80 MHz, $CDCl_3$): δ 7.92 (m, 2H), 7.89 (m, 2H), 7.67 (s, 1H), 7.54 (m, 4H), 2.61 (s, 3H). MS (ESI+): Calculated $C_{15}H_{13}NO_2$ as 239.09, [M+H] found 240.12 *m/z*. Characterized in accordance to the literature.[13]

**3p. *N*-phenyl 2-methoxybenzamide**

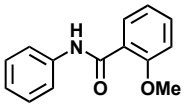

Followed the general procedure of amide synthesis (P4), product obtained as a white solid (20 mg, yield 43%). $^1$H-NMR (80 MHz, $CDCl_3$): δ 9.80 (s, 1H), 8.28 (m, 1H), 7.69 (m, 2H), 7.37 (m, 1H), 7.34 (m, 2H), 7.13 (m, 2H), 7.02 (m, 1H), 4.03 (s, 3H). MS (ESI+): Calculated $C_{14}H_{13}NO_2$ as 227.09, [M+H] found 228.23 *m/z*. Characterized in accordance to the literature.[12]

**3q. *N*-phenyl 3-ethylester benzamide**

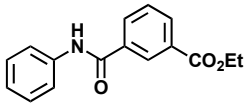

Followed the general procedure of amide synthesis (P4), product obtained as a white solid (16 mg, yield 47%), $^1$H-NMR (80 MHz, $CDCl_3$): δ 8.41 (s, 1H), 7.92 (d, 2H), 7.65 (dd, 1H), 7.39 (t, 2H), 7.30 (t, 2H), 7.21 (dd, 1H), 4.51 (q, 2H), 1.52 (t, 3H). MS (ESI+): Calculated $C_{16}H_{15}NO_3$ as 269.11, [M+H] found 270.08 *m/z*. Characterized in accordance to the literature.[14]

**3r. *N*-4-fluorophenyl-2-methoxybenzamide**

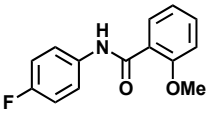

Followed the general procedure of amide synthesis (P4), product obtained as a yellow solid (13 mg, yield 27%). $^1$H-NMR (80 MHz, $CDCl_3$): δ 9.78 (s, 1H), 8.29-8.27 (m, 1H), 7.65-7.62 (m, 3H), 7.52-7.48 (m, 1H), 7.13 (t, H), 7.07-7.02 (m, 3H), 4.05 (s, 3H). MS (ESI+): Calculated $C_{14}H_{12}FNO_2$ as 245.09, [M+H] found 246.24 *m/z*. Characterized in accordance to the literature.[15]

**3s. *N*-4-fluorophenyl 4-methoxybenzamide**

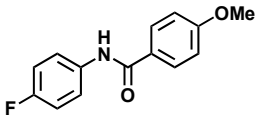

Followed the general procedure of amide synthesis (P4), product obtained as a white solid (27mg, yield 83%),[1]H-NMR (80 MHz, $CDCl_3$): δ 7.95 (d, 2H), 7.80 (m, 2H), 7.19 (m, 2H), 7.06 (d, 2H), 3.83 (s, 3H). MS (ESI+): Calculated $C_{14}H_{12}FNO_2$ as 245.09, [M+H] found 260.21 *m/z*. Characterized in accordance to the literature.[16]

**3t. *N*-2-methylphenyl 4-methoxybenzamide**

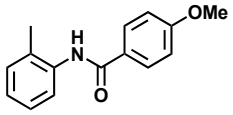

Followed the general procedure of amide synthesis (P4), product obtained as a white solid (24mg, yield 76%), [1]H-NMR (80 MHz, $CDCl_3$): δ 7.92 (s, 1H), 7.87 (m, 1H), 7.83 (dd, 1H), 7.17 (dd, 2H), 6.68 (d, 2H), 3.87 (s, 3H), 2.33 (s, 3H). MS (ESI+): Calculated $C_{15}H_{15}NO_2$ as 241.11, [M+H] found 242.13 *m/z*. Characterized in accordance to the literature.[17]

**3u. *N*-benzyl 4-chlorobenzamide**

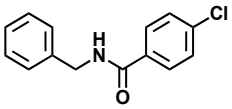

Followed the general procedure of amide synthesis (P4), product obtained as a white solid (14mg, yield 44%), 1H-NMR (80 MHz, CDCl3): δ 7.76 (d, 2H), 7.64 (d, 2H), 7.55 (t, 1H), 7.41 (t, 2H), 7.17 (d, 2H), 4.54 (d, 2H) . MS (ESI+): Calculated $C_{14}H_{12}ClNO$ as 245.06, [M+H] found 246.07 *m/z*. Characterized in accordance to the literature.[18]

**4a. *N*-phenyl propanamide**

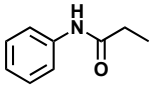

Followed the general procedure of amide synthesis (P4), product obtained as a white solid (19.6mg, yield 64%), [1]H-NMR (80 MHz, $CDCl_3$): δ = 7.52 (m, 2H), 7.33 (t, 2H), 7.11 (m, 2H), 2.39 (q, 2H), 1.25 (t, 3H, CH3). ). MS (ESI+): Calculated $C_9H_{11}NO$ as 149.08, [M+H] found 150.11 *m/z*. Characterized in accordance to the literature.[19]

**4b. *N*-4-trifluoromethylphenyl propanamide**

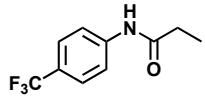

Followed the general procedure of amide synthesis (P4), product obtained as a white solid (26 mg, yield 60%). [1]H-NMR (300 MHz, $CDCl_3$): δ 7.59 (dd, 4H), 7.37 (bs, 1H), 2.41 (dd, 2H), 1.24 (t, 3H). [13]C-NMR (100 MHz, $CDCl_3$): 172.52, 141.12, 126.45, 124.24, 119.50, 118.82, 30.97, 9.66. MS (ESI+): Calculated $C_{10}H_{10}F_3NO$ as 217.07, [M+H] found 218.23 *m/z*, calculated 218.20. Spectra given, page S22.

**4c. *N*-4-fluorophenyl propanamide**

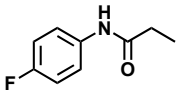

Followed the general procedure of amide synthesis (P4), product obtained as a white solid (13.7mg, yield 41%), [1]H-NMR (80 MHz, $CDCl_3$): δ = 7.97 (s, 1H), 4.43 (dd, 2H), 6.94 (t, 2H), 2.33 (q, 2H), 1.27 (t, 3H). MS (ESI+): Calculated $C_9H_{10}FNO$ as 167.07, [M+H] found 168.08 *m/z*. Characterized in accordance to the literature.[19]

**4d. *N*-2-nitrophenyl propanamide**

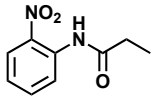

Followed the general procedure of amide synthesis (P4), product obtained as a yellow solid (22.8mg, yield 59%), $^1$H-NMR (80 MHz, $CDCl_3$): δ = 10.34 (s, 1H), 8.83 (dd, 1H), 8.22 (dd, 1H), 7.71 (m, 1H), 7.16 (m, 1H), 2.57 (q, 2H), 1.28 (t, 3H). MS (ESI+): Calculated $C_9H_{10}N_2O_3$ as 194.07, [M+H] found 195.13 *m/z*. Characterized in accordance to the literature.[20]

**4e. *N*-2-methoxyphenyl propanamide**

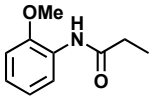

Followed the general procedure of amide synthesis (P4), product obtained as a brown oil (3.6 mg, yield 10%). $^1$H-NMR (80 MHz, $CDCl_3$): δ = 10.34 (s, 1H), 8.83 (dd, 1H), 8.22 (dd, 1H), 7.71 (m, 1H), 7.16 (m, 1H), 2.57 (q, 2H), 1.28 (t, 3H). MS (ESI+): Calculated $C_{10}H_{13}NO_2$ as 179.09, [M+H] found 180.06 *m/z*. Characterized in accordance to the literature.[20]

**4f. *N*-2,6-dimethylphenyl propanamide**

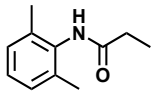

Followed the general procedure of amide synthesis (P4), product obtained as a white solid (3.5mg, yield 10%). $^1$H-NMR (80 MHz, $CDCl_3$): δ 7.94 (m, 2H), 7.59 (m, 1H), 2.41 (s, 6H), 2.54 (q, 2H), 1.23 (t, 3H). MS (ESI+): Calculated $C_{11}H_{15}NO$ as 177.12, [M+H] found 178.22 *m/z*. Characterized in accordance to the literature.[21]

**4g. *N*-2-methylphenyl propanamide**

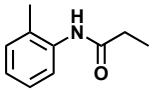

Followed the general procedure of amide synthesis (P4), product obtained as a white solid (10.4 mg, yield 32%). $^1$H-NMR (80 MHz, $CDCl_3$): δ = 7.68 (m, 1H), 7.37 (m, 1H), 7.31 (d, 1H), 7.17 (t, 1H), 2.38 (s, 2H), 2.30 (q, 2H), 1.22 (t, 3H). MS (ESI+): Calculated $C_{10}H_{13}NO$ as 163.10, [M+H] found 164.18 *m/z*. Characterized in accordance to the literature.[22]

**4h. *N*-3-methylphenyl propanamide**

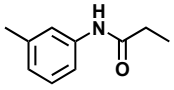

Followed the general procedure of amide synthesis (P4), product obtained as a white solid (10.2 mg, yield 31%). $^1$H-NMR (80 MHz, $CDCl_3$): δ = 7.72 (m, 1H), 7.37 (d, 1H), 7.31 (d, 1H), 7.15 (t, 1H), 6.90 (d, 1H), 2.37 (q, 2H), 2.31 (s, 3H), 1.21 (t, 3H). MS (ESI+): Calculated $C_{10}H_{13}NO$ as 163.10, [M+H] found 164.13 *m/z*. Characterized in accordance to the literature.[23]

**4j. *N*-phenethyl propanamide**

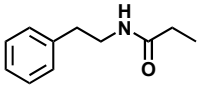

Followed the general procedure of amide synthesis (P4), product obtained as a white solid (7.8mg, yield 22%). $^1$H-NMR (80 MHz, $CDCl_3$): δ = 7.15 (m, 4H), 6.02 (s, 1H), 3.55 (q, 2H), 2.86 (t, 2H), 2.17 (q, 2H), 1.13 (t, 3H). MS (ESI+): Calculated $C_{11}H_{15}NO$ as 177.12, [M+H] found 178.02 *m/z*. Characterized in accordance to the literature.[22]

**4k. *N*-phenyl acetamide**

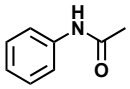

Followed the general procedure of amide synthesis (P4), product obtained as a white solid (11.6mg, yield 43%). $^1$H-NMR (80 MHz, $CDCl_3$): δ = 9.02 (s, 1H), 7.53 (d, 2H), 7.29 (t, 2H), 7.11 (t, 1H), 2.13 (s, 3H). MS (ESI+): Calculated $C_8H_9NO$ as 135.07, [M+H] found 136.05 *m/z*. Characterized in accordance to the literature.[22]

**4l. *N*-4-trifluoromethyl acetamide**

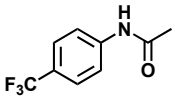

Followed the general procedure of amide synthesis (P4), product was obtained as a white solid (19.1mg, yield 47%). $^1$H-NMR (80 MHz, $CDCl_3$): δ = 10.28 (s, 1 H), 7.74 (m, 4H), 2.12 (s, 3H). MS (ESI+): Calculated $C_9H_8F_3NO$ as 203.06, [M+H] found 204.16 *m/z*. Characterized in accordance to the literature.[24]

**4m. *N*-2-methylphenyl acetamide**

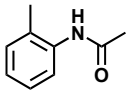

Followed the general procedure of amide synthesis (P4), product was obtained as a white solid (3.1 mg, yield 10%). $^1$H-NMR (80 MHz, $CDCl_3$): δ = 8.52 (s, 1H), 7.39 (s, 1H), 7.25 (m, 1H), 7.21 (t, 1H), 6.88 (t, J= 7.6 Hz, 1H), 2.33 (s, 3H), 2.16 (s, 3H). MS (ESI+): Calculated $C_9H_{11}NO$ as 149.08, [M+H] found 150.02 *m/z*. Characterized in accordance to the literature.[25]

**4n. *N*-3-methylphenyl acetamide**

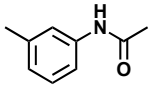

Followed the general procedure of amide synthesis (P4), product was obtained as a white solid (3.2 mg, yield 13%). $^1$H-NMR (80 MHz, $CDCl_3$): δ = 8.57 (s, 1H), 7.42 (m, 1H), 7.31 (m, 1H), 7.08 (t, 1H), 7.02 (t, 1H), 2.30 (s, 3H), 2.22 (s, 3H). MS (ESI+): Calculated $C_9H_{11}NO$ as 149.08, [M+H] found 150.08 *m/z*. Characterized in accordance to the literature.[26]

## 2.5.4. Calibration Curves

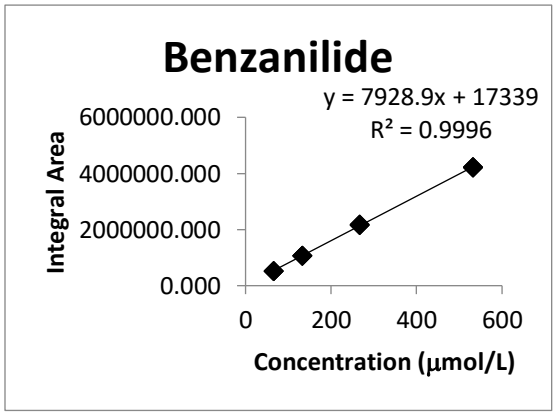


*Used with HPLC to determine benzanilide conversion.

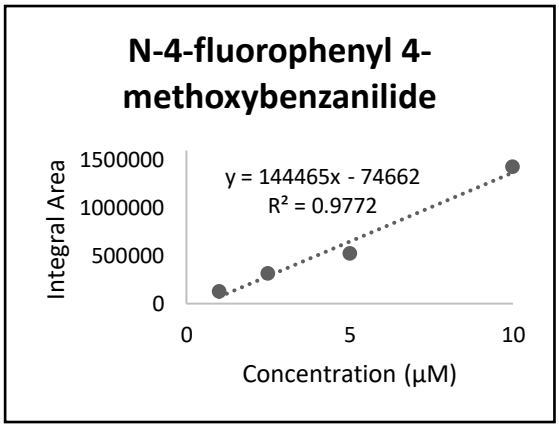

### 2.3.5. Optimization

**Figure S2.2.** Optimization of alkyl zinc iodide reaction conditions

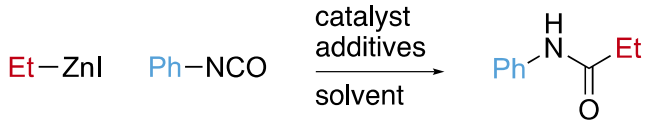


**1i** **2a** **4a** [a]

| Entry | Temperature (°C) | Additives [b] | Catalyst [c] | Conversion [d] |
|---|---|---|---|---|
| 1 | rt | - | - | 0% |
| 2 | rt | - | $[Rh(OH)(cod)]_2$ | 60% |
| 3 | 50 | - | $[Rh(OH)(cod)]_2$ | 60% |
| 4 | 0 | - | $[Rh(OH)(cod)]_2$ | 50% |
| 5 | rt | $NEt_3$ | $[Rh(OH)(cod)]_2$ | 10% |
| 6 | rt | PhOH | $[Rh(OH)(cod)]_2$ | 60% |
| 7 | rt | DBU | $[Rh(OH)(cod)]_2$ | 40% |
| 8 | rt | DBAD | $[Rh(OH)(cod)]_2$ | 50% |
| 9 | rt | - | $[Pd(PPh_3)_4]$ | 0% |
| 10 | rt | - | $Pd(OAc)_2$ | 0% |
| 11 | rt | - | $[RhCl(PPh_3)_3]$ | 0% |
| 12 | rt | - | $[Rh(Cl)(cod)]_2$ | 60% |

[a] Reaction conditions: **1a** (3 equiv., 0.6 mmol), phenyl isocyanate (1 equiv., 0.2 mmol), THF (2 mL), 18 h, under Ar. [b] Additive (1 equiv., 0.2 mmol). [c] 2.5 mol% catalyst charge was employed. [d] Conversions determined based on relative UPLC peak intensities compared to undesired side products.

### 2.3.6. Substrate Scope

**Figure S2.3.** Amide synthesis using organozinc iodides and isocyanates.

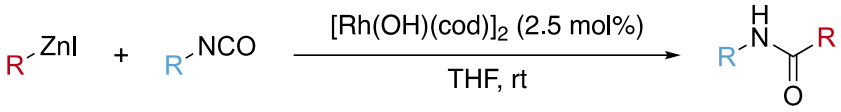


| Entry | Organozinc Reagent **1(a – m)** | Isocyanate **2(a – l)** | Amide Product **3(a – x) or 4(a – t)** | Yield [%] |
|---|---|---|---|---|
| 1 | 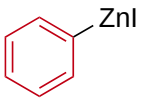 1a | 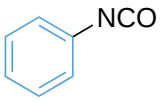 2a | 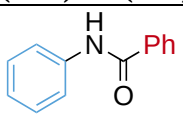 3a | 78 |
| 2 | 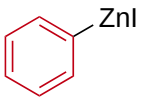 1a | 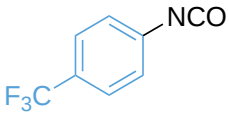 2b | 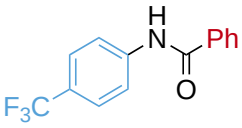 3b | 87 |
| 3 | 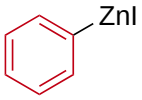 1a | 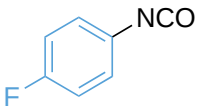 2c | 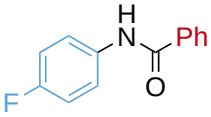 3c | 81 |
| 4 | 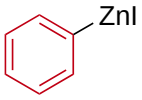 1a | 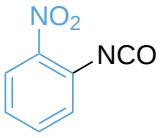 2d | 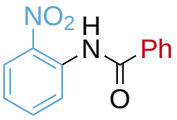 3d | 79 |
| 5 | 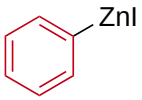 1a | 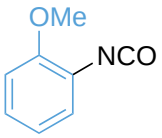 2e | 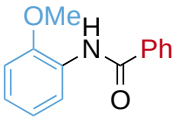 3e | 31 |
| 6 | 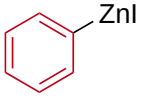 1a | 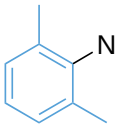 2f | 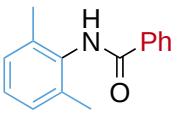 3f | 62 |
| 7 | 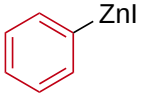 1a | 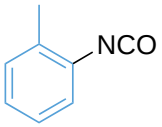 2g | 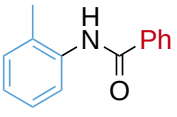 3g | 68 |
| 8 | 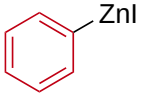 1a | 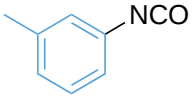 2h | 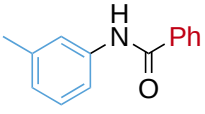 3h | 71 |

| Entry | Organozinc Reagent | Isocyanate | Amide Product | Yield [%] |
|---|---|---|---|---|
| 9 | 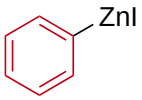 1a | 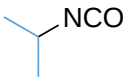 2i | 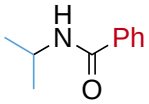 3i | 25 |
| 10 | 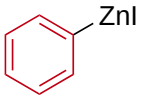 1a | 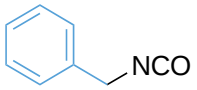 2j | 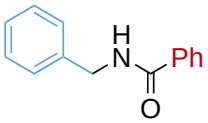 3j | 57 |
| 11 | 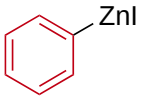 1a | 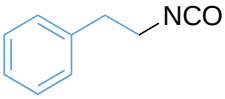 2k | 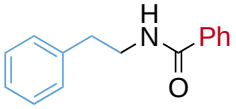 3k | 63 |
| 12 | 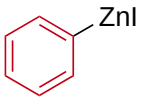 1a | 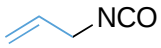 2l | 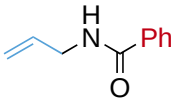 3l | 27 |
| 13 | 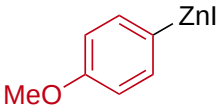 1b | 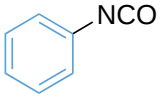 2a | 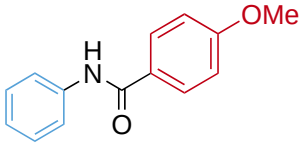 3m | 74 |
| 14 | 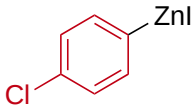 1c | 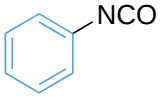 2a | 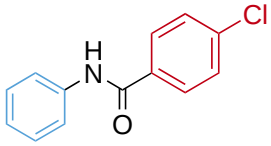 3n | 44 |
| 15 | 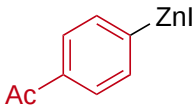 1d | 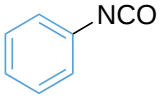 2a | 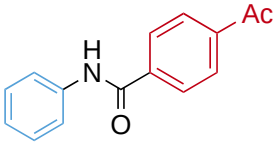 3o | 34 |
| 16 | 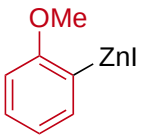 1e | 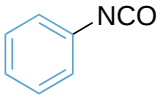 2a | 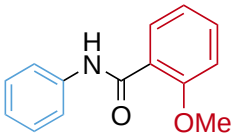 3p | 43 |
| 17 | 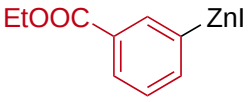 1f | 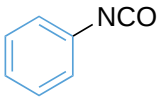 2a | 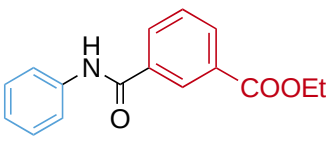 3q | 47 |

| Entry | Organozinc Reagent | Isocyanate | Amide Product | Yield [%] |
|---|---|---|---|---|
| 18 | 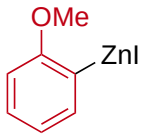 1e | 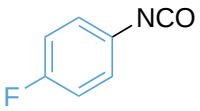 2c | 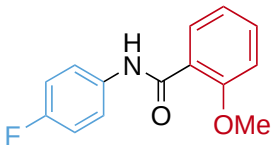 3r | 27 |
| 19 | 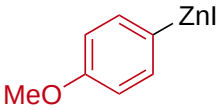 1b | 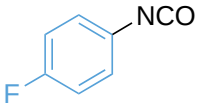 2c | 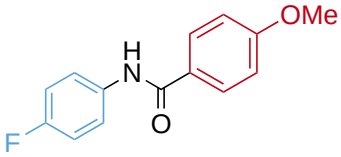 3s | 83 |
| 20 | 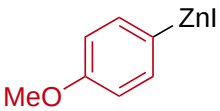 1b | 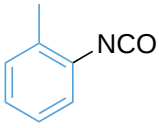 2g | 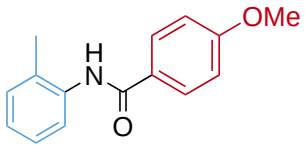 3t | 76 |
| 21 | 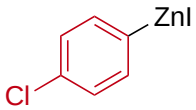 1c | 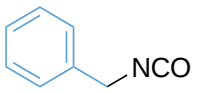 2j | 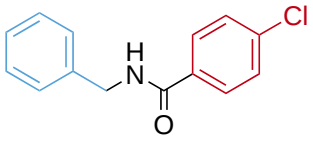 3u | 32 |
| 22 | 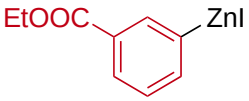 1f | 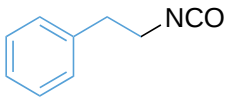 2k | 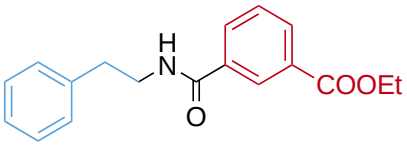 3v | Trace |
| 23 | 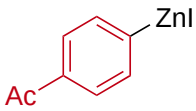 1d | 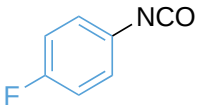 2c | 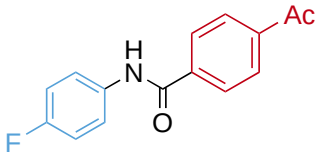 3w | Trace |
| 24 | 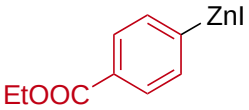 1g | 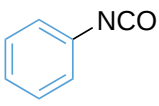 2a | 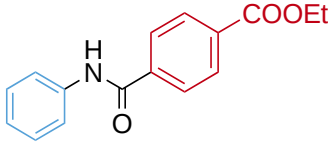 3x | Trace |
| 25 | 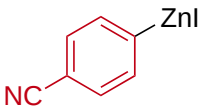 1h | 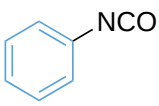 2a | 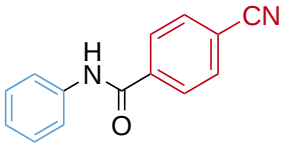 3y | 0 |
| 26 |  1i | 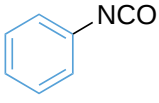 2a | 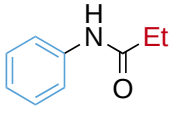 4a | 64 |

| Entry | Organozinc Reagent | Isocyanate | Amide Product | Yield [%] |
|---|---|---|---|---|
| 27 |  1i | 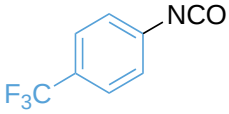 2b | 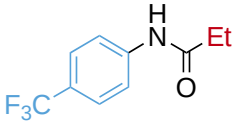 4b | 60 |
| 28 |  1i | 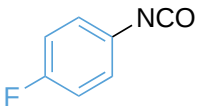 2c | 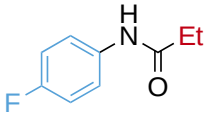 4c | 41 |
| 29 |  1i |  2d | 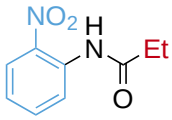 4d | 59 |
| 30 |  1i | 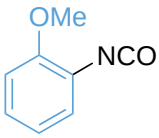 2e | 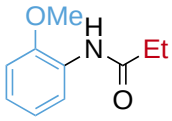 4e | 10 |
| 31 |  1i | 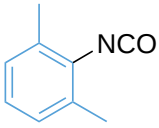 2f | 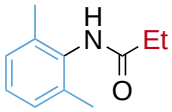 4f | 13 |
| 32 |  1i | 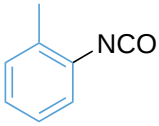 2g | 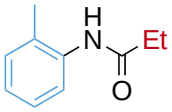 4g | 32 |
| 33 |  1i | 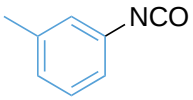 2h | 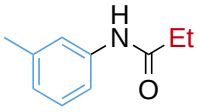 4h | 31 |
| 34 |  1i | 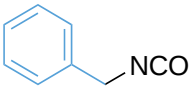 2j | 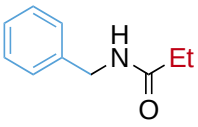 4i | Trace |
| 35 |  1i | 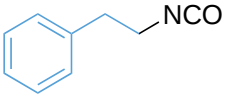 2k | 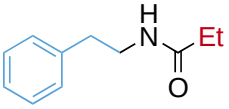 4j | 22 |
| 36 | 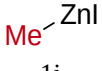 1j | 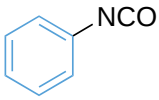 2a | 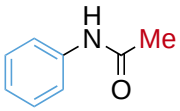 4k | 43 |

| Entry | Organozinc Reagent | Isocyanate | Amide Product | Yield [%] |
|---|---|---|---|---|
| 37 | 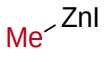 1j | 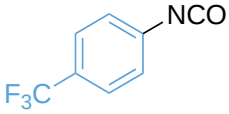 2b | 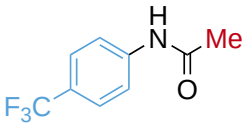 4l | 47 |
| 38 | 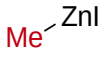 1j | 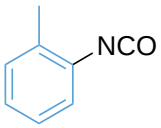 2g | 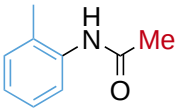 4m | 10 |
| 39 | 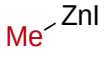 1j | 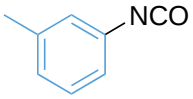 2h | 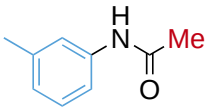 4n | 13 |
| 40 | 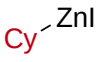 1k | 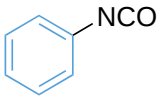 2a | 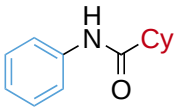 4o | Trace |
| 41 | 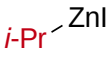 1l | 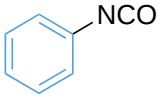 2a | 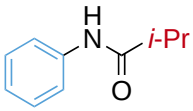 4p | 0 |
| 42 | 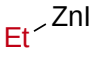 1i | 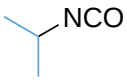 2i | 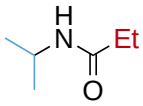 4q | 0 |
| 43 | 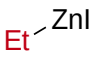 1i | 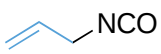 2l | 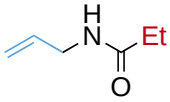 4r | 0 |
| 44 | 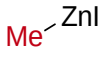 1j | 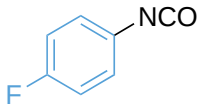 2c | 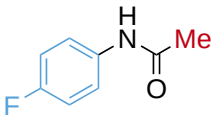 4s | 14 |
| 45 | 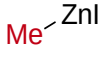 1j | 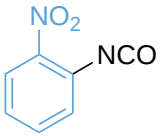 2d | 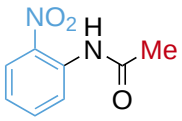 4t | Trace |

### 2.3.7. References

(1) Ikegami, R.; Koresawa, A.; Shibata, T.; Takagi, K. Functionalized Arylzinc Compounds in Ethereal Solvent: Direct Synthesis from Aryl Iodides and Zinc Powder and Application to Pd-Catalyzed Reaction with Allylic Halides. *The Journal of Organic Chemistry* **2003**, *68* (6), 2195–2199. https://doi.org/10.1021/jo026746s.

(2) Benischke, A. D.; Le Corre, G.; Knochel, P. Preparation of Polyfunctional Organozinc Halides by an InX3 - and LiCl-Catalyzed Zinc Insertion to Aryl and Heteroaryl Iodides and Bromides. *Chemistry - A European Journal* **2017**, *23* (4), 778–782. https://doi.org/10.1002/chem.201605139.

(3) Krasovskiy, A.; Malakhov, V.; Gavryushin, A.; Knochel, P. Efficient Synthesis of Functionalized Organozinc Compounds by the Direct Insertion of Zinc into Organic Iodides and Bromides. *Angewandte Chemie International Edition* **2006**, *45* (36), 6040–6044. https://doi.org/10.1002/anie.200601450.

(4) Wang, J.; Yin, X.; Wu, J.; Wu, D.; Pan, Y. Copper Catalyzed N-Arylation between Aryl Halides and Nitriles in Water: An Efficient Tandem Synthesis of Benzanilides. *TETRAHEDRON -LONDON-* **2013**, *69* (48), 10463–10469.

(5) Deshidi, R.; Rizvi, M. A.; Shah, B. A. Highly Efficient Dehydrogenative Cross-Coupling of Aldehydes with Amines and Alcohols. *RSC Adv.* **2015**, *5* (110), 90521–90524. https://doi.org/10.1039/C5RA17425B.

(6) Sheng, W.-J.; Ye, Q.; Yu, W.-B.; Liu, R.-R.; Xu, M.; Gao, J.-R.; Jia, Y.-X. CuSO4-Mediated Decarboxylative C–N Cross-Coupling of Aromatic Carboxylic Acids with Amides and Anilines. *Tetrahedron Letters* **2015**, *56* (4), 599–601. https://doi.org/10.1016/j.tetlet.2014.12.085.

(7) Bollenbach, M.; Aquino, P. G. V.; de Araújo-Júnior, J. X.; Bourguignon, J.-J.; Bihel, F.; Salomé, C.; Wagner, P.; Schmitt, M. Efficient and Mild Ullmann-Type N-Arylation of Amides, Carbamates, and Azoles in Water. *Chemistry* **2017**, *23* (55), 13676–13683. https://doi.org/10.1002/chem.201700832.

(8) Meng, G.; Lei, P.; Szostak, M. A General Method for Two-Step Transamidation of Secondary Amides Using Commercially Available, Air- and Moisture-Stable Palladium/NHC (N-Heterocyclic Carbene) Complexes. *Org. Lett.* **2017**, *19* (8), 2158–2161. https://doi.org/10.1021/acs.orglett.7b00796.

(9) Wu, W.; Zhang, Z.; Liebeskind, L. S. In Situ Carboxyl Activation Using a Silatropic Switch: A New Approach to Amide and Peptide Constructions. *J. Am. Chem. Soc.* **2011**, *133* (36), 14256–14259. https://doi.org/10.1021/ja2065158.

(10) Liu, Y.; Shi, S.; Achtenhagen, M.; Liu, R.; Szostak, M. Metal-Free Transamidation of Secondary Amides via Selective N–C Cleavage under Mild Conditions. *Org. Lett.* **2017**, *19* (7), 1614–1617. https://doi.org/10.1021/acs.orglett.7b00429.

(11) Xu, X.; Feng, H.; Huang, L.; Liu, X. Direct Amidation of Carboxylic Acids through an Active α-Acyl Enol Ester Intermediate. *J. Org. Chem.* **2018**, *83* (15), 7962–7969. https://doi.org/10.1021/acs.joc.8b00819.

(12) Wang, S.-M.; Zhao, C.; Zhang, X.; Qin, H.-L. Clickable Coupling of Carboxylic Acids and Amines at Room Temperature Mediated by SO2F2: A Significant Breakthrough for the Construction of Amides and Peptide Linkages. *Org. Biomol. Chem.* **2019**, *17* (16), 4087–4101. https://doi.org/10.1039/C9OB00699K.

(13) Qureshi, Z. S.; Revankar, S. A.; Khedkar, M. V.; Bhanage, B. M. Aminocarbonylation of Aryl Iodides with Primary and Secondary Amines in Aqueous Medium Using Polymer Supported Palladium-N-Heterocyclic Carbene Complex as an Efficient and Heterogeneous Recyclable Catalyst. *Catalysis Today* **2012**, *198* (1), 148–153. https://doi.org/10.1016/j.cattod.2012.03.039.

(14) Fang, W.; Deng, Q.; Xu, M.; Tu, T. Highly Efficient Aminocarbonylation of Iodoarenes at Atmospheric Pressure Catalyzed by a Robust Acenaphthoimidazolyidene Allylic Palladium Complex. *Org. Lett.* **2013**, *15* (14), 3678–3681. https://doi.org/10.1021/ol401550h.

(15) Feng, H.; Leng, L.; Liu, J.; Tang, Y.; Tang, P.; Zhang, C.; Tang, X.; Jiao, S. Optimization and Antifungal Activity of Amide Analogues. *Asian Journal of Chemistry* **2013**, *25*, 4029–4031.

(16) Xu, M.; Zhang, X.-H.; Shao, Y.-L.; Han, J.-S.; Zhong, P. The Synthesis of N-Arylated Amides via Copper(II) Triflate- Catalyzed Direct Oxygenation and N-Arylation of Benzylamines with Aryl Iodides. *Advanced Synthesis & Catalysis* **2012**, *354* (14–15), 2665–2670. https://doi.org/10.1002/adsc.201200424.

(17) Ma, Y.; Song, C.; Chai, Q.; Ma, C.; Andrus, M. B. Palladium-Imidazolium N-Heterocyclic Carbene-Catalyzed Carbonylative Amidation With Boronic Acids, Aryl Diazonium Ions, and Ammonia. *Synthesis* **2003**, *2003* (18), 2886–2889. https://doi.org/10.1055/s-2003-42478.

(18) Sawant, D. N.; Bagal, D. B.; Ogawa, S.; Selvam, K.; Saito, S. Diboron-Catalyzed Dehydrative Amidation of Aromatic Carboxylic Acids with Amines. *Org. Lett.* **2018**, *20* (15), 4397–4400. https://doi.org/10.1021/acs.orglett.8b01480.

(19) Luo, Q.-L.; Lv, L.; Li, Y.; Tan, J.-P.; Nan, W.; Hui, Q. An Efficient Protocol for the Amidation of Carboxylic Acids Promoted by Trimethyl Phosphite and Iodine. *European Journal of Organic Chemistry* **2011**, *2011* (34), 6916–6922. https://doi.org/10.1002/ejoc.201101030.

(20) Darvesh, S.; McDonald, R. S.; Darvesh, K. V.; Mataija, D.; Mothana, S.; Cook, H.; Carneiro, K. M.; Richard, N.; Walsh, R.; Martin, E. On the Active Site for Hydrolysis of Aryl Amides and Choline Esters by Human Cholinesterases. *Bioorg Med Chem* **2006**, *14* (13), 4586–4599. https://doi.org/10.1016/j.bmc.2006.02.021.

(21) Gowda, B. T.; Usha, K. M.; Jyothi, K. Infrared, 1H and 13C NMR Spectral Studies on Di- and Tri-Substituted N-Aryl Amides, 2,6-X2C6H3NHCOCH3 – IXi and 2,4,6-X3C6H2NHCOCH3 – IXi (X = Cl or CH3 and I = 0, 1, 2 or 3). *Zeitschrift für Naturforschung A* **2014**, *59* (1–2), 69–76. https://doi.org/10.1515/zna-2004-1-210.

(22) Guo, R.; Zhu, C.; Sheng, Z.; Li, Y.; Yin, W.; Chu, C. Silica Sulfuric Acid Mediated Acylation of Amines with 1,3-Diketones via CC Bond Cleavage under Solvent-Free Conditions. *Tetrahedron Letters* **2015**, *56* (45), 6223–6226. https://doi.org/10.1016/j.tetlet.2015.09.094.

(23) Kathiravan, S.; Nicholls, I. A. Monoprotected L-Amino Acid (l-MPAA), Accelerated Bromination, Chlorination, and Iodination of C(Sp2)−H Bonds by Iridium(III) Catalysis. *Chemistry – A European Journal* **2017**, *23* (29), 7031–7036. https://doi.org/10.1002/chem.201700280.

(24) Amić, A.; Molnar, M. An Improved and Efficient N-Acetylation of Amines Using Choline Chloride Based Deep Eutectic Solvents. *Organic Preparations and Procedures International* **2017**, *49* (3), 249–257. https://doi.org/10.1080/00304948.2017.1320914.

(25) Mo, X.; Morgan, T. D. R.; Ang, H. T.; Hall, D. G. Scope and Mechanism of a True Organocatalytic Beckmann Rearrangement with a Boronic Acid/Perfluoropinacol System under Ambient Conditions. *J Am Chem Soc* **2018**, *140* (15), 5264–5271. https://doi.org/10.1021/jacs.8b01618.

(26) Zand, Z.; Kazemi, F.; Partovi, A. Photocatalytic Synthesis of Anilides from Nitrobenzenes under Visible Light Irradiation: 2 in 1 Reaction. *J Photochem Photobiol B* **2015**, *152* (Pt A), 58–62. https://doi.org/10.1016/j.jphotobiol.2015.02.010.

## 2.3.8. Characterization

### 3a. *N*-phenyl benzamide (80 MHz, $CDCl_3$)

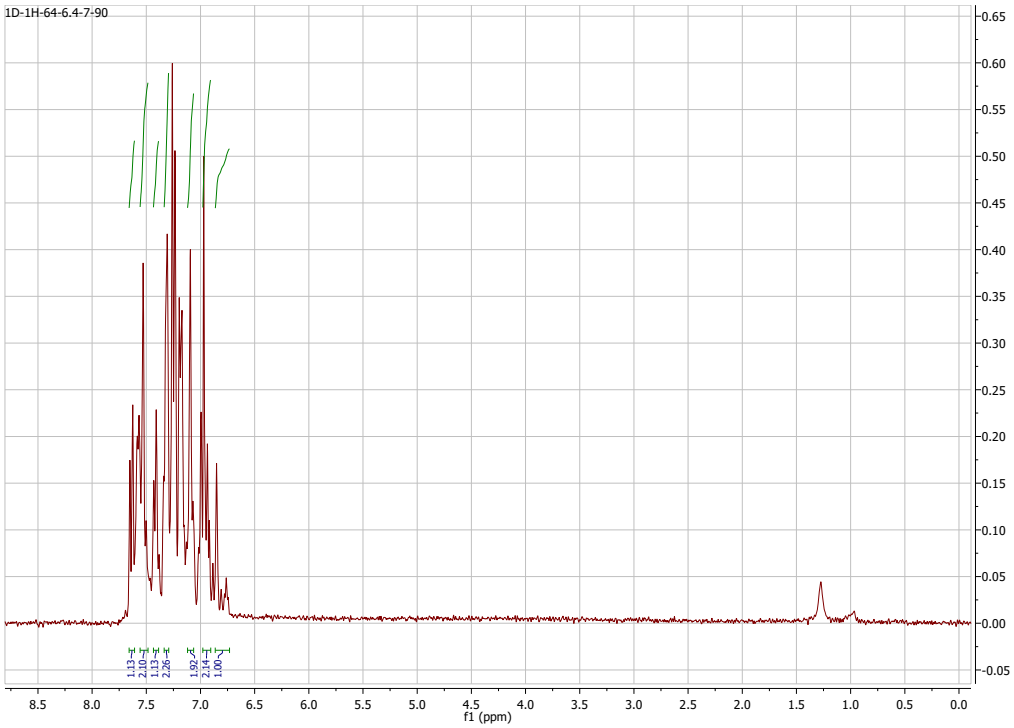


### 3b. *N*-4-trifluoromethylphenyl benzamide (80 MHz, $CDCl_3$)

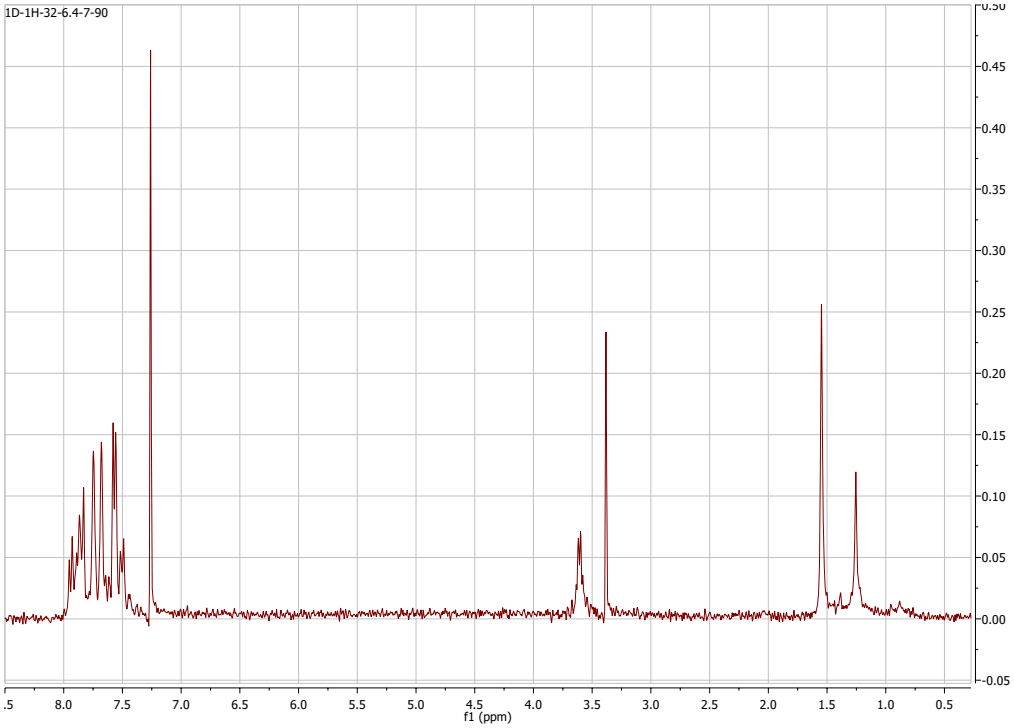

**3c. *N*-4-fluorophenyl benzamide** (80 MHz, $CDCl_3$)

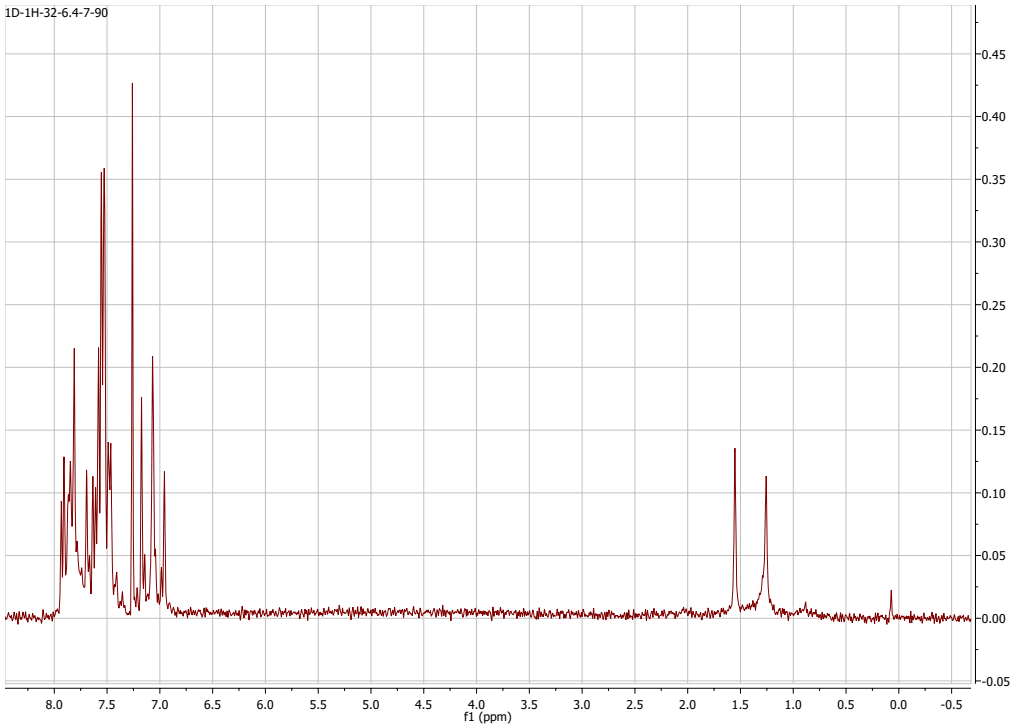


**3d. *N*-2-nitrophenyl benzamide** (80 MHz, $CDCl_3$)

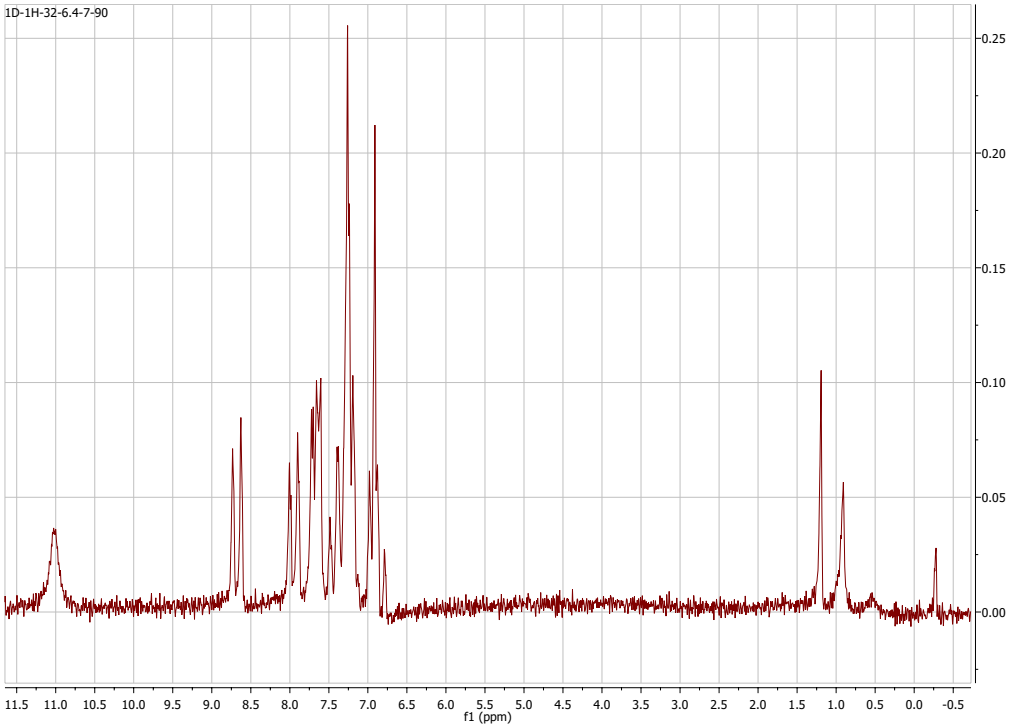

**3e. *N*-2-methoxyphenyl benzamide** (80 MHz, $CDCl_3$)

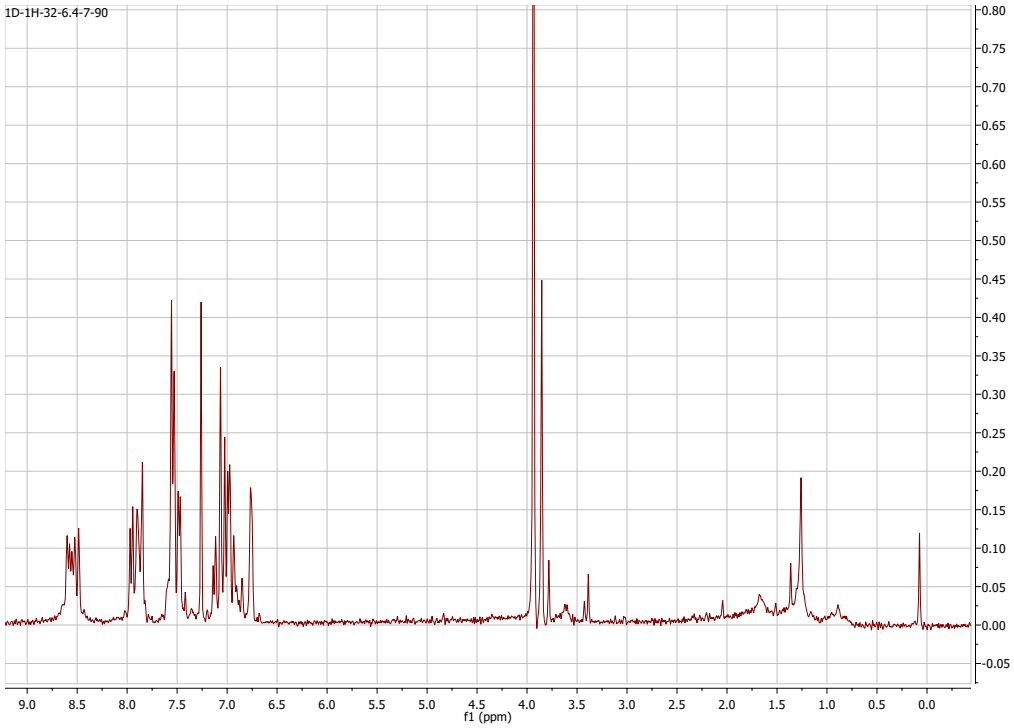


**3f. *N*-2,6-dimethylphenyl benzamide** (80 MHz, $CDCl_3$)

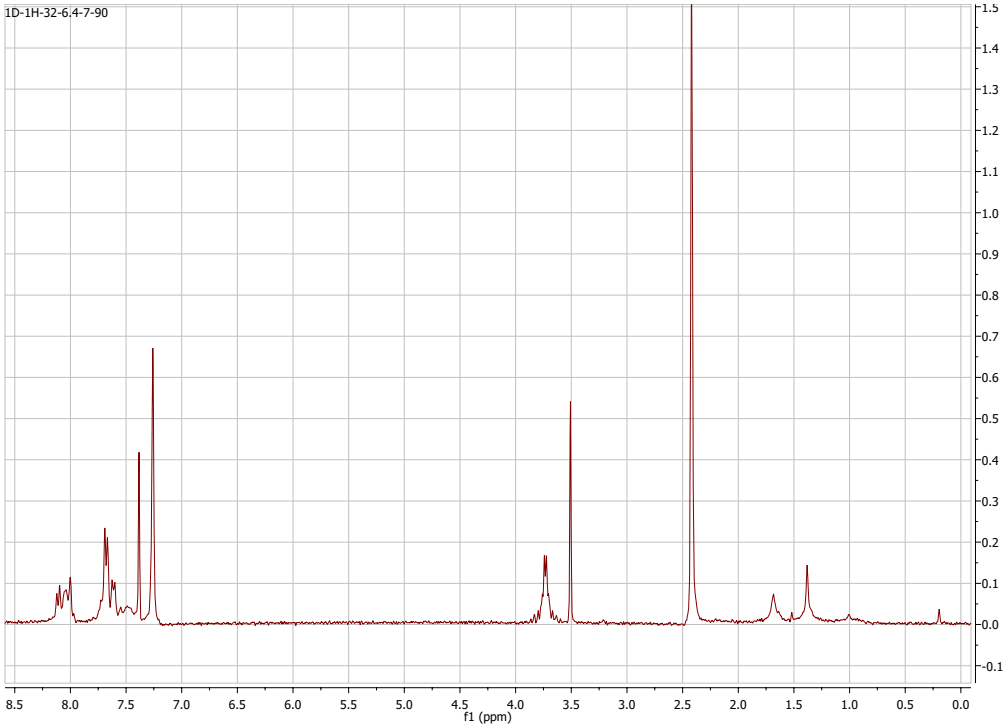

**3g. *N*-2-methylphenyl benzamide** (80 MHz, $CDCl_3$)

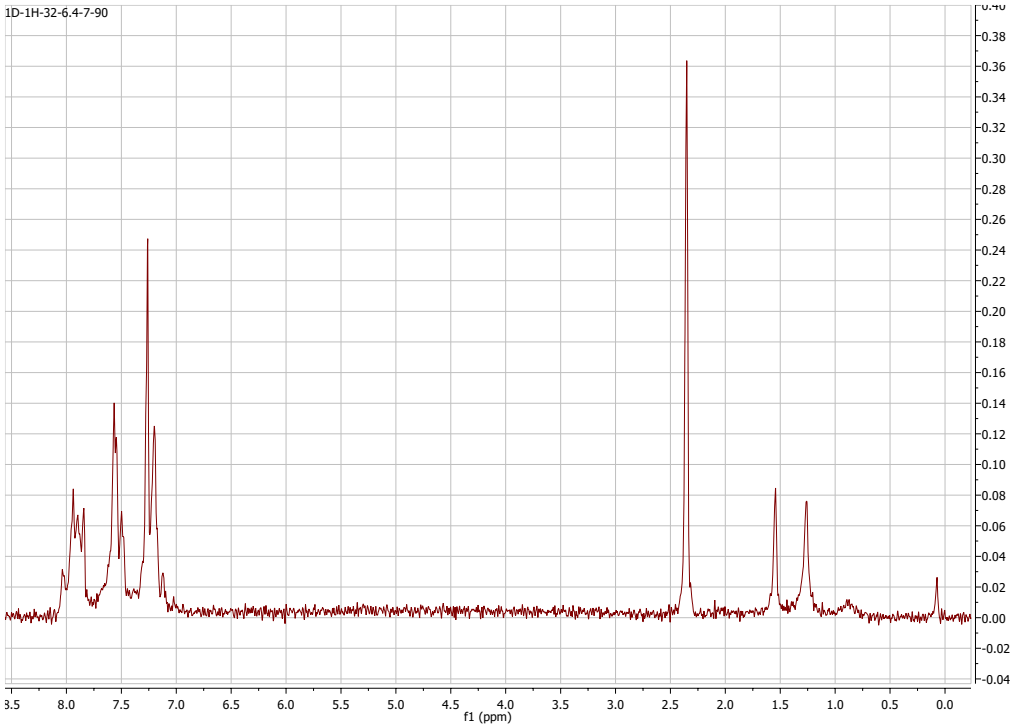


**3h. *N*-3-methylphenyl benzamide** (80 MHz, $CDCl_3$)

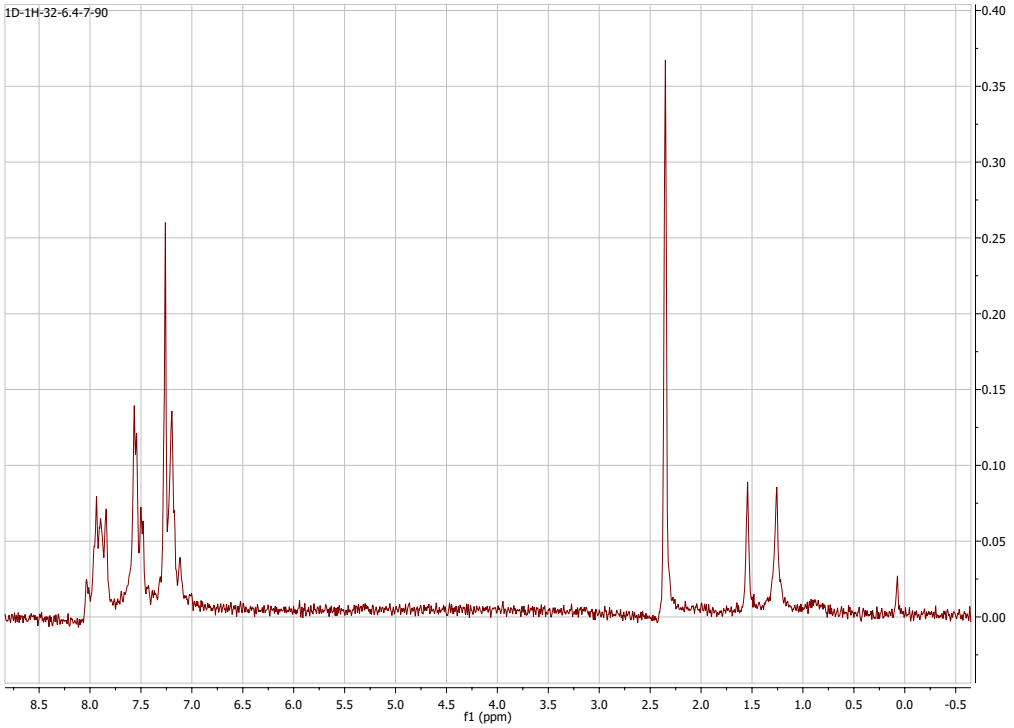

**3i. *N*-isopropyl benzamide** (80 MHz, $CDCl_3$)

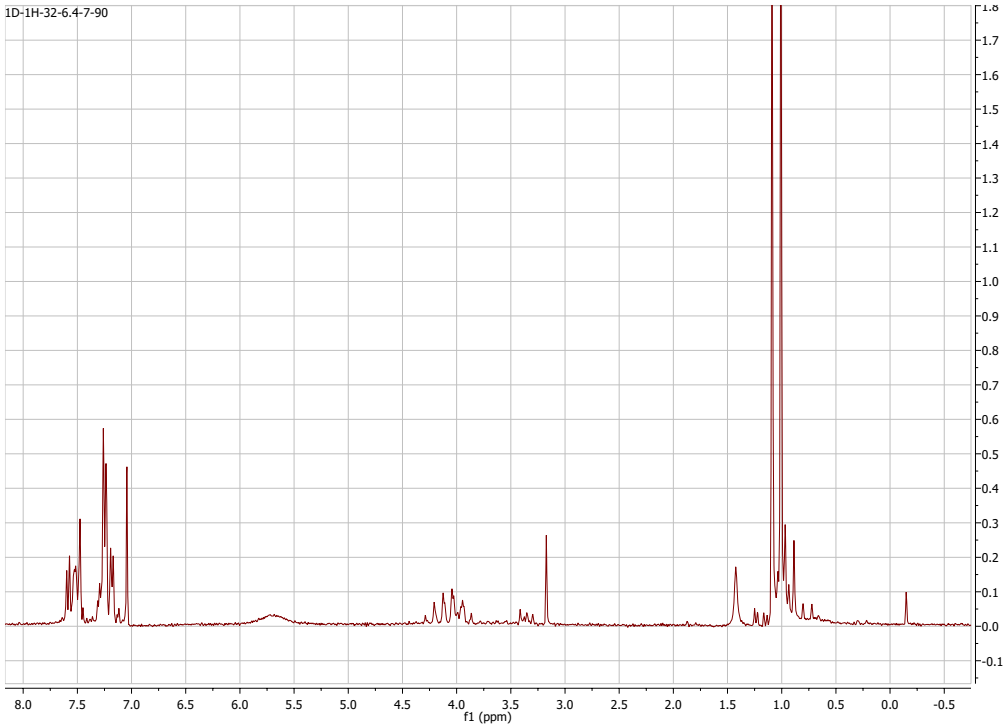


**3j. *N*-benzyl benzamide** (80 MHz, $CDCl_3$)

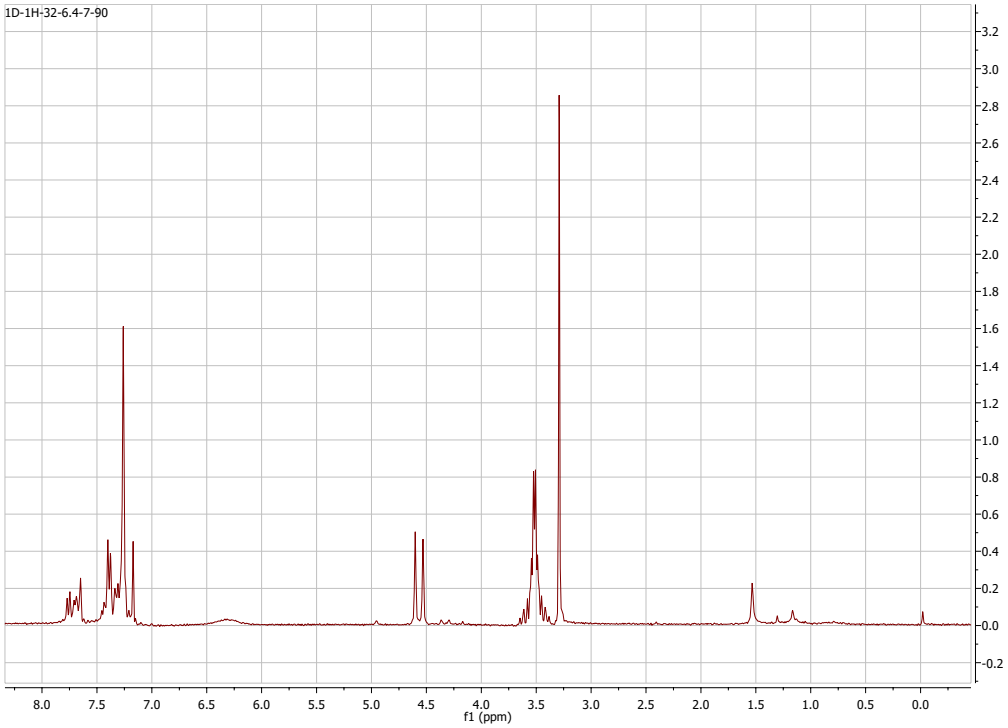

**3k. *N*-phenethyl benzamide** (80 MHz, $CDCl_3$)

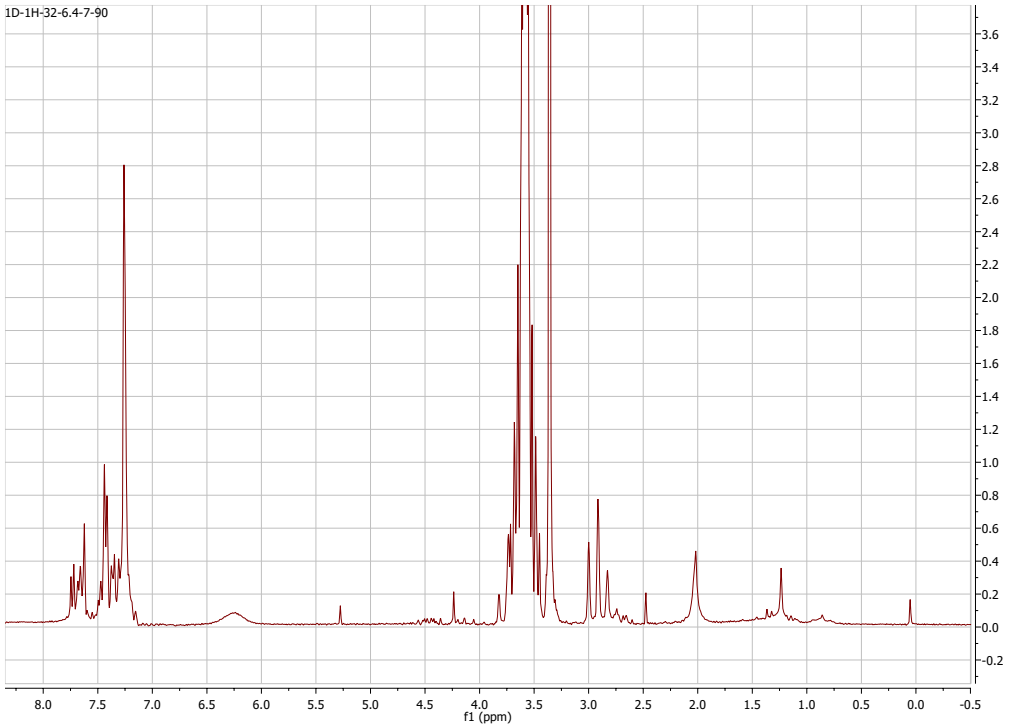


**3l. *N*-allyl benzamide** (80 MHz, $CDCl_3$)

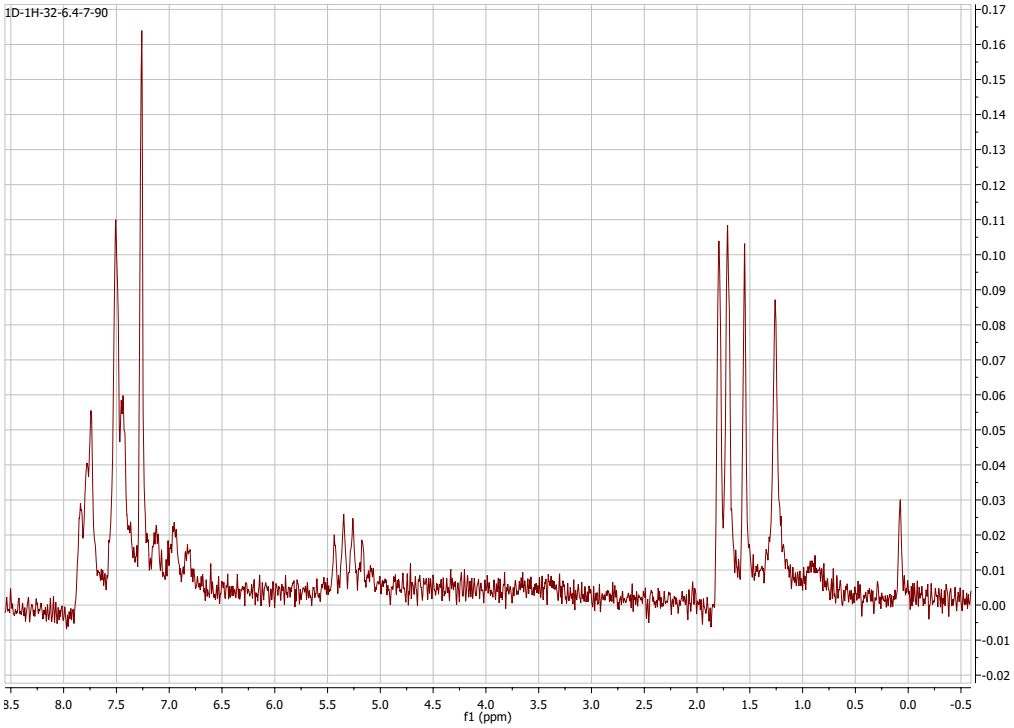

**3m. *N*-phenyl 4-methoxybenzamide** (80 MHz, $CDCl_3$)

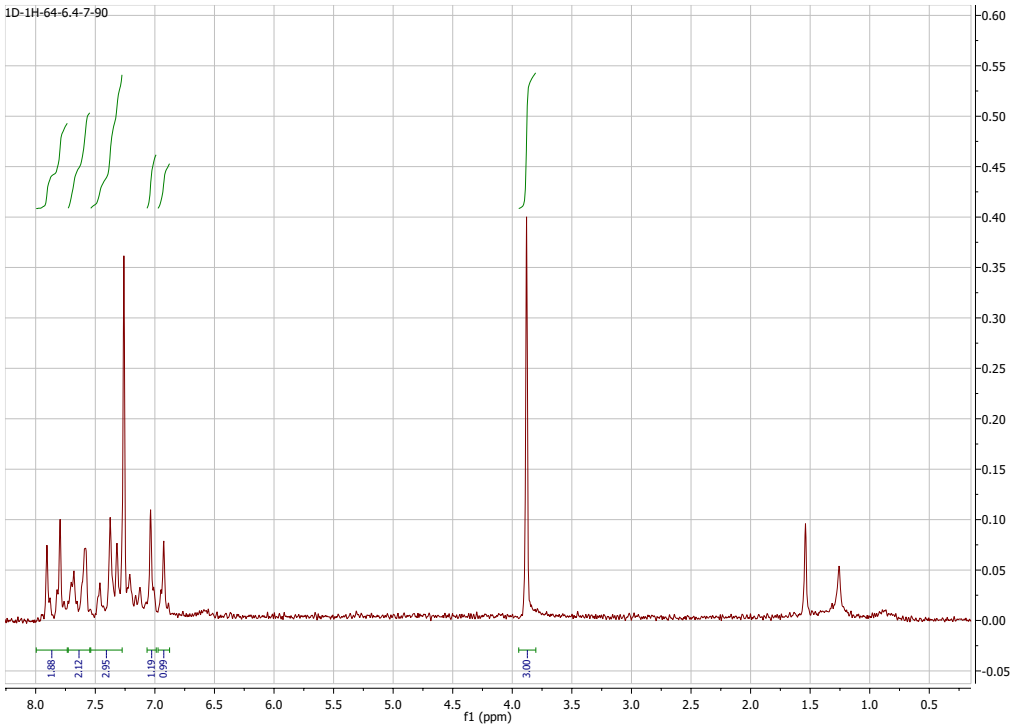


**3n. *N*-phenyl 4-chlorobenzamide** (80 MHz, $CDCl_3$)

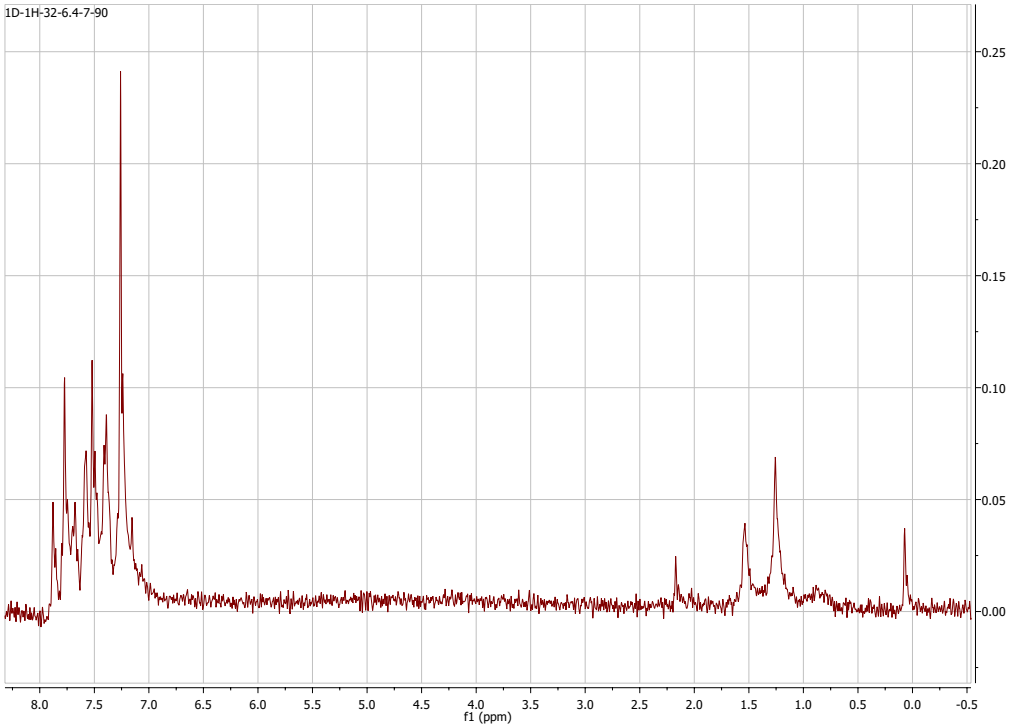

**3o. *N*-phenyl 4-acetylbenzamide** (80 MHz, $CDCl_3$)

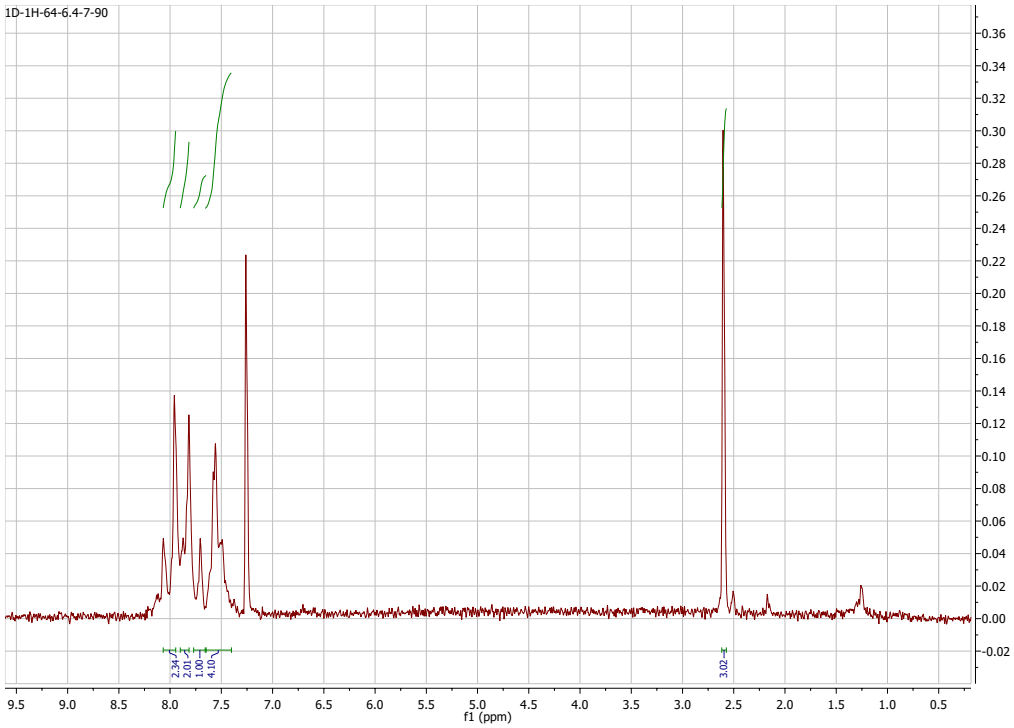


**3p. *N*-phenyl 2-methoxybenzamide** (80 MHz, $CDCl_3$)

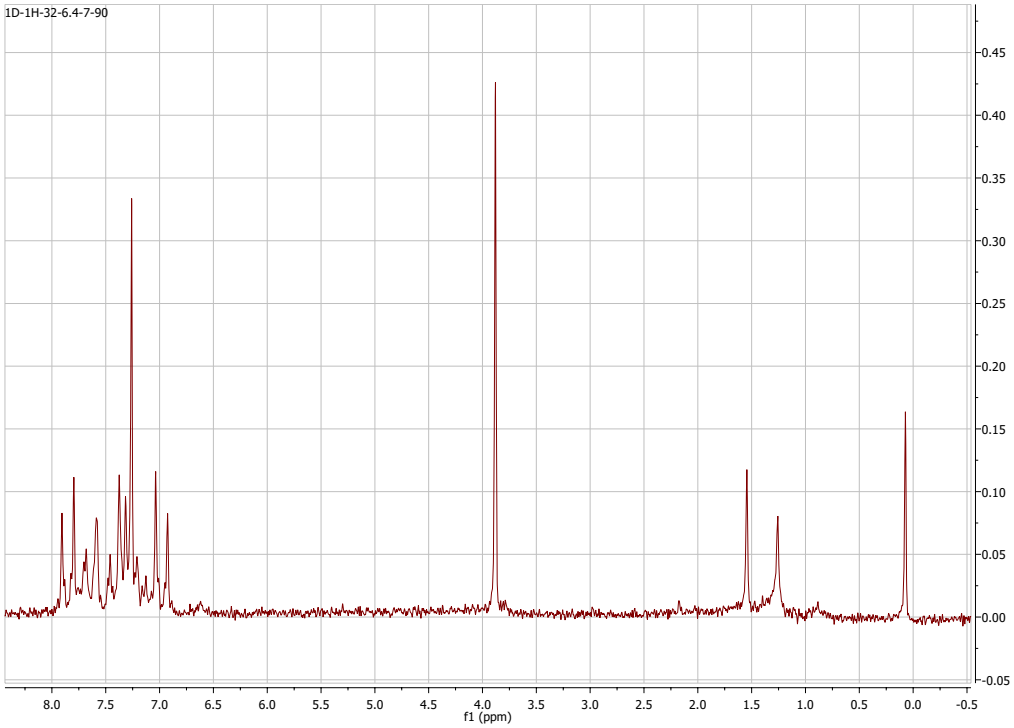

**3q. ethyl 3-(phenylcarbamoyl)benzoate** (80 MHz, $CDCl_3$)

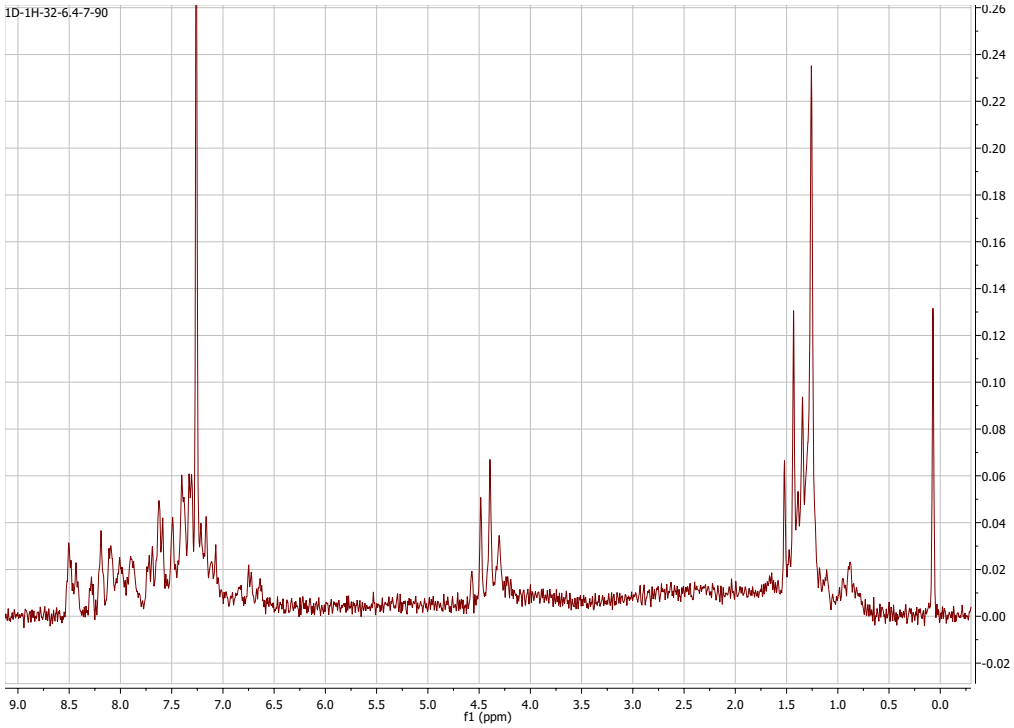


**3r. *N*-4-fluorophenyl 2-methoxybenzamide** (80 MHz, $CDCl_3$)

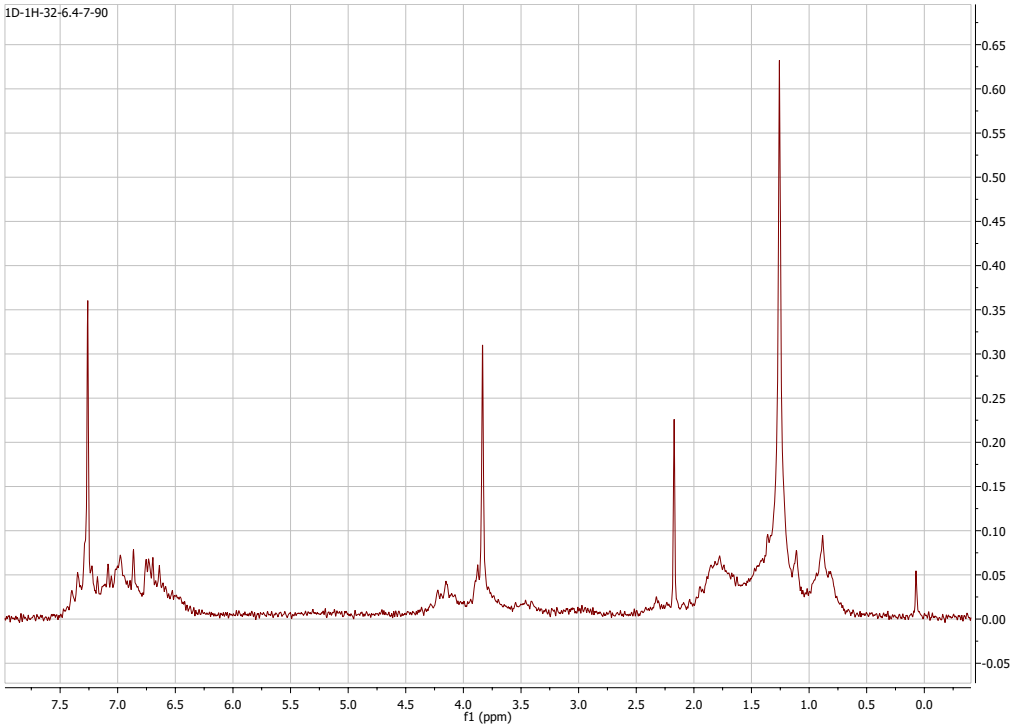

**3s. *N*-4-fluorophenyl 4-methoxybenzamide** (80 MHz, $CDCl_3$)

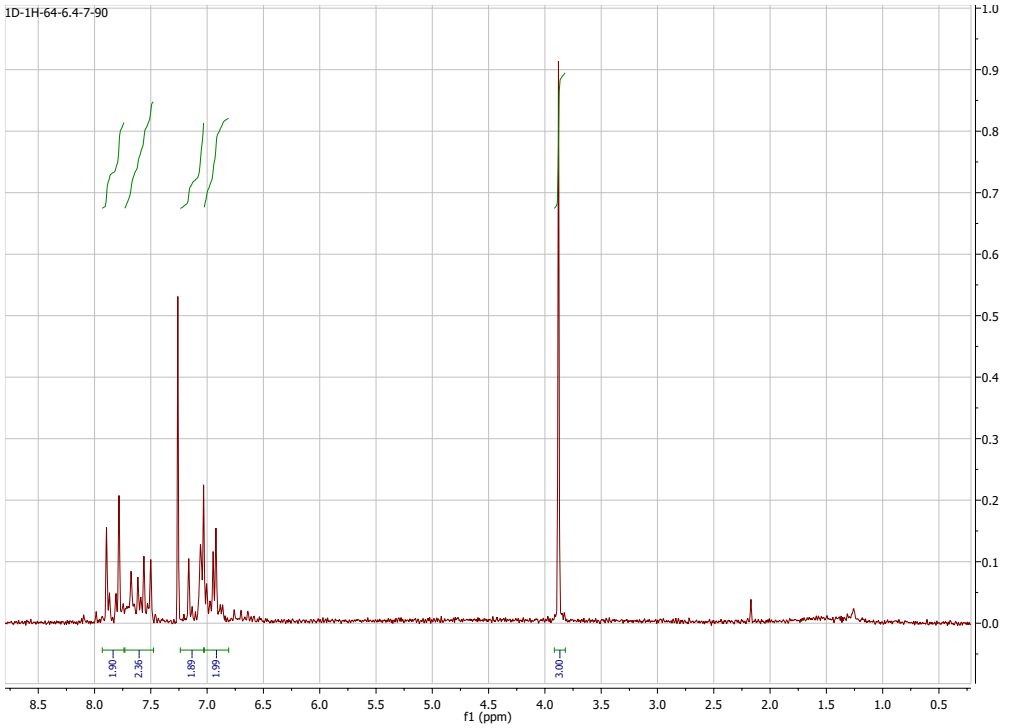


**3t. *N*-2-methylphenyl 4-methoxybenzamide** (80 MHz, $CDCl_3$)

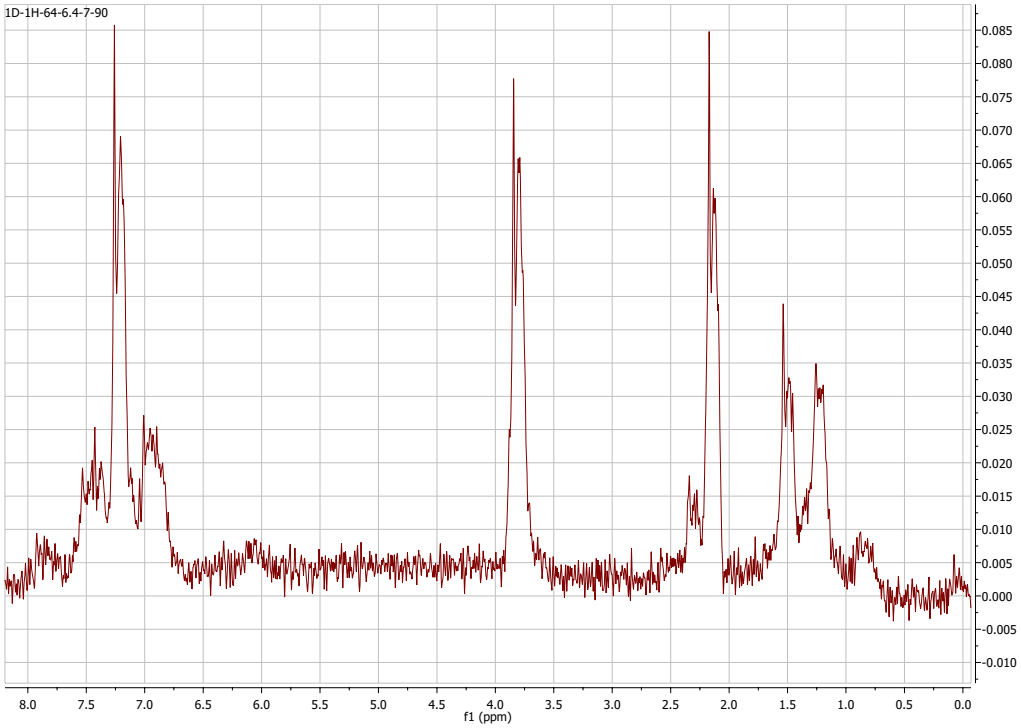

**3u. *N*-benzyl 4-chlorobenzamide** (80 MHz, $CDCl_3$)

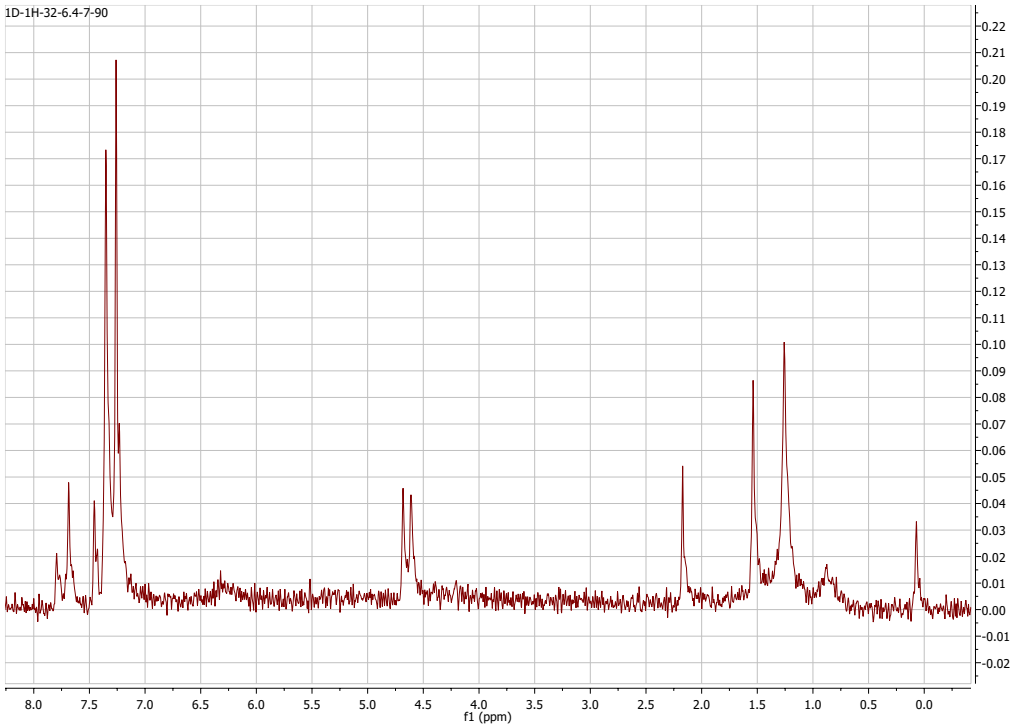


**4a. *N*-phenyl propanamide** (80 MHz, $CDCl_3$)

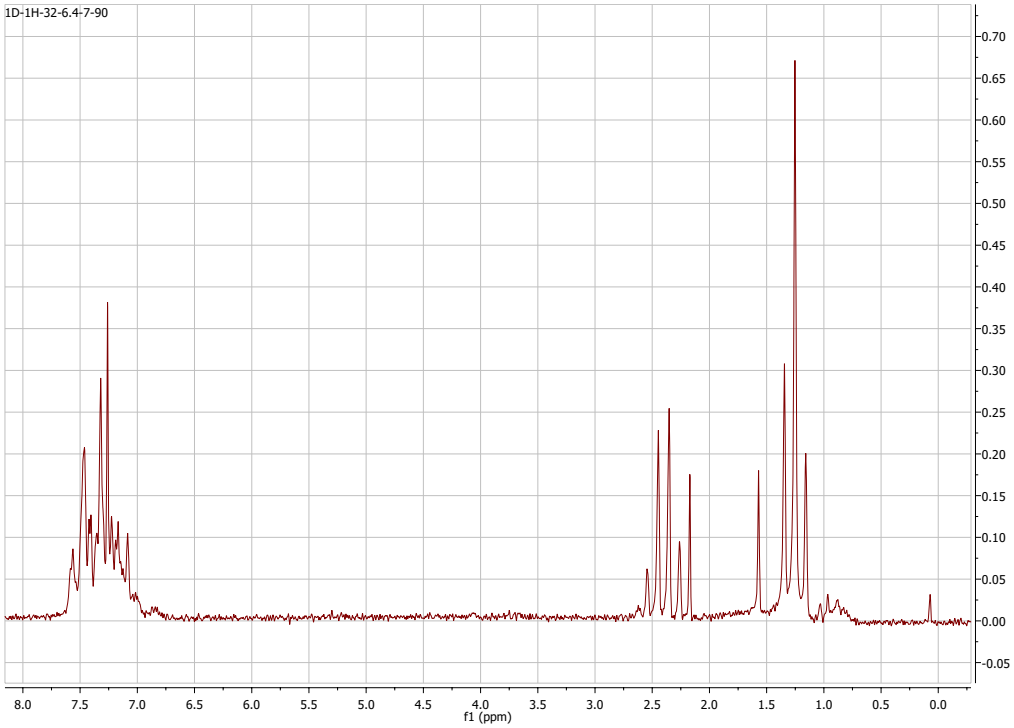

**4b. *N*-4-trifluoromethylphenyl propanamide**

$^{1}$H-NMR (300 MHz, $CDCl_3$): δ 7.59 (dd, 4H), 7.37 (bs, 1H), 2.41 (dd, 2H), 1.24 (t, 3H).

$^{13}$C-NMR (100 MHz, $CDCl_3$): 172.52, 141.12, 126.45, 124.24, 119.50, 118.82, 30.97, 9.66.

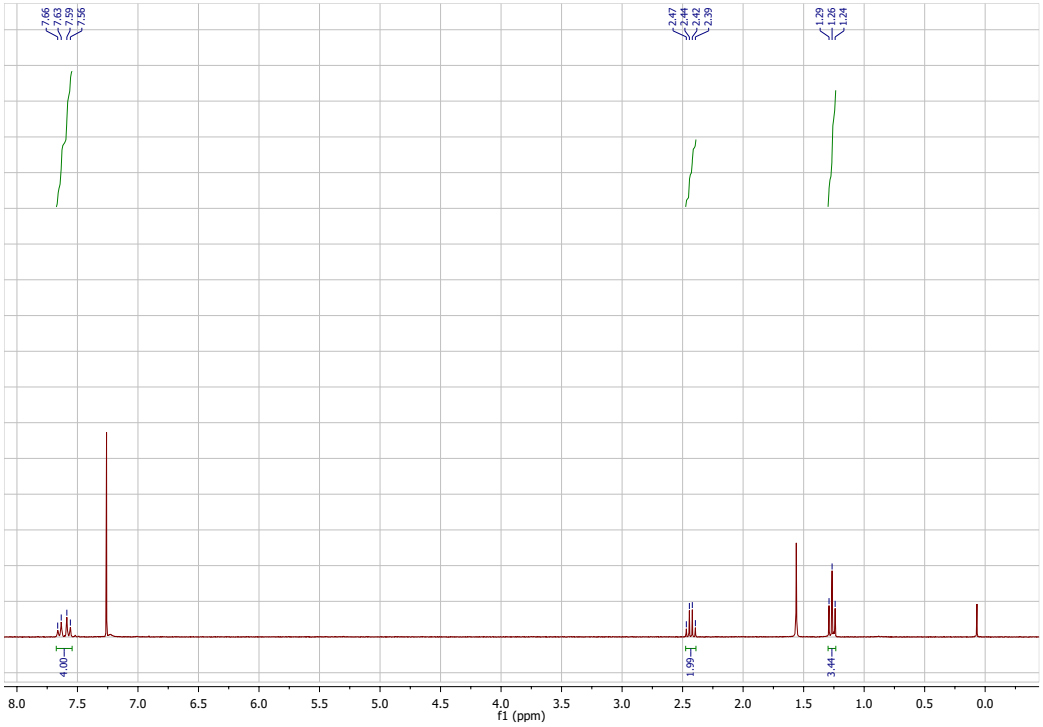


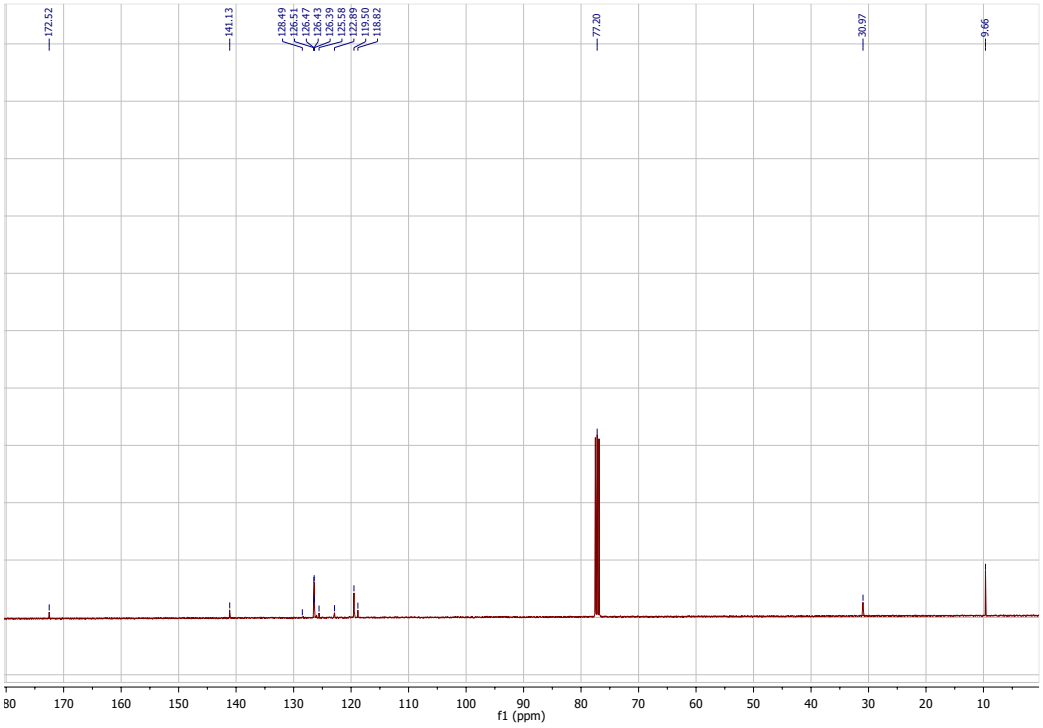

**4c. *N*-4-fluorophenyl propanamide** (80 MHz, $CDCl_3$)

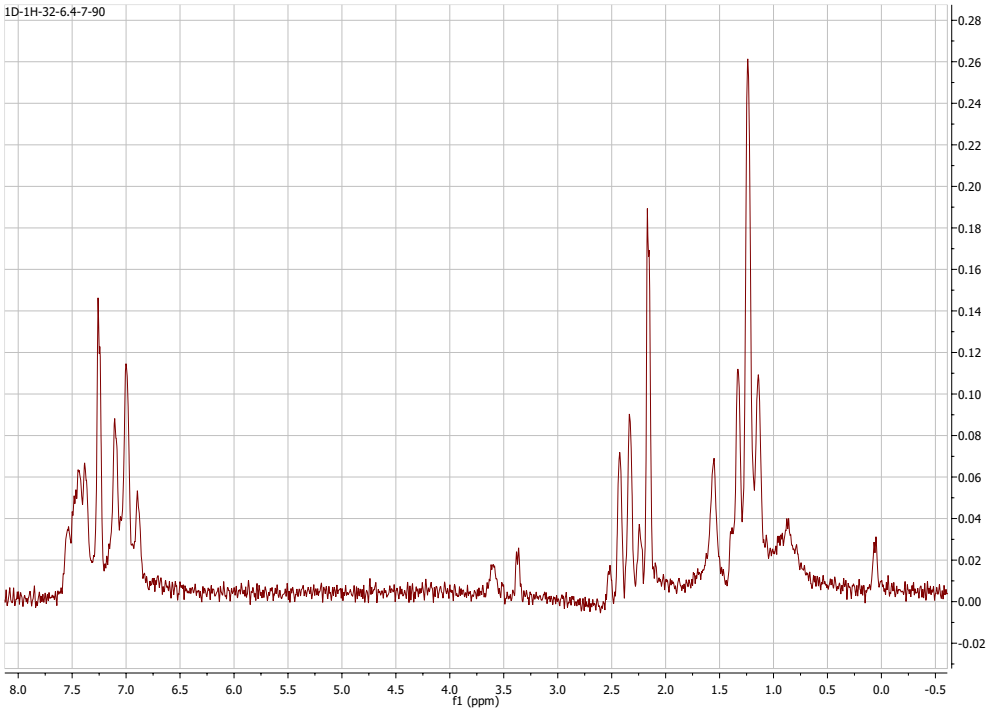


**4d. *N*-2-nitrophenyl propanamide** (80 MHz, $CDCl_3$)

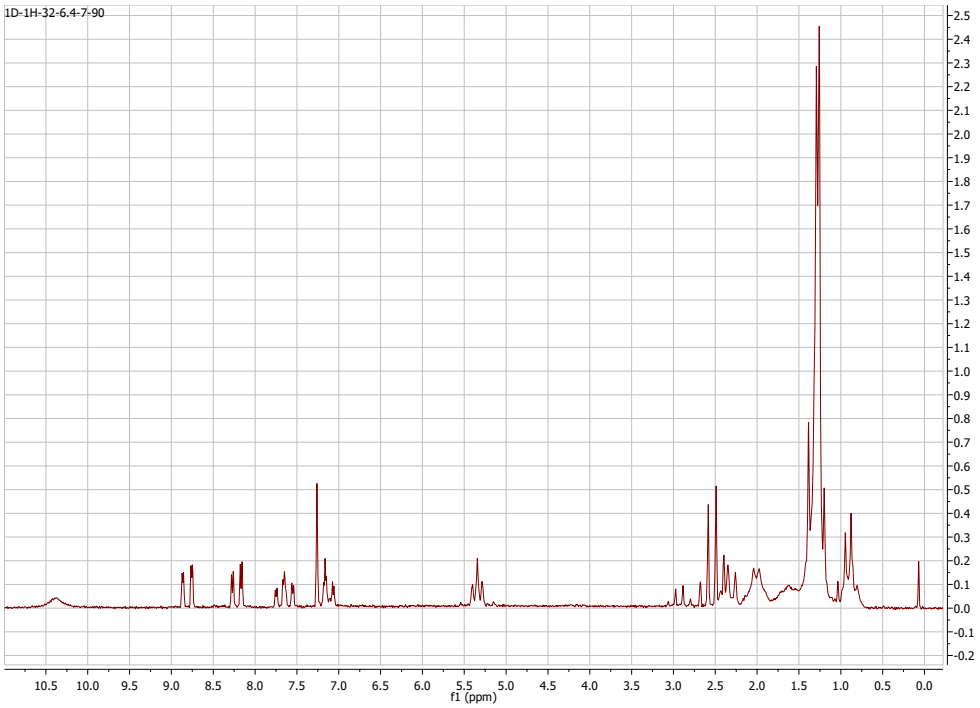

**4e. *N*-2-methoxyphenyl propanamide** (80 MHz, $CDCl_3$)

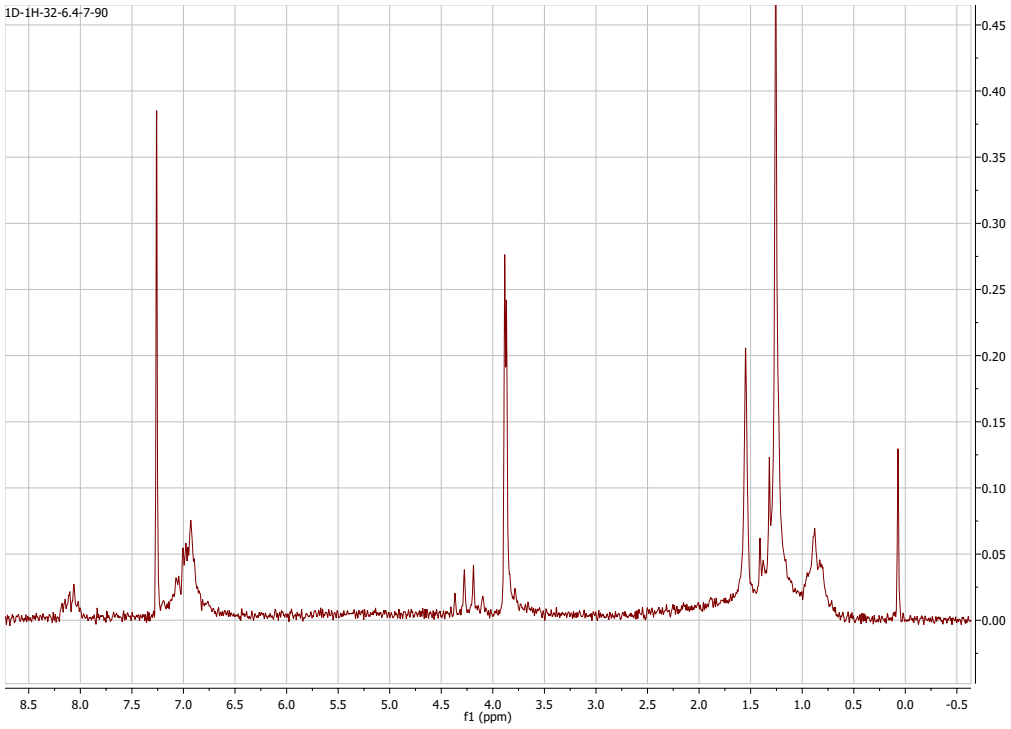


**4f. *N*-2,6-dimethylphenyl propanamide** (80 MHz, $CDCl_3$)

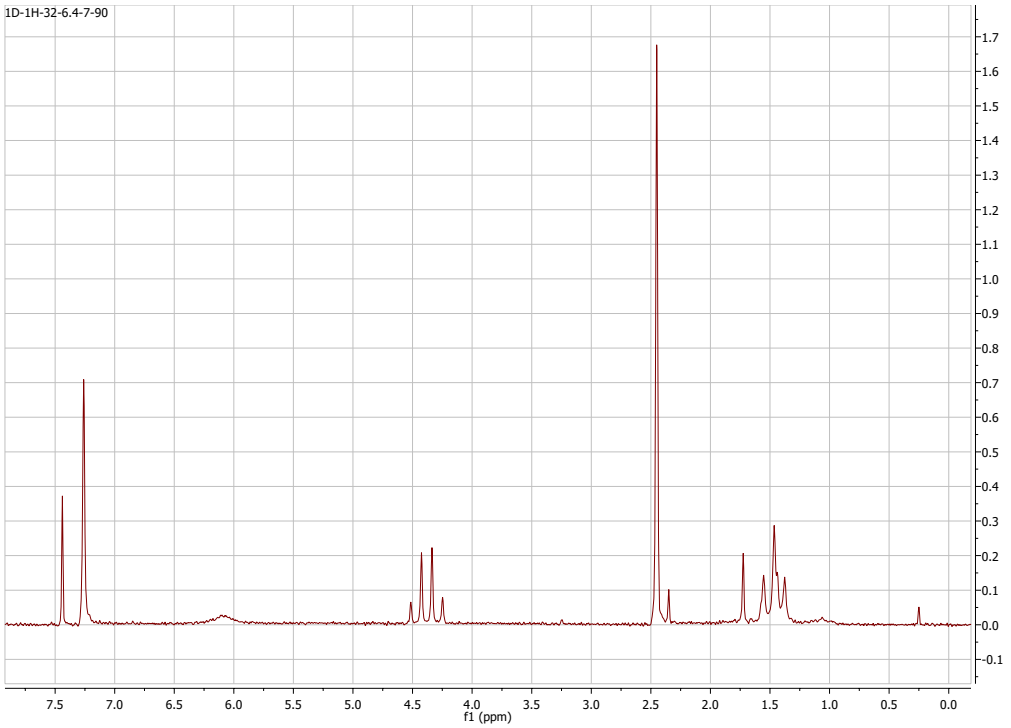

**4g. *N*-2-methylphenyl propanamide** (80 MHz, $CDCl_3$)

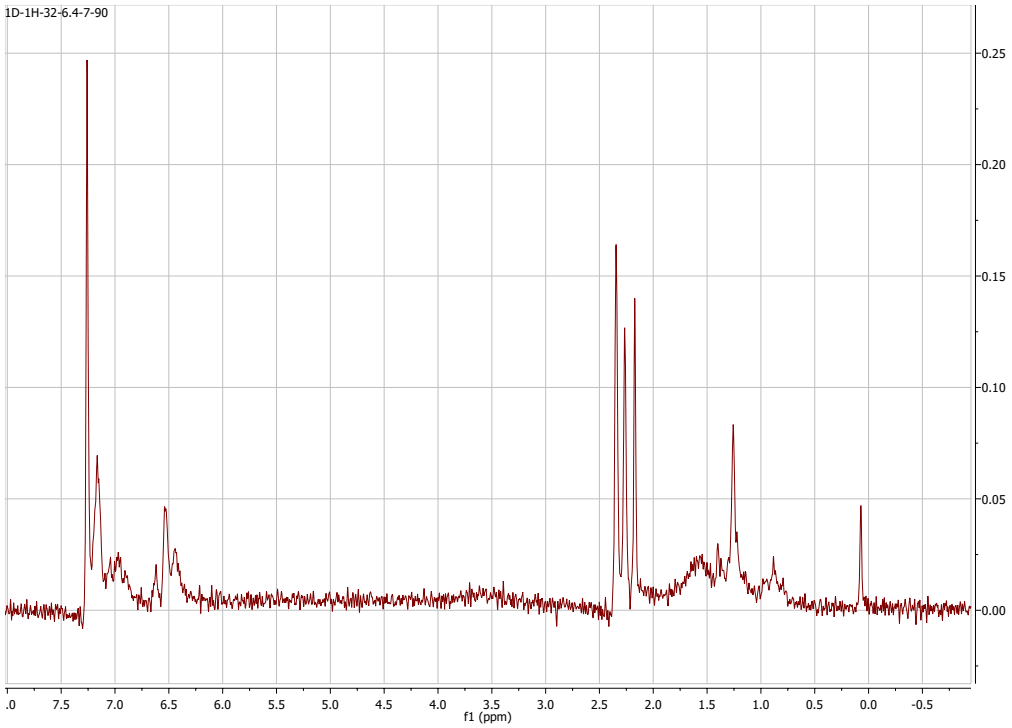


**4h. *N*-3-methylphenyl propanamide** (80 MHz, $CDCl_3$)

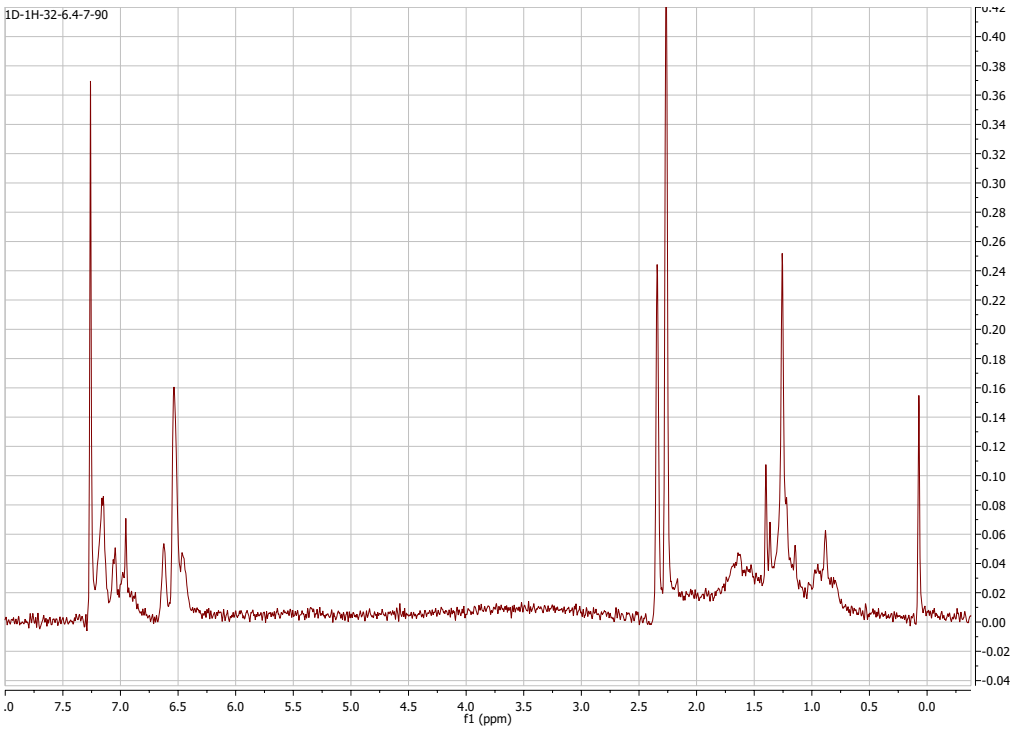

**4j. *N*-phenethyl propanamide** (UPLC trace)

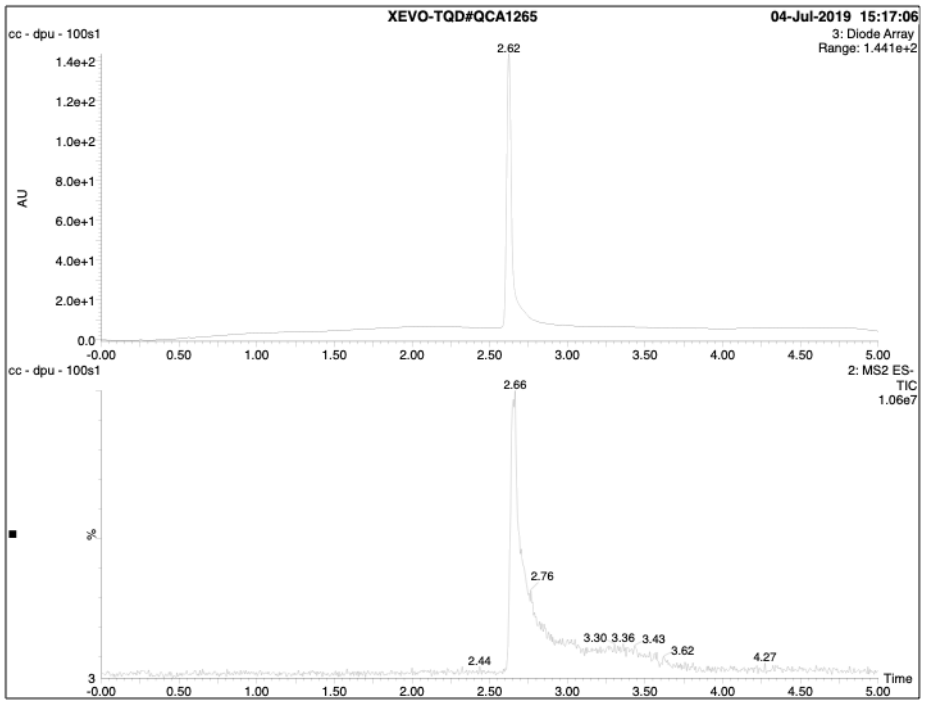


**4k. *N*-phenyl acetamide** (80 MHz, $CDCl_3$)

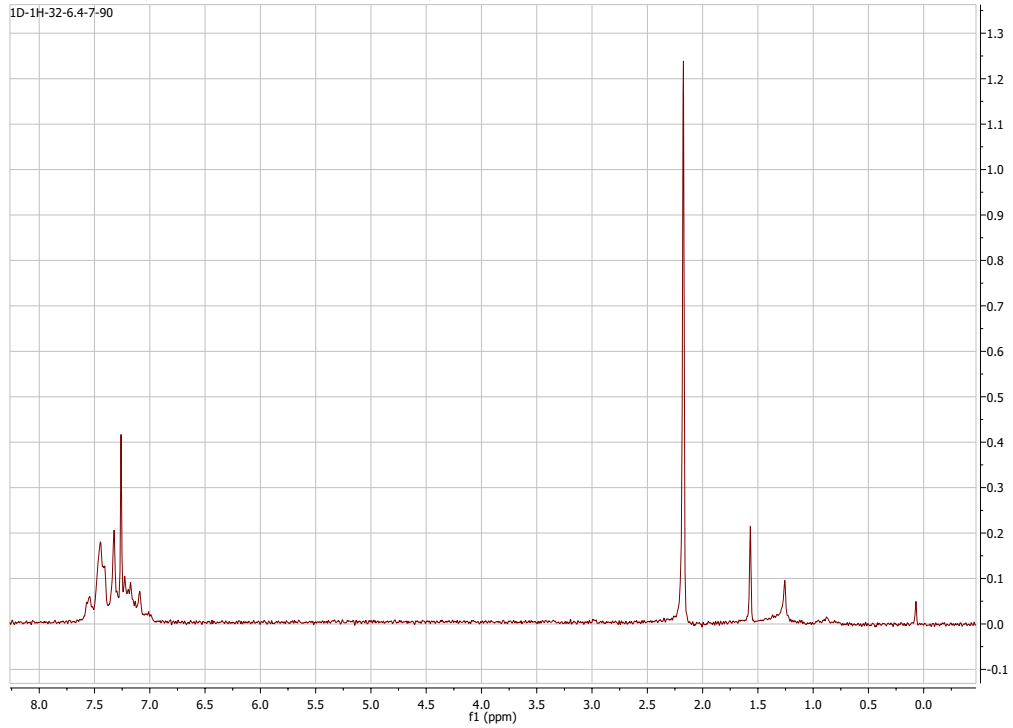

**4l. *N*-trifluoromethyl acetamide** (80 MHz, $CDCl_3$)

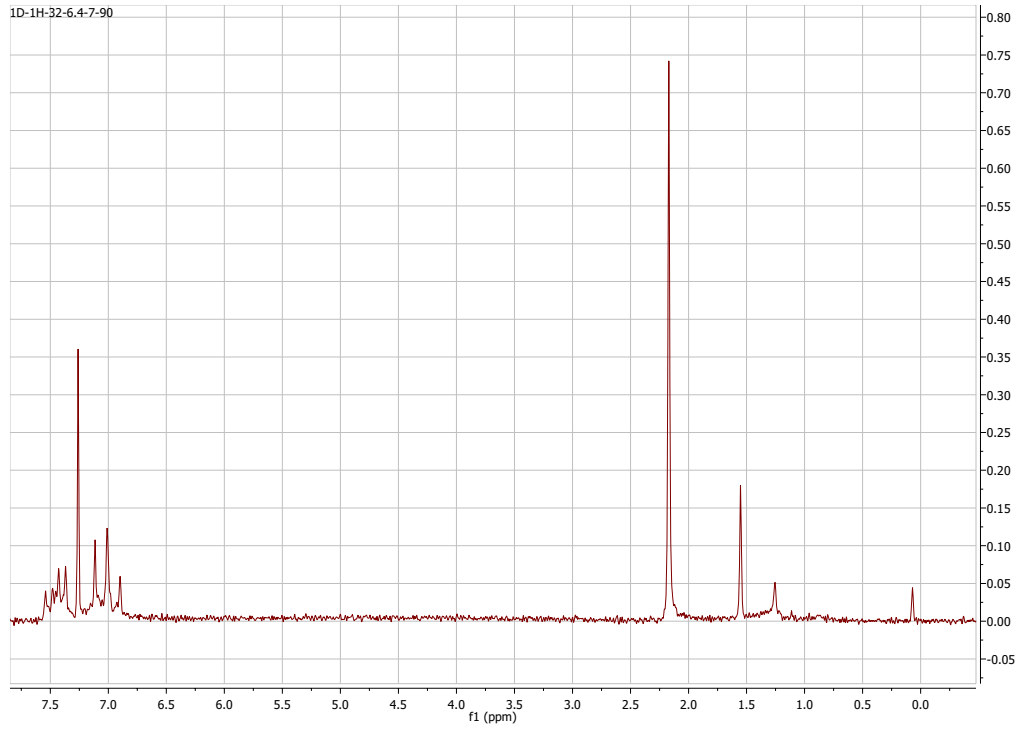


**4m. *N*-2-methylphenyl acetamide** (UPLC trace)

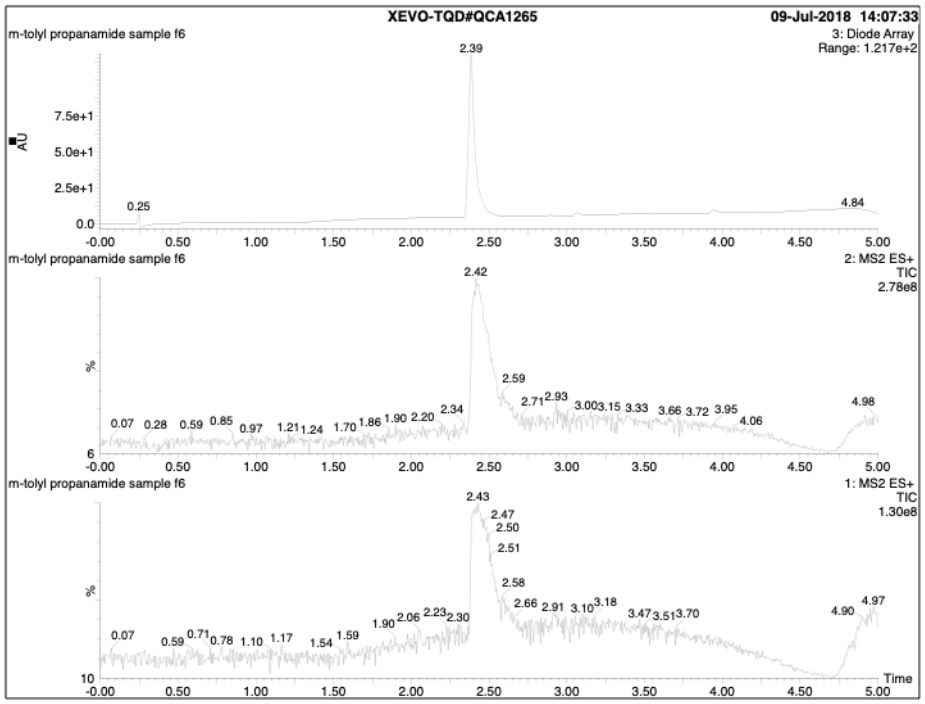

**4n. *N*-3-methylphenyl acetamide** (UPLC trace)

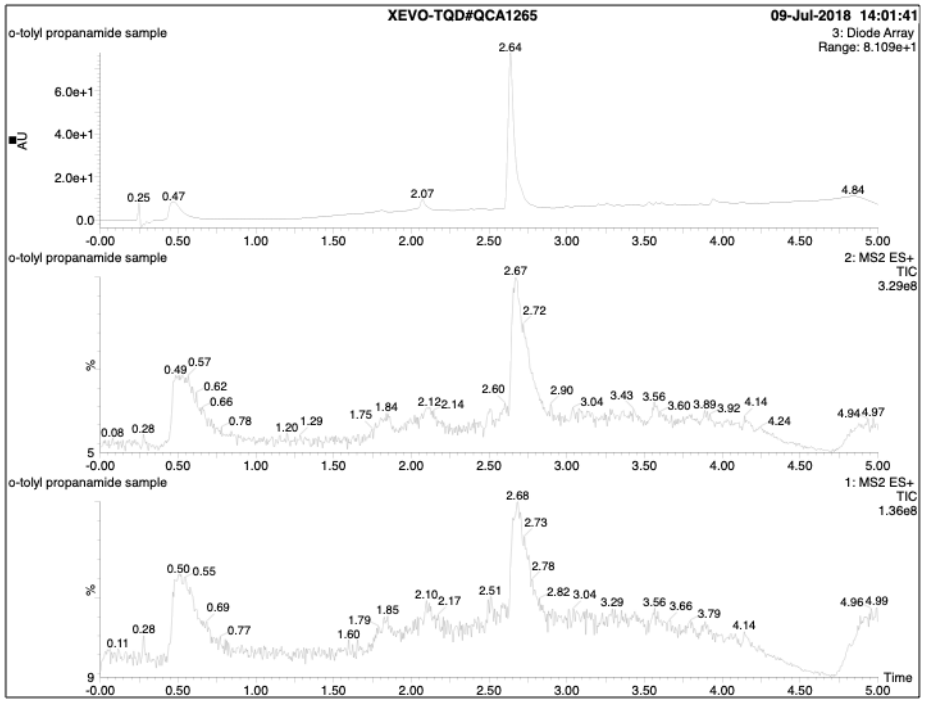

**6c. Ethyl 4-[(4-fluorophenyl)carbamoyl]benzoate**

$^{1}$H-NMR (300 MHz, $CDCl_3$): δ 8.13 (dd, 2H), 7.91 (dd, 2H), 7.61 (m, 2H), 7.07 (m, 2H), 4.41 (q, 2H), 1.42 (t, 3H)

$^{13}$C-NMR (75 MHz, $CDCl_3$): 165.7, 164.9, 159.7 (d, J = 243 Hz), 138.4, 133.6 (d, J = 3 Hz), 130.0, 127.0, 122.2 (d, J = 7.5 Hz), 115.8 (d, J = 22.5 Hz), 61.5, 14.3

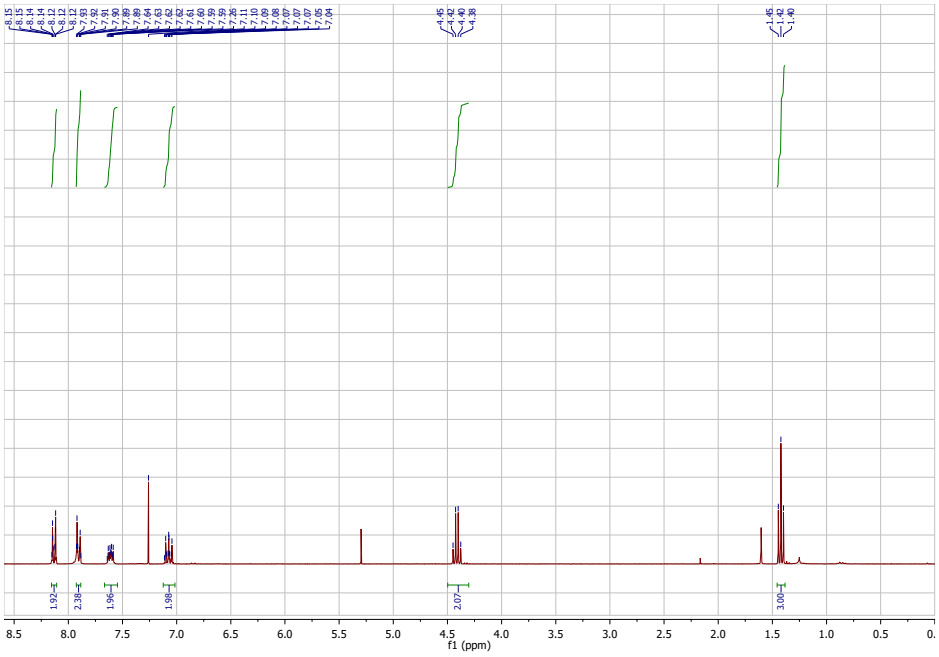

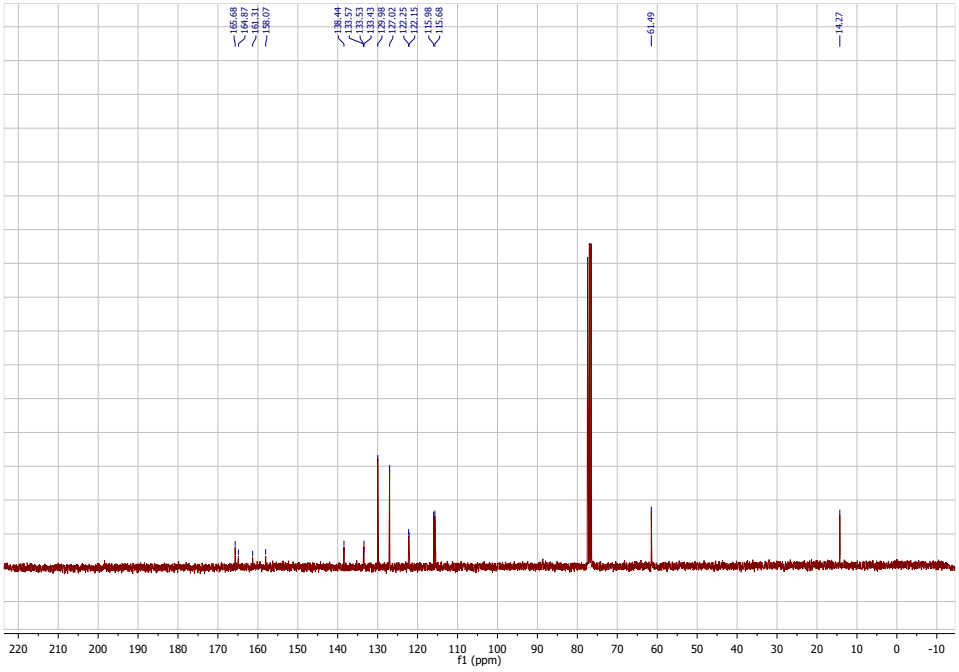

### 2.3.9. Representative HPLC Data

The peaks indicated by solid arrows are present in the chromatograms following coinjection of products with additional nonradioactive standard. The differences in elution times are due to UV-Vis and radiation detectors placed in series, and in all cases were consistent with delays observed at the time of acquisition. Due to modifications of the radioHPLC system, these delays have varied over the course of this project.

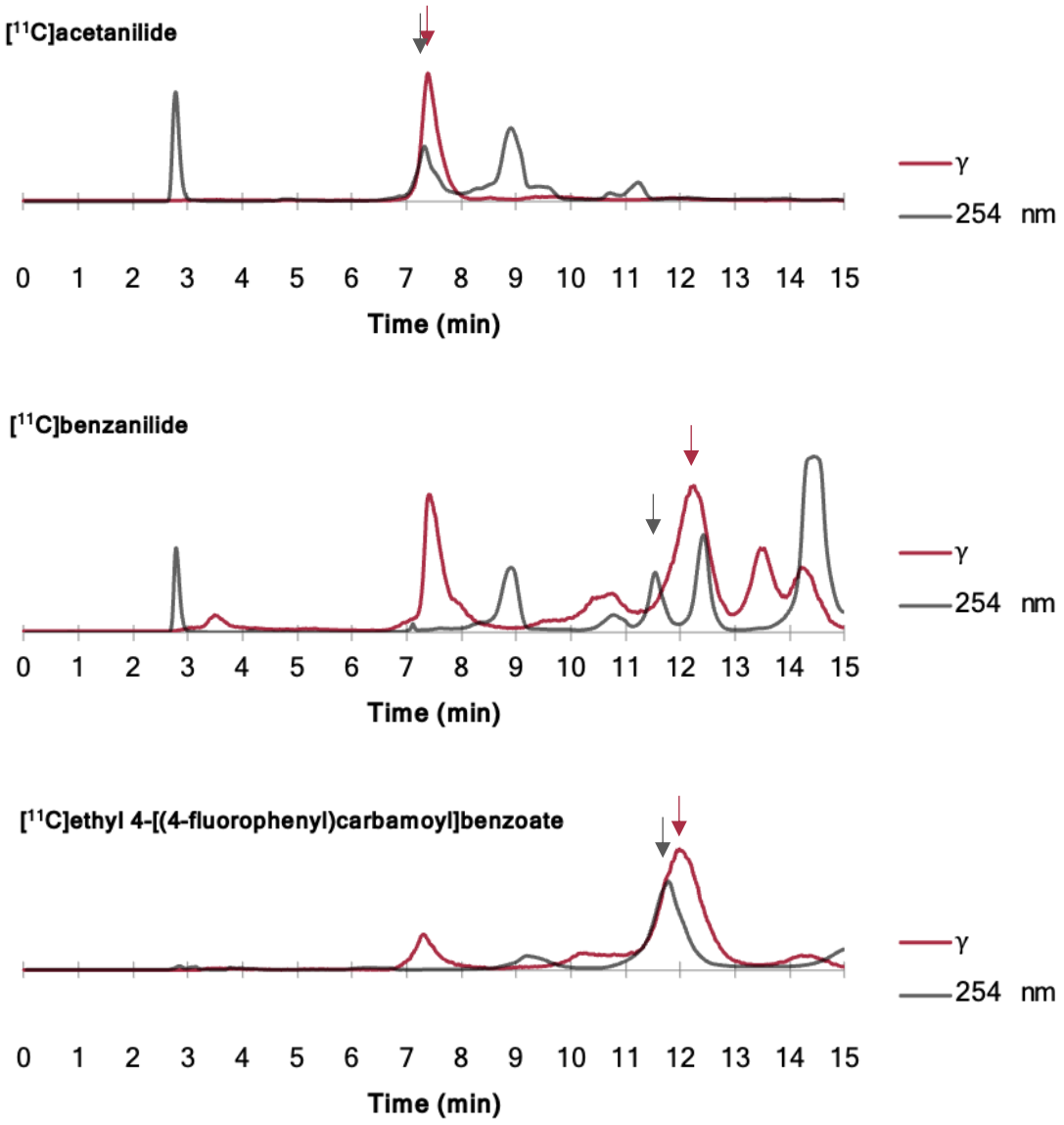

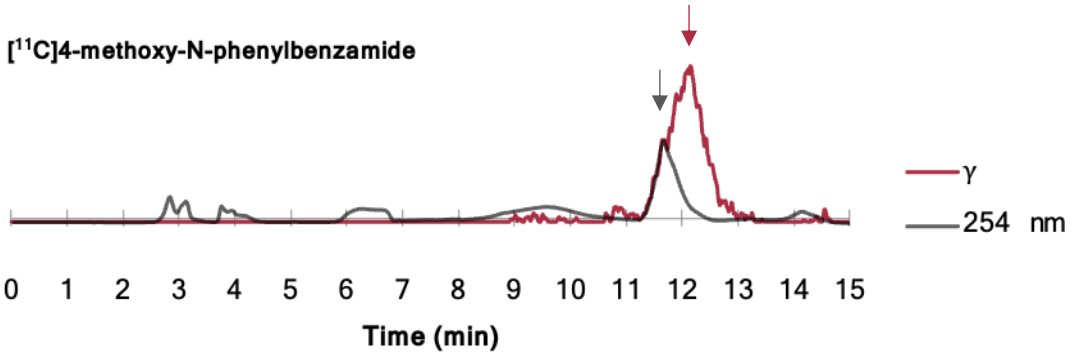
[11C]4-methoxy-N-phenylbenzamide
γ
254 nm
0 1 2 3 4 5 6 7 8 9 10 11 12 13 14 15
Time (min)

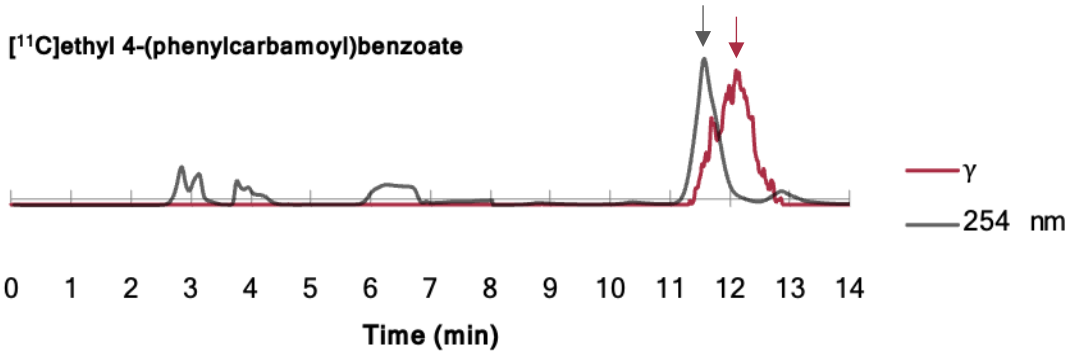
[11C]ethyl 4-(phenylcarbamoyl)benzoate
γ
254 nm
0 1 2 3 4 5 6 7 8 9 10 11 12 13 14
Time (min)

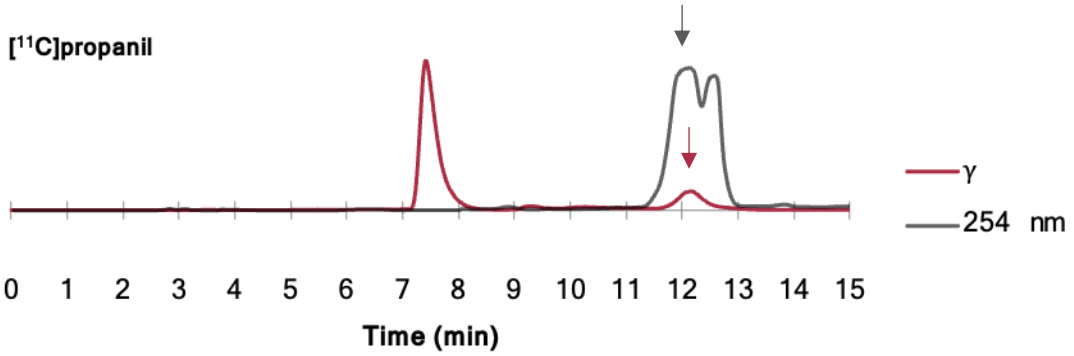
[11C]propanil
γ
254 nm
0 1 2 3 4 5 6 7 8 9 10 11 12 13 14 15
Time (min)

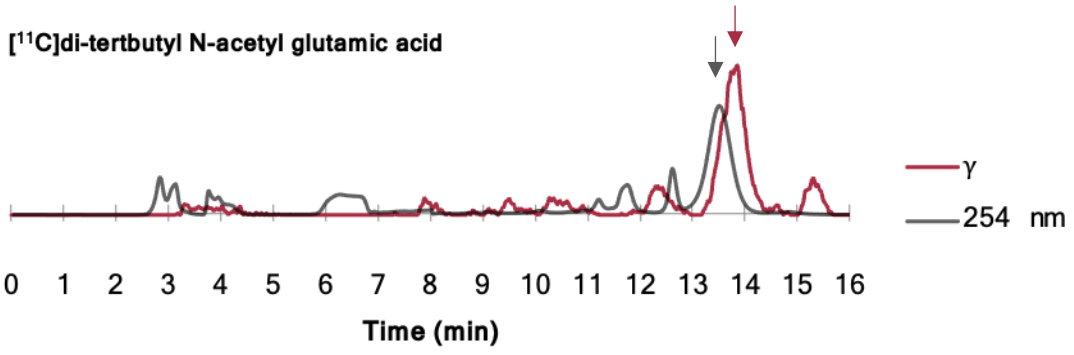
[11C]di-tertbutyl N-acetyl glutamic acid
γ
254 nm
0 1 2 3 4 5 6 7 8 9 10 11 12 13 14 15 16
Time (min)

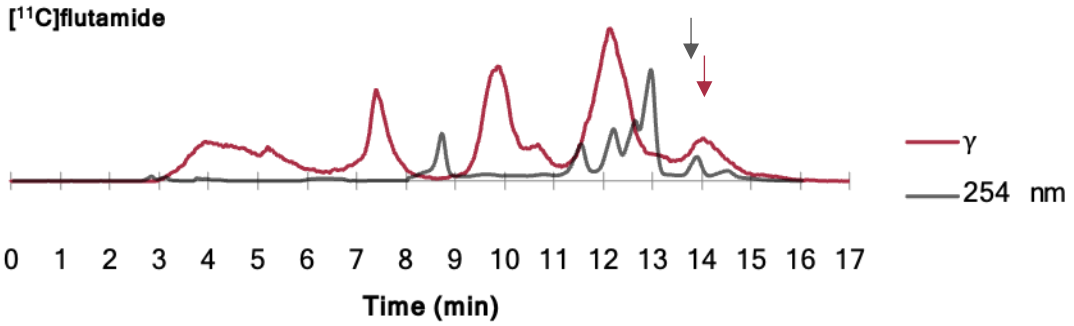


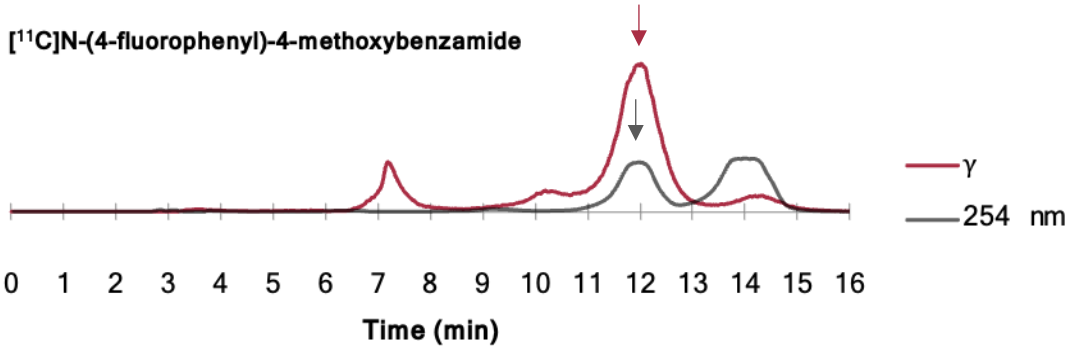


## ISOLATION OF [$^{11}$C]*N*-(4-fluorophenyl)-4-methoxybenzamide

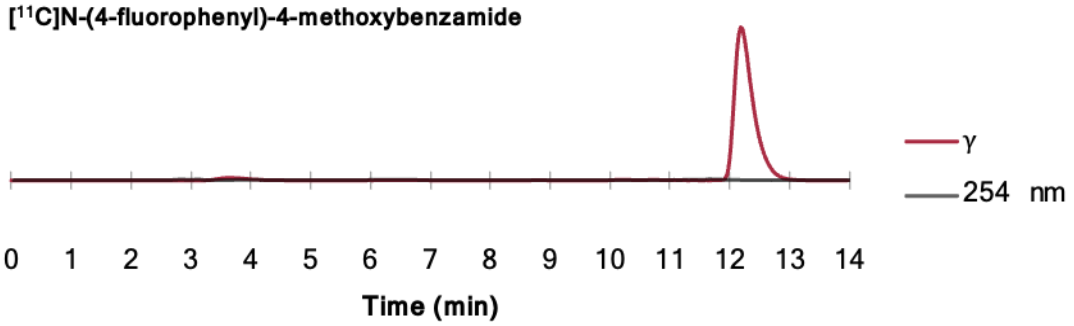


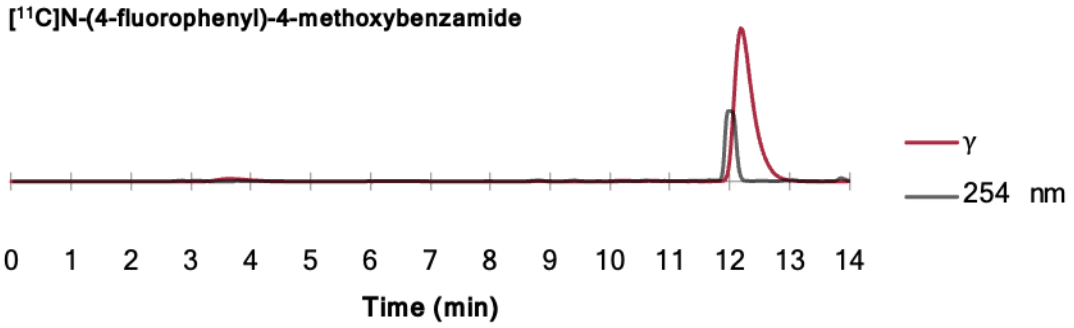

## 2.4. Extended Discussion

### 2.4.1. Lessons

*2.4.1.1. Alternative Organometallics*

While the yields of the derived $^{11}$C-amides in our study were sufficient for continued investigation, the intention with radiochemical method development is to target the preparation of practical radiotracer candidates; this demands diverse and robust tolerance for functionality to access compounds that are biologically active and/or akin to pharmaceuticals, and for easy-to-reproduce syntheses. For the former point, heteroaromatic systems are incredibly common in drug-like molecules, but were inaccessible using our rhodium-catalyzed addition of organozinc iodides. This was, we believe, a result of the rhodium catalyst and its interactions with *N* and *O*-groups. We evaluated alternative catalysts (as indicated in the publication, as well as others not listed) for their reactivity and tolerance, but found no improvements in reaction yield nor in functionality.

To the latter point, organozinc iodides are relatively difficult reagents to work with, due to their high sensitivity to water and a problematic quench that produces poorly soluble zinc hydroxide byproducts. While this was considered in the design of our methodology and was initially solved with an aqueous workup of our crude mixtures, performing extractions on radioactive products is not an efficient procedure nor one that can be easily adapted in radiotracer production facilities.

This led to the investigation of alternative organometallics. Our first inclination was to use organostannanes in place of organozinc halides, evaluating the nucleophile's effect on robustness (Figure 2.19). While we observed comparable yields, we did not notice any differences in functional group tolerance or access to more complex and diverse pharmaceutical scaffolds. Translation to carbon-11 chemistry also indicated limitations in yield. Given we felt our current catalytic systems (palladium-, platinum-, rhodium-based) were not sufficient, and that these strong organometallic precursors appeared restricted in their capabilities, we turned towards copper catalysis and boronic esters for an alternative scheme.

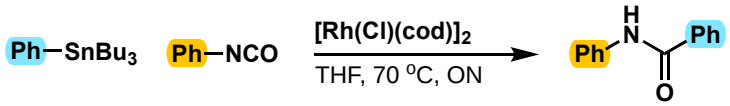


additive robustness assay

| | RCY (%) |
|---|---|
| **no change** | **36** |
| aniline | 21 |
| phenol | 53 |
| acetaldehyde | 53 |
| benzylamine | <1 |
| benzyl alcohol | 21 |
| 1-decyne | 0 |
| pyridine | 21 |
| indole | <1 |
| piperidine | <1 |
| morpholine | <1 |
| thiophene carboxylic acid | 7 |
| tetralone | 50 |

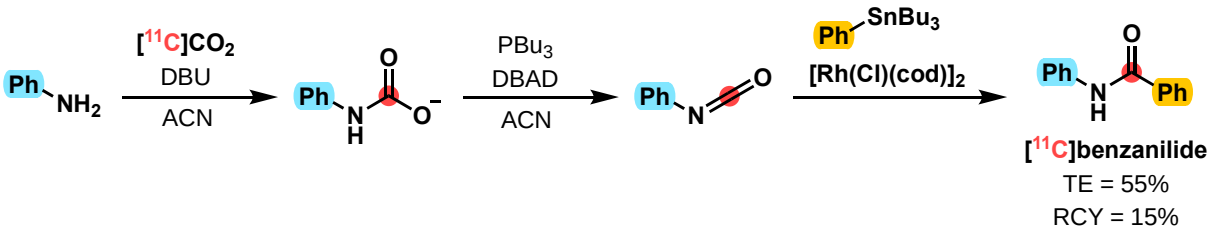


**[$^{11}$C]benzanilide**
TE = 55%
RCY = 15%

**Figure 2.19.** Rhodium-catalyzed reaction of isocyanates with organostannanes. A robustness assay evaluating a standard reaction in the presence of additives was used to test the effectiveness of organostannane nucleophiles. Poor tolerance for heteroatoms limited the translatability of the method for the preparation of carbon-11-labelled pharmaceuticals. Nonetheless, the method was translated and found to successfully provide product yield, albeit with lowered reactivity.

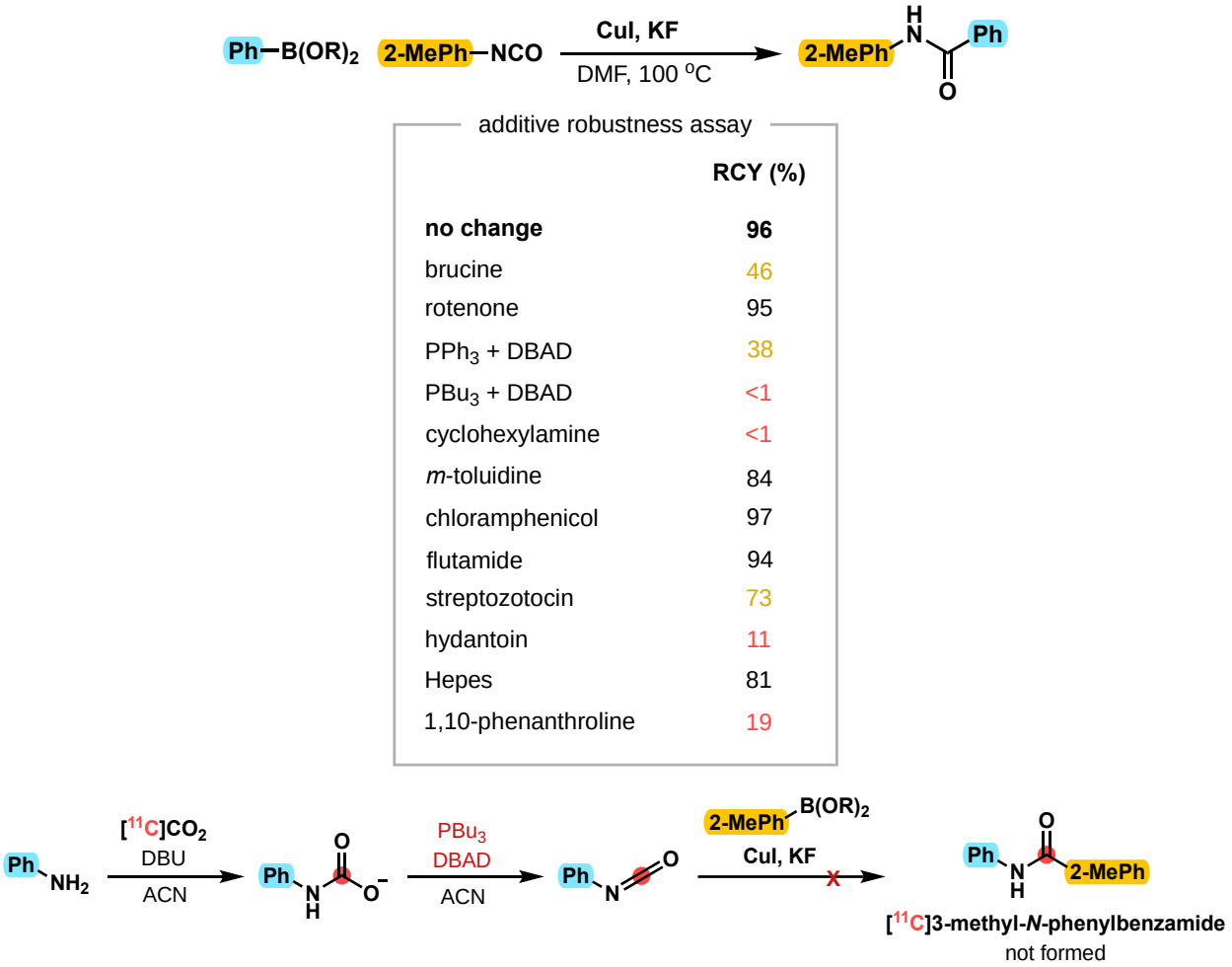


**Figure 2.20.** Copper-catalyzed reaction of isocyanates with boronic esters. A robustness assay was performed to determine the effectiveness of boronic esters at producing amides from isocyanates. Superior tolerance indicated the potential applicability for carbon-11 radiochemistry, however sensitivity to the Mitsunobu reagents and acidic conditions make *in situ* $^{11}$C-isocyanate formation a problem to address.

Development with stable isotopes was primarily conducted by a BSc candidate in our research group, Kirabo Nekesa; we once again performed a robustness assay, evaluating a baseline reaction's success in the presence of additives containing various functionalities and substituents (Figure 2.20). This study determined the method was capable of producing amides from isocyanates with much more tolerance for structurally diverse compounds, including heteroaromatic systems and drug-like functional groups. However, radiochemical translation proved more difficult due to the methods of preparing $^{11}$C-isocyanates ($POCl_3$ dehydration and Mitsunobu conversion) not being compatible with copper catalysis.

With this in mind, development of a possible substitute to traditional methods for $^{11}$C-isocyanate preparation may provide a reaction scheme that satisfies the requirements for copper catalysis, boronic esters, and $^{11}$C-amide preparation.

*2.4.1.2. Interrupted aza-Wittig using iminophosphoranes to synthesize $^{11}$C-carbonyls*

Current $^{11}$C-isocyanate syntheses are limited in their scope; acid dehydration with $POCl_3$ requires highly acidic conditions posing challenges for [$^{11}$C]$CO_2$ trapping as well as reactivity, while Mitsunobu conversions require high loading of azo reagents and phosphines that can be difficult to purify. An alternative approach to forming $^{11}$C-isocyanates that avoids these limitations therefore provides strong value for radiochemists.

Iminophosphoranes (or phosphinimines) are organophosphorus compounds with the structure $R_3P{=}NR'$. They have been shown to undergo the aza-Wittig reaction with $CO_2$ to produce isocyanates.[1] In the $^{11}$C space, van Tilburg *et al*. accessed unsymmetrical $^{11}$C-ureas through $^{11}$C-isocyanates derived from phenyltriphenylphosphinime.[2] Del Vecchio *et al.* developed the method further with cyclic $^{11}$C-ureas and $^{11}$C-carbamates through a Staudinger aza-Wittig sequence.[3] However, few linear carbamates were produced in low yields, and required both explosive azide precursors and forcing conditions with elevated temperatures.

As such, we sought to develop a robust methodology using [$^{11}$C]$CO_2$-fixation and iminophosphoranes to access $^{11}$C-ureas, $^{11}$C-carbamates, $^{11}$C-thiocarbamates, and $^{11}$C-amides without requiring highly acidic $POCl_3$, Mitsunobu reagents, explosive azides, toxic phosphines, and/or harsh conditions common in other methodologies (Figure 2.14).

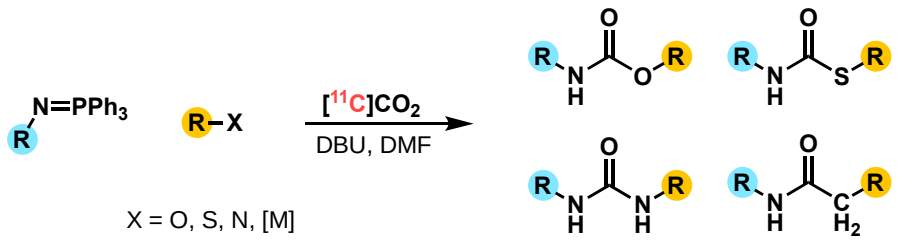


**Figure 2.14.** Interrupted aza-Wittig with iminophosphoranes. This methodology can access $^{11}$C-carbonyls, like $^{11}$C-carbamates, $^{11}$C-thiocarbamates, $^{11}$C-ureas, and $^{11}$C-amides from iminophosphorane precursors *via* an $^{11}$C-isocyanate intermediate.

This project was led by another graduate student in our group, Dr. Uzair Ismailani, and was later assisted by myself and a post-doctoral fellow, Dr. Maxime Munch. The development of the chemical method – discovering nucleophilic additions compatible with iminophosphorane-$CO_2$ coupling conditions with stable isotopes – was completed by Dr. Ismailani. With translation to radiochemistry, given my aforementioned work in adapting rhodium-mediated organozinc additions to $^{11}$C-isocyanates to a radiochemical system, we worked in cooperation to complete the same for iminophosphoranes.

Reactions were first tested manually. This was performed in reactors constructed in-house (Figure 2.15) by fitting a long test tube with a septum cap, then adding (a) a long needle for [$^{11}$C]$CO_2$ delivery, (b) an input needle for reagent addition, and (c) an output vent needle connected to a sodium hydroxide trap to capture any residual [$^{11}$C]$CO_2$. The septum was then painted with solidifying paste and the vial was purged with argon or nitrogen to ensure an isolated atmosphere. Following precursor loading and cyclotron production, [$^{11}$C]$CO_2$ was bubbled into the solution and allowed to trap. The reaction was left to run in a sand bath before being quenched and collected for analysis.

**Figure 2.15.** Manual radiosynthesis reaction vessel. Reactors were constructed using lab materials and used only once per reaction. Limitations in the amount of activity that can be produced, the reproducibility, and the technical difficulties associated with product purification if completed in manual reactors led to the automation of the method on a radiosynthesis unit.

While this methodology provided product yields, we quickly identified that we could not carry out high activity runs with reliable consistency, and so we turned towards the automation of the method using a radiosynthesis unit.

Adaptation of a manual method to an automated radiosynthesis unit carries with it many challenges. For starters, given the very low mass loading and volumes of solutions used in radiochemical reactions, as well as the careful handling and specific addition required for many reagents, the transfer of solutions throughout the unit's lines can be a major difficulty. Translation becomes just as much a technical difficulty as it is a chemistry problem.

We worked to acclimate the process of $^{11}$C-isocyanate synthesis from iminophosphorane precursors on an automated Synthra MeIplus Research radiosynthesis module (Figure 2.16). The time list – a series of commands delivered to the radiosynthesis unit for manipulation of valves and volume transport – developed for the organozinc work was adjusted and implemented for iminophosphorane chemistry. Following reaction completion, the solution was injected onto a built-in on-line HPLC column for purification. We completed this process for 11 representative substrates, including isolations for pharmaceutically relevant targets like [$^{11}$C]glibenclamide (62% isolated RCY), [$^{11}$C]URB694 (13% isolated RCY), and an antiarrhythmic compound (33% isolated RCY).

A

B

SR9009 Method 1min.tcf

| Time [min] | Function | Parameter |
|---|---|---|
| 0.00 | Valve Position | Reset all Valves |
| 0.05 | Valve Position | AC power relais = Position 2 |
| 0.10 | Digital Output | High Voltage = ON |
| 0.12 | Valve Position | V66 (He/NH3) = Position 2 |
| 0.14 | Valve Position | V1 Target / H2 = Position 2 |
| 0.16 | Valve Position | V2 CO2 Trap = Position 2 |
| 0.18 | Valve Position | V44 (Gas phase / direct) = Position 2 |
| 0.20 | Valve Position | V61 = Position 2 |
| 0.22 | Valve Position | V46 = Position 2 |
| 0.24 | Valve Position | V19 Reactor 1 vac = Position 2 |
| 0.26 | Valve Position | V22 Vacuum/Exhaust = Position 2 |
| 0.28 | Analog Output | No.1 = 1000 mV |
| 0.30 | Display Information | "Beam started?" |

**Figure 2.16.** Automated radiosynthesis unit. The Synthra MeIplus Research radiosynthesis unit can be used for radiochemical syntheses while operated remotely from behind lead shielding via programmed time lists of control commands. The synthesis unit itself (A) and a representative time list (B) are shown.

Our research group has continued to work with iminophosphoranes, this time extending to an application with prostate-specific membrane antigen (PSMA) radiotracer design. Several students have contributed to the project, including Dr. Ismailani, Dr. Munch, MSc candidate Abhishek Patel, BSc candidate Hala Almeneim, and BSc candidate Hunter Valley. My role throughout has been to assist with $^{11}$C implementation, having developed the method alongside Dr. Munch and Dr. Ismailani, and since then to oversee training and supervision for project development.

Most PSMA-targeting small molecule inhibitors first consist of a PSMA-binding domain; this is typically a urea-based binding motif, most often a glutamate-ureido core. These pharmacophores are then connected through a linker moiety to a chelator that can be labeled with various radiometals or radionuclides. While many promising candidates exist, a general and rapid method to radiolabel PSMA radioligand candidates would enable improved understanding of the structure-

activity relationship and aid in rational design of a new generation. Given the ureido center, [$^{11}$C]$CO_2$-fixation offers a methodological approach for library synthesis of PSMA candidates.

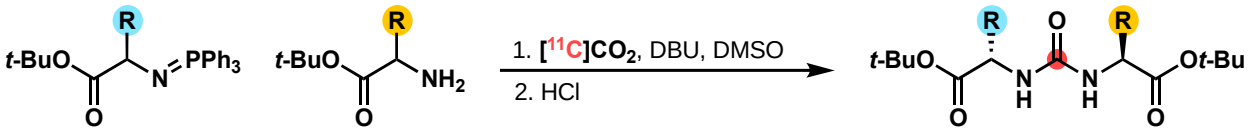


**Figure 2.17.** Proposed reaction scheme for general PSMA radioligand synthesis. Iminophosphorane reaction with [$^{11}$C]$CO_2$ and an amine nucleophile produces candidates for PSMA radiotracer development.

We envisioned a reaction scheme using $^{11}$C-isocyanates derived from iminophosphoranes reacting with amine nucleophiles to yield $^{11}$C-ureas (Figure 2.17). By sequentially alternating the iminophosphorane and nucleophilic amine, a catalogue of derivations can be produced. This approach was applied to a number of different urea substrates, of which many were isolated for subsequent PET imaging. This project is nearing completion and submission.

*2.4.1.3. Intramolecular Friedel-Crafts acylation of $^{11}$C-isocyanates*

Our work with isocyanates attracted the attention of an international research group seeking to form $^{11}$C-labelled α,β-aromatic lactams, in particular for the synthesis of [$^{11}$C]DPQ for imaging of poly (ADP-ribose) polymerase (PARP). We in turn supported a visit by Dr. Marius Ozenil from the Medical University of Vienna, Austria, in order to assist with translation of his methodology to carbon-11 and automated radiotracer production. Their method proceeds via an intramolecular $AlCl_3$-guided Friedel-Crafts acylation of isocyanates, first optimized using stable isotopes. Upon Dr. Ozenil's arrival to our facilities, we looked to prepare $^{11}$C-isocyanates *in situ* for subsequent cyclization. The established Mitsunobu conditions to convert amines to $^{11}$C-isocyanates proved to be incompatible and so we instead turned towards $POCl_3$ acid dehydration. This succeeded as, fortunately, the simultaneous addition of $POCl_3$ and $AlCl_3$ formed a Lewis-acid-base adduct displaying improved solubility and reactivity.

With this optimized methodology fully translated (Figure 2.18), Dr. Ozenil completed a substrate scope with amine precursors before returning to Vienna and completing the production and isolation of [$^{11}$C]DPQ.

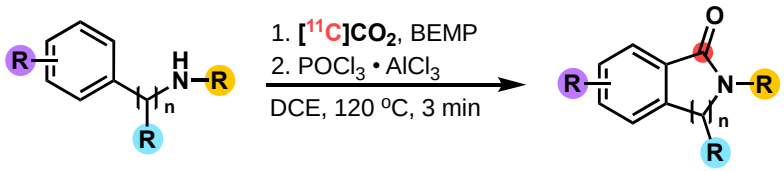


**Figure 2.18.** Intramolecular Friedel-Crafts acylation of [$^{11}$C]isocyanates. An $AlCl_3$-guided acylation of [$^{11}$C]isocyanates can yield α,β-aromatic lactams starting from amines and [$^{11}$C]$CO_2$.

### 2.5.2. Perspectives

*2.5.2.1. Conclusions*

In this section of the thesis, our aim was to develop a methodology to access $^{11}$C-amides for radiotracer production. In that task we succeeded, yielding several radiolabelled products in strong yields for continued investigation. The modular nature of $^{11}$C-carbonyl labelling was demonstrated, allowing for rapid alterations of both the organozinc halide and the amine to generate a diverse library of radiotracer candidates. This approach was further exemplified using iminophosphoranes and put into practice with the generation of PSMA probes. We also completed extensive investigation using stable isotopes, establishing yet another method that can be used to derive amides, and further improving on the understanding of isocyanate behaviour with transition metal catalysis.

While limitations in the diversity of products were elucidated, we could nonetheless access biologically active compounds that could be explored in imaging. The use of organozinc iodides appears to be feasible with many simple compounds and would be an option for the generation of $^{11}$C-amide radiotracer candidates.

*2.5.2.2. Future Directions*

Continued investigation into alternative catalytic systems and organometallics or other nucleophiles would allow for the discovery of a broadly applicable and general approach to $^{11}$C-amides. While our data suggests organostannanes may not be an ideal candidate for further investigation, boronic esters showed enough promise to merit attention.

Applications with organozinc iodides for imaging studies have yet to be explored but could show promise in the development of radiotracer candidates.

### 2.5.3. References

(1) Molina, P.; Alajarin, M.; Arques, A. Convenient Improved Syntheses of Isocyanates or Isothiocyanates from Amines. *Synthesis* **2002**, *1982*, 596–597. https://doi.org/10.1055/s-1982-29877.

(2) van Tilburg, E. W.; Windhorst, A. D.; van der Mey, M.; Herscheid, J. D. M. One-Pot Synthesis of [$^{11}$C]Ureas via Triphenylphosphinimines. *J Label Compd and Radiopharm* **2006**, *49* (4), 321–330. https://doi.org/10.1002/jlcr.1052.

(3) Del Vecchio, A.; Caillé, F.; Chevalier, A.; Loreau, O.; Horkka, K.; Halldin, C.; Schou, M.; Camus, N.; Kessler, P.; Kuhnast, B.; Taran, F.; Audisio, D. Late-Stage Isotopic Carbon Labeling of Pharmaceutically Relevant Cyclic Ureas Directly from $CO_2$. *Angewandte Chemie International Edition* **2018**, *57* (31), 9744–9748. https://doi.org/10.1002/anie.201804838.

# Chapter 3: Synthesis and Development of (*R*)- and (*S*)-[$^{11}$C]SR9009 Radiotracer Development

This chapter and discussion contains information from soon-to-be published studies.

- **FOCUS:** Mair et al. "Synthesis of (*R*)- and (*S*)-[$^{11}$C]SR9009 for Rev-erb Imaging" *Planned submission.* **2024**.
    - Contributions: Project lead, completed experiments, wrote manuscript.

## 3.1. Context

### 3.1.1. Rev-erb and the Circadian Clock

The daily systematic alterations in behaviour and physiology according to time and light exposure are known as circadian rhythms, triggered by the intrinsic timekeeping “circadian clock”. With an approximately 24-h period, these diurnal rhythms constitute an autonomous control center over expression, accumulation, and degradation of gene products therein establishing a molecular oscillation. At its core is a feedback loop of transcription factors directed and synchronized by external environmental stimuli like light exposure and food intake that trigger the suprachiasmatic nucleus (SCN), the internal clock pacemaker.[1–4]

The central role in regulation begins with the heterodimeric relationship of the brain and muscle Arnt-like protein 1 (BMAL1) and the circadian locomotor output cycles kaput (CLOCK). These two factors heterodimerize in the cytoplasm, promoting the expression of period (PER) and cryptochrome (CRY) genes, which then complex and translocate into the nucleus. With sufficient accumulation, PER:CRY inhibits the transcriptional activity of BMAL1:CLOCK, thereby limiting their own expression. This creates an oscillating pattern of expression with peaks of high and minimums of low expression.[1–4]

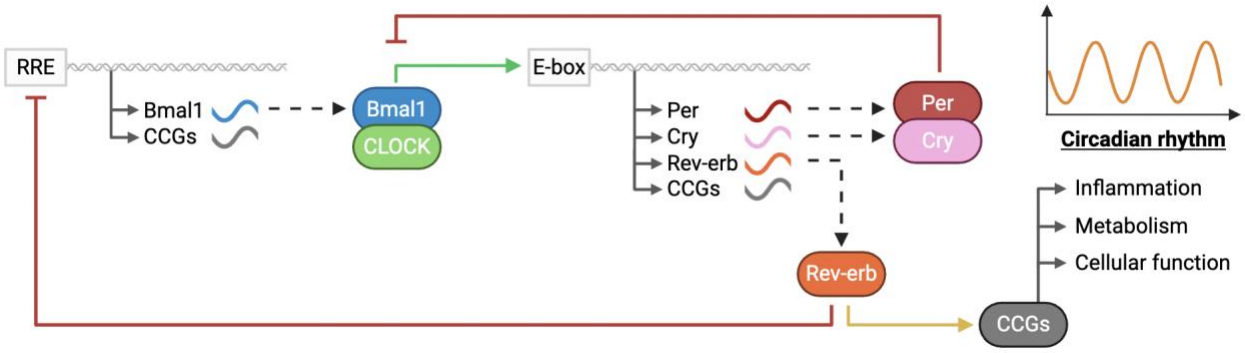


**Figure 3.1.** Circadian rhythm feedback loop. The body’s internal clock originates from a transcript feedback loop, regulated by its own products. Rev-erb acts as the master control protein while also imparting control over many clock-controlled genes (CCGs) implicated in inflammation, metabolism, and cellular function.

An additional arm of feedback comes from the induction of Rev-erb expression by BMAL1:CLOCK. Rev-erb itself represses the expression of BMAL1, providing an overarching

feedback loop and regulatory control. As a result, Rev-erb is viewed as the principal regulator of the circadian clock. These proteins belong to the nuclear receptor superfamily 1, group D (NR1D). There are two isoforms of the receptor: Rev-erbα (NR1D1) and Rev-erbβ (NR1D2). Current understanding is that Rev-erbα provides more control over the circadian machinery, with Rev-erbα knockout studies causing circadian disruption not conversely seen with Rev-erbβ knockout. That being said, the two are believed to work in concert for regulatory control and they are thought to play similar roles.[1–4]

Rev-erb and clock proteins further regulate additional genes (known as clock-controlled genes, CCGs) that are involved in biochemical pathways and cellular functions including inflammation and metabolism. In addition to their master control over the circadian period, these peripheral implications lead to an essential authority over biological functionality. Rev-erbα in particular is a potent regulator of metabolism in areas of the body like the liver, gastrointestinal tract, immune cells, muscles, adipose tissue, and in the heart.[1–4]

### 3.1.2. Cardiovascular Disease

Diurnal rhythms are observed in several heart-related physiological characteristics like clotting, the autonomic nervous system's alterations in contractility and heart rate, and in heart behaviour itself.[5–8] Beyond normal function, circadian rhythms play a key role in the onset, development and outcomes of many cardiovascular diseases like atherosclerosis, arrhythmias, and myocardial infarctions. Disruptions and asynchronicity in cardiac circadian rhythms can develop into cardiomyopathies and systolic dysfunction with outcomes leading to death.[9–12] Even the pathological incidence of cardiovascular diseases occurs over the 24-h rhythm: sudden cardiac death, arrhythmias, stroke, and pulmonary embolisms all occur most frequently in the early morning.[13]

Treating heart failure arising from the worsening of cardiac health following myocardial infarction remains a clinical challenge. While patients who suffer heart attacks frequently receive sufficient medical care to alleviate acute presentations of symptoms, the surgical reperfusion treatment triggers adverse inflammatory responses that lead to infarct expansion and terminal cardiac remodeling. This inflammation is driven by the NLR family pyrin domain containing 3 (NLRP3) protein expressed in macrophages, one of the main CCGs mediated by Rev-erb.[14,15]

Investigating pharmacological targeting of the circadian clock to mitigate the effects of NLRP3-driven inflammation is a natural area of interest.

### 3.1.3. SR9009

In understanding the vital role Rev-erb plays in circadian biology and its potential implications in clinical pathologies, synthetic ligands for its modulation are of research interest. Heme was identified as the natural, endogenous ligand of Rev-erb, coordinated by two key residues – a histidine on helix 11 and a cysteine on helix 3.[16] Following these findings, exploration into ligand scaffolds was used to identify potential ligands for exogeneous modulation. The first ligand identified was SR6452, later renamed to GSK4112.[17] The Rev-erb agonist was found to modulate CCG expression, however it was limited for *in vivo* use due to its systemic distribution and in its poor agonism of Rev-erb.[18] It nonetheless provided a base structure from which a class of compounds could be further derived with SAR analysis.[19]

From these structural improvements, two ligands have been further studied *in vivo*: SR9011 and SR9009.[20] With significantly more potency for Rev-erb than GSK4112, these two candidates – in particular, SR9009 – have been investigated for their pharmaceutical potential in biological control and regulation of the circadian clock. Additional candidates demonstrated possible activity for Rev-erb agonism, however they have yet to be explored in depth.[21] A more recent agonist, SLT1267, with a distinct chemical scaffold from SR9009 and its analogues has recently been characterized and is continuing to be investigated.[22]

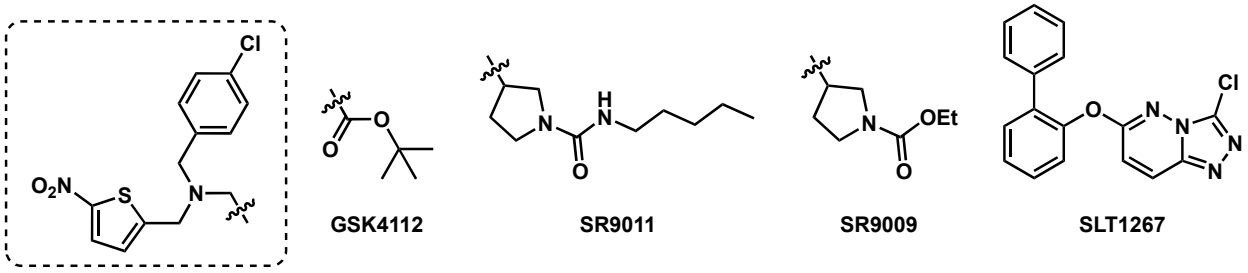


**Figure 3.2.** Most prominent Rev-erb agonists. The structures of most Rev-erb agonists contain a tertiary amine at its core with differences in one of the branch arms. The most commonly investigated are GSK4112, SR9011, and SR9009. A newer candidate, SLT1267, diverges from this core.

SR9009 is a tertiary amine containing three arms – a nitrothiophene, a chlorobenzylamine, and a pyrrolidine ethyl carbamate. Current approaches for its synthesis proceed with two subsequent reductive aminations, first forming a secondary amine with two branches before attaching the third.[21] The pyrrolidine in particular possesses a chiral stereocenter that can impart orientation in its final structure. These variations in stereochemistry can lead to differences in drug potency and efficacy,[23] and can even offer differing imaging profiles.[24] However, the current, patented, industry synthesis for producing SR9009 pharmaceutically uses racemic pyrrolidine, providing a mixture of products to be administered.[25]

While initially intended to be used for sleep-related disorders, SR9009 has been investigated for alternative clinical uses thanks to its regulation of Rev-erb and thus CCGs. One of the most predominant off-label indications stemmed from findings that Rev-erb modulates skeletal muscle oxidative capacity and therefore exercise capacity.[26] As such, abuse of SR9009 under the name Stenabolic has become a significant issue in the bodybuilding community, receiving a prohibition from the World Anti-Doping Agency. It has also been investigated for use in treating cancers like small-cell lung cancer,[27] and for supressing inflammation via inhibition of inflammasomes.[28] This anti-inflammatory effect is perhaps most relevant in the heart, where SR9009 administration has long demonstrated improvements in cardiac function and outcomes.[29–33] Dr. Tami Martino and her team specifically investigated SR9009's effects on treating cardiac reperfusion injury, in which just one day of treatment drastically improved infarct recovery and survival rate.[34]

Translation of these findings to clinical trials for use in human patients has however been delayed by Rev-erb-independent effects from SR9009 treatment. Using a Rev-erb deletion mouse model, SR9009 treatment was nonetheless found to demonstrate effects on cell proliferation and metabolism, suggesting off-target functionality that could account for any of its anti-inflammatory and cardioprotective behaviours.[35] Additional evaluations identified LXRα as an off-target pathway offering anti-cancer effects.[36] While GSK4112 had significantly higher selectivity for Rev-erb over LXRα, SR9009 has the opposite behaviour with strong selectivity for LXRα.[37]

With conflicting schools of thought, we theorized using [$^{11}$C]SR9009 to investigate its specific uptake in the heart could provide vital insight on the drug's mechanism of action. As previously discussed, $^{11}$C-carbamates are frequently prepared using [$^{11}$C]$CO_2$-fixation with amines, alkyl halides, and fixation bases like DBU and BEMP to mediate the reaction.[38,39] These methods offer an opportunity to access [$^{11}$C]SR9009 from an amine precursor.

### 3.1.4. Clarifications

Selection of a molecular target with a biochemical involvement in the clinical indication of interest is a typical first-step in the design and development of a radiotracer. By selecting a target with varied expression or activity depending on disease presence and/or severity, one may be able to successfully differentiate a patient compared to a healthy volunteer through imaging means; a radiotracer to this effect would be quite promising in a clinical space. The clinical value of [$^{11}$C]SR9009 still needs to be investigated, as it is widely expressed throughout the body and is temporally active as opposed to being linked to a disease-state.[1,2] Given this point, an SR9009-based radiotracer may have poor clinical value and could be found to be a poor imaging probe in the diagnosis of disease.

However, in pharmacological or molecular studies with a radiotracer, there is no requirement for medical or biochemical readout. In this intended study, investigation into the specific uptake across different tissues sufficiently justifies the development of a SR9009-based probe. With our intentions being to evaluate levels of uptake in the heart depending on the route of administration (intravenous, intraperitoneal, or subcutaneous injection), aspirations for disease-based imaging are secondary and not a marker of success for the radiotracer.

Furthermore, evidence of specific binding or a lack thereof does not invalidate SR9009 as a therapeutic. Regardless of its method of action, whether it be *via* Rev-erb in the heart or elsewhere in the body, or through downstream effects from LXRα, the phenotypic response of SR9009 treatment has nonetheless been positive and promising in pre-clinical models of heart failure. Investigation into its pharmacokinetic and pharmacodynamic behaviour with PET imaging provides additional information from which we can make educated decisions on continued target SAR, on therapeutic doses and regimens, on the mechanism of action like localization and biomarker correlation, and on additional research focuses into SR9009, Rev-erb, and their implications in cardiovascular health.

### 3.1.5. References


(1) Cho, H.; Zhao, X.; Hatori, M.; Yu, R. T.; Barish, G. D.; Lam, M. T.; Chong, L.-W.; DiTacchio, L.; Atkins, A. R.; Glass, C. K.; Liddle, C.; Auwerx, J.; Downes, M.; Panda, S.; Evans, R. M. Regulation of Circadian Behaviour and Metabolism by REV-ERB-α and REV-ERB-β. *Nature* **2012**, *485* (7396), 123–127. https://doi.org/10.1038/nature11048.

(2) Ikeda, R.; Tsuchiya, Y.; Koike, N.; Umemura, Y.; Inokawa, H.; Ono, R.; Inoue, M.; Sasawaki, Y.; Grieten, T.; Okubo, N.; Ikoma, K.; Fujiwara, H.; Kubo, T.; Yagita, K. REV-ERBα and REV-ERBβ Function as Key Factors Regulating Mammalian Circadian Output. *Sci Rep* **2019**, *9* (1), 10171. https://doi.org/10.1038/s41598-019-46656-0.

(3) Walker, W. H.; Walton, J. C.; DeVries, A. C.; Nelson, R. J. Circadian Rhythm Disruption and Mental Health. *Transl Psychiatry* **2020**, *10* (1), 1–13. https://doi.org/10.1038/s41398-020-0694-0.

(4) Ruan, W.; Yuan, X.; Eltzschig, H. K. Circadian Rhythm as a Therapeutic Target. *Nat Rev Drug Discov* **2021**, *20* (4), 287–307. https://doi.org/10.1038/s41573-020-00109-w.

(5) Shaw, E.; Tofler, G. H. Circadian Rhythm and Cardiovascular Disease. *Curr Atheroscler Rep* **2009**, *11* (4), 289–295. https://doi.org/10.1007/s11883-009-0044-4.

(6) Takeda, N.; Maemura, K. Circadian Clock and Cardiovascular Disease. *Journal of Cardiology* **2011**, *57* (3), 249–256. https://doi.org/10.1016/j.jjcc.2011.02.006.

(7) Thosar, S. S.; Butler, M. P.; Shea, S. A. Role of the Circadian System in Cardiovascular Disease. *J Clin Invest* **2018**, *128* (6), 2157–2167. https://doi.org/10.1172/JCI80590.

(8) Chellappa, S. L.; Vujovic, N.; Williams, J. S.; Scheer, F. A. J. L. Impact of Circadian Disruption on Cardiovascular Function and Disease. *Trends in Endocrinology & Metabolism* **2019**, *30* (10), 767–779. https://doi.org/10.1016/j.tem.2019.07.008.

(9) Morris, C. J.; Purvis, T. E.; Hu, K.; Scheer, F. A. J. L. Circadian Misalignment Increases Cardiovascular Disease Risk Factors in Humans. *Proceedings of the National Academy of Sciences* **2016**, *113* (10), E1402–E1411. https://doi.org/10.1073/pnas.1516953113.

(10) Rabinovich-Nikitin, I.; Lieberman, B.; Martino, T. A.; Kirshenbaum, L. A. Circadian-Regulated Cell Death in Cardiovascular Diseases. *Circulation* **2019**, *139* (7), 965–980. https://doi.org/10.1161/CIRCULATIONAHA.118.036550.

(11) Lecour, S.; Du Pré, B. C.; Bøtker, H. E.; Brundel, B. J. J. M.; Daiber, A.; Davidson, S. M.; Ferdinandy, P.; Girao, H.; Gollmann-Tepeköylü, C.; Gyöngyösi, M.; Hausenloy, D. J.; Madonna, R.; Marber, M.; Perrino, C.; Pesce, M.; Schulz, R.; Sluijter, J. P. G.; Steffens, S.; Van Linthout, S.; Young, M. E.; Van Laake, L. W. Circadian Rhythms in Ischaemic Heart Disease: Key Aspects for Preclinical and Translational Research: Position Paper of the ESC Working Group on Cellular Biology of the Heart. *Cardiovascular Research* **2022**, *118* (12), 2566–2581. https://doi.org/10.1093/cvr/cvab293.

(12) Young, M. E. The Cardiac Circadian Clock. *JACC: Basic to Translational Science* **2023**, *8* (12), 1613–1628. https://doi.org/10.1016/j.jacbts.2023.03.024.

(13) Crnko, S.; Du Pré, B. C.; Sluijter, J. P. G.; Van Laake, L. W. Circadian Rhythms and the Molecular Clock in Cardiovascular Biology and Disease. *Nat Rev Cardiol* **2019**, *16* (7), 437–447. https://doi.org/10.1038/s41569-019-0167-4.

(14) Franke, M.; Bieber, M.; Kraft, P.; Weber, A. N. R.; Stoll, G.; Schuhmann, M. K. The NLRP3 Inflammasome Drives Inflammation in Ischemia/Reperfusion Injury after Transient Middle Cerebral Artery Occlusion in Mice. *Brain, Behavior, and Immunity* **2021**, *92*, 221–231. https://doi.org/10.1016/j.bbi.2020.12.009.

(15) Ghafouri-Fard, S.; Shoorei, H.; Poornajaf, Y.; Hussen, B. M.; Hajiesmaeili, Y.; Abak, A.; Taheri, M.; Eghbali, A. NLRP3: Role in Ischemia/Reperfusion Injuries. *Front. Immunol.* **2022**, *13*. https://doi.org/10.3389/fimmu.2022.926895.

(16) Raghuram, S.; Stayrook, K. R.; Huang, P.; Rogers, P. M.; Nosie, A. K.; McClure, D. B.; Burris, L. L.; Khorasanizadeh, S.; Burris, T. P.; Rastinejad, F. Identification of Heme as the Ligand for the Orphan Nuclear Receptors REV-ERBα and REV-ERBβ. *Nat Struct Mol Biol* **2007**, *14* (12), 1207–1213. https://doi.org/10.1038/nsmb1344.

(17) Grant, D.; Yin, L.; Collins, J. L.; Parks, D. J.; Orband-Miller, L. A.; Wisely, G. B.; Joshi, S.; Lazar, M. A.; Willson, T. M.; Zuercher, W. J. GSK4112, a Small Molecule Chemical Probe for the Cell Biology of the Nuclear Heme Receptor Rev-Erbα. *ACS Chem. Biol.* **2010**, *5* (10), 925–932. https://doi.org/10.1021/cb100141y.

(18) Kumar, N.; Solt, L. A.; Wang, Y.; Rogers, P. M.; Bhattacharyya, G.; Kamenecka, T. M.; Stayrook, K. R.; Crumbley, C.; Floyd, Z. E.; Gimble, J. M.; Griffin, P. R.; Burris, T. P. Regulation of Adipogenesis by Natural and Synthetic REV-ERB Ligands. *Endocrinology* **2010**, *151* (7), 3015–3025. https://doi.org/10.1210/en.2009-0800.

(19) Kojetin, D. J.; Burris, T. P. REV-ERB and ROR Nuclear Receptors as Drug Targets. *Nat Rev Drug Discov* **2014**, *13* (3), 197–216. https://doi.org/10.1038/nrd4100.

(20) Solt, L. A.; Wang, Y.; Banerjee, S.; Hughes, T.; Kojetin, D. J.; Lundasen, T.; Shin, Y.; Liu, J.; Cameron, M. D.; Noel, R.; Yoo, S.-H.; Takahashi, J. S.; Butler, A. A.; Kamenecka, T. M.; Burris, T. P. Regulation of Circadian Behaviour and Metabolism by Synthetic REV-ERB Agonists. *Nature* **2012**, *485* (7396), 62–68. https://doi.org/10.1038/nature11030.

(21) Shin, Y.; Noel, R.; Banerjee, S.; Kojetin, D.; Song, X.; He, Y.; Lin, L.; Cameron, M. D.; Burris, T. P.; Kamenecka, T. M. Small Molecule Tertiary Amines as Agonists of the Nuclear Hormone Receptor Rev-Erbα. *Bioorganic & Medicinal Chemistry Letters* **2012**, *22* (13), 4413–4417. https://doi.org/10.1016/j.bmcl.2012.04.126.

(22) Murray, M. H.; Valfort, A. C.; Koelblen, T.; Ronin, C.; Ciesielski, F.; Chatterjee, A.; Veerakanellore, G. B.; Elgendy, B.; Walker, J. K.; Hegazy, L.; Burris, T. P. Structural Basis of Synthetic Agonist Activation of the Nuclear Receptor REV-ERB. *Nat Commun* **2022**, *13* (1), 7131. https://doi.org/10.1038/s41467-022-34892-4.

(23) McConathy, J.; Owens, M. J. Stereochemistry in Drug Action. *Primary Care Companion to The Journal of Clinical Psychiatry* **2003**, *5* (2), 70. https://doi.org/10.4088/pcc.v05n0202.

(24) Chau, W.-F.; Black, A. M. A.; Clarke, A.; Durrant, C.; Gausemel, I.; Khan, I.; Mantzilas, D.; Oulie, I.; Rogstad, A.; Trigg, W.; Jones, P. A. Exploration of the Impact of Stereochemistry on the Identification of the Novel Translocator Protein PET Imaging Agent [$^{18}$F]GE-180. *Nuclear Medicine and Biology* **2015**, *42* (9), 711–719. https://doi.org/10.1016/j.nucmedbio.2015.05.004.

(25) Kamenecka, T. M.; Burris, T. Modulators of Rev-Erb. WO2013033310A1, March 7, 2013.

(26) Woldt, E.; Sebti, Y.; Solt, L. A.; Duhem, C.; Lancel, S.; Eeckhoute, J.; Hesselink, M. K. C.; Paquet, C.; Delhaye, S.; Shin, Y.; Kamenecka, T. M.; Schaart, G.; Lefebvre, P.; Nevière, R.; Burris, T. P.; Schrauwen, P.; Staels, B.; Duez, H. Rev-Erb-α Modulates Skeletal Muscle Oxidative Capacity by Regulating Mitochondrial Biogenesis and Autophagy. *Nat Med* **2013**, *19* (8), 1039–1046. https://doi.org/10.1038/nm.3213.

(27) Shen, W.; Zhang, W.; Ye, W.; Wang, H.; Zhang, Q.; Shen, J.; Hong, Q.; Li, X.; Wen, G.; Wei, T.; Zhang, J. SR9009 Induces a REV-ERB Dependent Anti-Small-Cell Lung Cancer Effect through Inhibition of Autophagy. *Theranostics* **2020**, *10* (10), 4466. https://doi.org/10.7150/thno.42478.

(28) Hong, H.; Cheung, Y. M.; Cao, X.; Wu, Y.; Li, C.; Tian, X. Y. REV-ERBα Agonist SR9009 Suppresses IL-1β Production in Macrophages through BMAL1-Dependent Inhibition of Inflammasome. *Biochemical Pharmacology* **2021**, *192*, 114701. https://doi.org/10.1016/j.bcp.2021.114701.

(29) Zhang, L.; Zhang, R.; Tien, C.-L.; Chan, R. E.; Sugi, K.; Fu, C.; Griffin, A. C.; Shen, Y.; Burris, T. P.; Liao, X.; Jain, M. K. REV-ERBα Ameliorates Heart Failure through Transcription Repression. *JCI Insight* **2017**, *2* (17), e95177, 95177. https://doi.org/10.1172/jci.insight.95177.

(30) Stujanna, E. N.; Murakoshi, N.; Tajiri, K.; Xu, D.; Kimura, T.; Qin, R.; Feng, D.; Yonebayashi, S.; Ogura, Y.; Yamagami, F.; Sato, A.; Nogami, A.; Aonuma, K. Rev-Erb Agonist Improves Adverse Cardiac Remodeling and Survival in Myocardial Infarction through an Anti-Inflammatory Mechanism. *PLoS One* **2017**, *12* (12), e0189330. https://doi.org/10.1371/journal.pone.0189330.

(31) Li, H.; Song, S.; Tien, C.; Qi, L.; Graves, A.; Nasiotis, E.; Burris, T. P.; Zhao, Y.; Sun, Z.; Zhang, L. SR9009 Improves Heart Function after Pressure Overload Independent of Cardiac REV-ERB. *Front. Cardiovasc. Med.* **2022**, *9*. https://doi.org/10.3389/fcvm.2022.952114.

(32) Dierickx, P.; Zhu, K.; Carpenter, B. J.; Jiang, C.; Vermunt, M. W.; Xiao, Y.; Luongo, T. S.; Yamamoto, T.; Martí-Pàmies, Í.; Mia, S.; Latimer, M.; Diwan, A.; Zhao, J.; Hauck, A. K.; Krusen, B.; Nguyen, H. C. B.; Blobel, G. A.; Kelly, D. P.; Pei, L.; Baur, J. A.; Young, M. E.; Lazar, M. A. Circadian REV-ERBs Repress E4bp4 to Activate NAMPT-Dependent NAD+ Biosynthesis and Sustain Cardiac Function. *Nat Cardiovasc Res* **2022**, *1* (1), 45–58. https://doi.org/10.1038/s44161-021-00001-9.

(33) Song, S.; Tien, C.-L.; Cui, H.; Basil, P.; Zhu, N.; Gong, Y.; Li, W.; Li, H.; Fan, Q.; Min Choi, J.; Luo, W.; Xue, Y.; Cao, R.; Zhou, W.; Ortiz, A. R.; Stork, B.; Mundra, V.; Putluri, N.; York, B.; Chu, M.; Chang, J.; Yun Jung, S.; Xie, L.; Song, J.; Zhang, L.; Sun, Z. Myocardial Rev-Erb-Mediated Diurnal Metabolic Rhythm and Obesity Paradox. *Circulation* **2022**, *145* (6), 448–464. https://doi.org/10.1161/CIRCULATIONAHA.121.056076.

(34) Reitz, C. J.; Alibhai, F. J.; Khatua, T. N.; Rasouli, M.; Bridle, B. W.; Burris, T. P.; Martino, T. A. SR9009 Administered for One Day after Myocardial Ischemia-Reperfusion Prevents Heart Failure in Mice by Targeting the Cardiac Inflammasome. *Communications Biology* **2019**, *2* (1), 1–15. https://doi.org/10.1038/s42003-019-0595-z.

(35) Dierickx, P.; Emmett, M. J.; Jiang, C.; Uehara, K.; Liu, M.; Adlanmerini, M.; Lazar, M. A. SR9009 Has REV-ERB–Independent Effects on Cell Proliferation and Metabolism. *Proceedings of the National Academy of Sciences* **2019**, *116* (25), 12147–12152. https://doi.org/10.1073/pnas.1904226116.

(36) Xu, H.; Zhang, J.; Zheng, X.; Tan, P.; Xiong, X.; Yi, X.; Yang, Y.; Wang, Y.; Liao, D.; Li, H.; Wei, Q.; Ai, J.; Yang, L. SR9009 Inhibits Lethal Prostate Cancer Subtype 1 by Regulating the LXRα/FOXM1 Pathway Independently of REV-ERBs. *Cell Death Dis* **2022**, *13* (11), 1–14. https://doi.org/10.1038/s41419-022-05392-6.

(37) Trump, R. P.; Bresciani, S.; Cooper, A. W. J.; Tellam, J. P.; Wojno, J.; Blaikley, J.; Orband-Miller, L. A.; Kashatus, J. A.; Boudjelal, M.; Dawson, H. C.; Loudon, A.; Ray, D.; Grant, D.; Farrow, S. N.; Willson, T. M.; Tomkinson, N. C. O. Optimized Chemical Probes for REV-ERBα. *J. Med. Chem.* **2013**, *56* (11), 4729–4737. https://doi.org/10.1021/jm400458q.

(38) Hooker, J. M.; Reibel, A. T.; Hill, S. M.; Schueller, M. J.; Fowler, J. S. One-Pot, Direct Incorporation of [$^{11}$C]$CO_2$ into Carbamates. *Angewandte Chemie International Edition* **2009**, *48* (19), 3482–3485. https://doi.org/10.1002/anie.200900112.

(39) Wilson, A. A.; Garcia, A.; Houle, S.; Vasdev, N. Direct Fixation of [$^{11}$C]-$CO_2$ by Amines: Formation of [$^{11}$C-*Carbonyl*]-Methylcarbamates. *Org. Biomol. Chem.* **2009**, *8* (2), 428–432. https://doi.org/10.1039/B916419G.

## 3.2. Synthesis of (*R*)- and (*S*)-[$^{11}$C]SR9009 for Rev-erb Imaging

Braeden A. Mair,[1,2] Benjamin H. Rotstein*[1,2,4]

[1] Department of Chemistry and Biomolecular Sciences, University of Ottawa, Ottawa, Canada K1H 8M5

[2] University of Ottawa Heart Institute, Ottawa, Canada K1Y 4W7

[4] Department of Biochemistry, Microbiology and Immunology, University of Ottawa, Ottawa, Canada K1H 8M5

Manuscript in preparation.

### 3.2.1. Statement of the manuscript

The manuscript "Synthesis of (*R*)- and (*S*)-[$^{11}$C]SR9009 for Rev-erb Imaging" is currently in preparation for submission. In this paper, I detail the production of a synthetic route to SR9009 that retains stereochemistry, along with the translation to carbon-11.

I completed the development of an enantiopure synthetic route to (*R*)- and (*S*)-radiolabelling precursors. I optimized the radiochemical labelling of [$^{11}$C]SR9009, and developed the conditions for isolation. I wrote the manuscript with editing from Dr. Benjamin Rostein. All authors approved the final version. Continued investigation with PET imaging is expected to be carried out by future graduate students.

### 3.2.2. Abstract

Current approaches to clinical care for myocardial infarction often lead to a profound inflammatory response that can pathologically progress towards more severe cardiac morbidities and heart failure. The body's intrinsic circadian clock has a strong influence on inflammation and the recruitment of inflammasomes. Pharmacological inhibition of a key circadian regulator, Rev-erb, with the agonist (±)-SR9009 has demonstrated therapeutic potential for remediation of reperfusion injury and improvement of clinical outcomes. Further investigation into the dynamics of Rev-erb and its role in cardiovascular disease can be achieved with molecular imaging; positron emission tomography is a nuclear medicine imaging modality harnessing radioactive small molecules to visualize biochemical processes. Radiolabelling of SR9009 with the PET radionuclide carbon-11 ($^{11}$C) was completed and optimized for radiotracer production and subsequent imaging studies. Additionally, enantiopure syntheses were developed to provide (*R*)- and (*S*)-[$^{11}$C]SR9009 for comparative analysis.

### 3.2.3. Introduction

Ischemic heart disease leading to myocardial infarction is a leading cause of morbidity and mortality.[1] Most patients make it to the hospital in time to receive the standard of care – reperfusion, the process of blockade removal within the artery thus restoring flow to the infarcted tissue – however this triggers a rapid inflammatory response known as 'reperfusion injury' in which the infarct region expands, and the heart undergoes deleterious cardiac remodelling with risk of pathological progression towards heart failure.[2] Although we cannot currently identify specific individuals at risk with sufficient precision, an alternative strategy is to therapeutically minimize this inflammatory trigger, reducing progression towards cardiac injury and improving clinical outcomes.[3,4]

Recent studies suggest a strong circadian influence on inflammatory processes warranting additional investigation into these pathways.[5,6] The circadian clock is an approximately 24-hour biological cycle that regulates behavioural and physiological functions. It is comprised of a primary feedback loop, containing transcription factors BMAL1 and CLOCK that heterodimerize to promote transcription of Period (PER) and Cryptochrome (CRY) genes. PER and CRY proteins inhibit transcriptional activity of the BMAL1/CLOCK heterodimer thereby repressing their own expression. A secondary loop modulates BMAL1 transcription; CLOCK and BMAL1 induce Rev-erb expression, which then ultimately represses BMAL1.[7] As a result, Rev-erb is thought to be a vital regulator of the circadian clock and the time-dependent oscillation of biochemical functionality.

Rev-erb proteins are members of the nuclear receptor superfamily 1, group D (NR1D). There are two forms of the receptor, Rev-erbα (NR1D1) and Rev-erbβ (NR1D2), and while more is currently known about the function of Rev-erbα, they're believed to play similar roles.[8] This important function in modulating circadian rhythm imparts regulatory control of copious biochemical processes including metabolism and inflammatory response.[9] In particular, the circadian regulatory mechanism plays an essential role in inflammasome and immunocyte recruitment to infarcted myocardial tissue.[10] With this understanding, subsequent the discovery of heme as the natural ligand of Rev-erb,[11,12] synthetic agonists and antagonists were designed for pharmaceutical intervention of the critical machinery.[13]

One such pharmaceutic is SR9009, a Rev-erb agonist with promising results for therapeutic intervention in the treatment of post-myocardial ischemia reperfusion injury.[14] However, SR9009

has, perhaps contradictorily, been found to act independent of Rev-erb in cell proliferation and metabolism, and in the immunological treatment of lethal prostate cancer subtype 1.[15,16] Investigation into the localization of administered SR9009 can elucidate which regulatory pathway offers primary control over inflammatory response and thus cardiac repair. Additionally, valuable information on the biochemical behaviour of Rev-erb can be gained from probing its dynamics post-myocardial infarction along with the effects of agonism with inhibitors like SR9009.

Positron emission tomography (PET) is a non-invasive, nuclear medicine imaging technique used to visualize biochemical processes by harnessing the decay properties of radiolabelled probes. Radiotracers, often drug-like as small molecules or peptides, are prepared by labelling with radioactive isotopes which, upon decay, can be visualized using PET cameras. Carbon-11 ($^{11}$C) is a frequently used PET isotope with a half-life of 20.4 minutes. Due to the abundance of carbon in organic scaffolding, carbon-11 is an invaluable radioisotope thanks to the theoretical potential to label any organic drug molecule. Carbon-11 is most frequently produced from a cyclotron as carbon dioxide, and several methods have been developed to apply this in radiochemical syntheses to achieve more complex radiotracer candidates.[17,18] As simultaneously discovered by Hooker et al. and Wilson et al., $^{11}$C-carbamates can be accessed with [$^{11}$C]$CO_2$ direct from the cyclotron.[19,20] This radiosynthesis offers a potential route towards radiolabelling SR9009 to reveal crucial findings on its pharmaceutical properties.

We describe herein a novel synthetic approach, followed by radiosynthesis of (*R*)- and (*S*)-[$^{11}$C]SR9009 for the purposes of PET analysis in murine models.

### 3.2.4. Materials and Methods

*3.2.4.1. Precursor and Standard Synthesis*

SR9009 has two enantiomeric forms, (*R*)- and (*S*)-SR9009, dependent on the stereochemistry of the bond connecting the pyrrolidine. Due to potential differences in imaging and pharmaceutical characteristics[21–23] it was important to first develop a synthetic route that begins with enantiopure starting materials and avoids racemization throughout. SR9009 was therefore prepared by a multistep pathway according to literature methods with minor modifications to ensure conservation of the stereocenter.[13] Polarimetry was used to validate enantiomeric enrichment – 10 mg of sample was dissolved in dichloromethane and tested on the polarimeter.

*N*-(4-chlorobenzyl)-1-(5-nitrothiophen-2-yl)methanamine (**3**): 5-nitrothiophene-2-carboxaldehyde (**1**, 0.57 g, 3.6 mmol) was added to a solution of 4-chlorobenzylamine (**2**, 0.44 mL, 3.6 mmol) in dichloroethane (12.0 mL) at room temperature. After the mixture was stirred for 5 min, sodium triacetoxyborohydride (1.10 g, 5.0 mmol) was added at room temperature. The solution was stirred for 16 hours before the mixture was quenched with saturated aqueous $NaHCO_3$. Extraction with EtOAc and purification via column chromatography (20–60% EtOAc in hexanes) provides the title compound as a pale-yellow oil (26%). $^1$H-NMR (80 MHz, $CDCl_3$): δ 7.80 (m, 1H), 7.30 (m, 4H), 6.87 (m, 1H), 3.99 (m, 2H), 3.83 (s, 2H). MS-ESI: *m/*z calculated $C_{12}H_{11}ClN_2O_2S$ as 282.02, [M+H] found as 283.04.

*Tert*-butyl 3-formylpyrrolidine-1-carboxylate (**5R** and **5S**): To a solution of (R or S)-*tert*-butyl 3-(hydroxymethyl)pyrrolidine-1-carboxylate (**4R** or **4S**) in DCM (0.17 M) was added Dess-Martin Periodinane (1.5 equiv.) at room temperature. To the stirred solution was then slowly added $H_2O$ (1.1 equiv.) after which the suspension turned completely white. Stirring was continued for 1 h followed by the addition of $Et_2O$ (0.02 M w.r.t the alcohol) and the resulting suspension was gently concentrated *in vacuo* to a few mL after which $Et_2O$ was added. The solution was washed with 1:1 $NaHCO_3$ and $Na_2S_2O_3$ until the phases become clear. Extraction with $Et_2O$ and purification via column chromatography (20–60% EtOAc in hexanes) provides the title compound as a colourless oil (30% R, 28% S). $^1$H-NMR (80 MHz, $CDCl_3$): δ 9.69 (s, 1H), 3.75–3.44 (m, 4H), 3.38–2.87 (m, 1H), 2.27–2.08 (m, 2H), 1.46 (s, 9H). LR MS-ESI: *m/*z calculated $C_6H_9NO_3$ as 143.06, [M+H – *t*Bu] found as 144.01.

*Tert*-butyl-3-({[(4-chlorobenzyl)(5-nitrothiophen-2-yl)methyl]amino}methyl)pyrrolidine-1-carboxylate (**6R** and **6S**): To a solution of *N*-(4-chlorobenzyl)-1-(5-nitrothiophen-2-yl)methanamine (**3**, 70 mg) in DCE (1 mL) was added *tert*-butyl 3-formylpyrrolidine-1-carboxylate (**5R** or **5S**, 74 mg) followed by $NaBH(OAc)_3$ (106 mg). The reaction was left at room temperature with stirring overnight. The mixture was diluted with EtOAc and saturated aqueous $NaHCO_3$ and the layers were separated. The organic layer was washed with saturated aqueous $NaHCO_3$, brine, dried with $MgSO_4$, concentrated, and purified by column chromatography (30–70% EtOAc in hexanes) to give the title compound (46% R, 51% S), which was then immediately deprotected. LR MS-ESI: *m/z* calculated $C_{18}H_{20}ClN_3O_4S$ as 409.09, [M+H – *t*Bu] found as 410.24.

3-({[(4-chlorophenyl)methyl][(5-nitrothiophen-2-yl)methyl]azaniumyl}methyl)pyrrolidin-1-ium dichloride salt (**7R** and **7S**, precursor): To a vial of **6R** or **6**S was added 2 mL of 4 M HCl

in dioxane. The reaction mixture was stirred for 1 hour, then concentrated to yield the title compound. $^{1}$H-NMR (80 MHz, $CDCl_3$): δ 7.77 (m, 1H), 7.29 (m, 4H), 6.83 (m, 1H), 3.73 (m, 2H), 2.95–3.69 (m, 6H), 2.44 (m, 3H), 1.88 (m, 1H), 1.44 (m, 1H). LR MS-ESI: *m/z* calculated $C_{17}H_{20}ClN_3O_2S$ as 365.10, [M+H] found as 366.22.

Ethyl-3-({[(4-chlorophenyl)methyl][(5-nitrothiophen-2-yl)methyl]amino}methyl) pyrrolidine-1-carboxylate (**8R** and **8S**, standard): To a solution of **7R** or **7S** in DCM (2 mL) was added $NEt_3$ (0.1 mL) and ethyl chloroformate (0.1 mL). The reaction was stirred for 1 h, before being diluted with EtOAc and saturated aqueous $NaHCO_3$, and being separated. The organic layer was dried with $MgSO_4$, concentrated, and purified by column chromatography (30–70% EtOAc in hexanes) to give the title compound (70%). $^{1}$H-NMR (80 MHz, $CDCl_3$): δ 7.79 (m, 1H), 7.31 (m, 4H), 6.85 (m, 1H), 4.12 (m, 2H), 3.74 (m, 2H), 3.60 (m, 2H), 3.11 (m, 4H), 2.46 (m, 2H), 1.84 (m, 3H), 1.25 (m, 3H). LR MS-ESI: *m/z* calculated $C_{20}H_{24}ClN_3O_4S$ as 437.12, [M+H] found as 438.10.

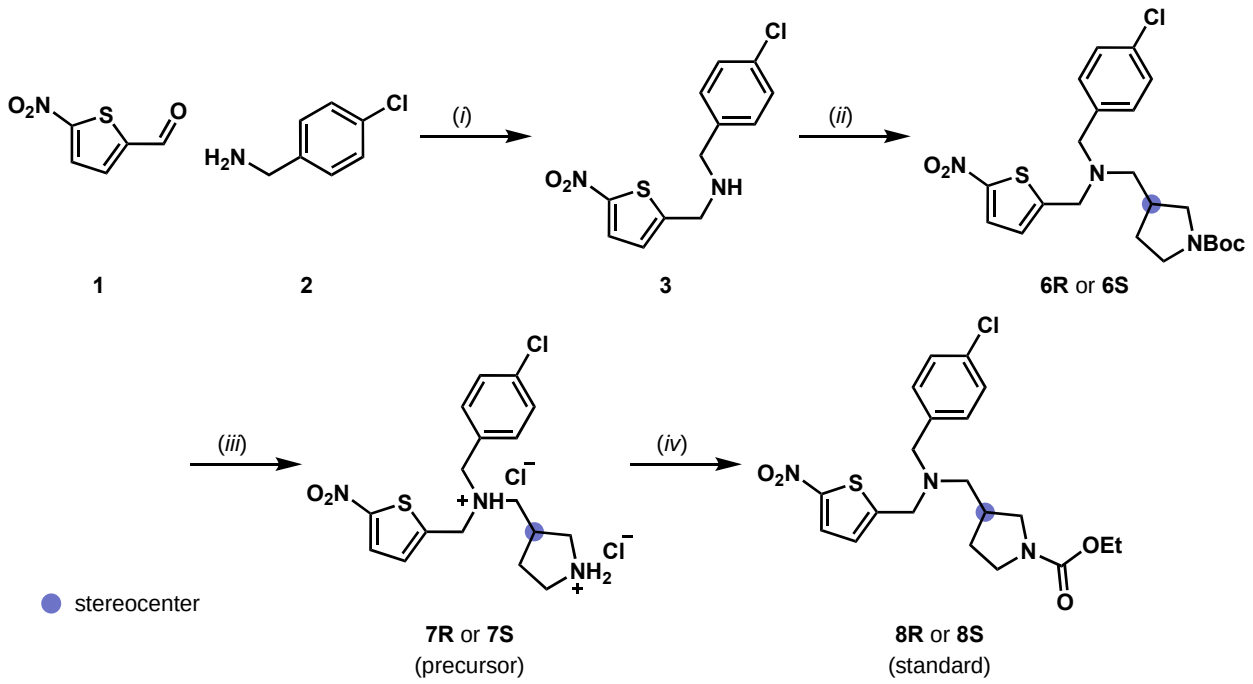


**Figure 3.3.** Synthesis of [$^{11}$C]SR9009 standard and precursor. Reagents and conditions: (i) $NaBH(OAc)_3$, DCE, r.t., 24 h, 26%; (ii) (*R*)-1-Boc-pyrrolidine-3-carboxaldehyde or (*S*)-1-Boc-pyrrolidine-3-carboxaldehyde (prepared as previously described), $NaBH(OAc)_3$, DCE, r.t., 1 h, 46% R yield, 51% S yield; (iii) 4 M HCl in dioxane, r.t., 1 h, quantitative; (iv) $NEt_3$, ethyl chloroformate, DCM, r.t., 1 h, yield 70% R yield, 72% S yield.

*3.2.4.2. Radiotracer Synthesis*

Radiochemistry was performed on a Synthra MeIplus Research module. Solutions of precursor (**7R** or **7S**, 25 mM), bromoethane (300 mM.), and BEMP (75 mM) were prepared in anhydrous *N*,*N*-dimethylformamide (DMF). Aliquots (100 μL) of each were added directly to the reactor, which was then sealed. [$^{11}$C]Carbon dioxide ([$^{11}$C]$CO_2$) produced from the cyclotron was trapped in a steel coil at -180 °C, which was then subsequently heated to 25 °C under a stream of helium at 3 mL/min to deliver [$^{11}$C]$CO_2$ into the reaction solution. The amount of [$^{11}$C]$CO_2$ was monitored until peak activity, after which the reactor was sealed off and left to react for 10 minutes at 40 °C. For optimization studies, 700 μL of 1 M HCl was added to the reactor, the solution was purged with helium, and the resulting mixture was transferred to a vial fitted with a vent needle. The crude reaction was sampled and analyzed by radioHPLC to determine radiochemical conversion (RCC) and trapping efficiency (TE). RCC was determined by integration of radiation detector chromatograms. TE was determined from decay-corrected measurements of activity in the post-quench solution to the peak activity in the steel coil.

For preparative studies, the crude mixture was diluted with 0.7 mL of 0.1 M AMF before being purified by high-performance liquid chromatography (HPLC) using a Luna C18 column (10 μ, 100 Å, 250 x 10 mm) with increasing concentrations of acetonitrile in 0.1 M ammonium formate (70% for 7 minutes, 90% for 13 minutes). The product was collected in a bulk vessel charged with 20 mL of $H_2O$ and passed through a Sep-Pak C18 Plus Light cartridge. The cartridge was first washed with 10 mL of $H_2O$ before being eluted with multiple fractions of 0.1 mL of EtOH. The most concentrated fraction was selected and diluted with saline (1.9 mL), after which the contents were passed through a 0.22 μm sterile filter. Quality control analysis was performed with co-injection of the nonradioactive standard using a Waters 2695 Alliance HPLC equipped with a Phenomenex Luna C18 (10 μm, 100 Å, 250 mm x 4.6 mm) column, Waters 2487 Dual λ Absorbance Detector, and a Carroll & Ramsey Associates 105-S high-sensitivity radiation detector. Radiochemical yield (RCY) and molar activity ($A_m$) were decay-corrected to end of synthesis.

### 3.2.5. Results and Discussion

*3.2.5.1. Enantiopure Synthesis*

Treatment of 5-nitrothiophene-2-carboxaldehyde (**1**) with chlorobenzylamine (**2**) in the presence of sodium triacetoxyborohydride provided the secondary amine **3**. This was further reacted with both (*R*)- and (*S*)-pyrrolidine carboxaldehyde prepared from oxidations of their corresponding alcohol to yield the tertiary amines **6R** and **6S**. This intermediate could then be Boc-deprotected to provide the radiolabelling precursor (**7R** and **7S**), and then further reacted with triethylamine and ethyl chloroformate to access (*R*)- and (*S*)-SR9009 (**8R** or **8S**). Stereochemistry was retained throughout the synthesis, as measured by polarimetry (protected precursor S = -12.6, R = +13.2; standard S = -9.0, R = +10.6). The precursor was prepared as a hydrochloride salt to be stored for longer periods of time.

*3.2.5.2. Radiochemistry*

Initial attempts to label the precursor according to literature methods resulted in no reaction (Figure 3.4). Conditions were therefore first narrowed down with a model substrate to conserve precursor (Supplemental Figure S1). Additional base improved trapping but led to significant degradation of the precursor and therefore no reactivity (entry 2). Lowering the temperature drastically improved the yields, providing both (*R*)- and (*S*)-[$^{11}$C]SR9009 in 7 and 6% yields (entries 3–4). Continued lowering of the temperature disabled reactivity (entries 5–6). Due to the poor stability of the precursor in the basic medium, a 1-minute reaction was attempted with a significant improvement to conversion and doubling of the yields (entry 7). Alternative bases did not perform as well as BEMP (entries 8–9).

Automated radiosynthesis was established to produce (*R*)- and (*S*)-[$^{11}$C]SR9009 in 13% decay-corrected yield 20 minutes after [$^{11}$C]$CO_2$ delivery. Molar activity was determined to be 6 GBq $\mu$mol$^{-1}$ at the end of synthesis.

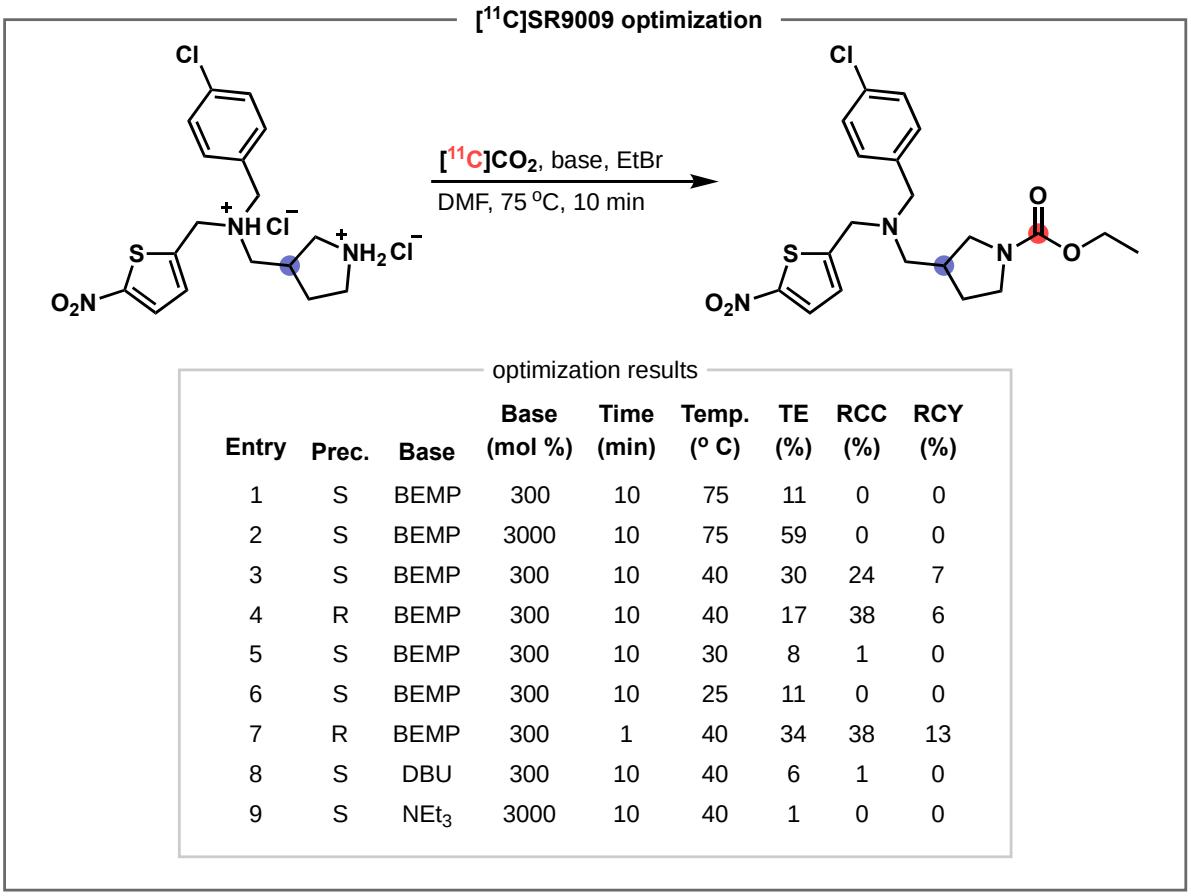


| Entry | Prec. | Base | Base (mol %) | Time (min) | Temp. (° C) | TE (%) | RCC (%) | RCY (%) |
|---|---|---|---|---|---|---|---|---|
| 1 | S | BEMP | 300 | 10 | 75 | 11 | 0 | 0 |
| 2 | S | BEMP | 3000 | 10 | 75 | 59 | 0 | 0 |
| 3 | S | BEMP | 300 | 10 | 40 | 30 | 24 | 7 |
| 4 | R | BEMP | 300 | 10 | 40 | 17 | 38 | 6 |
| 5 | S | BEMP | 300 | 10 | 30 | 8 | 1 | 0 |
| 6 | S | BEMP | 300 | 10 | 25 | 11 | 0 | 0 |
| 7 | R | BEMP | 300 | 1 | 40 | 34 | 38 | 13 |
| 8 | S | DBU | 300 | 10 | 40 | 6 | 1 | 0 |
| 9 | S | $NEt_3$ | 3000 | 10 | 40 | 1 | 0 | 0 |

**Figure 3.4.** Radiochemical optimization for [$^{11}$C]SR9009. Conditions were evaluated to determine their effects on trapping efficiency and radiochemical conversion.

### 3.2.6. Conclusion

In conclusion, [$^{11}$C]SR9009 has been labelled using optimized [$^{11}$C]$CO_2$-fixation radiochemistry. Both enantiomers of the labelling precursors were prepared with stereochemically-conserving syntheses to target (*R*)- and (*S*)-[$^{11}$C]SR9009 for imaging. Animal studies can subsequently be performed to determine localization and dynamics of Rev-erb within murine models.

### 3.2.7. Acknowledgement

The authors would like to thank Dr. Tami Martino and Dr. Cristine Reitz for their discussions on SR9009, and the role of the circadian clock in cardiovascular disease.

### 3.2.8. References

(1) Laforgia, P. L.; Auguadro, C.; Bronzato, S.; Durante, A. The Reduction of Mortality in Acute Myocardial Infarction: From Bed Rest to Future Directions. *International Journal of Preventive Medicine* **2022**, *13* (1), 56. https://doi.org/10.4103/ijpvm.IJPVM_122_20.

(2) Neri, M.; Riezzo, I.; Pascale, N.; Pomara, C.; Turillazzi, E. Ischemia/Reperfusion Injury Following Acute Myocardial Infarction: A Critical Issue for Clinicians and Forensic Pathologists. *Mediators of Inflammation* **2017**, *2017* (1), 7018393. https://doi.org/10.1155/2017/7018393.

(3) Frangogiannis, N. G. Regulation of the Inflammatory Response in Cardiac Repair. *Circulation Research* **2012**, *110* (1), 159–173. https://doi.org/10.1161/CIRCRESAHA.111.243162.

(4) Epelman, S.; Liu, P. P.; Mann, D. L. Role of Innate and Adaptive Immune Mechanisms in Cardiac Injury and Repair. *Nat Rev Immunol* **2015**, *15* (2), 117–129. https://doi.org/10.1038/nri3800.

(5) Zeng, Y.; Guo, Z.; Wu, M.; Chen, F.; Chen, L. Circadian Rhythm Regulates the Function of Immune Cells and Participates in the Development of Tumors. *Cell Death Discov.* **2024**, *10* (1), 1–17. https://doi.org/10.1038/s41420-024-01960-1.

(6) Aziz, I. S.; McMahon, A. M.; Friedman, D.; Rabinovich-Nikitin, I.; Kirshenbaum, L. A.; Martino, T. A. Circadian Influence on Inflammatory Response during Cardiovascular Disease. *Current Opinion in Pharmacology* **2021**, *57*, 60–70. https://doi.org/10.1016/j.coph.2020.11.007.

(7) Buhr, E. D.; Takahashi, J. S. Molecular Components of the Mammalian Circadian Clock. In *Circadian Clocks*; Kramer, A., Merrow, M., Eds.; Springer: Berlin, Heidelberg, 2013; pp 3–27. https://doi.org/10.1007/978-3-642-25950-0_1.

(8) Ikeda, R.; Tsuchiya, Y.; Koike, N.; Umemura, Y.; Inokawa, H.; Ono, R.; Inoue, M.; Sasawaki, Y.; Grieten, T.; Okubo, N.; Ikoma, K.; Fujiwara, H.; Kubo, T.; Yagita, K. REV-ERBα and REV-ERBβ Function as Key Factors Regulating Mammalian Circadian Output. *Sci Rep* **2019**, *9* (1), 10171. https://doi.org/10.1038/s41598-019-46656-0.

(9) Fagiani, F.; Di Marino, D.; Romagnoli, A.; Travelli, C.; Voltan, D.; Di Cesare Mannelli, L.; Racchi, M.; Govoni, S.; Lanni, C. Molecular Regulations of Circadian Rhythm and Implications for Physiology and Diseases. *Sig Transduct Target Ther* **2022**, *7* (1), 1–20. https://doi.org/10.1038/s41392-022-00899-y.

(10) Alibhai, F. J.; Tsimakouridze, E. V.; Chinnappareddy, N.; Wright, D. C.; Billia, F.; O'Sullivan, M. L.; Pyle, W. G.; Sole, M. J.; Martino, T. A. Short-Term Disruption of Diurnal Rhythms After Murine Myocardial Infarction Adversely Affects Long-Term Myocardial Structure and Function. *Circulation Research* **2014**, *114* (11), 1713–1722. https://doi.org/10.1161/CIRCRESAHA.114.302995.

(11) Raghuram, S.; Stayrook, K. R.; Huang, P.; Rogers, P. M.; Nosie, A. K.; McClure, D. B.; Burris, L. L.; Khorasanizadeh, S.; Burris, T. P.; Rastinejad, F. Identification of Heme as the Ligand for the Orphan Nuclear Receptors REV-ERBα and REV-ERBβ. *Nat Struct Mol Biol* **2007**, *14* (12), 1207–1213. https://doi.org/10.1038/nsmb1344.

(12) Yin, L.; Wu, N.; Curtin, J. C.; Qatanani, M.; Szwergold, N. R.; Reid, R. A.; Waitt, G. M.; Parks, D. J.; Pearce, K. H.; Wisely, G. B.; Lazar, M. A. Rev-Erbα, a Heme Sensor That Coordinates Metabolic and Circadian Pathways. *Science* **2007**, *318* (5857), 1786–1789. https://doi.org/10.1126/science.1150179.

(13) Solt, L. A.; Wang, Y.; Banerjee, S.; Hughes, T.; Kojetin, D. J.; Lundasen, T.; Shin, Y.; Liu, J.; Cameron, M. D.; Noel, R.; Yoo, S.-H.; Takahashi, J. S.; Butler, A. A.; Kamenecka, T. M.; Burris, T. P. Regulation of Circadian Behaviour and Metabolism by Synthetic REV-ERB Agonists. *Nature* **2012**, *485* (7396), 62–68. https://doi.org/10.1038/nature11030.

(14) Reitz, C. J.; Alibhai, F. J.; Khatua, T. N.; Rasouli, M.; Bridle, B. W.; Burris, T. P.; Martino, T. A. SR9009 Administered for One Day after Myocardial Ischemia-Reperfusion Prevents Heart Failure in Mice by Targeting the Cardiac Inflammasome. *Communications Biology* **2019**, *2* (1), 1–15. https://doi.org/10.1038/s42003-019-0595-z.

(15) Dierickx, P.; Emmett, M. J.; Jiang, C.; Uehara, K.; Liu, M.; Adlanmerini, M.; Lazar, M. A. SR9009 Has REV-ERB–Independent Effects on Cell Proliferation and Metabolism. *Proceedings of the National Academy of Sciences* **2019**, *116* (25), 12147–12152. https://doi.org/10.1073/pnas.1904226116.

(16) Xu, H.; Zhang, J.; Zheng, X.; Tan, P.; Xiong, X.; Yi, X.; Yang, Y.; Wang, Y.; Liao, D.; Li, H.; Wei, Q.; Ai, J.; Yang, L. SR9009 Inhibits Lethal Prostate Cancer Subtype 1 by Regulating the LXRα/FOXM1 Pathway Independently of REV-ERBs. *Cell Death Dis* **2022**, *13* (11), 1–14. https://doi.org/10.1038/s41419-022-05392-6.

(17) Rotstein, B. H.; Liang, S. H.; Holland, J. P.; Collier, T. L.; Hooker, J. M.; Wilson, A. A.; Vasdev, N. $^{11}CO_2$ Fixation: A Renaissance in PET Radiochemistry. *Chem Comm* **2013**, *49* (50), 5621. https://doi.org/10.1039/c3cc42236d.

(18) Rotstein, B. H.; Liang, S. H.; Placzek, M. S.; Hooker, J. M.; Gee, A. D.; Dollé, F.; Wilson, A. A.; Vasdev, N. $^{11}C$=O Bonds Made Easily for Positron Emission Tomography Radiopharmaceuticals. *Chem Soc Rev* **2016**, *45* (17), 4708–4726. https://doi.org/10.1039/C6CS00310A.

(19) Hooker, J. M.; Reibel, A. T.; Hill, S. M.; Schueller, M. J.; Fowler, J. S. One-Pot, Direct Incorporation of [$^{11}C]CO_2$ into Carbamates. *Angewandte Chemie International Edition* **2009**, *48* (19), 3482–3485. https://doi.org/10.1002/anie.200900112.

(20) Wilson, A. A.; Garcia, A.; Houle, S.; Vasdev, N. Direct Fixation of [$^{11}C$]-$CO_2$ by Amines: Formation of [$^{11}C$-*Carbonyl*]-Methylcarbamates. *Org. Biomol. Chem.* **2009**, *8* (2), 428–432. https://doi.org/10.1039/B916419G.

(21) Chau, W.-F.; Black, A. M. A.; Clarke, A.; Durrant, C.; Gausemel, I.; Khan, I.; Mantzilas, D.; Oulie, I.; Rogstad, A.; Trigg, W.; Jones, P. A. Exploration of the Impact of Stereochemistry on the Identification of the Novel Translocator Protein PET Imaging Agent [$^{18}F$]GE-180. *Nuclear Medicine and Biology* **2015**, *42* (9), 711–719. https://doi.org/10.1016/j.nucmedbio.2015.05.004.

(22) McConathy, J.; Owens, M. J. Stereochemistry in Drug Action. *Prim Care Companion CNS Disord* **2003**, *5* (2), 23324. https://doi.org/10.4088/PCC.v05n0202.

(23) Brocks, D. R. Drug Disposition in Three Dimensions: An Update on Stereoselectivity in Pharmacokinetics. *Biopharmaceutics & Drug Disposition* **2006**, *27* (8), 387–406. https://doi.org/10.1002/bdd.517.

## 3.3. Supplementary Information

### 3.3.1. Characterization

*N*-(4-chlorobenzyl)-1-(5-nitrothiophen-2-yl)methanamine

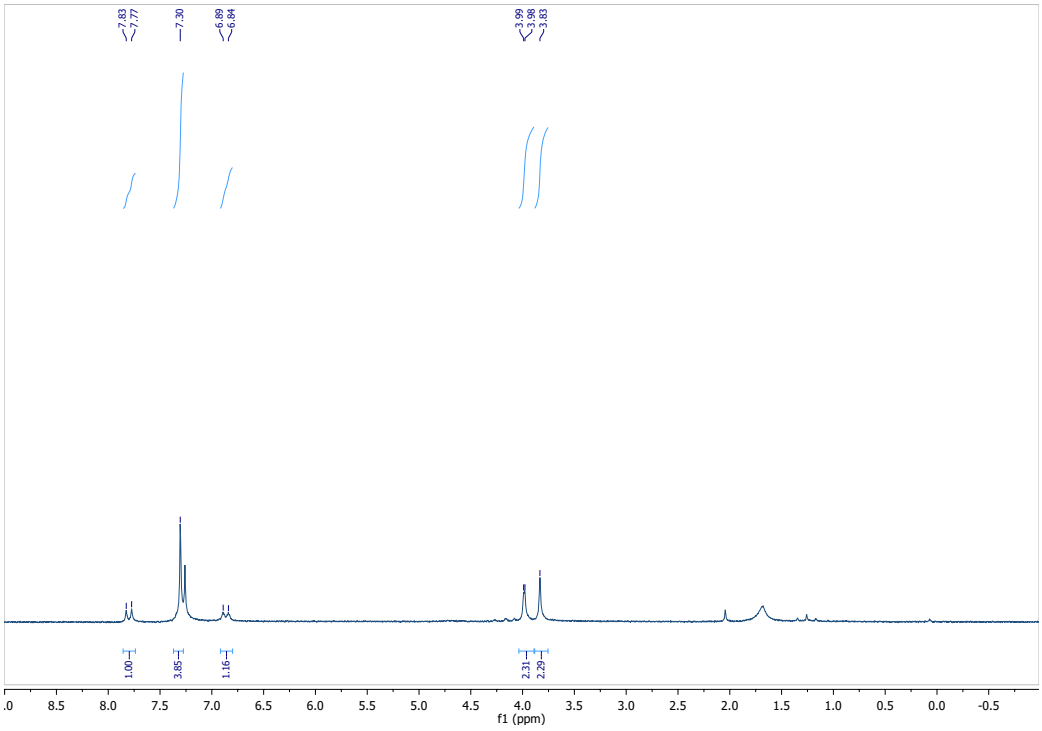

*Tert*-butyl 3-formylpyrrolidine-1-carboxylate

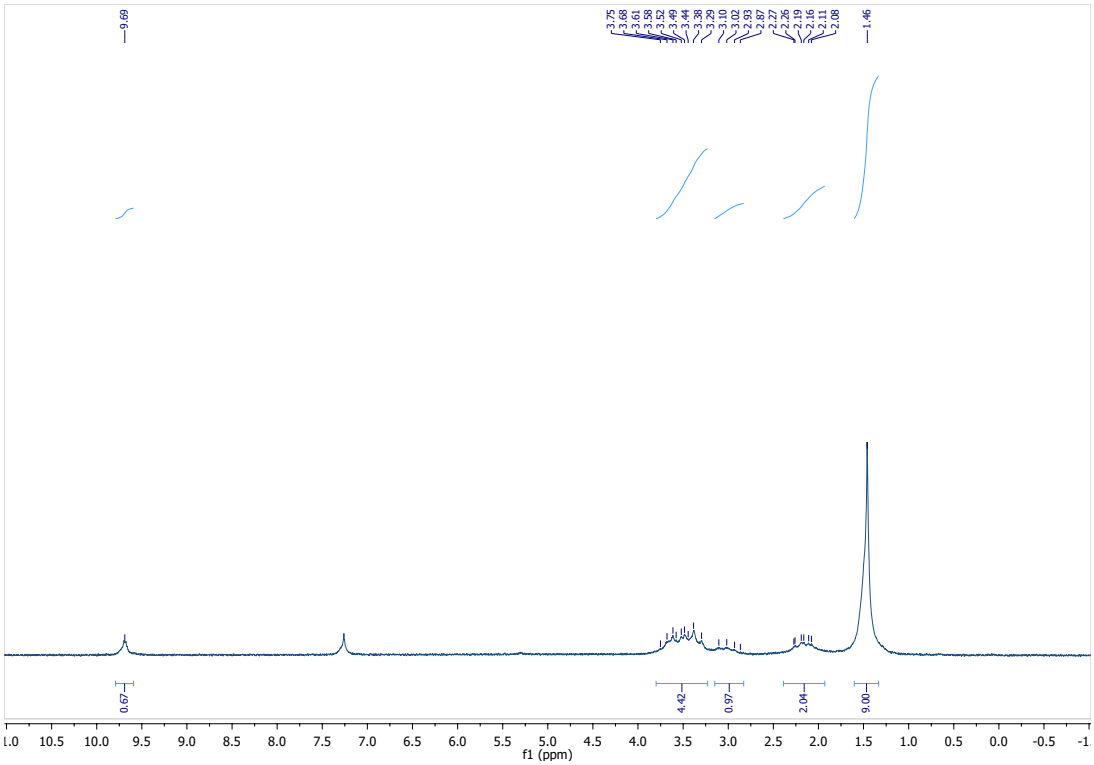

*N*-(4-chlorobenzyl)-1-(5-nitrothiophen-2-yl)-*N*-(pyrrolidine-3-ylmethyl)methanamine (contains residual EtOAc)

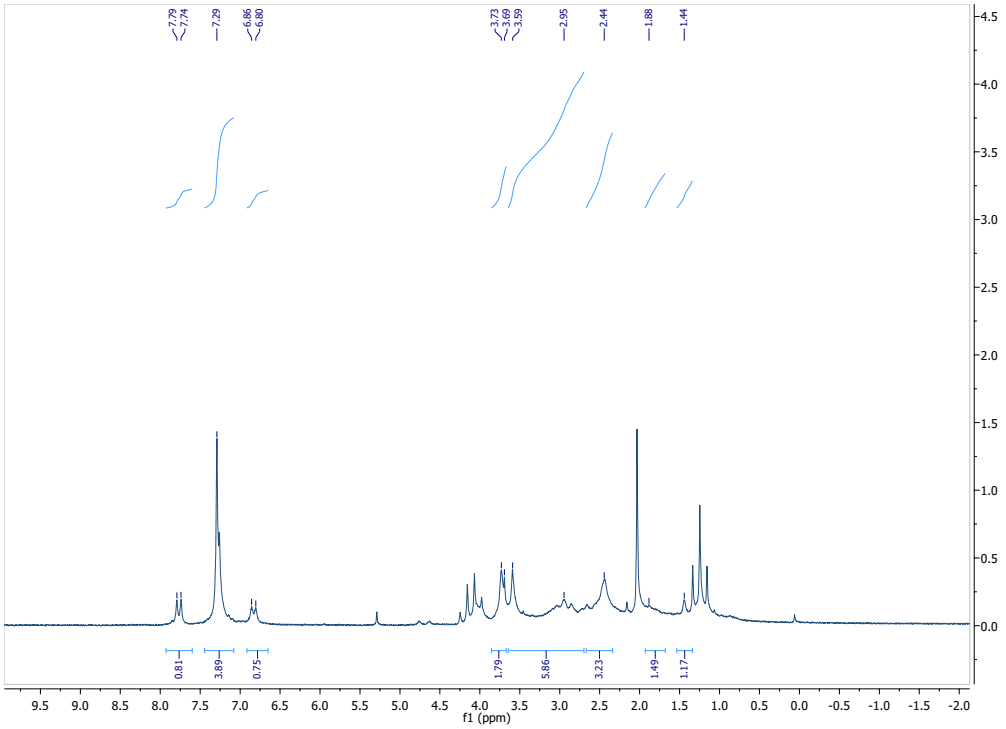


Ethyl-3-({[(4-chlorophenyl)methyl][(5-nitrothiophen-2-yl)methyl]amino}methyl) pyrrolidine-1-carboxylate (*R*)

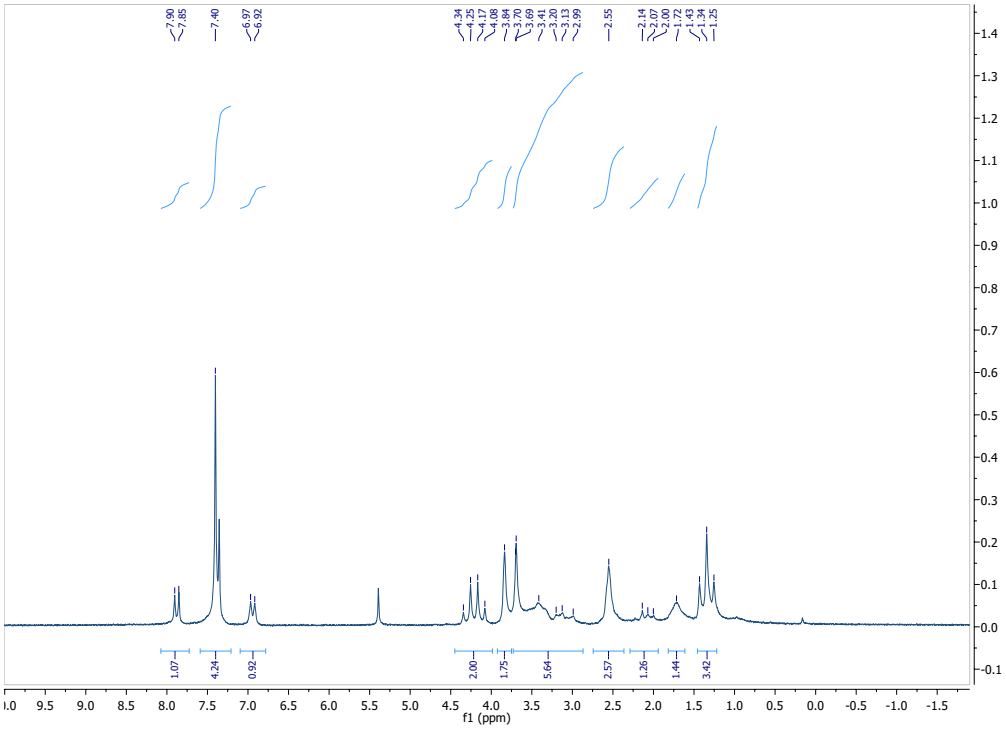

(*S*)

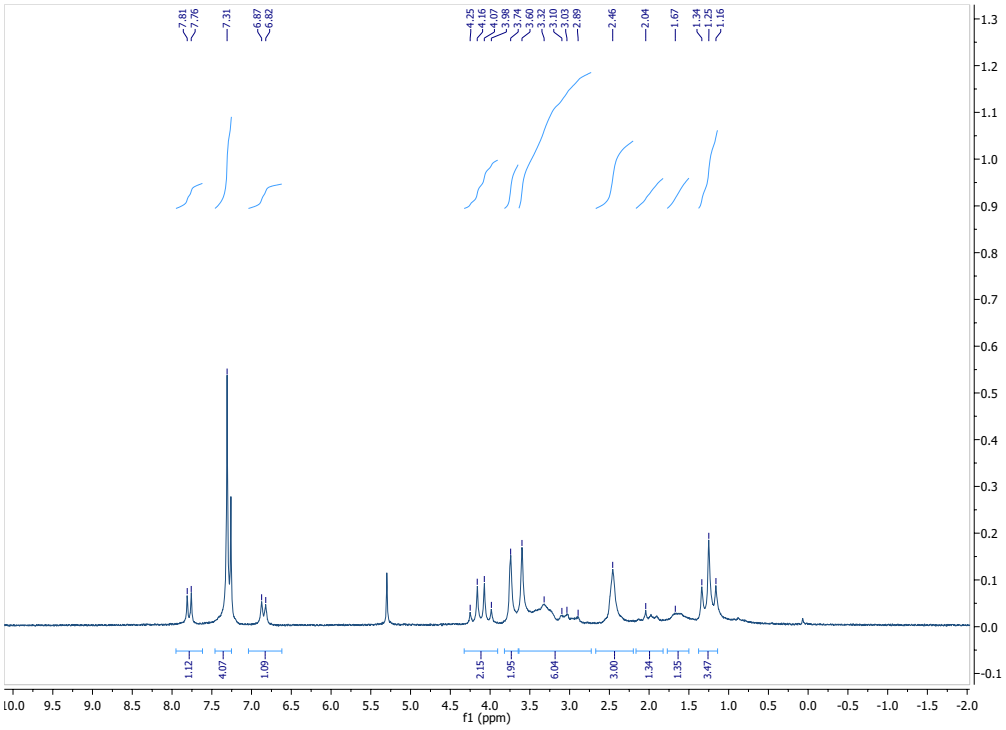
7.81
7.76
7.31
6.87
6.82
4.25
4.16
4.07
3.98
3.74
3.60
3.32
3.10
3.03
2.89
2.46
2.04
1.67
1.34
1.25
1.16
1.12
4.07
1.09
2.15
1.95
6.04
3.00
1.34
1.35
3.47
f1 (ppm)

## 3.4. Extended Discussion

### 3.4.1. Lessons

Given the poor throughput yield of the precursor synthesis, to conserve product we turned towards a model substrate for establishing a baseline on reaction conditions. Both 2-phenylpiperidine and 4-phenylpiperidine were evaluated; the presence of a conjugated system branching from a heterocycloalkane offered a representative reaction scaffold with which we could optimize more efficiently. The amine in both piperidine and pyrrolidine have similar $pK_a$'s (~11), and therefore should offer similarities in their behaviour with $^{11}C$-carboxylation.

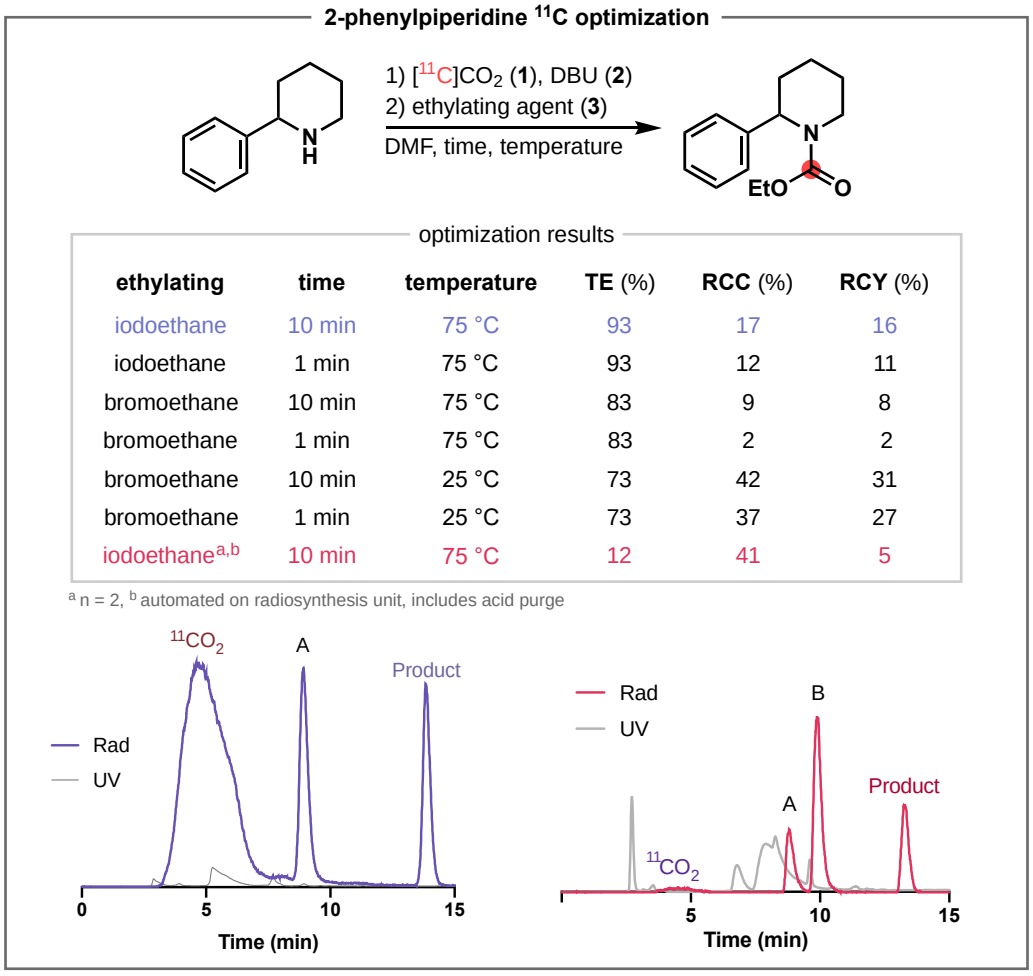


**Figure 3.5.** Model optimization with 2-phenylpiperidine. Initial manual optimization of 2-phenylpiperidine proceeded accordingly. However, upon addition of an acid purge in the automated synthesis, a secondary product formed in high yields. This model was therefore deemed inaccurate for optimization.

Beginning first with 2-phenylpiperidine, we completed a brief optimization scope evaluating the literature conditions (Figure 3.6). We began to narrow down conditions that improved the synthesis, like a decrease in temperature, but upon translation to an automated radiosynthesis unit we discovered a new major side product forming (product B). We theorized that this product was an intramolecular ring closure, forming a tetrahydropyridine isoindolone, a class of compounds known as valmerins.[1] After working with similar targets in our work with intramolecular Friedel-crafts acylations as described in a previous chapter, we tested a readily available standard to confirm the identity of the valmerins side product. Our hypothesis was that this was occurring through formation of the desired carbamate, followed by extrusion of an ethanol leaving group to form the new ring (Figure 3.7).

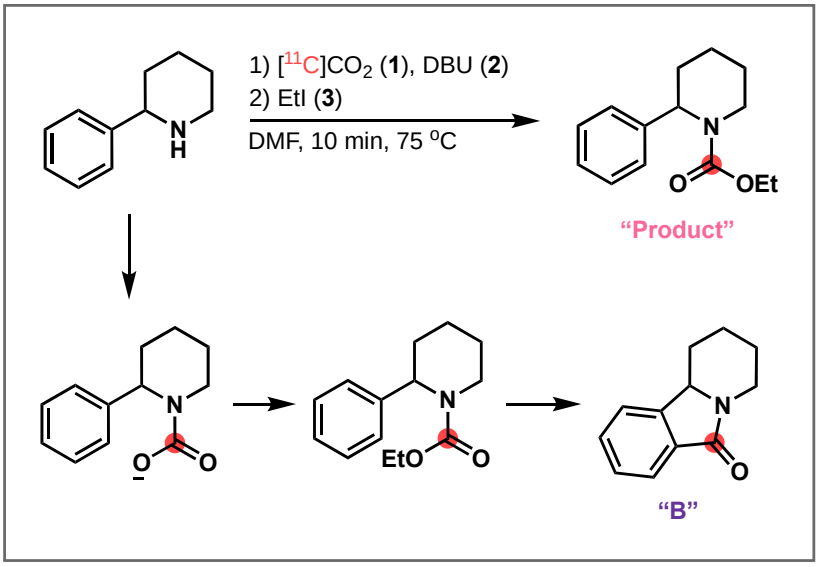


**Figure 3.6.** Proposed mechanism for valmerin synthesis. The primary side product is believed to occur by initial formation of the desired product, followed by a ring closure mediated by base in the reaction pot.

Determining that this would not be an accurate model for labelling of SR9009, we instead evaluated 4-phenylpiperidine using the established literature conditions with iodoethane and DBU at 75 °C, providing the desired product in 6% RCY overall (Figure 3.8). Yields doubled by switching to a milder ethylating agent in bromoethane. We sought to evaluate the identity of the major side product, believing it to possibly be an adduct of $^{11}CO_2$ and DBU with the ethylating agent that forms prior to the $^{11}C$-carboxylation of the amine; we tested the differences in the

reaction when the ethylating agent was added separately *after* bubbling of $^{11}CO_2$ and observed significant improvements in conversion. This side product was eliminated however, and yields improved dramatically, when using BEMP in place of DBU – we yielded our desired product in 43% RCY with near quantitative conversion.

**4-phenylpiperidine $^{11}$C optimization**

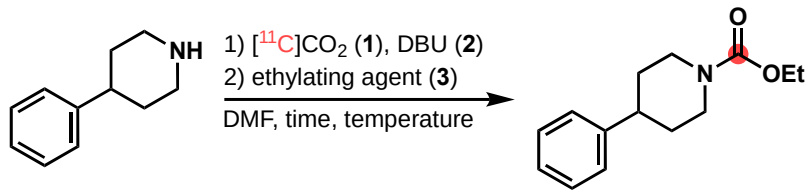


optimization results

| ethylating | time | temperature | TE (%) | RCC (%) | RCY (%) |
|---|---|---|---|---|---|
| iodoethane | 10 min | 75 °C | 15 | 43 | 6 |
| iodoethane | 10 min | 100 °C | 16 | 22 | 4 |
| bromoethane | 10 min | 75 °C | 17 | 83 | 14 |
| bromoethane | 10 min | 100 °C | 25 | 82 | 21 |
| bromoethane | 10 min | 50 °C | 27 | 55 | 15 |
| bromoethane | 5 min | 75 °C | 20 | 75 | 15 |
| bromoethane | 1 min | 75 °C | 25 | 65 | 16 |
| bromoethane[a] | 10 min | 100 °C | 13 | 90 | 12 |
| bromoethane[b] | 10 min | 100 °C | 11 | 85 | 9 |
| bromoethane[c] | 10 min | 100 °C | **44** | **98** | **43** |
| ethyl triflate | 10 min | 75 °C | 4 | 0 | 0 |

[a] order of addition: dbu/amine + $co_2$, then etbr; [b] 2 equiv DBU [c] BEMP instead of DBU

**Figure 3.7.** Model optimization with 4-phenylpiperidine. Optimization was determined to be more appropriate with the 4-phenylpiperidine scaffold to avoid the intramolecular side product observed previously. Upon changing to BEMP and a milder ethylating agent in bromoethane, the reaction yields improved dramatically.

Translation to the SR9009 precursor scaffold presented significant side products as well. Most could be explained by precursor/standard degradation; evaluations of stability for SR9009 and its precursor under the reaction conditions indicated exceptionally poor tolerance for basic conditions, and thus strict control of equivalents of BEMP were necessary. Additional side products were not identified.

### 3.4.2. Perspectives

#### *3.4.2.1. Conclusions*

In this part of the thesis, we wished to develop a radiotracer based on the Rev-erb agonist, SR9009. We adapted and optimized a literature method for the preparation of $^{11}$C-carbamates in order to access [$^{11}$C]SR9009 for imaging studies. An enantioselective precursor synthesis was developed to produce (*R*)- and (*S*)-[$^{11}$C]SR9009, both to provide a novel approach to yield enantiopure product, and to evaluate differences in imaging characteristics based on the chosen enantiomer.

#### *3.4.2.2. Future Directions*

Imaging with [$^{11}$C]SR9009 will follow. Assessment of specific uptake into tissues or organs of interest is merely the beginning of potential imaging studies that can be performed, however. Given the time-dependent expression of Rev-erb as a result of the feedback loop of the circadian cycle, evaluations of tracer uptake and distribution at various times throughout the day could provide interesting differences to observe. Nearly every cell contains its own circadian clock, and so variations in when certain tissues express Rev-erb at its highest level of expression could result in image characteristics that vary by the hour.

Additionally, while imaging studies in healthy mice could provide useful conclusions on levels of uptake (potentially indicating the mechanism of action of SR9009), an evaluation of the radiotracer's potential in disease applications would be an avenue of interest. Determining whether differing levels of expression of Rev-erb could be an indication of disease state could offer prognostic and diagnostic value for [$^{11}$C]SR9009.

Furthermore, radiotracers provide value in assisting with SAR and drug design, allowing for evaluation of target binding and probe pharmacokinetics without investing financially into the development of a drug. Whether SR9009 or its similar analogues acts on Rev-erb or alternatively through, for example, LXRα, can be determined using imaging in a rapid and efficient manner. Additional candidates can be evaluated using this demonstrated method.

### 3.4.3. References

(1) Boulahjar, R.; Ouach, A.; Matteo, C.; Bourg, S.; Ravache, M.; le Guével, R.; Marionneau, S.; Oullier, T.; Lozach, O.; Meijer, L.; Guguen-Guillouzo, C.; Lazar, S.; Akssira, M.; Troin, Y.; Guillaumet, G.; Routier, S. Novel Tetrahydropyrido [1,2-α]isoindolone Derivates (Valmerins): Potent Cyclin-Dependent Kinase/Glycogen Synthase Kinase 3 Inhibitors with Antiproliferative Activities and Antitumor Effects in Human Tumor Xenografts. *Journal of Medicinal Chemistry* **2012**, 55, 9589–9606. https://doi.org/10.1021/jm3008536.

## Chapter 4: Synthesis of $^{11}$C-Amino Acids
## Novel Method Development

This chapter and discussion contains information from multiple published studies.

- **FOCUS:** Mair et al. "Carbon-11-Carboxylate Exchange in α-Amino Acids" *Planned submission to Canadian Journal of Chemistry.*
    - Contributions: Project lead, completed experiments, wrote manuscript.
- Doyle, Mair et al. "A practical guide for the preparation of C1-labeled α-amino acids using aldehyde catalysis with isotopically labeled $CO_2$" *Nat. Prot.* **2024**. doi: 10.1038/s41596-024-00974-4.
    - Contributions: Developed $^{11}$C method, wrote $^{11}$C section of manuscript.
- Bsharat and Doyle, Munch, Mair et al. "Aldehyde-catalyses carboxylate exchange in α-amino acids with isotopically labelled $CO_2$" *Nat. Chem.* **2022**, 14, 1367–1374. doi: 10.1038/s41557-022-01074-0.
    - Contributions: Assisted with and completed $^{11}$C development and experiments.
- Munch, Mair et al. "Photocatalyzed radiosynthesis of $^{11}$C-phenylacetic acids" *J. Label. Compd. Radiopharm.* **2023**, 1–6. doi: 10.1002/jlcr.4073.
    - Contributions: Assisted with and finished $^{11}$C experiments.

## 4.1. Context

### 4.1.1. Carbon Isotope Exchange

While labelling with deuterium and tritium has been explored extensively,[1] the direct exchange of carbon isotopes has long been a difficult and relatively underappreciated topic. However, a recent increase in the exploration of carbon isotope exchange (CIE) has developed strategies for labelling with carbon-13, carbon-14 and with carbon-11.[2,3] The pioneering methods – palladium-catalyzed CIE of acid chlorides with [$^{14}$C]CO,[4] nickel-mediated exchange with [$^{14}$C]$CO_2$,[5,6] and a [$^{14}$C]$CO_2$ conversion of aromatic carboxylates in the presence of a copper salt[7] – paved the way for continued exploration of carbon labelling using isotopic exchange scaffolds.

These techniques would later inform extension to carbon-13 and carbon-11 labelling. In 2020, the research groups of Davide Audisio and of Rylan Lundgren independently reported carboxylate isotope replacement using [$^{13}$C]$CO_2$ to access phenylacetic acids for the pharmaceutically-relevant labelling of non-steroidal anti-inflammatory drugs (Figure 4.1).[8,9] Audisio *et al.*, in collaboration with the group of Magnus Schou, notably explored the first example of CIE using [$^{11}$C]$CO_2$ with faster reaction times. These methods however used conditions that were relatively harsh, and so they were later improved by the same groups in 2021 by harnessing photochemical strategies to overcome limitations (Figure 4.2).[10,11]

Carbon-11 isotopic exchange suffers from a major limitation in the way of low molar activities, given that the final product is identical to the initial precursor, albeit with $^{11}$C in place of $^{nat}$C. This may not always be problematic: in cases where there is already an abundance of the stable form endogenous to the body, like amino acids, there will always be a high mass dose of the non-radioactive counterpart and as such molar activity is not as vital. Nonetheless, alternative methodologies ensuring higher molar activity are valuable tools. To this end, we established a method for the synthesis of $^{11}$C-phenylacetic acids using photochemical carboxylation of alkylbenzene derivatives (Figure 4.2).[12] Work largely completed by Dr. Maxime Munch in our research group required completion of the carbon-11 scope as well as preparative isolation for demonstration of its potential applicability to imaging. To that end, I contributed to addressing the technical challenges of photochemical radiolabelling, to the synthesis of the remaining scope targets, and to the isolation of [$^{11}$C]fenoprofen as a target compound. This work succeeded in improving molar activities, although only moderately, warranting extended investigation.

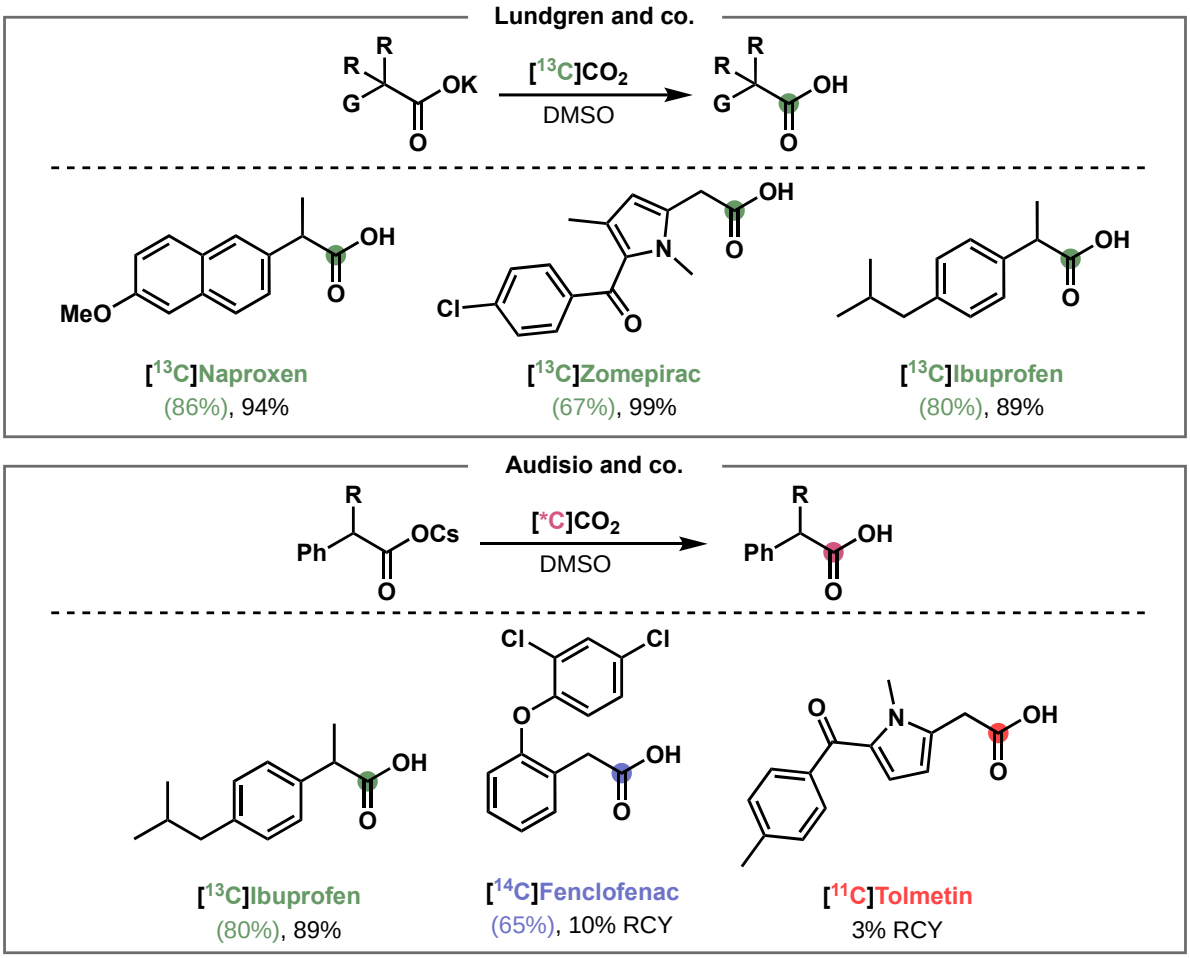


**Figure 4.1.** Early adoption of carbon-13 and carbon-11 isotope exchange. While many of the methodologies were first discovered using carbon-14, attempts to label with alternative carbon isotopes soon appeared, beginning with the work from Lundgren and Audisio. Lundgren and co. accessed carbon-13 labelled non-steroidal anti-inflammatory drugs like naproxen and ibuprofen to demonstrate the methodology; carbon-13 incorporation and product yield were used to indicate reaction success. Independently but in parallel, Audisio and co. targeted carbon-13, carbon-14 and the first iteration of carbon-11 carbon isotope exchange to access similar products; incorporations of carbon-13 and carbon-14 as well as radiochemical yields for carbon-14 and carbon-11 were used to measure reaction performance.

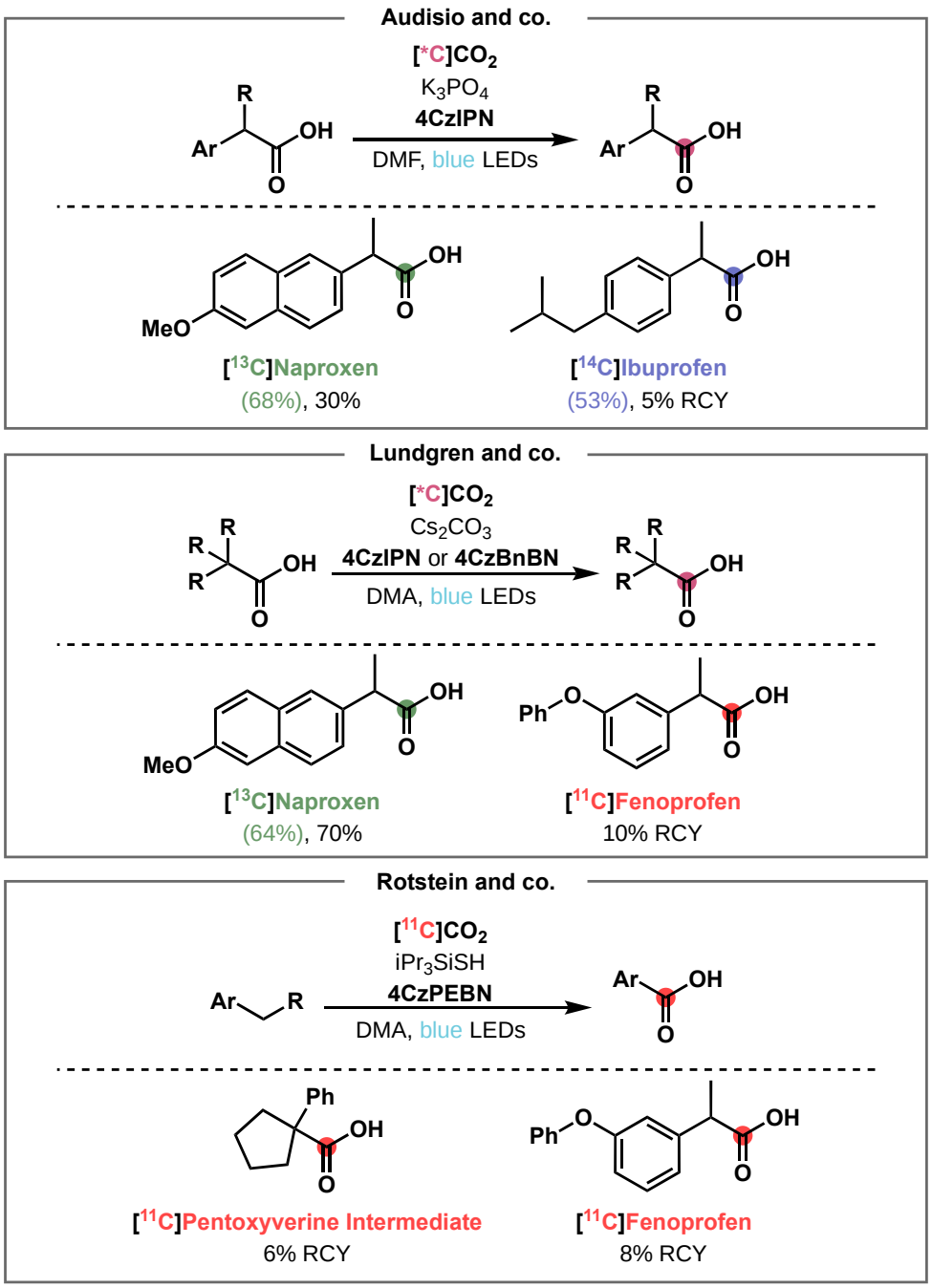


**Figure 4.2.** Photochemical $^{11}$C-carboxylations. Due to harsh reaction conditions with thermal methods, the groups of Audisio and Lundgren sought photochemical frameworks to access similar carbon isotope exchange reactions. These methodologies were used to access carbon-13-, carbon-14- and carbon-11-labelled products under the catalysis of carbazole-containing photocatalysts. Our group followed with work specific to carbon-11 labelling and its required conditions, using a C–H carboxylation.

### 4.1.2. $^{11}$C-Amino Acids

The critical role played by amino acids (AAs) in vital biological functions is apparent, with key involvement in protein synthesis, neurotransmission, and cell signalling. Given their frequent transport throughout and consumption within the body, labelled amino acids offer significant value for PET imaging, most notably in the study of cancer biology.[13] In fact, labelled amino acids may offer an improvement over commonly used [$^{18}$F]FDG due to lower baseline uptake into glucose-consuming tissues like the brain, heart, and areas of inflammation.[14]

Many synthetic approaches exist, though there is no one single preferred and generalized strategy for their labelling. The Strecker reaction is perhaps one of the most common methods for $^{11}$C-amino acid preparation, using an aldehyde and an amine in the presence of [$^{11}$C]HCN (Figure 4.3), and was first exemplified with [$^{11}$C]aminocyclopentanecarboxylic acid.[15] The reaction, however, required carrier-added cyanide – i.e. delivered alongside stable isotope gas to assist with reaction kinetics – that can be problematic for dose formulation. Following this work however was the development of amino acids, like [$^{11}$C]valine,[16] as well as [$^{11}$C]leucine and [$^{11}$C]tryptophan.[17]

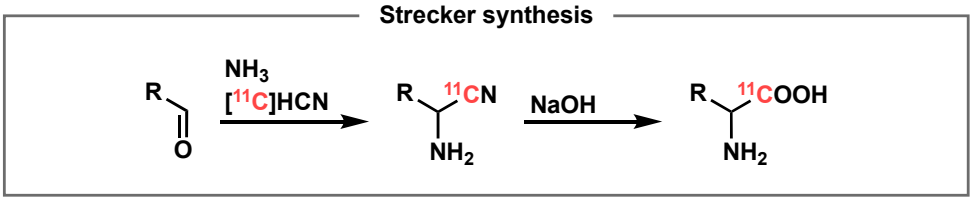


**Figure 4.3.** Strecker synthesis for $^{11}$C-amino acids. The Strecker synthesis is a general radiolabelling methodology to prepare α-amino acids. While it is currently the most widely applicable method in the literature, it requires a custom apparatus for the production of [$^{11}$C]HCN.

Upon the discovery of no-carrier-added carbon-11 delivery techniques amenable to the Strecker reaction, methods to access [$^{11}$C]phenylalanine, [$^{11}$C]leucine and [$^{11}$C]valine were established, followed by modifications in 2003 for improved attempts at [$^{11}$C]phenylalanine and [$^{11}$C]tyrosine.[18,19] Improvements to carbon-11 chemistry assisted further in the progression of the method, resulting in an automated synthesis that obviates the need for immediate purification and specialized delivery systems for [$^{11}$C]HCN by instead using [$^{11}$C]NaCN.[20]

An alternative approach to the synthesis of $^{11}$C-amino acids utilizes Schiff base precursors, condensed amines and aldehydes, in which the α-carbon's reactivity is elevated (Figure 4.4).[21,22]

Various extended iterations exist,[23–28] including [$^{11}$C]$CH_3I$ methylations of the α-carbon.[29,30] Naturally, $^{11}$C-methylations of homocysteine are a logical labelling site as well,[31,32] although they are limited exclusively to the preparation of [$^{11}$C]methionine.

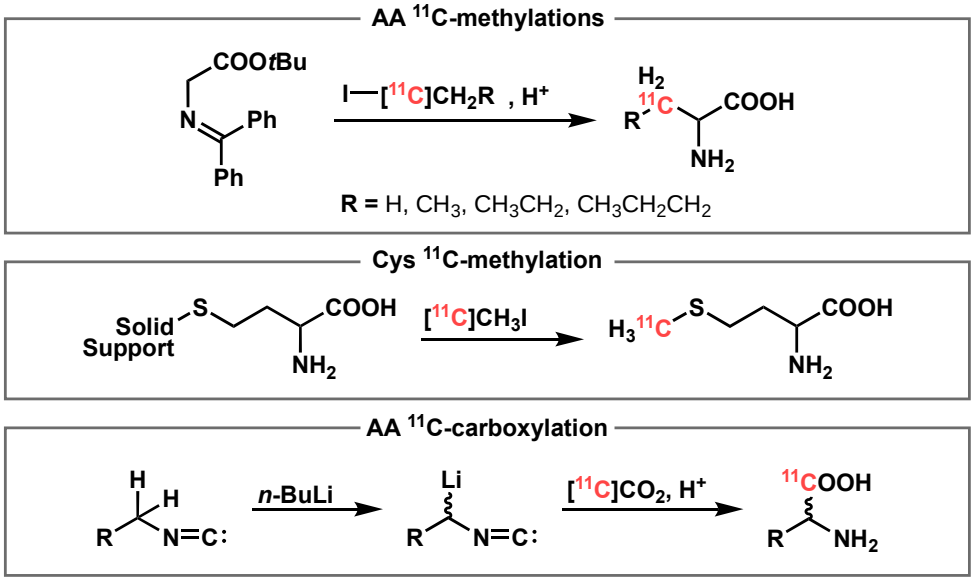


**Figure 4.4.** Alternative methods for $^{11}$C-AA synthesis. Methylations using [$^{11}$C]$CH_3I$ can be used to access specific amino acids. Carboxylations with lithiated precursors have also been developed.

Despite being relatively underexplored in the literature, $^{11}$C-carboxylations with [$^{11}$C]$CO_2$ direct from the cyclotron would provide a reliable and simple method for accessing $^{11}$C-amino acids. A methodology with [$^{11}$C]$CO_2$ carboxylation of α-lithioisocyanides was identified, and used to provide [$^{11}$C]glycine and [$^{11}$C]phenylalanine,[33] [$^{11}$C]lysine,[34] [$^{11}$C]tyrosine,[35] and [$^{11}$C]proline.[36]

The most used PET $^{11}$C-AA radiotracer is [$^{11}$C]methionine, typically for brain tumour imaging.[37,38] Few others have been translated to regular clinical production with most studies only having been performed with small animals and preclinical work. Others like [$^{11}$C]tyrosine,[39] [$^{11}$C]DOPA,[40] and [$^{11}$C]glutamine[41] have been investigated in smaller studies, but have yet to be fully validated for rotation in imaging. A potential area of interest for PET imaging is in the evaluation of oxidative metabolism of branched-chain amino acids (BCAA) in cardiac homeostasis, with underlying mechanisms having been recently identified.[42] As such, labelling of [$^{11}$C]leucine, [$^{11}$C]isoleucine, and/or [$^{11}$C]valine offers valuable opportunities for novel investigation into this newly explored relationship.

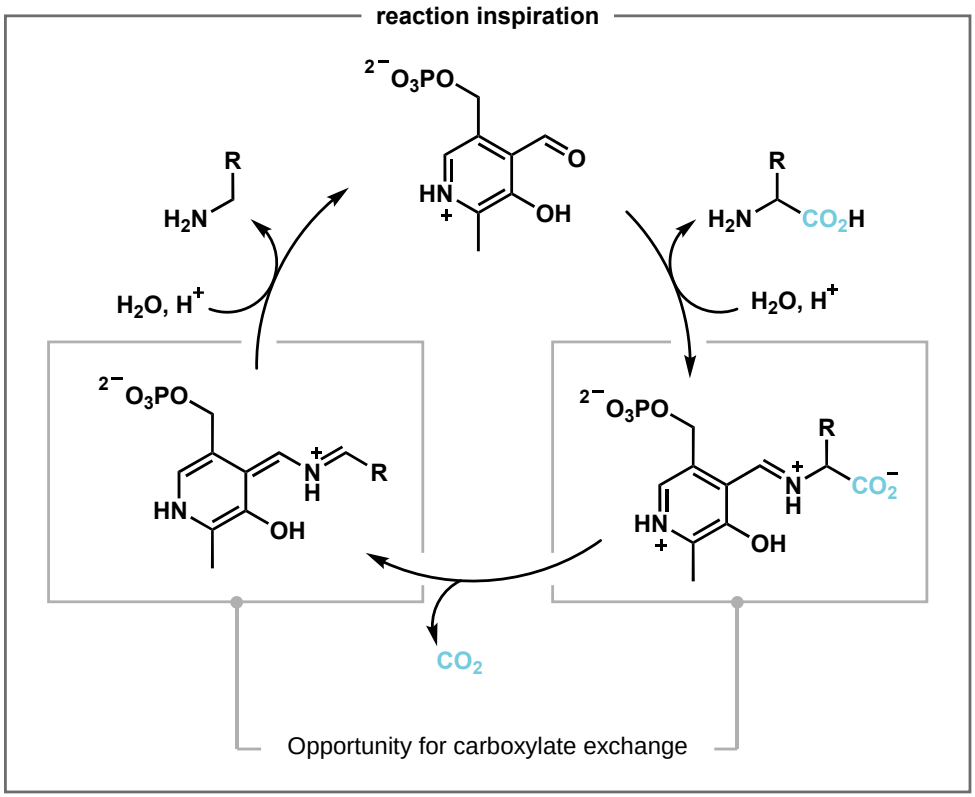


**Figure 4.5.** Aromatic amino acid decarboxylase and carboxylate exchange. The enzymatic extrusion of $CO_2$ from amino acids is a reversible process. Observing condensation of amino acids with pyridoxal phosphate into a Schiff base, this reaction scaffold offers the potential for inspiration into $^{11}$C-AA labelling.

### 4.1.3. Aldehyde-catalysed carboxylate exchange in α-amino acids with labelled $CO_2$

Given the importance of carbon-11-labelled amino acids, as well as the value in isotopically labelled α-amino acids with alternative labels like carbon-13 and carbon-14, we sought to develop a general approach to their preparation. In the specific case of amino acids, their spontaneous rates of decarboxylation are extremely slow due to being unable to stabilize the anion formed.[43] However, nature achieves the extrusion of $CO_2$ from α-amino acids using aromatic amino acid decarboxylases – these convert amino acids into imines via a condensation with pyridoxal phosphate, and decarboxylate to form an aza-allyl intermediate that can be hydrolysed to an amine (Figure 4.5).[44,45] With this being a reversible process, we saw an opportunity for a potential re-carboxylation with labelled $CO_2$.

Carbon dioxide's utility as a labelling synthon has been demonstrated thus far in this thesis by harnessing fixation techniques with trapping bases. We instead envisioned an aldehyde-catalysed

isotopic exchange reaction, which was realized for labelling with carbon-14, carbon-13 and carbon-11.[46] Following condensation of amino acids with an aryl aldehyde catalyst, the Schiff base was exposed to $*CO_2$ to provide labelled products (Figure 4.6). Various aldehyde catalysts were examined with carbon-13 labelling; it was determined that electron-deficient and electrophilic catalysts like those containing strong electron-withdrawing groups give fast initial rates of carboxylate exchange but are consumed and degrade rapidly leading to a lower final incorporation of the label. Conversely, electron-rich catalysts like 4-anisaldehyde progress at a relatively slow rate but result in higher concentrations of labelled product.

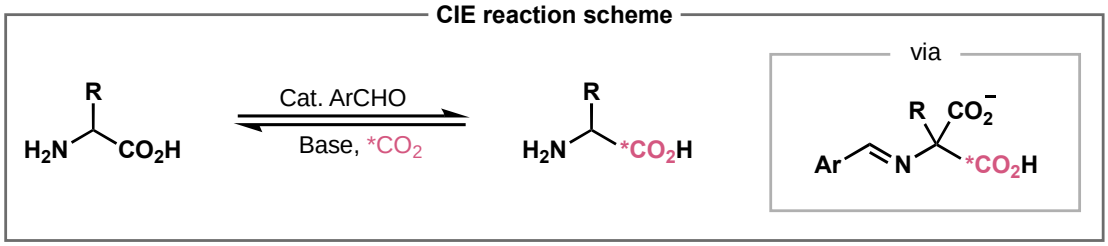


**Figure 4.6.** Carbon isotope exchange reaction scheme. The conversion of α-amino acids into their isotopically labelled counterparts using $*CO_2$ can be performed with the presence of aldehyde catalyst via a carboxylation/decarboxylation pathway.

This reaction scheme was performed with carbon-14 for the labelling of phenylalanine and with carbon-13 to access a diverse scope of α-amino acids. The reaction process leads to racemization of the amino acid, creating a mixture of the L- and D-isomers. To overcome this process, literature methods like dynamic kinetic resolution and enzyme-catalysed conversions were used with carbon-13 products to ensure enrichment of the desired form. Additionally, attempts to perform enzymatic resolutions have been shown to be successful with carbon-11 radiochemistry.[47] Chromatographic resolution could also be performed to separate both the L- and D-products.

In parallel to the work with carbon-13 and carbon-14, Dr. Maxime Munch and I developed the method for radiolabelling with carbon-11. We worked in tandem, simultaneously building a substrate scope with aromatic, aliphatic, and polar sidechain products including tyrosine, tryptophan, leucine, methionine, lysine, glutamine, phenylalanine, and non-proteinogenic products thyroxine and glutathione (Figure 4.7). Following our publication in *Nature Chemistry*, we looked

to target the production and isolation of $^{11}$C-amino acids for imaging studies. I took over as the project lead, further optimizing and simplifying the approach for routine production and developing a reliable isolation of racemic [$^{11}$C]phenylalanine. The method as well as the labelling with carbon-13 and carbon-14 were further detailed in a *Nature Protocol* article.[48]

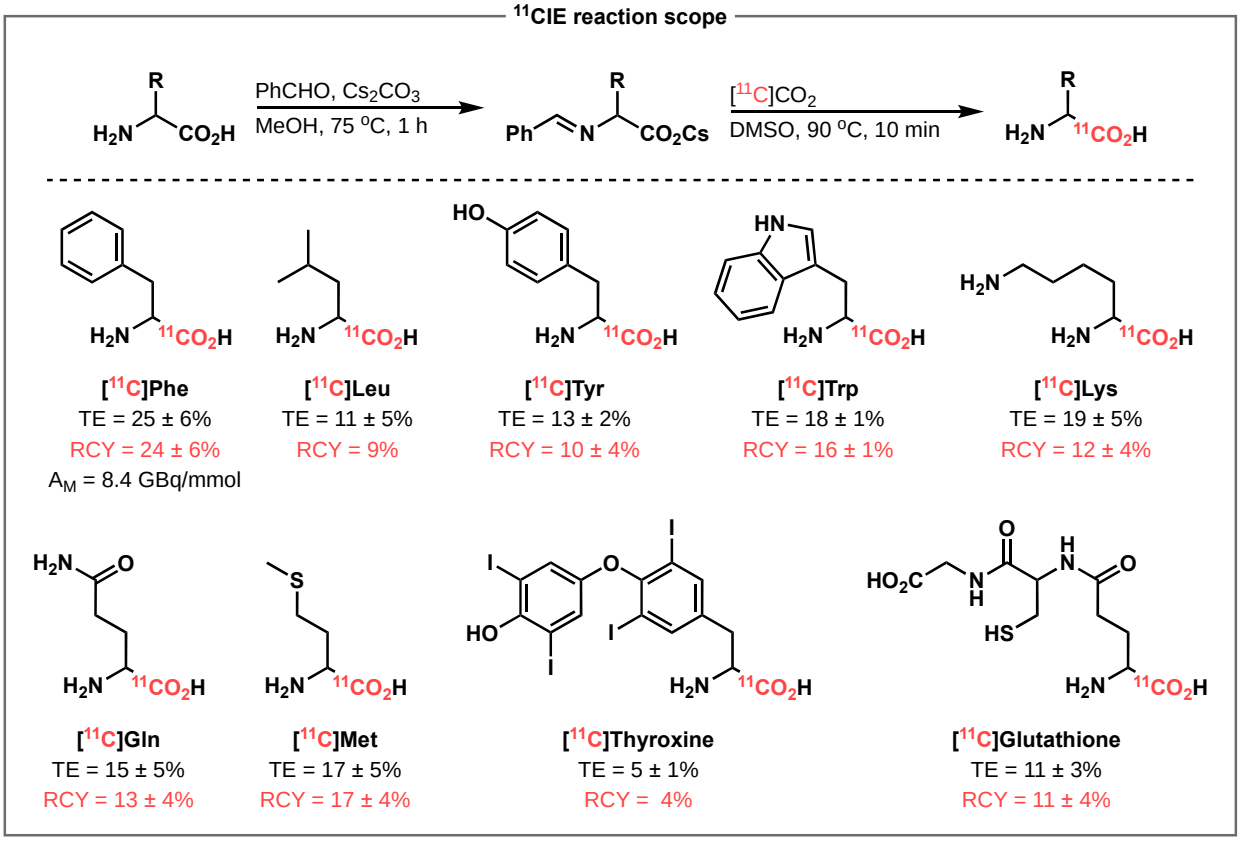


**Figure 4.7.** $^{11}$C-AA substrate scope. Imines were prepared immediately prior to radiolabelling performed on a Synthra MeIplus synthesis module. Final products were evaluated by radio-HPLC to determine yield. TE = trapping efficiency. RCY = radiochemical yield. $A_M$ = molar activity.

### 4.1.4. References


(1) Kopf, S.; Bourriquen, F.; Li, W.; Neumann, H.; Junge, K.; Beller, M. Recent Developments for the Deuterium and Tritium Labeling of Organic Molecules. *Chem. Rev.* **2022**, *122* (6), 6634–6718. https://doi.org/10.1021/acs.chemrev.1c00795.

(2) Hinsinger, K.; Pieters, G. The Emergence of Carbon Isotope Exchange. *Angewandte Chemie International Edition* **2019**, *58* (29), 9678–9680. https://doi.org/10.1002/anie.201905368.

(3) Labiche, A.; Malandain, A.; Molins, M.; Taran, F.; Audisio, D. Modern Strategies for Carbon Isotope Exchange. *Angewandte Chemie International Edition* **2023**, *62* (36), e202303535. https://doi.org/10.1002/anie.202303535.

(4) Gauthier, D. R. Jr.; Rivera, N. R.; Yang, H.; Schultz, D. M.; Shultz, C. S. Palladium-Catalyzed Carbon Isotope Exchange on Aliphatic and Benzoic Acid Chlorides. *J. Am. Chem. Soc.* **2018**, *140* (46), 15596–15600. https://doi.org/10.1021/jacs.8b09808.

(5) Kingston, C.; Wallace, M. A.; Allentoff, A. J.; deGruyter, J. N.; Chen, J. S.; Gong, S. X.; Bonacorsi, S. Jr.; Baran, P. S. Direct Carbon Isotope Exchange through Decarboxylative Carboxylation. *J. Am. Chem. Soc.* **2019**, *141* (2), 774–779. https://doi.org/10.1021/jacs.8b12035.

(6) Tortajada, A.; Duan, Y.; Sahoo, B.; Cong, F.; Toupalas, G.; Sallustrau, A.; Loreau, O.; Audisio, D.; Martin, R. Catalytic Decarboxylation/Carboxylation Platform for Accessing Isotopically Labeled Carboxylic Acids. *ACS Catal.* **2019**, *9* (7), 5897–5901. https://doi.org/10.1021/acscatal.9b01921.

(7) Destro, G.; Loreau, O.; Marcon, E.; Taran, F.; Cantat, T.; Audisio, D. Dynamic Carbon Isotope Exchange of Pharmaceuticals with Labeled $CO_2$. *J. Am. Chem. Soc.* **2019**, *141* (2), 780–784. https://doi.org/10.1021/jacs.8b12140.

(8) Kong, D.; Moon, P. J.; Lui, E. K. J.; Bsharat, O.; Lundgren, R. J. Direct Reversible Decarboxylation from Stable Organic Acids in Dimethylformamide Solution. *Science* **2020**, *369* (6503), 557–561. https://doi.org/10.1126/science.abb4129.

(9) Destro, G.; Horkka, K.; Loreau, O.; Buisson, D.-A.; Kingston, L.; Del Vecchio, A.; Schou, M.; Elmore, C. S.; Taran, F.; Cantat, T.; Audisio, D. Transition-Metal-Free Carbon Isotope Exchange of Phenyl Acetic Acids. *Angewandte Chemie International Edition* **2020**, *59* (32), 13490–13495. https://doi.org/10.1002/anie.202002341.

(10) Kong, D.; Munch, M.; Qiqige, Q.; Cooze, C. J. C.; Rotstein, B. H.; Lundgren, R. J. Fast Carbon Isotope Exchange of Carboxylic Acids Enabled by Organic Photoredox Catalysis. *J. Am. Chem. Soc.* **2021**, *143* (5), 2200–2206. https://doi.org/10.1021/jacs.0c12819.

(11) Babin, V.; Talbot, A.; Labiche, A.; Destro, G.; Del Vecchio, A.; Elmore, C. S.; Taran, F.; Sallustrau, A.; Audisio, D. Photochemical Strategy for Carbon Isotope Exchange with $CO_2$. *ACS Catal.* **2021**, *11* (5), 2968–2976. https://doi.org/10.1021/acscatal.0c05344.

(12) Munch, M.; Mair, B. A.; Adi, M.; Rotstein, B. H. Photocatalyzed Radiosynthesis of $^{11}$C-Phenylacetic Acids. *Journal of Labelled Compounds and Radiopharmaceuticals* **2024**, *67* (6), 211–216. https://doi.org/10.1002/jlcr.4073.

(13) Jager, P. L.; Vaalburg, W.; Pruim, J.; Vries, E. G. E. de; Langen, K.-J.; Piers, D. A. Radiolabeled Amino Acids: Basic Aspects and Clinical Applications in Oncology*. *Journal of Nuclear Medicine* **2001**, *42* (3), 432–445.

(14) Sun, A.; Liu, X.; Tang, G. Carbon-11 and Fluorine-18 Labeled Amino Acid Tracers for Positron Emission Tomography Imaging of Tumors. *Front. Chem.* **2018**, *5*. https://doi.org/10.3389/fchem.2017.00124.

(15) Hayes, R. L.; Washburn, L. C.; Wieland, B. W.; Sun, T. T.; Turtle, R. R.; Butler, T. A. Carboxyl-Labeled $^{11}$C-1-Aminocyclopentanecarboxylic Acid, a Potential Agent for Cancer Detection. *Journal of Nuclear Medicine* **1976**, *17* (8), 748–751.

(16) Washburn, L. C.; Wieland, B. W.; Sun, T. T.; Hayes, R. L.; Butler, T. A. [1-$^{11}$C] DL-Valine, A Potential Pancreas-Imaging Agent. *Journal of Nuclear Medicine* **1978**, *19* (1), 77–83.

(17) Hayes, R. L.; Washburn, L. C.; Wieland, B. W.; Sun, T. T.; Anon, J. B.; Butler, T. A.; Callahan, A. P. Synthesis and Purification of $^{11}$C-Carboxyl-Labeled Amino Acids. *The International Journal of Applied Radiation and Isotopes* **1978**, *29* (3), 186–187. https://doi.org/10.1016/0020-708X(78)90142-4.

(18) Iwata, R.; Ido, T.; Takahashi, T.; Nakanishi, H.; Iida, S. Optimization of [$^{11}$C]HCN Production and No-Carrier-Added [1-$^{11}$C]Amino Acid Synthesis. *International Journal of Radiation Applications and Instrumentation. Part A. Applied Radiation and Isotopes* **1987**, *38* (2), 97–102. https://doi.org/10.1016/0883-2889(87)90003-7.

(19) Studenov, A. R.; Szalda, D. E.; Ding, Y.-S. Synthesis of No-Carrier-Added C-11 Labeled D- and L-Enantiomers of Phenylalanine and Tyrosine for Comparative PET Studies. *Nuclear Medicine and Biology* **2003**, *30* (1), 39–44. https://doi.org/10.1016/S0969-8051(02)00349-9.

(20) Xing, J.; Brooks, A. F.; Fink, D.; Zhang, H.; Piert, M. R.; Scott, P. J. H.; Shao, X. High-Yielding Automated Convergent Synthesis of No-Carrier-Added [$^{11}$C-*Carbonyl*]-Labeled Amino Acids Using the Strecker Reaction. *Synlett* **2016**, *28*, 371–375. https://doi.org/10.1055/s-0036-1588638.

(21) Kilbourn, M. R.; Dischino, D. D.; Welch, M. J. Synthesis of DL-[3-$^{11}$C]Phenylalanine. *The International Journal of Applied Radiation and Isotopes* **1984**, *35* (7), 603–605. https://doi.org/10.1016/0020-708X(84)90103-0.

(22) Antoni, G.; Långström, B. Synthesis of Racemic [3-$^{11}$C]-Labelled Alanine, 2-Aminobutyric Acid, Norvaline, Norleucine, Leucine and Phenylalanine and Preparation of L-[3-$^{11}$C]Alanine and L-[3-$^{11}$C]Phenylalanine. *Journal of Labelled Compounds and Radiopharmaceuticals* **1987**, *24* (2), 125–143. https://doi.org/10.1002/jlcr.2580240203.

(23) Långström, B.; Stridsberg, B. Syntheses of Racemic [1-$^{11}$C]-Alanine and Partially Resolved [3-$^{11}$C]-Alanine. *The International Journal of Applied Radiation and Isotopes* **1979**, *30* (3), 151–153. https://doi.org/10.1016/0020-708X(79)90122-4.

(24) Antoni, G.; Långström, B.; Famini, G. R.; Taft, R. W.; Fischer, G. W. Asymmetric Synthesis of L-2-Amino[3-$^{11}$C]Butyric Acid, L-[3-$^{11}$C]Norvaline and L-[3-$^{11}$C]Valine. *Acta Chem. Scand.* **1987**, *41b*, 511–517. https://doi.org/10.3891/acta.chem.scand.41b-0511.

(25) Fasth, K.-J.; Antoni, G.; Langström, B. Asymmetric Synthesis of L-[3-$^{11}$C]Alanine and L-[3-$^{11}$C]Phenylalanine by a Phase-Transfer Alkylation Reaction. *J. Chem. Soc., Perkin Trans. 1* **1988**, No. 12, 3081–3084. https://doi.org/10.1039/P19880003081.

(26) Oppolzer, W.; Moretti, R.; Zhou, C. Asymmetric Alkylations of a Sultam-Derived Glycine Equivalent: Practical Preparation of Enantiomerically Pure α-Amino Acids. *Helvetica Chimica Acta* **1994**, *77* (8), 2363–2380. https://doi.org/10.1002/hlca.19940770823.

(27) Filp, U.; Pees, A. L.; Taddei, C.; Pekošak, A.; Gee, A. D.; Windhorst, A. D.; Poot, A. J. Efficient Synthesis of $^{11}$C-Acrylesters, $^{11}$C-Acrylamides and Their Application in Michael Addition Reactions for PET Tracer Development. *European Journal of Organic Chemistry* **2017**, *2017* (34), 5154–5162. https://doi.org/10.1002/ejoc.201700932.

(28) Pekošak, A.; Filp, U.; Škrinjar, J.; Poot, A. J.; Windhorst, A.D. A rapid and highly enantioselective C–$^{11}$C bond formation of L-[$^{11}$C]phenylalanine *via* chiral phase-transfer catalysis. *Organic & Biomolecular Chemistry* **2017**, 15, 570–575. https://doi.org/10.1039/C6OB02633H.

(29) Chaly, T.; Diksic, M. Synthesis of "No-Carrier-Added" α-[$^{11}$C] Methyl-L-Tryptophan. *Journal of Nuclear Medicine* **1988**, *29* (3), 370–374.

(30) Popkov, A.; Nádvorník, M.; Kružberská, P.; Lyčka, A.; Lehel, S.; Gillings, N. Towards Stereoselective Radiosynthesis of α-[$^{11}$C]Methyl-Substituted Aromatic α-Amino Acids – a Challenge of Creation of Quaternary Asymmetric Centre in a Very Short Time. *Journal of Labelled Compounds and Radiopharmaceuticals* **2007**, *50* (5–6), 370–374. https://doi.org/10.1002/jlcr.1268.

(31) Comar, D.; Cartron, J.-C.; Maziere, M.; Marazano, C. Labelling and Metabolism of Methionine-Methyl-$^{11}$C. *Eur J Nucl Med* **1976**, *1* (1), 11–14. https://doi.org/10.1007/BF00253260.

(32) Schmitz, F.; Plenevaux, A.; Del-Fiore, G.; Lemaire, C.; Comar, D.; Luxen, A. Fast Routine Production of L-[$^{11}$C-*Methyl*]Methionine with $Al_2O_3KF$. *Applied Radiation and Isotopes* **1995**, *46* (9), 893–897. https://doi.org/10.1016/0969-8043(95)00181-C.

(33) Vaalburg, W.; Beerling-van der Molen, H. D.; Reiffers, S.; Rijskamp, A.; Woldring, M. G.; Wynberg, H. Preparation of Carbon-11 Labelled Phenylalanine and Phenylglycine by a New Amino Acid Synthesis. *The International Journal of Applied Radiation and Isotopes* **1976**, *27* (3), 153–157. https://doi.org/10.1016/0020-708X(76)90126-5.

(34) Bolster, J. M.; Vaalburg, W.; Van Dijk, T. H.; Zijlstra, J. B.; Paans, A. M. J.; Wynberg, H.; Woldring, M. G. Syntheses of Carbon-11 Labelled Ornithine and Lysine. Preliminary Accumulation Studies in Rats with Walker 256 Carcinosarcoma. *The International Journal of Applied Radiation and Isotopes* **1985**, *36* (4), 263–267. https://doi.org/10.1016/0020-708X(85)90082-1.

(35) Bolster, J. M.; Vaalburg, W.; Paans, A. M. J.; van Dijk, T. H.; Elsinga, P. H.; Zijlstra, J. B.; Piers, D. A.; Mulder, N. H.; Woldring, M. G.; Wynberg, H. Carbon-11 Labelled Tyrosine to Study Tumor Metabolism by Positron Emission Tomography (PET). *Eur J Nucl Med* **1986**, *12* (7), 321–324. https://doi.org/10.1007/BF00263811.

(36) Bolster, J. M.; Hoeve, W. T.; Vaalburg, W.; Van Dijk, T. H.; Zijlstra, J. B.; Paans, A. M. J.; Wynberg, H.; Woldring, M. G. The Preparation of Carbon-11 Labelled Proline for Positron Emission Tomography. Preliminary Distribution Studies in Rats with Walker 256 Carcinosarcoma. *The International Journal of Applied Radiation and Isotopes* **1985**, *36* (5), 339–343. https://doi.org/10.1016/0020-708X(85)90272-8.

(37) Långström, B.; Antoni, G.; Gullberg, P.; Halldin, C.; Malmborg, P.; Någren, K.; Rimland, A.; Svärd, H. Synthesis of L- and D-[*Methyl*-$^{11}$C]Methionine. *Journal of Nuclear Medicine* **1987**, *28* (6), 1037–1040.

(38) Lilja, A.; Bergström, K.; Hartvig, P.; Spännare, B.; Halldin, C.; Lundqvist, H.; Långstrom, B. Dynamic Study of Supratentorial Gliomas with L-*Methyl*-$^{11}$C-Methionine and Positron Emission Tomography. *AJNR: American Journal of Neuroradiology* **1985**, *6* (4), 505.

(39) Ginkel, R. J. van; Kole, A. C.; Nieweg, O. E.; Molenaar, W. M.; Pruim, J.; Koops, H. S.; Vaalburg, W.; Hoekstra, H. J. L-[1-$^{11}$C]-Tyrosine PET to Evaluate Response to Hyperthermic Isolated Limb Perfusion for Locally Advanced Soft-Tissue Sarcoma and Skin Cancer. *Journal of Nuclear Medicine* **1999**, *40* (2), 262–267.

(40) Hartvig, P.; ågren, H.; Reibring, L.; Tedroff, J.; Bjurling, P.; Kihlberg, T.; Långström, B. Brain Kinetics of L-[β-$^{11}$C]DOPA in Humans Studied by Positron Emission Tomography. *J. Neural Transmission* **1991**, *86* (1), 25–41. https://doi.org/10.1007/BF01250373.

(41) Qu, W.; Oya, S.; Lieberman, B. P.; Ploessl, K.; Wang, L.; Wise, D. R.; Divgi, C. R.; Chodosh, L. P.; Thompson, C. B.; Kung, H. F. Preparation and Characterization of L-[5-$^{11}$C]-Glutamine for Metabolic Imaging of Tumors. *Journal of Nuclear Medicine* **2012**, *53* (1), 98–105. https://doi.org/10.2967/jnumed.111.093831.

(42) McGarrah, R. W.; White, P. J. Branched-Chain Amino Acids in Cardiovascular Disease. *Nat Rev Cardiol* **2023**, *20* (2), 77–89. https://doi.org/10.1038/s41569-022-00760-3.

(43) Snider, M. J.; Wolfenden, R. The Rate of Spontaneous Decarboxylation of Amino Acids. *J. Am. Chem. Soc.* **2000**, *122* (46), 11507–11508. https://doi.org/10.1021/ja002851c.

(44) Li, T.; Huo, L.; Pulley, C.; Liu, A. Decarboxylation Mechanisms in Biological System. *Bioorganic Chemistry* **2012**, *43*, 2–14. https://doi.org/10.1016/j.bioorg.2012.03.001.

(45) Claes, L.; Janssen, M.; De Vos, D. E. Organocatalytic Decarboxylation of Amino Acids as a Route to Bio-Based Amines and Amides. *ChemCatChem* **2019**, *11* (17), 4297–4306. https://doi.org/10.1002/cctc.201900800.

(46) Bsharat, O.; Doyle, M. G. J.; Munch, M.; Mair, B. A.; Cooze, C. J. C.; Derdau, V.; Bauer, A.; Kong, D.; Rotstein, B. H.; Lundgren, R. J. Aldehyde-Catalysed Carboxylate Exchange in α-Amino Acids with Isotopically Labelled $CO_2$. *Nat. Chem.* **2022**, *14* (12), 1367–1374. https://doi.org/10.1038/s41557-022-01074-0.

(47) Barrio, J. R.; Keen, R. E.; Ropchan, J. R.; MacDonald, N. S.; Baumgartner, F. J.; Padgett, H. C.; Phelps, M. E. L-[1-$^{11}$C]Leucine: Routine Synthesis by Enzymatic Resolution. *24* (6).

(48) Doyle, M. G. J.; Mair, B. A.; Sib, A.; Bsharat, O.; Munch, M.; Derdau, V.; Rotstein, B. H.; Lundgren, R. J. A Practical Guide for the Preparation of C1-Labeled α-Amino Acids Using Aldehyde Catalysis with Isotopically Labeled $CO_2$. *Nat Protoc* **2024**, 1–33. https://doi.org/10.1038/s41596-024-00974-4.

## 4.2. Carbon-11-Carboxylate Exchange in α-Amino Acids

Braeden A. Mair,[1,2] Maxime Munch,[2,3] Abhishek Patel,[2,3] Ariel Buchler,[1,2] Benjamin H. Rotstein*[1,2,3]

[1] Department of Chemistry and Biomolecular Sciences, University of Ottawa, Ottawa, Canada K1H 8M5

[2] University of Ottawa Heart Institute, Ottawa, Canada K1Y 4W7

[3] Department of Biochemistry, Microbiology and Immunology, University of Ottawa, Ottawa, Canada K1H 8M5

Pending submission to the Canadian Journal of Chemistry, Radiochemistry Special Issue.

### 4.2.1. Statement of the manuscript

The manuscript "Carbon-11-Carboxylate Exchange in α-Amino Acids" is in preparation for a planned submission to the special issue for Radiochemistry in the Canadian Journal of Chemistry. In this paper, I elaborate on the optimization of a method to access $^{11}$C-amino acids for purposes of PET imaging following our work in *Nature Chemistry* and *Nature Protocols*. Pilot imaging with [$^{11}$C]leucine was performed to evaluate feasibility.

Imine stability testing was performed by Abhishek Patel (BSc Candidate) under my guidance. The reaction condition scope was developed by me and Dr. Maxime Munch (PDF) in collaboration. I completed the aldehyde catalyst evaluation, with assistance from Abhishek Patel in the preparation of imine precursors. I evaluated the chiral catalyst and developed isolation conditions, with additional assistance from Abhishek Patel. I produced [$^{11}$C]leucine for imaging, with assistance from Ariel Buchler (PhD Candidate) for animal handling and PET. I wrote the manuscript with editing from Dr. Benjamin Rotstein and Abhishek Patel. All authors approved the final version. Extended investigation into imaging is expected to be performed by Abhishek Patel.

### 4.2.2. Abstract

Radiolabeled amino acids offer a broad spectrum of applications in clinical care and pharmaceutical development. Traditional methods of labelling are limited in their availability, requiring specialized synthetic requirements, and robustness, targeting only a select list of amino acids. We discovered a simple and efficient approach using aldehyde-catalysed carboxylate exchange to access labelled α-amino acids; this method can be used to prepare $^{11}$C-amino acids. Seeking enrichment of the carbon-11 methodology, and the preparation of radiotracers suitable for animal imaging, we explored further optimization and probe development. In this article we detail precursor stability, the evaluation of aldehyde catalysts, optimal reaction conditions, and the production of enantiopure radiolabelled amino acids. We then tested [$^{11}$C]leucine, a branched-chain amino acid, in the interest of investigating oxidative metabolism in cardiovascular disease.

**Keywords:** Carbon-11, carboxylation, amino acids, radiochemistry, catalysis

### 4.2.3. Introduction

Positron emission tomography (PET) is a non-invasive nuclear medicine technology for *in vivo* molecular imaging. Carbon-11 ($^{11}C$, $t_{1/2}$ = 20.4 min) is a short-lived PET isotope commonly used for labelling of small molecules and peptides; carbon's presence in all organic molecules presents the opportunity for isotopologue labelling without any structural modifications. Carbon-11-labelled amino acids (AAs) offer significant potential as PET imaging agents, to be used for disease monitoring, prognostication and therapeutic evaluation, and for biochemical profiling of pharmacodynamics and pharmacokinetics of potential drug candidates.[1] AA-based radiotracers have become especially valuable for the study of cancer biology due to increased uptake, and aromatic AAs have found a place in the evaluation and diagnosis of neurological disorders.[2,3]

Leading strategies for labelling AAs are *via* the Strecker reaction with [$^{11}C$]HCN,[4–8] with which many cyclotrons and radiosynthesis units are not equipped to deliver, or methylation with [$^{11}C$]$CH_3I$, albeit only in applicable cases (such as with [$^{11}C$]methionine). Alternative approaches harness $^{11}C$-carboxylations using activated lithiated precursors;[9] these can provide several essential amino acids but require tedious organic syntheses to prepare and often have post-labelling steps to achieve the desired product.[10–12] Specific syntheses for labelling of the side chain exist, but are not widely applicable to all amino acid targets.[13] Furthermore with a short decay half-life, carbon-11 necessitates rapid, late-stage label-incorporation often not compatible with traditional literature methodologies.

Understanding a need for a general and efficient approach to $^{11}C$-amino acids, we developed an isotopic exchange reaction scheme harnessing aldehyde catalysis to direct a cycle of carboxylation and decarboxylation with labelled $CO_2$.[14,15] This process can be realized with the use of simple aldehyde catalysts to form Schiff base intermediates, and can access most proteinogenic targets. Our method was developed for the use of carbon-13 and carbon-14, as well as for carbon-11 using [$^{11}C$]$CO_2$ produced directly from the cyclotron. However, limitations in relative reactivity with carbon-11 were elucidated. In addition, techniques used for enantiomeric resolution proved useful for carbon-13 labelling but have yet to be translated to our carboxylation process.

With that consideration, we sought to enrich the labelling methodology to be amenable to conditions that suit carbon-11, its handling, and its short half-life. We also wished to identify an

approach to enantiopure $^{11}$C-amino acids. We herein detail the carbon-11 optimization of our carboxylate exchange to access labelled α-amino acids.

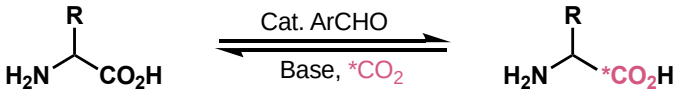


**Figure 4.8.** Synthesis of $^{11}$C-amino acids using carbon isotope exchange.

### 4.2.4. Results and Discussion

*4.2.4.1. Imine Precursors*

In order to promote quicker reaction times necessary for carbon-11 implementation, imines were pre-formed using a condensation of amino acids with aldehydes in methanol. This proved essential for improving the reactivity. The condensation proceeds quantitatively, verified by $^{1}$H NMR to observe the presence of an aldehyde proton peak. Each imine is individually prepared in advance of radiolabelling. While we initially attempted to prepare imines in a much larger batch scale from which we could take aliquots for radiolabelling, this approach proved ineffective due to insolubility of the isolated imine precursor. Using individually prepared imines, we instead assessed their stability over time to determine their approximate shelf-lives. Monitoring the gradual degradation of our synthesized imine determined that the condensed product should be kept for no more than a week, with significant degradation observed by that time.

We further evaluated the stability of the imine under the reaction conditions. Imines were prepared using three aldehyde catalysts: benzaldehyde, an electron-deficient substituted 4-fluorobenzaldehyde, and an electron-rich 4-methoxybenzaldehyde. These were dissolved in deuterated dimethyl sulfoxide ($d_6$-DMSO) before being subjected to similar conditions to our radiolabelling – heated to 90 °C, bubbled with $CO_2$ for 45 seconds – and then left to react for 10 minutes with $CO_2$ atmosphere. Upon completion, the samples were evaluated by NMR (Supplemental Figure S1–S3). The 4-methoxybenzaldehyde imine was found to have the most significant decomposition to either the free aldehyde or a degradation product, with only 81% of the imine remaining. Conversely, the 4-fluorobenzaldehyde exhibited the slowest decomposition, with 93% of the imine remaining after the simulated reaction. The baseline benzaldehyde displayed 90% imine stability after 10 minutes. With these variations in imine stability within our

reaction window, it became apparent the importance of the nature of the aldehyde catalyst in order to maximize yield.

#### *4.2.4.2. $^{11}$C-Labelling Optimization*

Conditions for the carbon-11 isotopic exchange reaction were evaluated with both 4-methoxybenzaldehyde, the model catalyst used in optimization for carbon-13 chemistry, and with benzaldehyde, a baseline catalyst with sufficient imine stability. Adaptation of the standard conditions established by our colleagues at the University of Alberta provided poor translatability limited by the reaction time (Figure 4.9, entry 1). Alterations in temperature and catalyst loading, reacting under the presence of base to mediate the reaction, or using a different catalyst provided only marginal improvements to the reaction yield (entries 2–6).

Pre-formed imines offered great value by obviating the need for formation *in situ*. This significantly improved reaction yields (entry 8), and with higher imine concentration we achieved the standard reaction for [$^{11}$C]phenylalanine in 24% RCY with benzaldehyde (entry 9) and 15% RCY with 4-methoxybenzaldehyde (entry 10).

A faster reaction time could not be achieved with higher temperatures (entry 12), nor can the yields be improved with longer times (entry 13). Lower cesium carbonate loading resulted in comparable trapping and conversion (entries 14–15), while higher amounts of cesium carbonate decreased reactivity (entry 16). The reaction proceeds only slightly worse with $K_3PO_4$ in place of $Cs_2CO_3$, but could not be performed with $Li_2CO_3$ due to insolubility (entries 18–19).

Additives were evaluated for their effects on the reaction: bases like DABCO, TMEDA and NaOH, as well as the crown ether 18-Crown-6 and chelator Kryptofix 222, provided only minor decreases in yield (entries 20–24). Increased loading of base disabled the reaction entirely (entries 25–27).

**$^{11}$CIE reaction optimization**


optimization results

| Entry | R | [imine] (M) | $Cs_2CO_3$ (mol %) | Aldehyde (mol %) | Time (min) | Temp. (° C) | $V_{DMSO}$ (mL) | Additive | TE (%) | RCC (%) | RCY (%) |
|---|---|---|---|---|---|---|---|---|---|---|---|
| 1 | OMe | 0.1 [a] | 40 | 20 | 10 | 70 | 0.50 | - | 10 | 24 | 2 |
| 2 | OMe | 0.1 [a] | 40 | 20 | 10 | 70 | 0.50 | DBU [b] | 12 | 16 | 2 |
| 3 | OMe | 0.1 [a] | 40 | 60 | 10 | 90 | 0.50 | - | 8 | 80 | 6 |
| 4 | OMe | 0.1 [a] | 40 | 60 | 10 | 90 | 0.50 | DBU [b] | 15 | 56 | 8 |
| 5 | OMe | 0.1 [a] | 40 | 80 | 10 | 90 | 0.50 | DBU [b] | 9 | 89 | 8 |
| 6 | H | 0.1 [a] | 40 | 80 | 10 | 90 | 0.50 | DBU [b] | 13 | 46 | 6 |
| 7 | H | 0.1 | 50 | 100 | 10 | 70 | 0.50 | - | 13 | 74 | 10 |
| 8 | H | 0.1 | 50 | 100 | 10 | 90 | 0.50 | - | 15 | 99 | 14 |
| 9 | H | 0.2 | 50 | 100 | 10 | 90 | 0.75 | - | 25 | 95 | 24 |
| 10 | OMe | 0.2 | 50 | 100 | 10 | 90 | 0.75 | - | 16 | 97 | 15 |
| 11 | H | 0.2 [a] | 50 | 100 | 10 | 90 | 0.75 | - | 13 | 90 | 12 |
| 12 | H | 0.2 | 50 | 100 | 5 | 110 | 0.75 | - | 19 | 97 | 18 |
| 13 | H | 0.2 | 50 | 100 | 20 | 90 | 0.75 | - | 22 | 99 | 22 |
| 14 | H | 0.2 | 40 | 100 | 10 | 90 | 0.75 | - | 28 | 94 | 26 |
| 15 | H | 0.2 | 40 | 100 | 10 | 110 | 0.75 | - | 27 | 99 | 27 |
| 16 | H | 0.2 | 100 | 100 | 10 | 90 | 0.75 | - | 10 | 95 | 10 |
| 17 | H | 0.2 | 50 | 100 | 10 | 90 | 0.75 [c] | - | 18 | 99 | 18 |
| 18 | H | 0.2 | 0 [d] | 100 | 10 | 90 | 0.75 | - | 17 | 97 | 16 |
| 19 | H | 0.2 | 0 [e] | 100 | 10 | 90 | 0.75 | - | 0 | 0 | 0 |
| 20 | H | 0.2 | 50 | 100 | 10 | 90 | 0.75 | DABCO [b] | 17 | 98 | 17 |
| 21 | H | 0.2 | 50 | 100 | 10 | 90 | 0.75 | TMEDA [b] | 21 | 99 | 21 |
| 22 | H | 0.2 | 50 | 100 | 10 | 90 | 0.75 | NaOH [f] | 20 | 95 | 19 |
| 23 | H | 0.2 | 50 | 100 | 10 | 90 | 0.75 | 18C6 [b] | 23 | 97 | 22 |
| 24 | H | 0.2 | 0 [g] | 100 | 10 | 90 | 0.75 | K222 [b] | 25 | 56 | 14 |
| 25 | H | 0.2 | 50 | 100 | 10 | 90 | 0.75 | KOtBu [h] | 12 | 0 | 0 |
| 26 | H | 0.2 | 50 | 100 | 10 | 90 | 0.75 | DBU [i] | 19 | 0 | 0 |
| 27 | H | 0.2 | 50 | 100 | 10 | 90 | 0.75 | DABCO [i] | 51 | 0 | 0 |

[a] imines prepared *in situ* with 100% ArCHO and AA, [b] 50 mol %, [c] $d_6$-DMSO, [d] $K_3PO_4$ (50 mol %), [e] $Li_2CO_3$ (50 mol %), [f] 10 mol %, [g] $K_2CO_3$ (50 mol %), [h] 100 mol %, [i] 200 mol %

**Figure 4.9.** Radiochemical optimization for the preparation of $^{11}$C-amino acids.

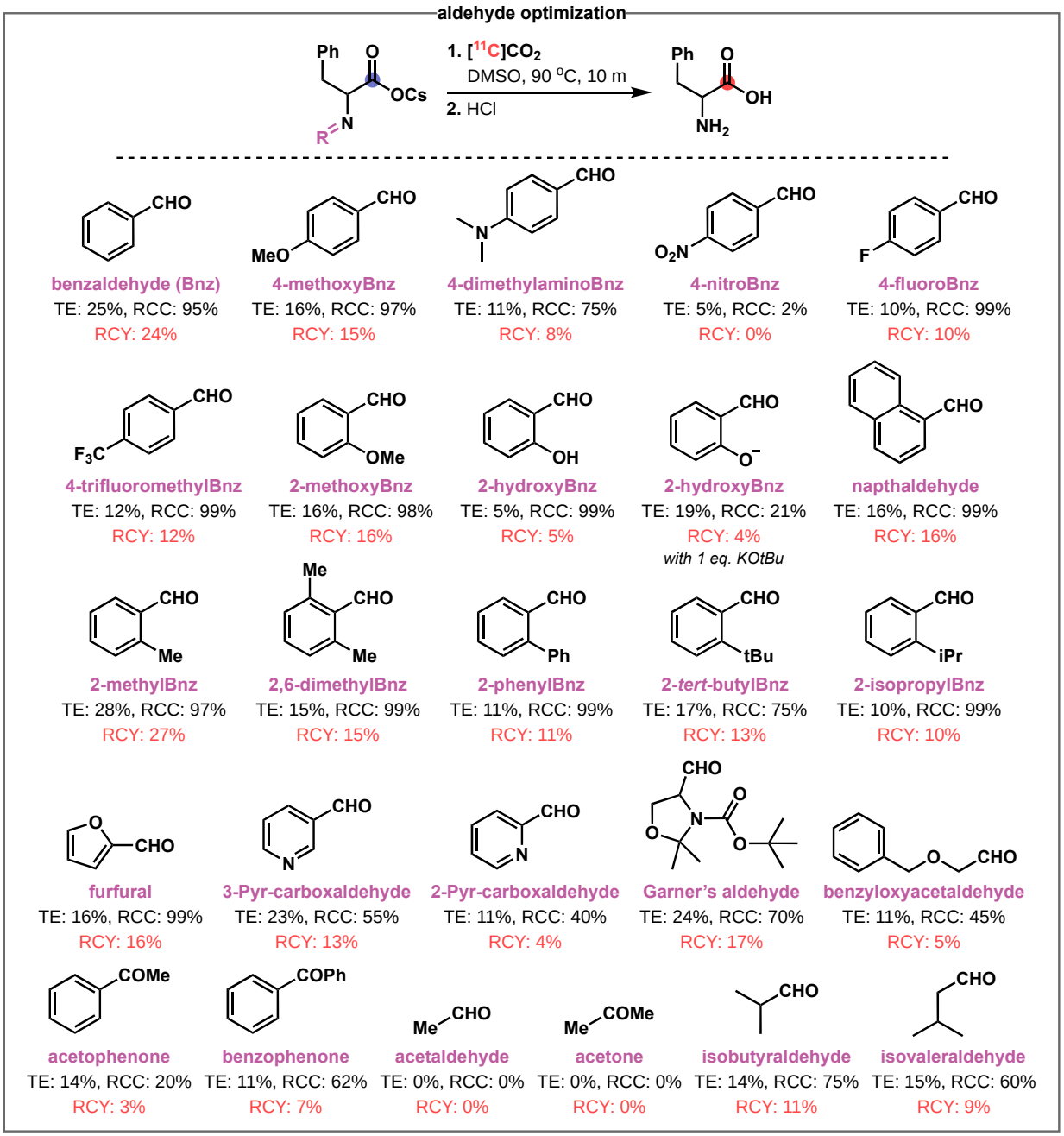


**Figure 4.10.** Aldehyde catalyst evaluation.

### *4.2.4.3. Aldehyde Catalysts*

The aldehyde catalyst was assessed for effects on reactivity (Figure 4.10). Electronics were evaluated in both the *ortho*- and *para*- positions with only moderate decreases in yield. Sterics appeared to offer improvements initially, but did not stand with further addition of bulk. Heteroatom-containing catalysts demonstrated slight decreases in yield. Ketones like

acetophenone and benzophenone exhibited significant decreases in reaction effectiveness, whereas acetaldehyde and acetone were found to be volatile under the conditions and lead to no reaction.

*4.2.4.4. Chiral Catalyst*

An enantioselective carbon isotope exchange using a chiral aldehyde catalyst was evaluated with carbon-13 and carbon-14 conditions.[16] We tested the application of these axially chiral urea-tethered aldehydes for enantioselective radiosynthesis (Figure 4.11). The reaction only proceeded using phenylalanine and without base, unlike the conditions for carbon-13 and carbon-14 labelling. Despite the lower yields, the enantiomeric ratio was determined to be 67:33, indicating minor enrichment of the desired enantiomer (Supplemental Figure S4). Restrictions in reaction time however limited the capacity for complete enrichment and for elevated yields.

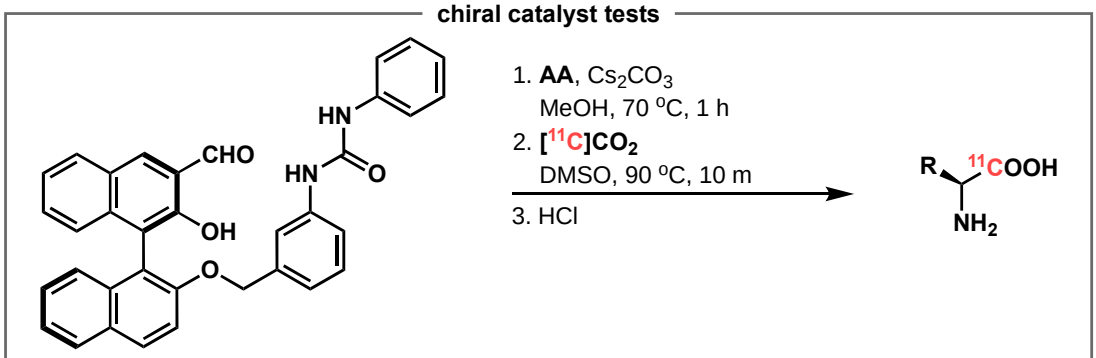


optimization results

| amino acid | base | TE (%) | RCC (%) | RCY (%) | er |
|---|---|---|---|---|---|
| leu | DBU [a] | 31 | 0 | 0 | 0:0 |
| leu | - | 0 | 0 | 0 | 0:0 |
| phe | DBU [a] | 36 | 0 | 0 | 0:0 |
| phe | - | 5 | 38 | 2 | 67:33 |
| phe | DABCO [a] | 15 | 0 | 0 | 0:0 |
| phe | TMEDA [b] | 0 | 0 | 0 | 0:0 |
| phe | KO*t*Bu [b] | 12 | 0 | 0 | 0:0 |
| phe | KO*t*Bu [a] | 21 | 0 | 0 | 0:0 |

[a] 2 equiv. [b] 1 equiv.

**Figure 4.11.** Chiral catalyst evaluation.

*4.2.4.5. Chiral Resolution*

To separate the two enantiomers formed in the production of (±)-$^{11}$C-AAs, we developed an enantiomeric resolution using chromatographic separation with chiral recognition. The Astec Chirobiotic™ T column contains the glycopeptide teicoplanin, which possesses 23 chiral centers capable of altering the retention times of two enantiomers, most frequently with amino acids.[17] Optimization of the resolution of the two enantiomers suggested 20% methanol in water as the ideal mobile phase; L- and D-leucine could be resolved on a preparative scale with a nearly 3 minute difference in their elution times (Supplemental Figure S4.5).

Attempts to isolate L-[$^{11}$C]leucine from D-[$^{11}$C]leucine were successful, however due to low residence time of the L-enantiomer on the column, significant co-elution with the similarly eluted unreacted [$^{11}$C]$CO_2$ remained a major problem (Supplemental Figure S6). To remedy this, given leucine's poor solubility in organic solvents, subsequent the preparative injection the column was purged with 90% methanol in water to elute [$^{11}$C]$CO_2$ before changing to the 20% mobile phase for resolution of the two enantiomers. This approach successfully provided L-[$^{11}$C]leucine sufficient for further study.

*4.2.4.6. PET Imaging with [$^{11}$C]Leucine*

In parallel, to evaluate feasibility for animal studies, (±)-[$^{11}$C]leucine was isolated for imaging (Supplemental Figure S7). Doses of 250 μCi in 200 μL of saline were injected into two C57BL/6 mice (1 M, 1 F) and imaged for 60 minutes (Figure 4.12). Radiotracer localization was visualized primarily in the liver, albeit with measurable uptake in the heart. Given the many roles AAs can play within the body as well as both their incorporation into proteins and their degradation into amines that are reused in biochemical cycles, further analysis with compartmental modeling would be necessary to evaluate accurate tracer distribution.

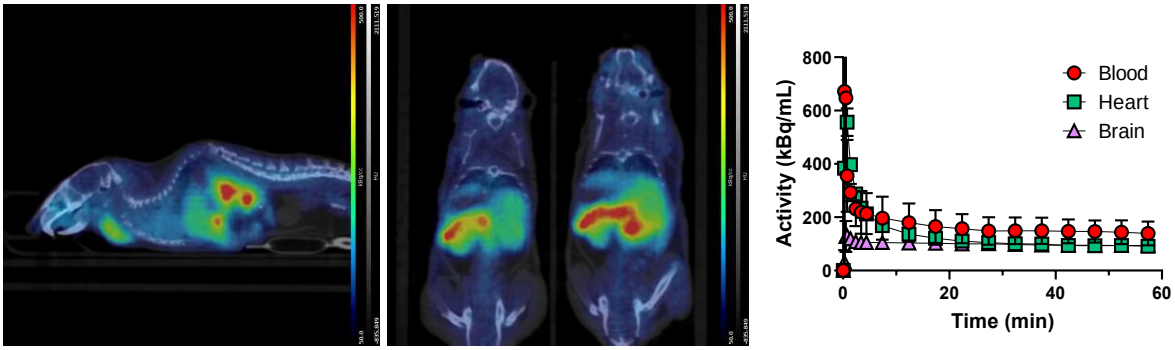


**Figure 4.12.** PET imaging with [$^{11}$C]leucine in C57BL/6 mice.

### 4.2.5. Conclusion

In conclusion, we sought to enrich our carbon isotopic exchange reaction for the preparation of carbon-11-labelled α-amino acids. Pre-formation of the imine intermediate significantly improved reactivity. Several aldehyde catalysts were found to be tolerated, however significant improvements to radiochemical yields were not elucidated. While the use of a chirally-locked catalyst did not provide sufficient enrichment or yield, we developed a chromatographic resolution to prepare enantiopure $^{11}$C-amino acids for imaging in animals. A pilot evaluation showed measurable uptake sufficient for extended study and further modeling.

### 4.2.6. Experimental

Imine Preparation: Amino acid (0.15 mmol, 1 equiv.) and $Cs_2CO_3$ (24.4 mg, 0,075 mmol, 0.05 equiv.) were added to a vial equipped with a stir bar which was then sealed, equipped with an exhaust needle, and filled with argon by performing three vacuum/argon re-filling cycles. Anhydrous MeOH (750 μL) and catalytic aldehyde (0.15 mmol, 1 equiv.) were then added, and the reaction mixture was heated to 70 $^{o}$C for 1 h while stirring. The vial was then equipped with an exhaust needle and the solvent was removed by flowing argon over the reaction mixture which was cooled to room temperature. The crude material was dried *in vacuo* for 1 h and then used directly for the radiolabelling experiment.

Cyclotron Production: No-carrier-added [$^{11}$C]$CO_2$ was generated by the $^{14}$N(p,α)$^{11}$C nuclear reaction after bombardment of a gas target filled with a pressurized $N_2/O_2$ mixture using a 11 MeV Siemens CTI Eclipse HP/RD Hybrid Cyclotron (University of Ottawa Heart Institute PET Radiochemistry Facility). After beaming for 120 seconds at 55 μA, around 7.4 GBq of [$^{11}$C]$CO_2$

was produced. After end-of-bombardment, target content was transferred to a Synthra MeIPlus Research module using a helium flow. [$^{11}$C]$CO_2$ was flowed through a nitrogen oxides trapping cartridge and cold-trapped at -180 $^{o}$C. After recording peak activity in the cold trap, [$^{11}$C]$CO_2$ was transferred to the reaction vessel by heating the trap to 25 $^{o}$C and flowing helium at a flow rate of 3 mL/min.

Radiochemistry: Imine precursor was dissolved in anhydrous DMSO (750 μL) and subsequently transferred to the synthesis module reactor. The reactor was sealed and flushed with He. After [$^{11}$C]$CO_2$ production and delivery, the reactor was heated to 90 $^{o}$C for 10 min while stirring. After 10 min the reactor was cooled to 30 $^{o}$C, then 0.45 mL of 1 M HCl was added to the vessel. Helium was then bubbled into the reaction mixture for 1 minute to remove most of the unreacted [$^{11}$C]$CO_2$. Confirmation of radiolabelled compound identity was then performed by radio-HPLC.

### 4.2.7. References


(1) Pekošak, A.; Filp, U.; Poot, A. J.; Windhorst, A. D. From Carbon-11-Labeled Amino Acids to Peptides in Positron Emission Tomography: The Synthesis and Clinical Application. *Mol Imaging Biol* **2018**, *20* (4), 510–532. https://doi.org/10.1007/s11307-018-1163-5.

(2) Jager, P. L.; Vaalburg, W.; Pruim, J.; Vries, E. G. E. de; Langen, K.-J.; Piers, D. A. Radiolabeled Amino Acids: Basic Aspects and Clinical Applications in Oncology*. *Journal of Nuclear Medicine* **2001**, *42* (3), 432–445.

(3) Huang, C.; McConathy, J. Radiolabeled Amino Acids for Oncologic Imaging. *Journal of Nuclear Medicine* **2013**, *54* (7), 1007–1010. https://doi.org/10.2967/jnumed.112.113100.

(4) Hayes, R. L.; Washburn, L. C.; Wieland, B. W.; Sun, T. T.; Turtle, R. R.; Butler, T. A. Carboxyl-Labeled $^{11}$C-1-Aminocyclopentanecarboxylic Acid, a Potential Agent for Cancer Detection. *Journal of Nuclear Medicine* **1976**, *17* (8), 748–751.

(5) Washburn, L. C.; Wieland, B. W.; Sun, T. T.; Hayes, R. L.; Butler, T. A. [1-$^{11}$C] DL-Valine, A Potential Pancreas-Imaging Agent. *Journal of Nuclear Medicine* **1978**, *19* (1), 77–83.

(6) Hayes, R. L.; Washburn, L. C.; Wieland, B. W.; Sun, T. T.; Anon, J. B.; Butler, T. A.; Callahan, A. P. Synthesis and Purification of $^{11}$C-Carboxyl-Labeled Amino Acids. *The International Journal of Applied Radiation and Isotopes* **1978**, *29* (3), 186–187.

https://doi.org/10.1016/0020-708X(78)90142-4.

(7) Studenov, A. R.; Szalda, D. E.; Ding, Y.-S. Synthesis of No-Carrier-Added C-11 Labeled D- and L-Enantiomers of Phenylalanine and Tyrosine for Comparative PET Studies. *Nuclear Medicine and Biology* **2003**, *30* (1), 39–44. https://doi.org/10.1016/S0969-8051(02)00349-9.

(8) Xing, J.; Brooks, A. F.; Fink, D.; Zhang, H.; Piert, M. R.; Scott, P. J. H.; Shao, X. High-Yielding Automated Convergent Synthesis of No-Carrier-Added [$^{11}$C-Carbonyl]-Labeled Amino Acids Using the Strecker Reaction. *Synlett* **2016**, *28*, 371–375.
https://doi.org/10.1055/s-0036-1588638.

(9) Vaalburg, W.; Beerling-van der Molen, H. D.; Reiffers, S.; Rijskamp, A.; Woldring, M. G.; Wynberg, H. Preparation of Carbon-11 Labelled Phenylalanine and Phenylglycine by a New Amino Acid Synthesis. *The International Journal of Applied Radiation and Isotopes* **1976**, *27* (3), 153–157. https://doi.org/10.1016/0020-708X(76)90126-5.

(10) Bolster, J. M.; Vaalburg, W.; Van Veen, W.; Van Dijk, Th.; Van der Molen, H. D.; Wynberg, H.; Woldring, M. G. Synthesis of No-Carrier-Added L- and D-[1-$^{11}$C]-DOPA. *The International Journal of Applied Radiation and Isotopes* **1983**, *34* (12), 1650–1652.
https://doi.org/10.1016/0020-708X(83)90019-4.

(11) Bolster, J. M.; Vaalburg, W.; Paans, A. M. J.; van Dijk, T. H.; Elsinga, P. H.; Zijlstra, J. B.; Piers, D. A.; Mulder, N. H.; Woldring, M. G.; Wynberg, H. Carbon-11 Labelled Tyrosine to Study Tumor Metabolism by Positron Emission Tomography (PET). *Eur J Nucl Med* **1986**, *12* (7), 321–324. https://doi.org/10.1007/BF00263811.

(12) Bolster, J. M.; Vaalburg, W.; Elsinga, Ph. H.; Wynberg, H.; Woldring, M. G. Synthesis of DL-[1-$^{11}$C]Methionine. *International Journal of Radiation Applications and Instrumentation. Part A. Applied Radiation and Isotopes* **1986**, *37* (10), 1069–1070.
https://doi.org/10.1016/0883-2889(86)90047-X.

(13) Antoni, G.; Kihlberg, T.; Långström, B. 11C: Labeling Chemistry and Labeled Compounds. In *Handbook of Nuclear Chemistry*; Vértes, A., Nagy, S., Klencsár, Z., Lovas, R. G., Rösch, F., Eds.; Springer US: Boston, MA, 2011; pp 1977–2019.
https://doi.org/10.1007/978-1-4419-0720-2_41.

(14) Bsharat, O.; Doyle, M. G. J.; Munch, M.; Mair, B. A.; Cooze, C. J. C.; Derdau, V.; Bauer, A.; Kong, D.; Rotstein, B. H.; Lundgren, R. J. Aldehyde-Catalysed Carboxylate Exchange in α-Amino Acids with Isotopically Labelled $CO_2$. *Nat. Chem.* **2022**, *14* (12), 1367–1374.

https://doi.org/10.1038/s41557-022-01074-0.

(15) Doyle, M. G. J.; Mair, B. A.; Sib, A.; Bsharat, O.; Munch, M.; Derdau, V.; Rotstein, B. H.; Lundgren, R. J. A Practical Guide for the Preparation of C1-Labeled α-Amino Acids Using Aldehyde Catalysis with Isotopically Labeled $CO_2$. *Nat Protoc* **2024**, *19* (7), 2147–2179. https://doi.org/10.1038/s41596-024-00974-4.

(16) Doyle, M. G. J.; Bsharat, O.; Sib, A.; Derdau, V.; Lundgren, R. J. Enantioselective Carbon Isotope Exchange. *J. Am. Chem. Soc.* **2024**, *146* (28), 18804–18810. https://doi.org/10.1021/jacs.4c03685.

(17) Berthod, A.; Liu, Y.; Bagwill, C.; Armstrong, D. W. Facile Liquid Chromatographic Enantioresolution of Native Amino Acids and Peptides Using a Teicoplanin Chiral Stationary Phase. *Journal of Chromatography A* **1996**, *731* (1), 123–137. https://doi.org/10.1016/0021-9673(95)01198-6.

## 4.3. Supplementary Information

### 4.3.1. Imine Stability

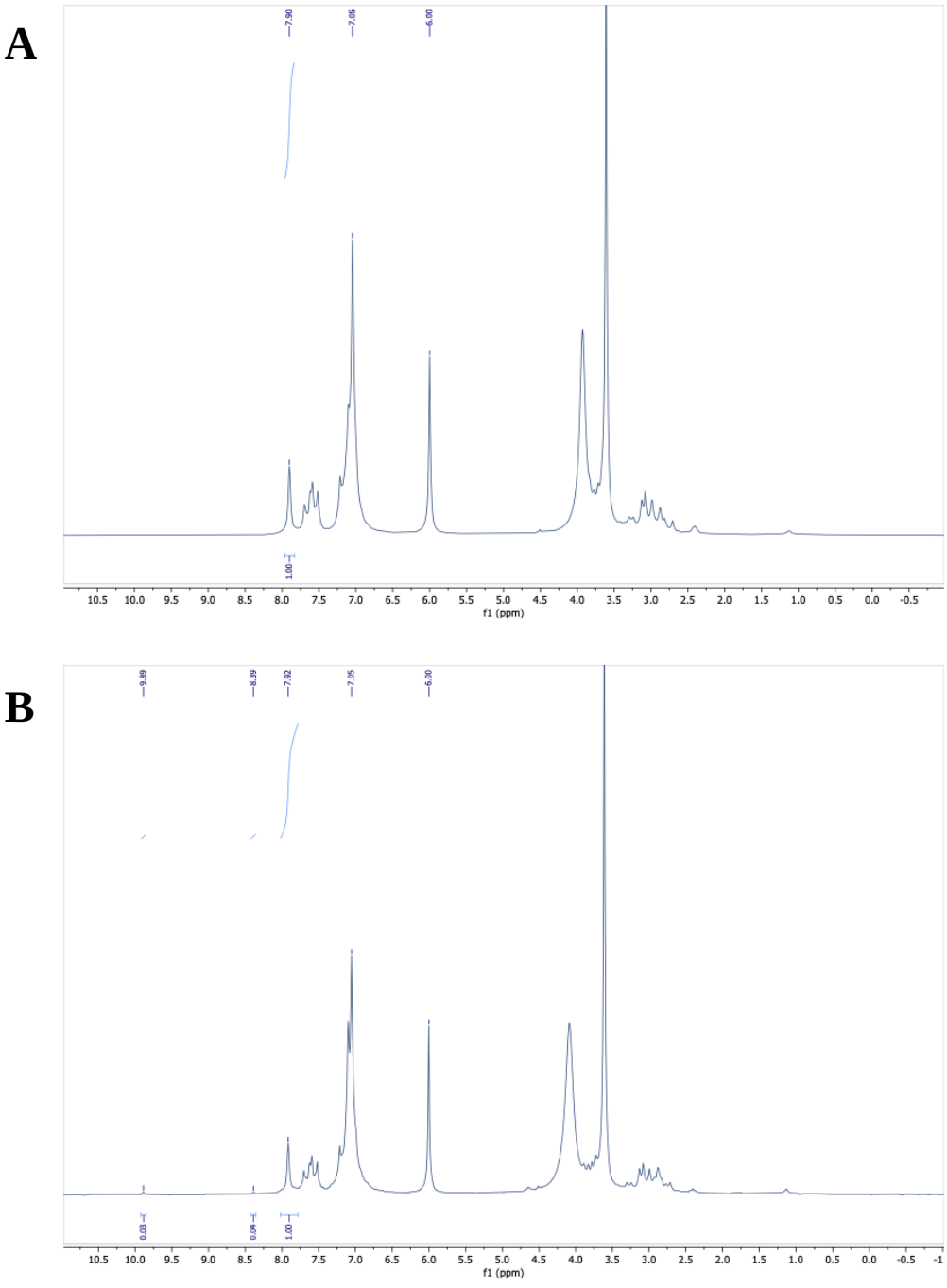


**Figure S4.1.** Stability tests with 4-fluorobenzaldehyde. (a) $^{1}$H-NMR of imine. (b) $^{1}$H-NMR of imine after reaction conditions.

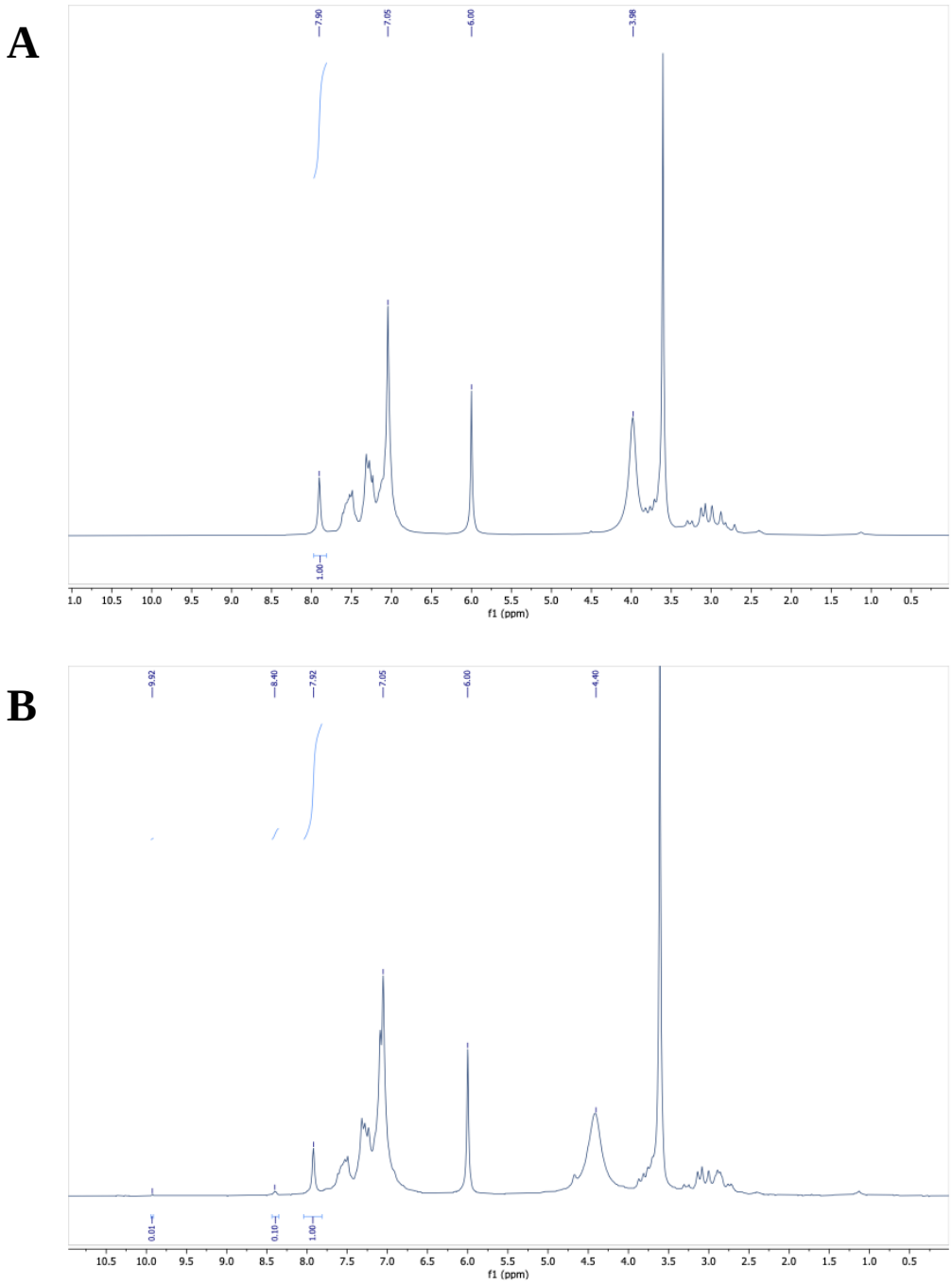


**Figure S4.2.** Stability tests with benzaldehyde. (a) $^{1}$H-NMR of imine. (b) $^{1}$H-NMR of imine after reaction conditions.

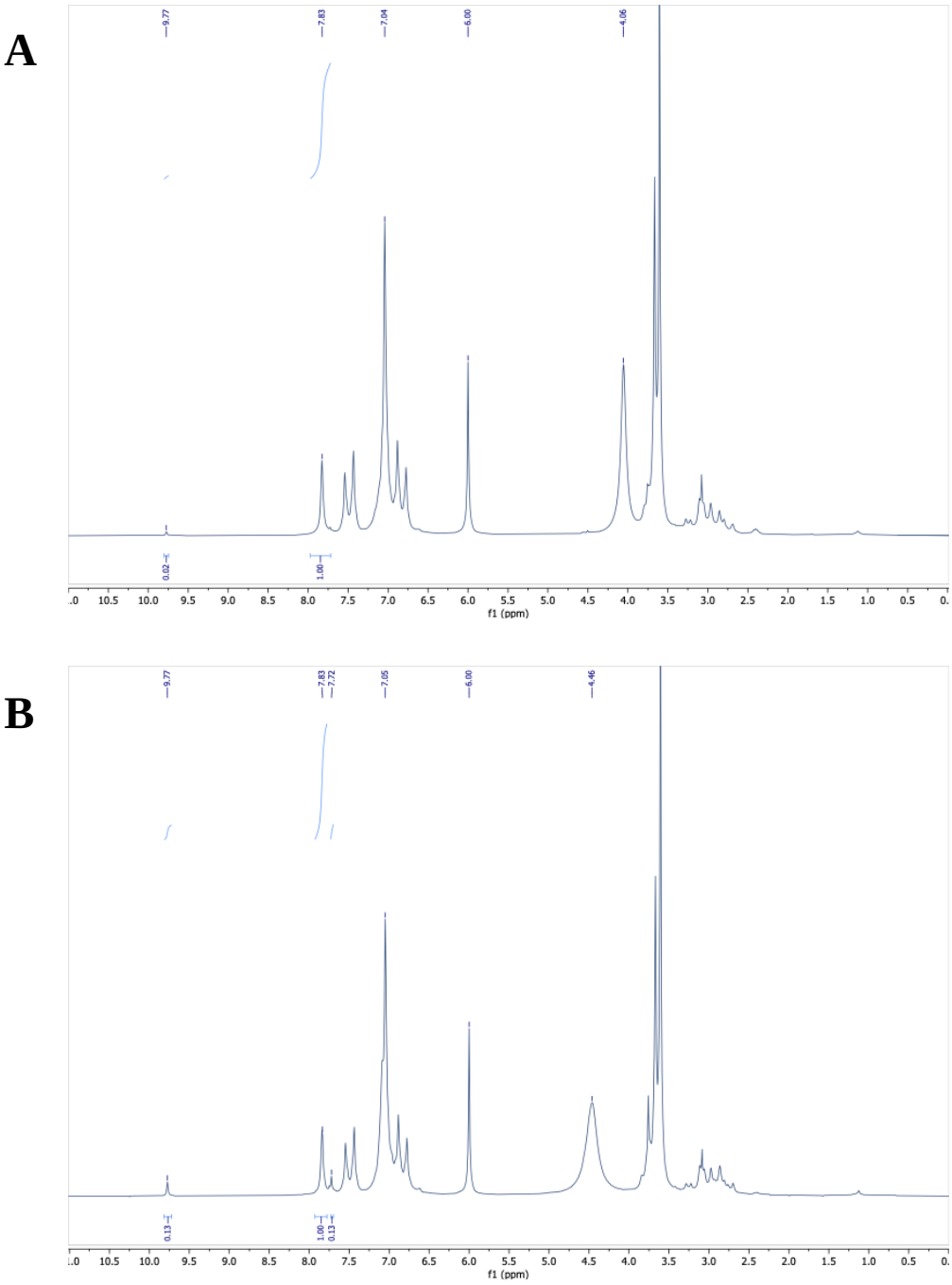


**Figure S4.3.** Stability tests with 4-methoxybenzaldehyde. (a) $^{1}$H-NMR of imine. (b) $^{1}$H-NMR of imine after reaction conditions.

### 4.3.2. Chiral Catalyst

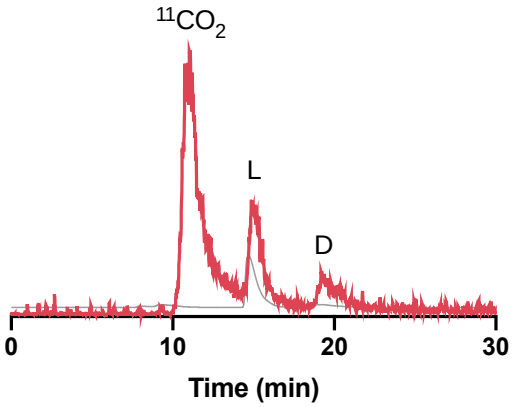


**Figure S4.4.** L- and D-[$^{11}$C]phenylalanine with partial L-enrichment. Red is γ, grey is UV.

### 4.3.3. Chiral Resolution

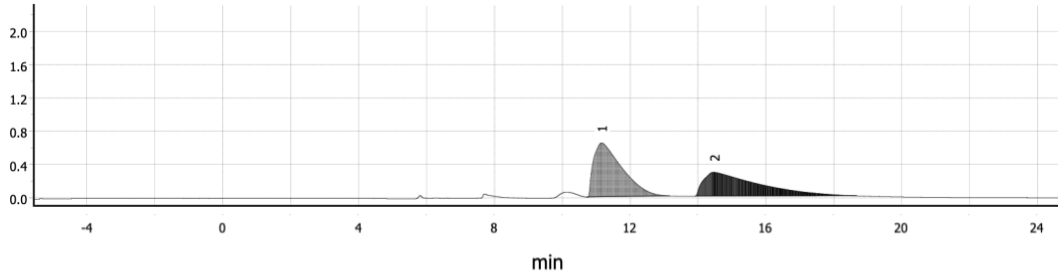


**Figure S4.5.** Preparative resolution of L- and D-leucine.

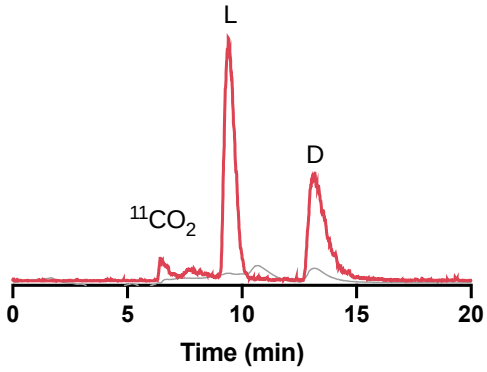


**Figure S4.6.** Analytical resolution of $^{11}CO_2$, L- and D-[$^{11}$C]leucine. Red is γ, grey is UV.

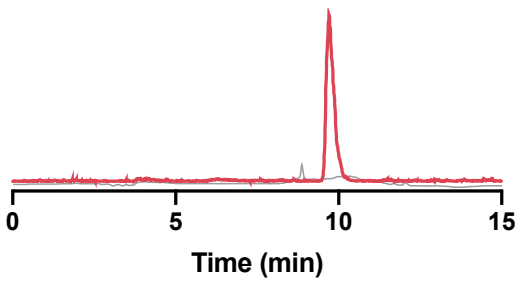


**Figure S4.7.** Isolation of [$^{11}$C]leucine. Red is γ, grey is UV.

### 4.3.4. Representative NMRs

Benzaldehyde w/ Phe:

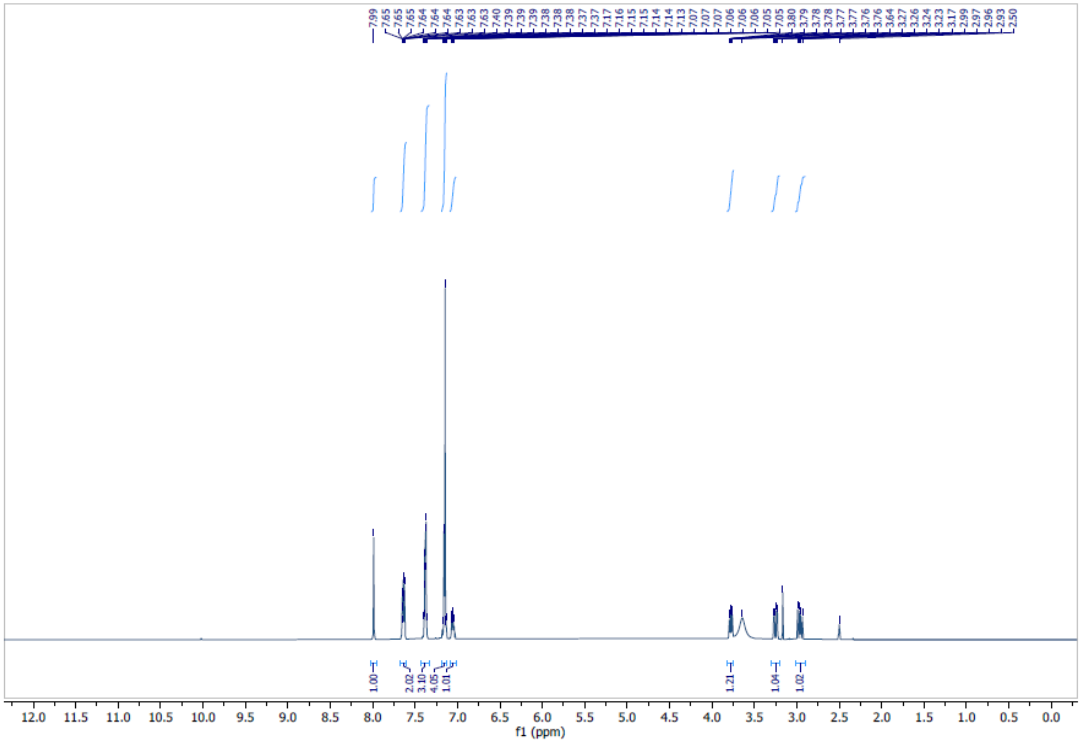


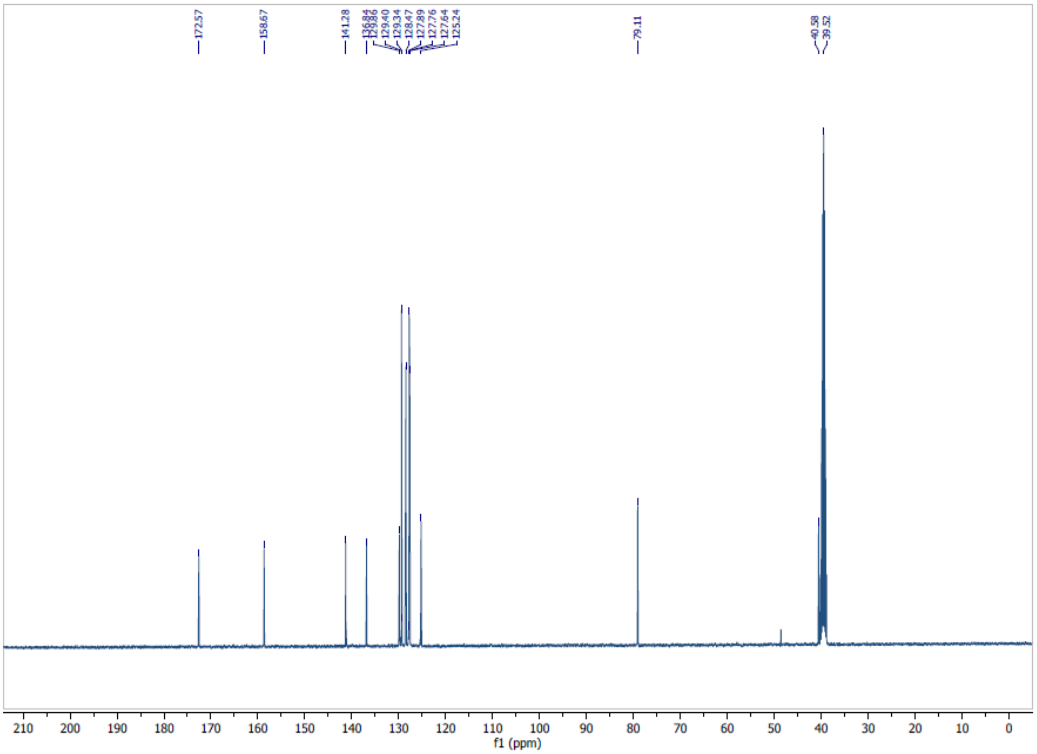

Benzaldehyde w/ Tyr:

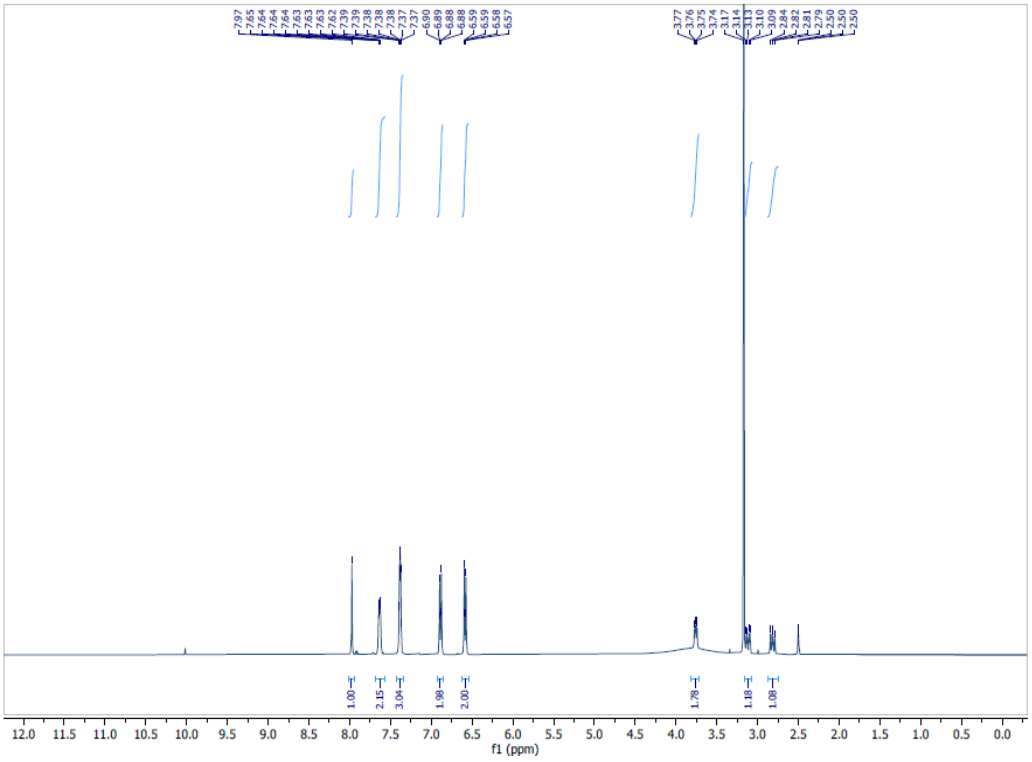


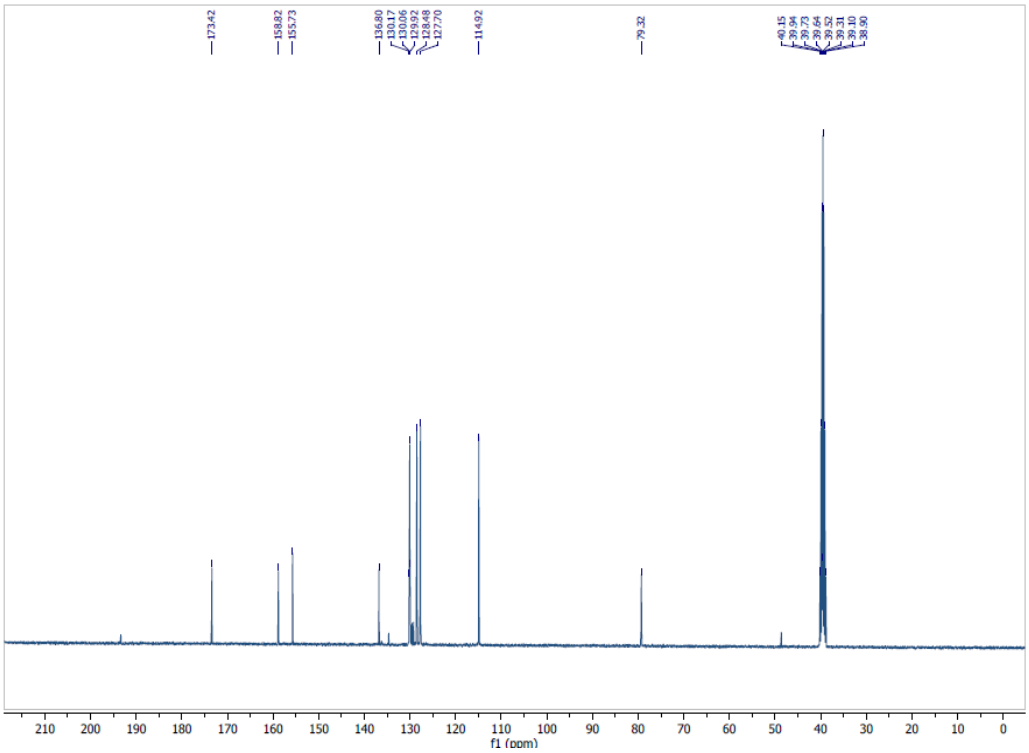

Benzaldehyde w/ Trp:

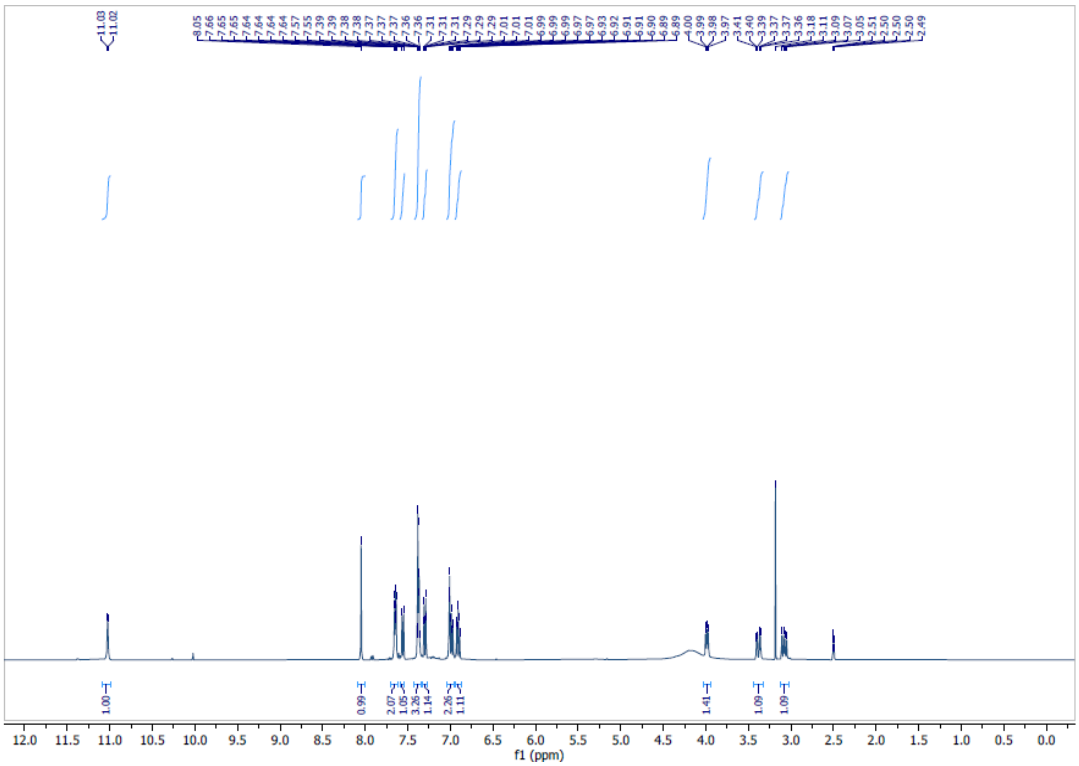


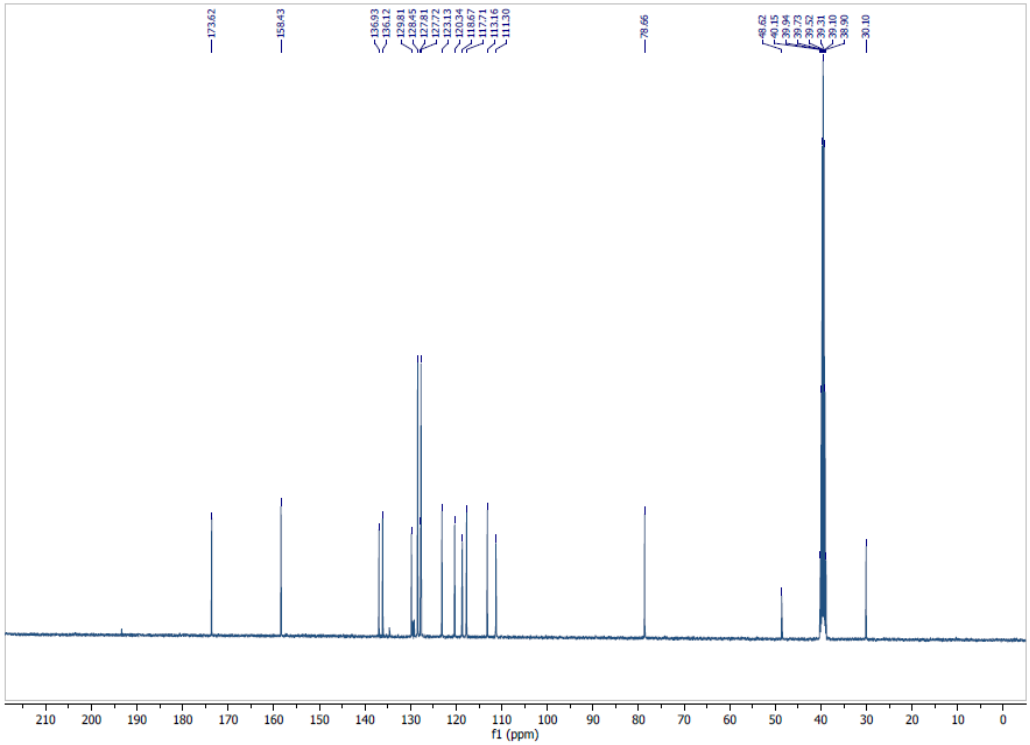

Benzaldehyde w/ Met:

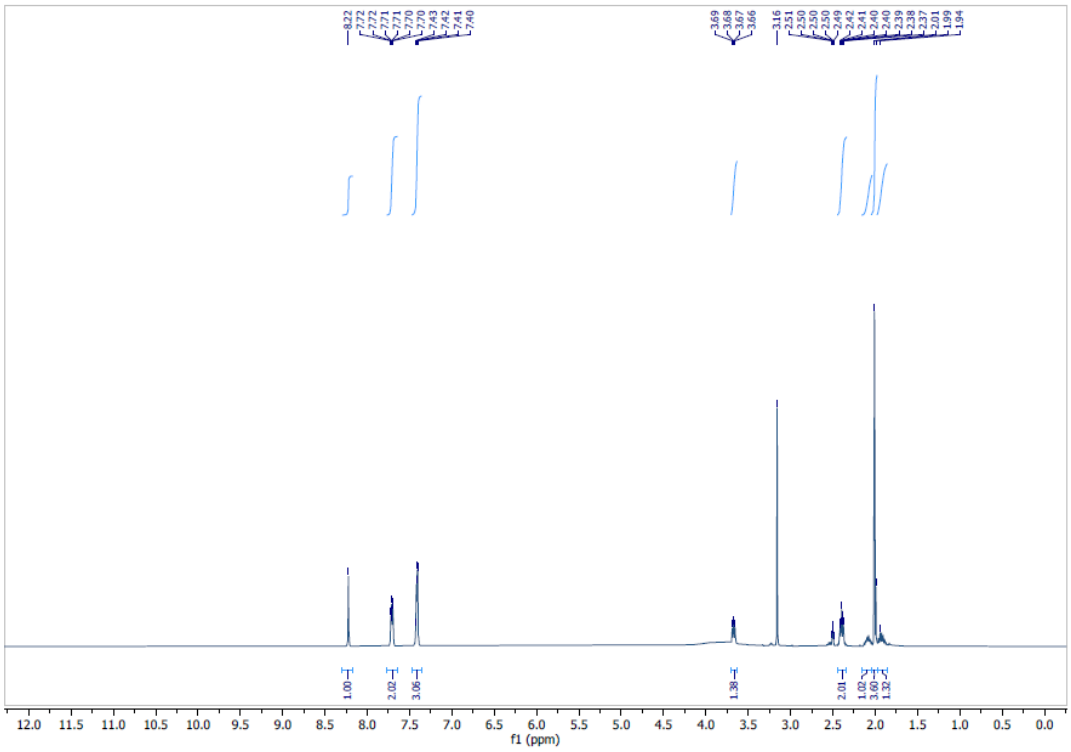


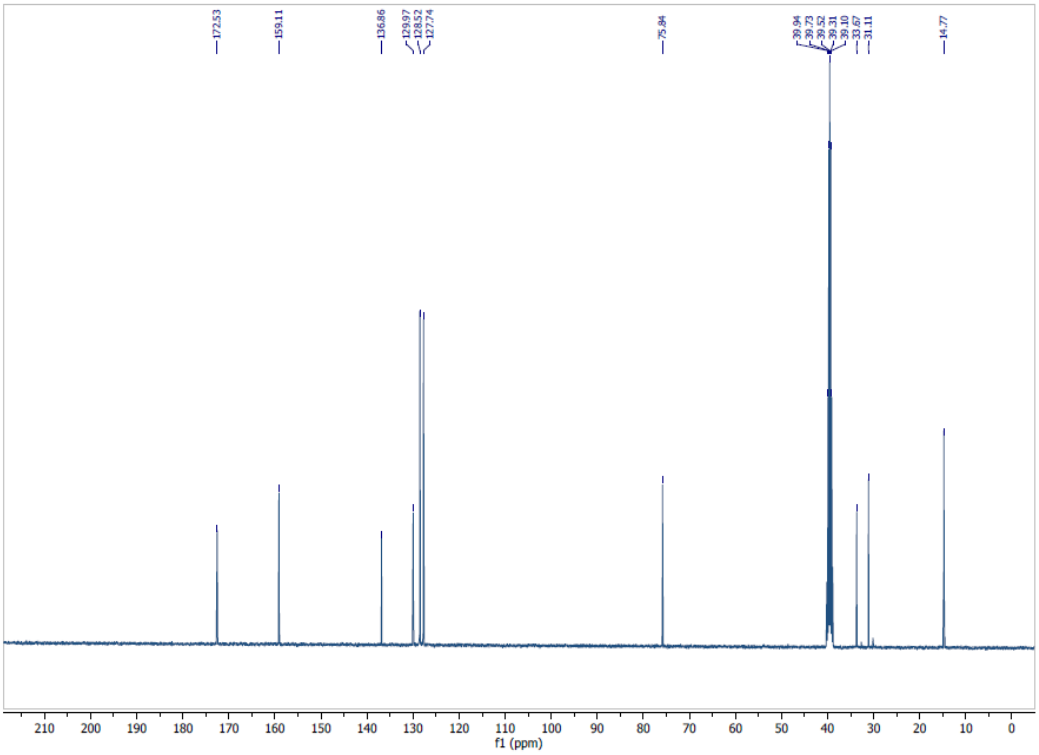

Benzaldehyde w/ Leu:

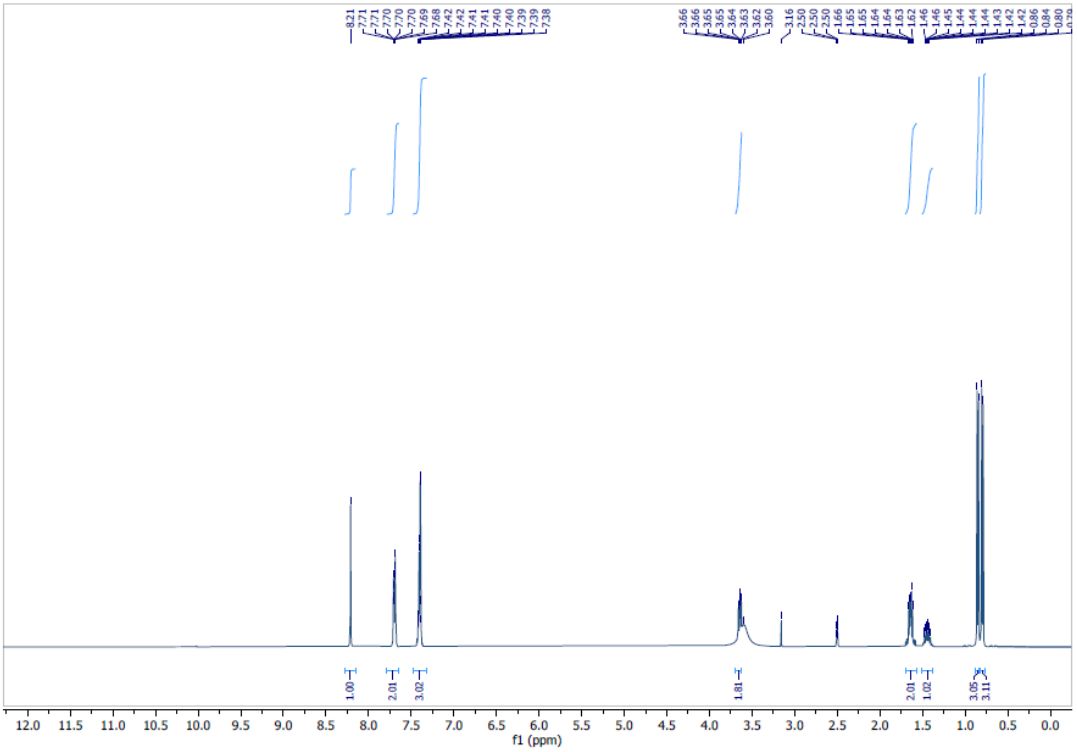


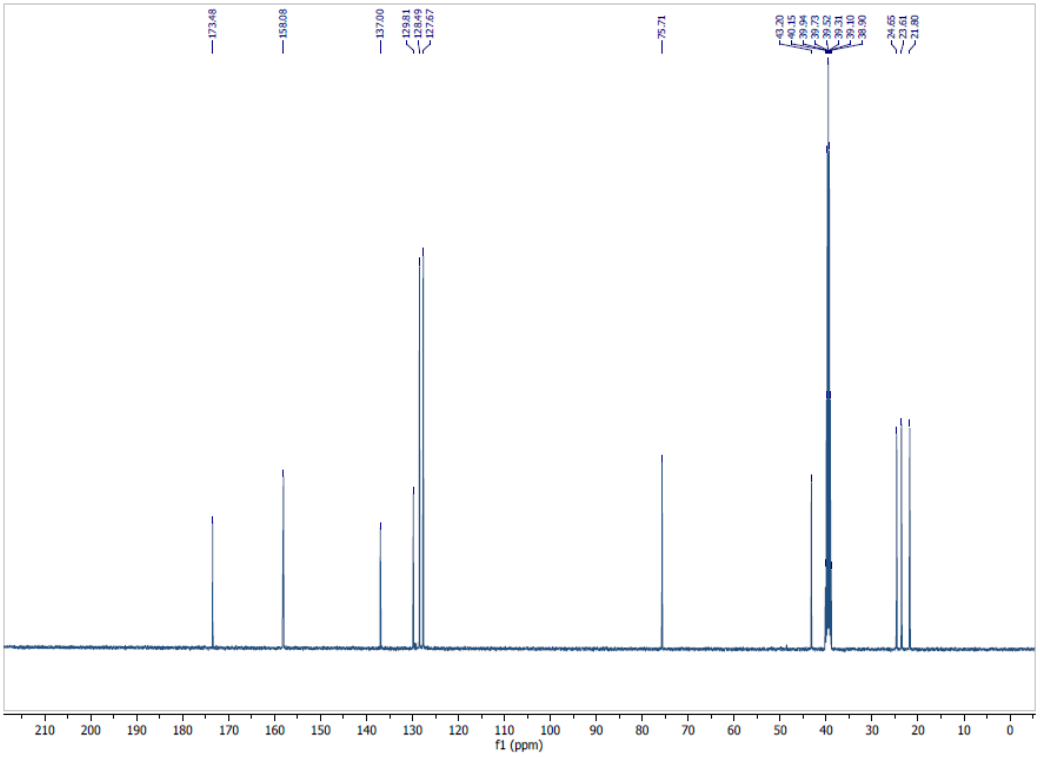

Benzaldehyde w/ Glutathione:

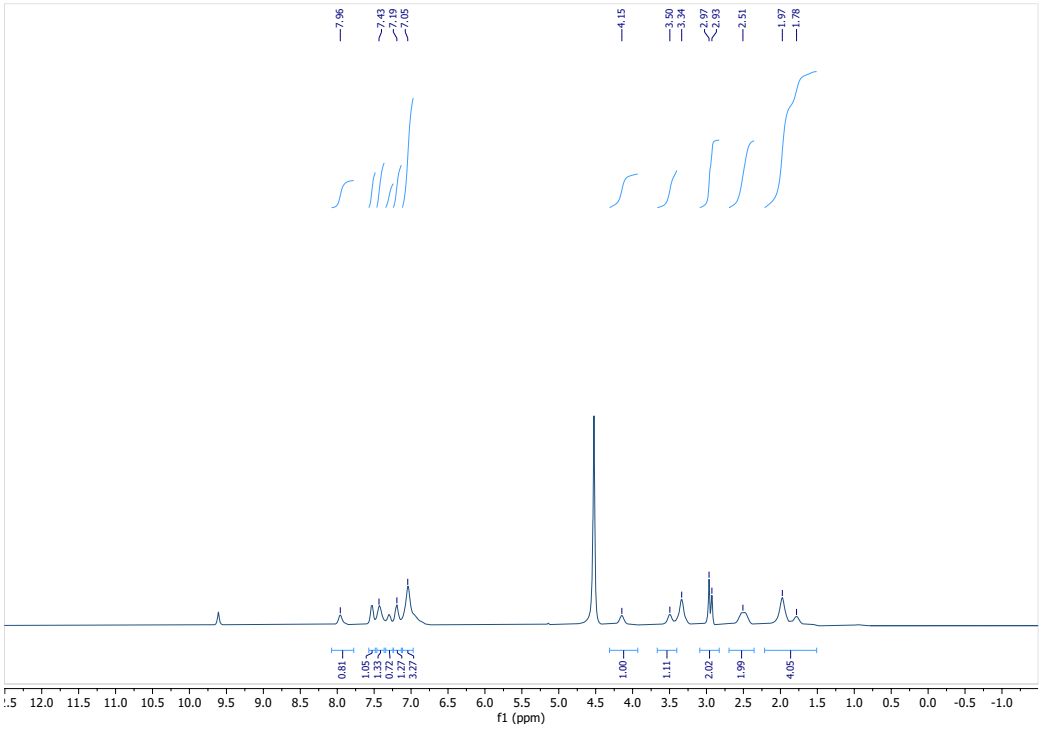

Benzaldehyde w/ Thyroxine:

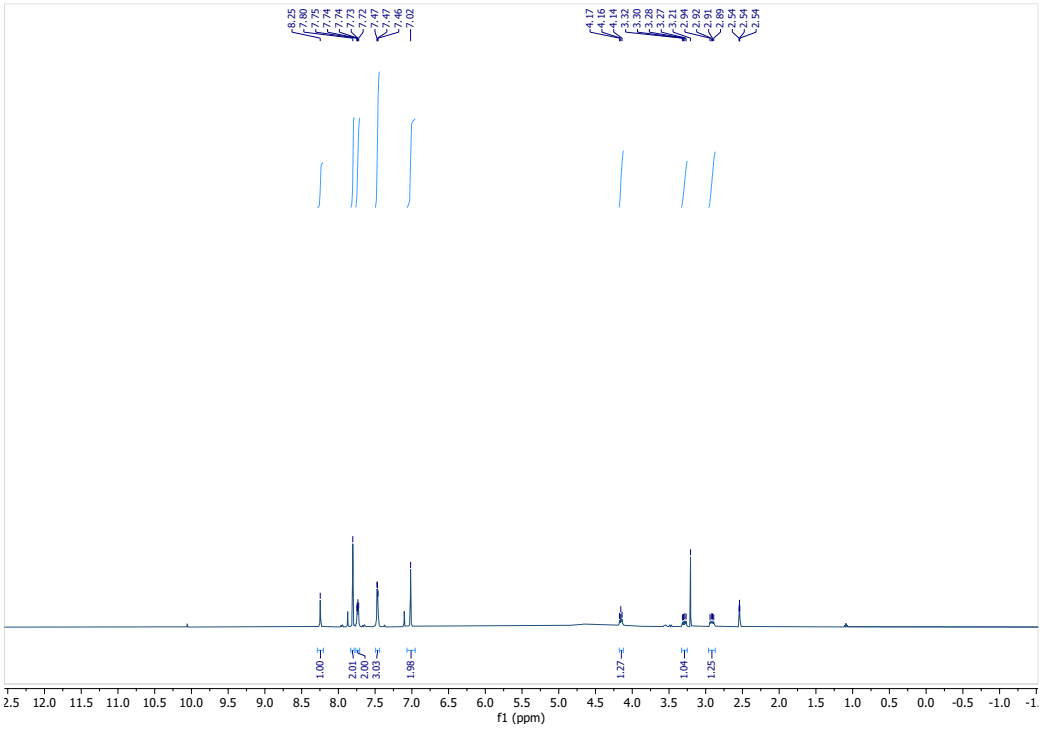


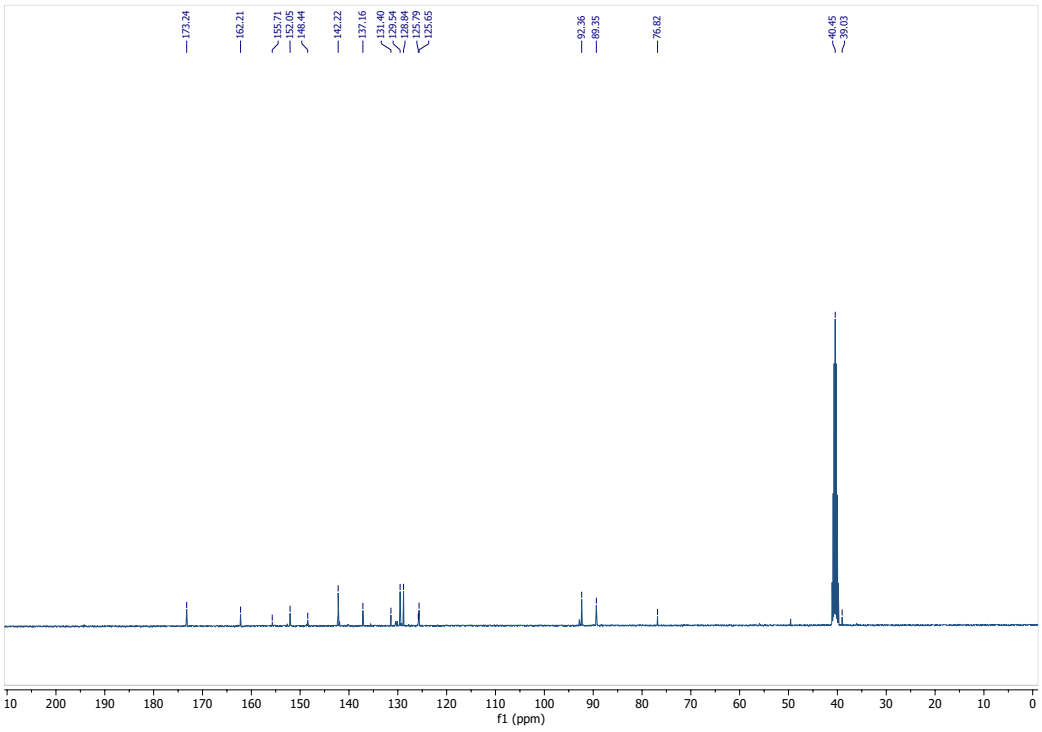

2-Pyridinecarboxaldehyde w/ Phe:

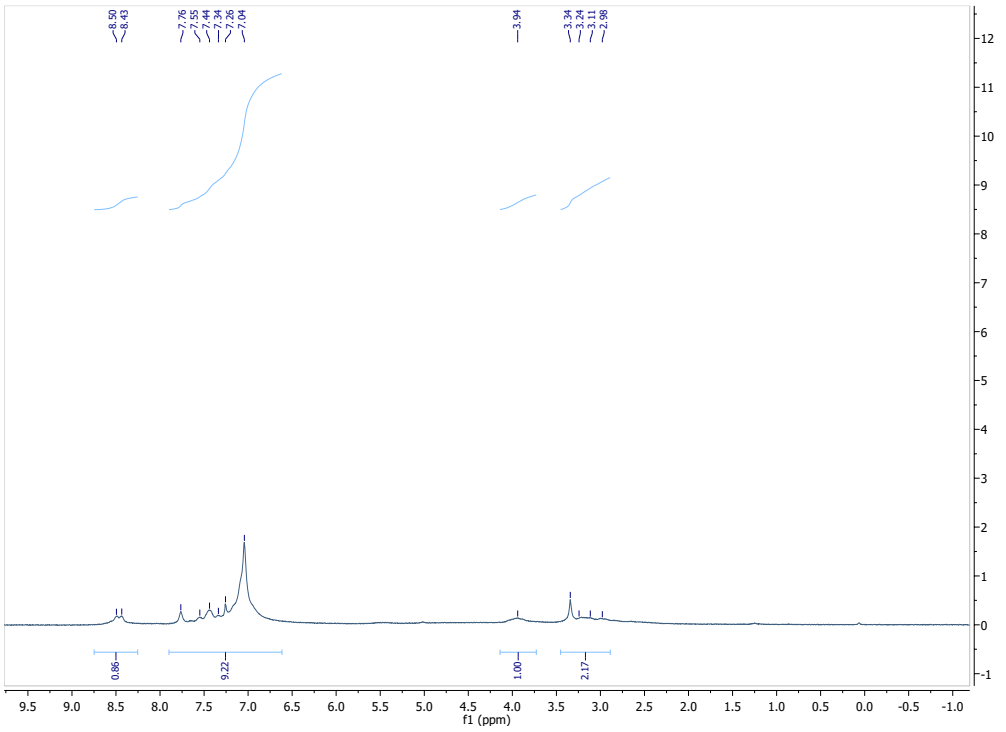


3-Pyridinecarboxaldehyde w/ Phe:

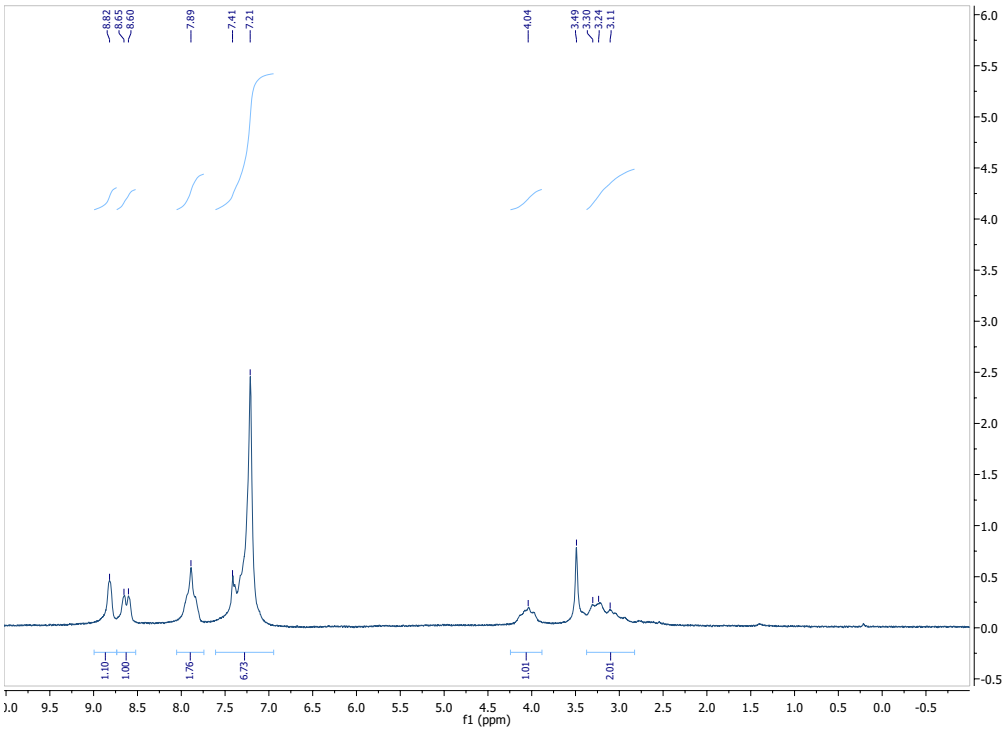

2-Phenylbenzaldehyde w/ Phe:

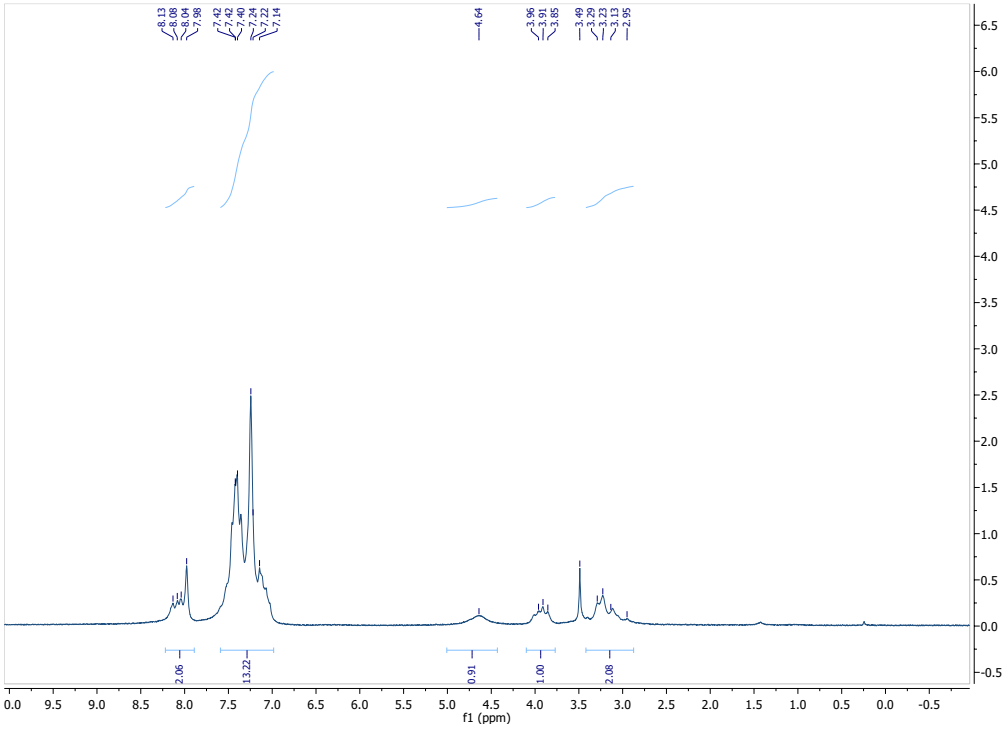

## 4.4. Extended Discussion

### 4.4.1. Lessons

Insight into the mechanism of $^{11}$C-carboxylation was completed in parallel to the work with $^{13}$C from the University of Alberta. The reaction was initially hypothesized to proceed through an aza-allyl anion intermediate formed following decarboxylation of the imine species. This offered a potential scaffold for "transfer carboxylation", beginning first with one amino acid and driving carboxylation at an alternative site to derive an entirely different amino acid (Figure 4.13). A process like this would aid in improving molar activity for $^{11}$C-synthesis, as the starting state would differ from the final product. We tested this by condensation of phenylglycine with isovaleraldehyde in an attempt to observe carboxylation at both sites from the aza-allyl anion intermediate. However, in doing so we did not observe any leucine product, suggesting the aza-allyl anion intermediate may not be involved in the reaction mechanism.

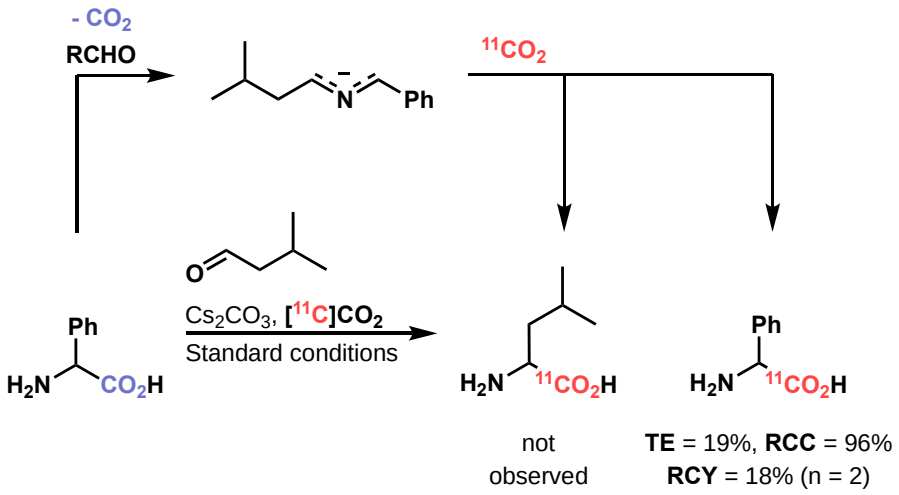


**Figure 4.13.** Transfer carboxylation. An approach to access $^{11}$C-AAs without using the same AA precursor offers potential improvements in molar activity. However, this transfer carboxylation technique did not proceed as predicted, also indicating the reaction had to be proceeding through an alternative intermediate than hypothesized.

In Alberta, further study of the mechanism with carbon-13 supported an alternative intermediate; addition of $D_2O$ under standard conditions lead to the observation of both $CO_2$ and H/D exchange, with <1% yield of the proto-/deutero-decarboxylation product that would form from an aza-allyl anion. Furthermore, while acetone could be used to catalyse carboxylate

exchange, a non-enolizable amino acid like 2-aminoisobutyric acid yielded no product. In place of the aza-allyl anion, the carboxylation of an imino-enol intermediate followed by decarboxylation was suggested.

An additional challenge in producing radiolabelled amino acids comes from enantioselectivity of the method. Given the methodology leads to the racemization of the selected amino acids upon decarboxylation, an approach to separation would be necessary. Methodologies used in the separation of $^{13}$C-amino acids are generally incompatible with the time constraints of carbon-11, like nickel-mediated dynamic kinetic resolution. In an attempt to recreate a literature method for enzymatic resolution of D- and L-amino acids, we constructed a column containing an immobilized D-amino acid oxidase/catalase enzyme complex with a Sepharose support. The oxidase is capable of selectively deaminating D-amino acids, thus allowing for more efficient separation of a ketoacid from the remaining L-amino acid.

While this method had been demonstrated to work with [$^{11}$C]leucine prepared *via* Strecker synthesis with [$^{11}$C]HCN, it proceeded far too slowly to be amenable to our conditions. In the case of the Strecker method, a very low quantity of amino acid product is prepared; by contrast, our methodology begins with amino acids as the starting material and thus comes with much higher loading to be processed by the enzymatic system. As such, the optimum incubation time of 15 minutes determined by Barrio *et al*. was not sufficient and thus the method was not viable for enantiomeric resolution.

### 4.4.2. Perspectives

#### *4.4.2.1. Conclusions*

In this chapter, we targeted new methodologies to access labelled amino acids using carbon isotope exchange. We sought improvements for $^{11}$C-amino acid synthesis that suit the specific conditions set out by radiosynthetic requirements. A sizeable scope of potential catalytic aldehydes was assessed with only minor variations in reactivity observed. We also evaluated a chiral catalyst with the intention of pushing carboxylation to one face, selectively enriching towards L- or D-amino acids; the approach worked, but only provided minor enrichment and low yields in the given reaction time.

Chiral resolution was used to isolate L-[$^{11}$C]leucine for imaging studies. BCAAs have recently become an imaging target of interest for diagnosis and evaluation of cardiovascular

conditions due to elevated oxidative metabolism within the damaged heart. As such, pilot images were collected using racemic [$^{11}$C]leucine as a proof-of-concept in a mouse model.

*4.4.2.2. Future Directions*

Continued investigation into imaging with [$^{11}$C]leucine can offer important information for BCAA metabolism. Assessments of specific uptake into tissues of interest can be performed to determine the baseline distribution; with this understanding, pharmacological blockade can be employed to evaluate the impact of key proteins and transporters. BCAAs undergo a transport process into the cytosol where they either undergo incorporation into proteins or a metabolic deconstruction process yielding intermediate coenzymes and free $CO_2$ (Figure 4.16). Key enzymes like BCAT and BCKDH as well as transporters like LAT1 and SLC25A44 are instrumental to the manipulation of BCAAs like leucine once in the cellular space. Pharmacologic manipulation of these processes can provide insight into the rates of oxidative metabolism and can be used to model the distribution of [$^{11}$C]leucine once injected in the body.

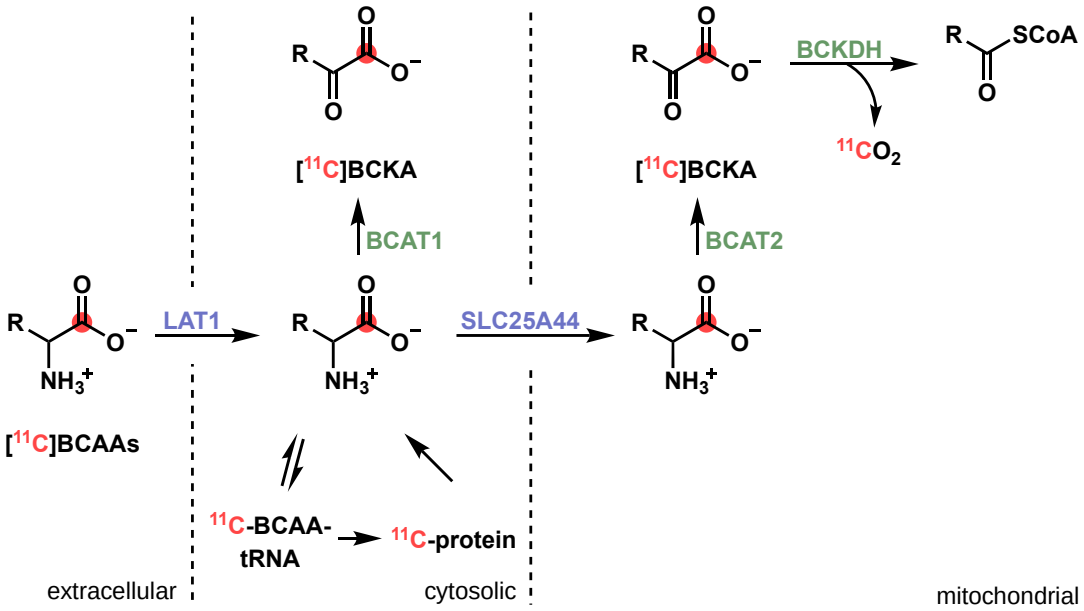


**Figure 4.14.** [$^{11}$C]BCAA outcomes in the body. Amino acids are transported into the cell where they can be integrated into proteins or degraded into intermediates for other biochemical cycles and pathways. Given the retention of the carbon-11 label, determining the rates of these processes can allow for accurate quantification of images.

# Chapter 5: Pharmacological Outcomes and Metabolism of [$^{18}$F]Flubrobenguane Radiotracer Analysis

This chapter and discussion contains information from multiple published studies.

- **FOCUS:** Mair et al. "Pharmacological and metabolic parameters of [$^{18}$F]flubrobenguane in clinical imaging populations" *J. Nucl. Cardiol.* **2023**, 30, 2089–2095. doi: 10.1007/s12350-023-03338-9.
    - Contributions: Project lead, coordinated two imaging sites, completed all experiments and analysis, wrote manuscript.
- Zelt, Britt, Mair et al. "Regional distribution of fluorine-18-flubrobenguane and carbon-11-hydroxephedrine for cardiac PET imaging of sympathetic innervation" *J. Am. Coll. Cardiol. Img.*. **2021**, 14 (7), 1425–1436. doi: 10.1016/j.jcmg.2020.09.026.
    - Contributions: Performed blood analysis, metabolic outcome assessment, reviewed manuscript.

## 5.1. Context

### 5.1.1. Radiotracer Metabolism

#### *5.1.1.1. Compartmental Modeling*

The accurate analysis of PET images is instrumental for its interpretation. An important consideration is the outcome of the injected radiotracer, whether it be uptake into on- and off-target tissues, elimination to excretory organs, or metabolic transformations into a different compound. As such, compartmental models are constructed to account for all radioactivity within the body.[1–5] The biochemical state in which a radiochemical species can be found following injection are known as compartments; within each the activity is considered to be homogenously distributed. Change in concentration within one compartment is a function of the concentrations in other compartments, and thus the compartmental model can be described in terms of linear, first-order differential equations that depict and describe characteristics like tracer perfusion, transport, uptake and washout.

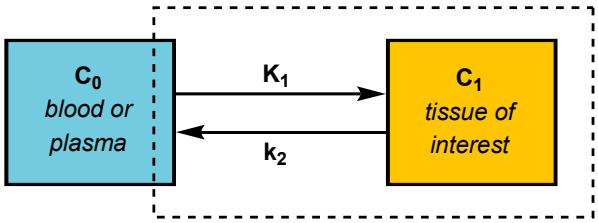


**Figure 5.1.** One-tissue compartment model. Radiotracer distribution in the body is depicted with compartmental models that track the different states of the radionuclide. The 1TCM is the simplest expression, however more complex models are often required to quantify probe kinetics.

Plasma or blood pool tends to be the first component of the model, although it is not itself a compartment. The injected radiotracer into the blood stream is instead a measurable quantity, and thus can be used to derive additional parameters or can aid in reducing the model to the lowest number of compartments for ease of analysis. The simplest model is that of the one-tissue compartment model (Figure 5.1). It is comprised of the blood pool and a compartment for the isotope in tissue, with rates of transport between. The transport between the blood pool into the tissue represents perfusion, and thus a model like this accurately describes freely diffusible tracers such as [$^{15}$O]water or [$^{13}$N]ammonia.

In practice, compartmental models are often far more complicated and have to consider all processes that the radiotracer is subjected to within the body. It is therefore important to clarify that it is not the radiotracer itself that is modelled, but the instances of radioactivity as a whole. The parent compound can undergo changes within a given tissue, whether it be incorporation into other larger molecules like in the case of amino acid integration into peptides and proteins, or a process like metabolism in which the radiotracer is degraded.

*5.1.1.2. Radiometabolites*

The metabolic outcome of a radiotracer is of great importance; at least one metabolite of the injected radiotracer will retain the radiolabel and is therefore known as a radiometabolite. Proper quantification demands accounting for these given that both the parent radiotracer and its radiometabolic products will contribute to the collected PET image.[6–9] If the radiometabolite is lipophilic enough to migrate to other tissues or if significant concentrations of radiometabolite exist in the plasma, it must also be factored into the modelling and subtracted from uptake data.

Blood samples are often drawn during imaging to evaluate the concentration of parent compound over the course of the scan. A constant blood sampling technique like arterial cannulation can be used for quantitative data analysis but can be invasive and inconvenient for many patient cohorts. Venous sampling is less invasive of a procedure than arterial sampling, however it is dependent on the sampling site and on radiotracer clearance. In place of blood sampling one can also use a reference tissue time-activity-curve, but this requires a region in which there is no specific uptake of the radiotracer while also possessing similar non-specific binding as the tissue or organ of interest. Additionally, it needs to be sufficiently close to the target organ so as to be visible in the same PET image but with enough distance to not have spillover from adjacent radioactivity hotspots. This can be especially difficult to satisfy for both brain and cardiac PET imaging and so sampling remains the gold standard.

These samples are then treated to isolate plasma, within which the fraction of parent compound is measured using high-performance liquid chromatography.[10] From there, kinetic modeling fitting the data to a mathematical function can be completed.

*5.1.1.3. Input Function*

The input (or delivery) function is a measurement of the concentration of parent compound within plasma as a function of time. It plays a vital role in image interpretation in order to normalize tissue uptake across different organs, different patients, and different studies entirely.[11] While arterial input functions can be technically challenging and invasive for patients, image-derived input functions are frequently regarded as a more practical alternative.[12,13]

Obtaining a radiometabolite-corrected input function requires multiple steps:

1. Measurement of whole blood and plasma activity to derive the plasma-to-whole blood ratio – PBR(t)
2. Parent fraction in plasma, determined by HPLC analysis of plasma samples – PF(t)
3. Analysis of binding to proteins circulating in plasma to determine the freely distributed, unbound radiotracer – $f_P$

Following the development of these corrections, in which imaging alone is not sufficient, the input function can then be used alongside either arterial blood sample concentrations or image-derived volumes of interest drawn in tissues of interest.

### 5.1.2. Cardiac ANS Imaging

The autonomic nervous system is a network of neurons controlling the body's involuntary functions and internal organs.[14] It is made up of the sympathetic nervous system (SNS), often known as the "fight or flight" system in which it prepares the body for action, the parasympathetic nervous system (PNS), coined the "rest and digest system" to regulate the body at rest, and the enteric nervous system, which is dedicated to control of the gastrointestinal tract. The sympathetic and parasympathetic systems play integral roles in cardiac function with essential mediation of blood flow, contractility, and heart rate.[15,16]

Parasympathetic neurons originate from the brain stem's nucleus ambiguus *via* the vagus nerve, projecting into cardiac ganglia where acetylcholine is released. Conversely, sympathetic neurons extend from the locus coeruleus to ganglia where norepinephrine is released into the synaptic cleft. While parasympathetic fibres are mainly present throughout the atrium, the sympathetic nervous system is prevalent throughout the ventricular myocardium. The heart is

under continuous control from the PNS whereas it is activated during periods of stress from the SNS. Altered autonomic function is characteristic of several cardiac pathologies, and so physicians turn towards molecular imaging techniques like PET to diagnose and evaluate these conditions. From this interest, several radiotracer options have arisen (Figure 5.2).[17–22]

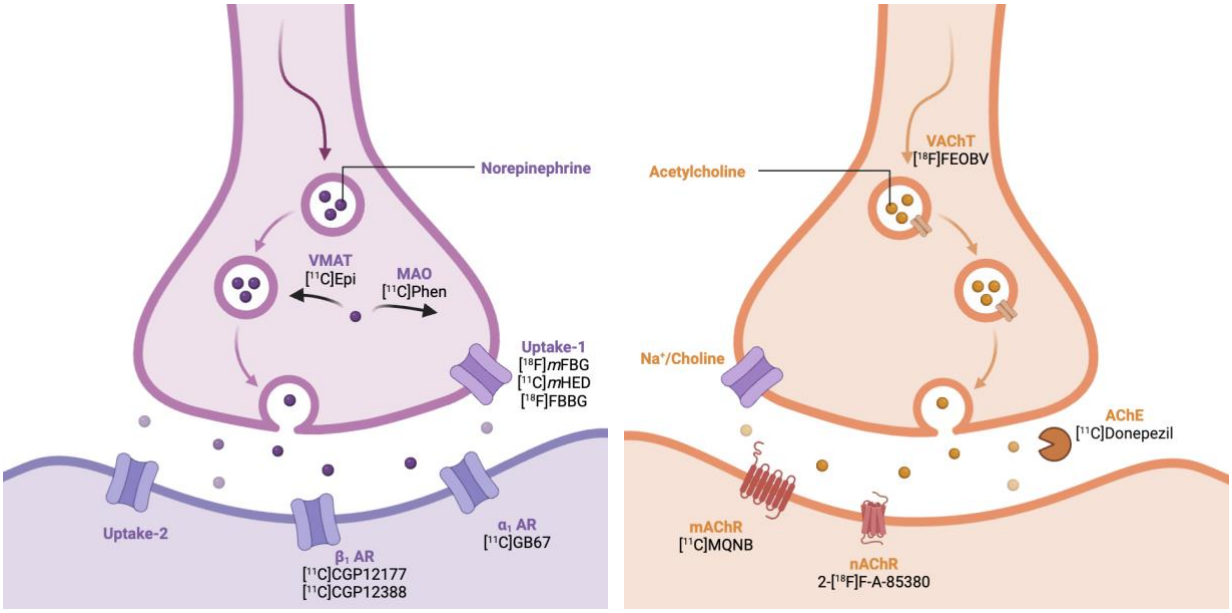


**Figure 5.2.** Autonomic nervous system PET imaging. Neuronal imaging has been investigated for diagnosis and evaluation of cardiovascular diseases. Several radiotracers for the sympathetic nervous system (purple, left) and the parasympathetic nervous system (orange, right) have been developed and studied for cardiac PET.

*5.1.2.1. PNS Imaging*

Research and development of radiotracers targeting the cardiac parasympathetic nervous system has historically been limited. While there has been significant work on developing imaging agents for the brain, very little has been successful in imaging myocardial PNS activity.[23] Examples like the postsynaptic muscarinic receptor-targeting [$^{11}$C]methiodide quinuclidinyl benzilate ([$^{11}$C]MQNB) and acetylcholine esterase's [$^{11}$C]donepezil have been investigated, but neither has shown enough promise for extension to clinical validation and regular usage. [$^{18}$F]Fluoroethoxybenzovesamicol ([$^{18}$F]FEOBV) is used for imaging the vesicular acetylcholine transporter and while it has predominantly been investigated in the brain,[24,25] recent research into its use in imaging cardiac innervation has shown promise.[26]

*5.1.2.2. SNS Imaging*

To date, the most extensively used radiotracers for imaging sympathetic innervation are [$^{123}$I]*meta*-iodobenzylguanidine ([$^{123}$I]mIBG) using SPECT, and [$^{11}$C]*meta*-hydroxyephedrine ([$^{11}$C]HED) for PET imaging (Figure 5.3). The former has predominantly been used in imaging of the whole myocardium rather than region-specific determinations, largely due to the limited spatial resolution for SPECT imaging. Interest in modernizing and developing a PET radiotracer using [$^{123}$I]mIBG's benzylguanidine scaffold led to the development of an alternative, [$^{18}$F]*meta*-fluorobenzylguanidine ([$^{18}$F]mFBG),[27] as well as pre-clinical evaluations completed within our lab.[28] Continued investigations into its mechanism of action and tracer kinetics are ongoing, however it has already begun to be investigated for clinical use for cardiac sympathetic imaging.[29]

Alternatively, [$^{11}$C]HED represents the most frequently used radiotracer for neuronal imaging, with routine production in some radiochemistry facilities and PET clinics. However, carbon-11 radiotracers are limited in their potential for distribution, requiring an on-site cyclotron and operating facility, and thus a fluorine-18 alternative offers great value. Addressing that need, a novel $^{18}$F-labelled radiotracer known as flubrobenguane (LMI1195 or N-[3-bromo-4-(3-[$^{18}$F]fluoropropoxy)benzyl]guanidine) was developed.

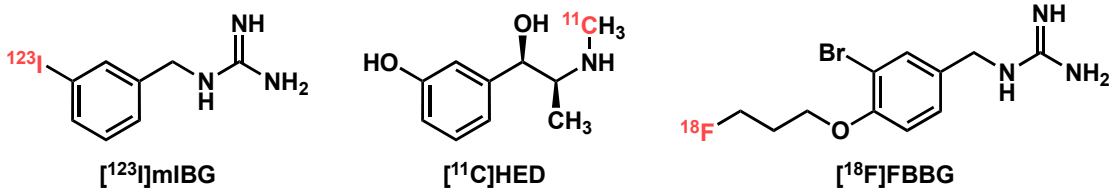


**Figure 5.3.** Radiotracers for sympathetic innervation. [$^{123}$I]mIBG, [$^{11}$C]HED, and the more recently explored [$^{18}$F]FBBG are used for imaging cardiac neuronal activity.

### 5.1.3. [$^{18}$F]Flubrobenguane

*5.1.3.1. Fluorine-18*

Fluorine-18 ($^{18}$F, $t_{1/2}$ = 109.7 min) is the predominant PET radioisotope alongside carbon-11. It is produced most frequently by a cyclotron with the proton bombardment of enriched [$^{18}$O]water. This leads to the production of aqueous [$^{18}$F]fluoride ([$^{18}$F]$F^-$) which can be used as a nucleophile in organic synthesis. Alkyl [$^{18}$F]fluorides are typically prepared with nucleophilic substitutions displacing leaving groups (-OTf, -OTs, halides, etc). Due to its longer half-life, $^{18}$F

is the ideal isotope for radiolabelling with the intention of distribution to off-site imaging centers. Radiotracers like [$^{18}$F]FDG, [$^{18}$F]fluorodopa, [$^{18}$F]flumazenil, and [$^{18}$F]florbetapir remain amongst the most commonly used in PET imaging as a result of their half-life and their dispensation.

#### *5.1.3.2. FBBG*

Flubrobenguane (FBBG) resembles [$^{123}$I]mIBG in its benzylguanidine core and behaves similarly in its pharmacokinetics and distribution in preclinical animal models.[30] However, in an effort to improve its distribution and functionality as a radiotracer, it's labelled instead with fluorine-18. Also like [$^{123}$I]mIBG, FBBG is a substrate for the norepinephrine transporter, a protein responsible for sodium chloride-dependent reuptake of norepinephrine and dopamine from the synaptic cleft into the presynaptic neuron.

Its use in a patient cohort of healthy volunteers proved successful and found feasibility in the determination of myocardial sympathetic activity.[31] With this data in mind, and with the fluorine-18 radiolabel, FBBG is well positioned to become the new gold standard for PET imaging of cardiac innervation in place of [$^{11}$C]HED.

### 5.1.4. [$^{18}$F]FBBG vs [$^{11}$C]HED for cardiac PET imaging of sympathetic innervation

#### *5.1.4.1. Summary*

In a previously published study, we evaluated FBBG in clinically relevant patient cohorts for the assessment of myocardial sympathetic nerve function.[32] This was compared in parallel to [$^{11}$C]HED. Participants (25), including healthy volunteers and those with ischemic and non-ischemic cardiomyopathy, were administered FBBG and HED in separate imaging sessions and then compared. FBBG and HED were found to have a strong correlation in measuring global innervation and regional denervation within the myocardium. Notably, the ventricular retention was remarkably similar for both radiotracers, with no significant differences found in radiotracer behaviour at the regional level. As such, this study confirmed the viability of FBBG for use in a clinical setting evaluating neuronal activity in the myocardium, and established its applicability in evaluating cardiomyopathies.

*5.1.4.2. Limitations*

A major limitation in this study was the use of corrections to the input function that were derived from studies with healthy volunteers from Sinusas *et al.*[31] While these may still be suitable, pathologies relevant for imaging (like ischemic and non-ischemic cardiomyopathy) may have differences in tracer distribution, uptake and washout, and so cohort-specific (or at the very least non-healthy) corrections may be necessary. This was further remarked by Sinusas in a response to the publication.[33]

*5.1.4.3. Contributions*

During each scan, venous blood samples were collected from a cannula placed in a vein in the antecubital fossa of the opposite arm to injection at a series of timepoints (0.5, 1, 2, 5, 10, 20, 30, 40, 60 min). The samples were contained in heparinized tubes and stored on ice to be transported from the clinical PET room to a radiochemistry wet lab. There, samples were treated to either HPLC or SPE separation to analyse the percent of activity attributed to parent compound. This process is described in detail in the following section and publication.

### 5.1.5. References


(1) Anderson, D. H. *Compartmental Modeling and Tracer Kinetics*; Levin, S., Series Ed.; Lecture Notes in Biomathematics; Springer: Berlin, Heidelberg, 1983; Vol. 50. https://doi.org/10.1007/978-3-642-51861-4.

(2) Gunn, R. N.; Gunn, S. R.; Cunningham, V. J. Positron Emission Tomography Compartmental Models. *J Cereb Blood Flow Metab* **2001**, *21* (6), 635–652. https://doi.org/10.1097/00004647-200106000-00002.

(3) Lammertsma, A. A. Radioligand Studies: Imaging and Quantitative Analysis. *European Neuropsychopharmacology* **2002**, *12* (6), 513–516. https://doi.org/10.1016/S0924-977X(02)00100-1.

(4) Schmidt, K. C.; Turkheimer, F. E. Kinetic Modeling in Positron Emission Tomography. *Q J Nucl Med* **2002**, *46* (1), 70–85.

(5) Lammertsma, A. A. Compartmental Modeling in Emission Tomography. In *Handbook of Particle Detection and Imaging*; Grupen, C., Buvat, I., Eds.; Springer: Berlin, Heidelberg, 2012; pp 1065–1081. https://doi.org/10.1007/978-3-642-13271-1_42.

(6) Huang, S. C.; Barrio, J. R.; Yu, D.; Chen, B.; Grafton, S.; Melega, W. P.; Hoffman, J. M.; Satyamurthy, N.; Mazziotta, J. C.; Phelps, M. E. Modelling Approach for Separating Blood Time Activity Curves in Positron Emission Tomographic Studies. *Phys. Med. Biol.* **1991**, *36* (6), 749. https://doi.org/10.1088/0031-9155/36/6/004.

(7) Burger, C.; Buck, A. Tracer Kinetic Modelling of Receptor Data with Mathematical Metabolite Correction. *Eur J Nucl Med* **1996**, *23* (5), 539–545. https://doi.org/10.1007/BF00833389.

(8) Tonietto, M.; Veronese, M.; Rizzo, G.; Zanotti-Fregonara, P.; Lohith, T. G.; Fujita, M.; Zoghbi, S. S.; Bertoldo, A. Improved Models for Plasma Radiometabolite Correction and Their Impact on Kinetic Quantification in PET Studies. *J Cereb Blood Flow Metab* **2015**, *35* (9), 1462–1469. https://doi.org/10.1038/jcbfm.2015.61.

(9) Tonietto, M.; Rizzo, G.; Veronese, M.; Fujita, M.; Zoghbi, S. S.; Zanotti-Fregonara, P.; Bertoldo, A. Plasma Radiometabolite Correction in Dynamic PET Studies: Insights on the Available Modeling Approaches. *J Cereb Blood Flow Metab* **2016**, *36* (2), 326–339. https://doi.org/10.1177/0271678X15610585.

(10) Hilton, J.; Yokoi, F.; Dannals, R. F.; Ravert, H. T.; Szabo, Z.; Wong, D. F. Column-Switching HPLC for the Analysis of Plasma in PET Imaging Studies. *Nuclear Medicine and Biology* **2000**, *27* (6), 627–630. https://doi.org/10.1016/S0969-8051(00)00125-6.

(11) Bentourkia, M. Determination of the Input Function at the Entry of the Tissue of Interest and Its Impact on PET Kinetic Modeling Parameters. *Mol Imaging Biol* **2015**, *17* (6), 748–756. https://doi.org/10.1007/s11307-015-0895-8.

(12) Zanotti-Fregonara, P.; Chen, K.; Liow, J.-S.; Fujita, M.; Innis, R. B. Image-Derived Input Function for Brain PET Studies: Many Challenges and Few Opportunities. *J Cereb Blood Flow Metab* **2011**, *31* (10), 1986–1998. https://doi.org/10.1038/jcbfm.2011.107.

(13) Feng, D. D.; Chen, K.; Wen, L. Noninvasive Input Function Acquisition and Simultaneous Estimations With Physiological Parameters for PET Quantification: A Brief Review. *IEEE Transactions on Radiation and Plasma Medical Sciences* **2020**, *4* (6), 676–683. https://doi.org/10.1109/TRPMS.2020.3010844.

(14) McCorry, L. K. Physiology of the Autonomic Nervous System. *Am J Pharm Educ* **2007**, *71* (4), 78.

(15) Hasan, W. Autonomic Cardiac Innervation: Development and Adult Plasticity. *Organogenesis* **2013**, *9* (3), 176. https://doi.org/10.4161/org.24892.

(16) Hadaya, J.; Ardell, J. L. Autonomic Modulation for Cardiovascular Disease. *Frontiers in Physiology* **2020**, *11*, 617459. https://doi.org/10.3389/fphys.2020.617459.

(17) Goldstein, D. S.; Chang, P. C.; Eisenhofer, G.; Miletich, R.; Finn, R.; Bacher, J.; Kirk, K. L.; Bacharach, S.; Kopin, I. J. Positron Emission Tomographic Imaging of Cardiac Sympathetic Innervation and Function. *Circulation* **1990**, *81* (5), 1606–1621. https://doi.org/10.1161/01.cir.81.5.1606.

(18) Goldstein, D. S. Imaging of the Autonomic Nervous System: Focus on Cardiac Sympathetic Innervation. *Semin Neurol* **2003**, *23* (4), 423–433. https://doi.org/10.1055/s-2004-817726.

(19) Travin, M. I. Imaging of Cardiac Autonomic Innervation with SPECT and PET. *Curr Cardiovasc Imaging Rep* **2013**, *7* (1), 9242. https://doi.org/10.1007/s12410-013-9242-0.

(20) Thackeray, J. T.; Bengel, F. M. PET Imaging of the Autonomic Nervous System. *Q J Nucl Med Mol Imaging* **2016**, *60* (4), 362–382.

(21) Boutagy, N. E.; Sinusas, A. J. Recent Advances and Clinical Applications of PET Cardiac Autonomic Nervous System Imaging. *Curr Cardiol Rep* **2017**, *19* (4), 33. https://doi.org/10.1007/s11886-017-0843-0.

(22) Thackeray, J. T.; Bengel, F. M. PET Imaging of Autonomic Innervation and Receptors. In *Cardiac CT, PET & MR*; John Wiley & Sons, Ltd, 2019; pp 203–235. https://doi.org/10.1002/9781118754467.ch6.

(23) Le Guludec, D.; Delforge, J.; Dollé, F. Imaging the Parasympathetic Cardiac Innervation with PET. In *Autonomic Innervation of the Heart: Role of Molecular Imaging*; Slart, R. H. J. A., Tio, R. A., Elsinga, P. H., Schwaiger, M., Eds.; Springer: Berlin, Heidelberg, 2015; pp 111–135. https://doi.org/10.1007/978-3-662-45074-1_6.

(24) Cyr, M.; Parent, M. J.; Mechawar, N.; Rosa-Neto, P.; Soucy, J.-P.; Aliaga, A.; Kostikov, A.; Maclaren, D. A. A.; Clark, S. D.; Bedard, M.-A. PET Imaging with [$^{18}$F]Fluoroethoxybenzovesamicol ([$^{18}$F]FEOBV) Following Selective Lesion of Cholinergic Pedunculopontine Tegmental Neurons in Rat. *Nucl Med Biol* **2014**, *41* (1), 96–101. https://doi.org/10.1016/j.nucmedbio.2013.10.004.

(25) Aghourian, M.; Legault-Denis, C.; Soucy, J.-P.; Rosa-Neto, P.; Gauthier, S.; Kostikov, A.; Gravel, P.; Bédard, M.-A. Quantification of Brain Cholinergic Denervation in Alzheimer's Disease Using PET Imaging with [$^{18}$F]-FEOBV. *Mol Psychiatry* **2017**, *22* (11), 1531–1538. https://doi.org/10.1038/mp.2017.183.

(26) Saint-Georges, Z.; Zayed, V. K.; Dinelle, K.; Cassidy, C.; Soucy, J.-P.; Massarweh, G.; Rotstein, B.; Nery, P. B.; Guimond, S.; deKemp, R.; Tuominen, L. First-in-Human Imaging and Kinetic Analysis of Vesicular Acetylcholine Transporter Density in the Heart Using [$^{18}$F]FEOBV PET. *J Nucl Cardiol* **2021**, *28* (1), 50–54. https://doi.org/10.1007/s12350-020-02323-w.

(27) Garg, P. K.; Garg, S.; Zalutsky, M. R. Synthesis and Preliminary Evaluation of *Para*- and *Meta*-[$^{18}$F]Fluorobenzylguanidine. *Nuclear Medicine and Biology* **1994**, *21* (1), 97–103. https://doi.org/10.1016/0969-8051(94)90135-X.

(28) Ismailani, U. S.; Buchler, A.; Farber, G.; Pekošak, A.; Farber, E.; MacMullin, N.; Suuronen, E. J.; Vasdev, N.; Beanlands, R. S. B.; de Kemp, R. A.; Rotstein, B. H. Cardiac Sympathetic Positron Emission Tomography Imaging with Meta-[$^{18}$F]Fluorobenzylguanidine Is Sensitive to Uptake-1 in Rats. *ACS Chem. Neurosci.* **2021**, *12* (22), 4350–4360. https://doi.org/10.1021/acschemneuro.1c00575.

(29) Grkovski, M.; Zanzonico, P. B.; Modak, S.; Humm, J. L.; Narula, J.; Pandit-Taskar, N. F-18 Meta-Fluorobenzylguanidine PET Imaging of Myocardial Sympathetic Innervation. *Journal of Nuclear Cardiology* **2022**, *29* (6), 3179–3188. https://doi.org/10.1007/s12350-021-02813-5.

(30) Yu, M.; Bozek, J.; Lamoy, M.; Guaraldi, M.; Silva, P.; Kagan, M.; Yalamanchili, P.; Onthank, D.; Mistry, M.; Lazewatsky, J.; Broekema, M.; Radeke, H.; Purohit, A.; Cdebaca, M.; Azure, M.; Cesati, R.; Casebier, D.; Robinson, S. P. Evaluation of LMI1195, a Novel $^{18}$F-Labeled Cardiac Neuronal PET Imaging Agent, in Cells and Animal Models. *Circ Cardiovasc Imaging* **2011**, *4* (4), 435–443. https://doi.org/10.1161/CIRCIMAGING.110.962126.

(31) Sinusas, A. J.; Lazewatsky, J.; Brunetti, J.; Heller, G.; Srivastava, A.; Liu, Y.-H.; Sparks, R.; Puretskiy, A.; Lin, S.; Crane, P.; Carson, R. E.; Lee, L. V. Biodistribution and Radiation Dosimetry of LMI1195: First-in-Human Study of a Novel $^{18}$F-Labeled Tracer for Imaging Myocardial Innervation. *J Nucl Med* **2014**, *55* (9), 1445–1451. https://doi.org/10.2967/jnumed.114.140137.

(32) Zelt, J. G. E.; Britt, D.; Mair, B. A.; Rotstein, B. H.; Quigley, S.; Walter, O.; Garrard, L.; Robinson, S.; Mielniczuk, L. M.; deKemp, R. A.; Beanlands, R. S. Regional Distribution of Fluorine-18-Flubrobenguane and Carbon-11-Hydroxyephedrine for Cardiac PET Imaging of Sympathetic Innervation. *JACC: Cardiovascular Imaging* **2021**, *14* (7), 1425–1436. https://doi.org/10.1016/j.jcmg.2020.09.026.

(33) Sinusas, A. J.; Liu, C. Multi-Tracer Positron Emission Tomography Quantification of Sympathetic Innervation: Tracer Similarity But Not Equivalence∗. *JACC: Cardiovascular Imaging* **2021**, *14* (7), 1437–1439. https://doi.org/10.1016/j.jcmg.2020.10.007.

## 5.2. Pharmacological and metabolic parameters of flubrobenguane in clinical imaging populations

Braeden A. Mair,[1,2] Jason G.E. Zelt,[2,3] Kirabo Nekesa,[1,2] Zacharie Saint-Georges,[2,4,5] Katie Dinelle,[5] Myriam Adi,[1,2] Simon Robinson,[6] Lisa M. Mielniczuk,[2] Jakov Shlik,[5,7] Rob S. Beanlands,[2] Robert A. deKemp,[2] Benjamin H. Rotstein*[1,2,8]

[1] Department of Chemistry and Biomolecular Sciences, University of Ottawa, Ottawa, Canada K1H 8M5

[2] University of Ottawa Heart Institute, Ottawa, Canada K1Y 4W7

[3] Department of Medicine, Faculty of Medicine, University of Ottawa, Ottawa, Canada

[4] Department of Cellular and Molecular Medicine, University of Ottawa, Ottawa, Canada

[5] The University of Ottawa Institute of Mental Health Research at the Royal, Ottawa, Canada

[6] Lantheus Medical Imaging, Inc., North Billerica, MA

[7] Department of Psychiatry, University of Ottawa, Ottawa, Canada

[8] Department of Biochemistry, Microbiology and Immunology, University of Ottawa, Ottawa, Canada K1H 8M5

Mair et al. *J. Nucl. Cardiol.* **2023**, 30, 2089–2095.

https://doi.org/10.1007/s12350-023-03338-9

### 5.2.1. Statement of the manuscript

The manuscript "Pharmacological and metabolic parameters of [$^{18}$F]flubrobenguane in clinical imaging populations" was accepted into *Journal of Nuclear Cardiology* and published on July 26, 2023. In this paper, I detail the development of an HPLC and SPE method for metabolic analysis of blood samples derived from patients undergoing [$^{18}$F]FBBG imaging, followed by the derivation of an input function for clinical populations.

Blood samples were collected at two separate sites – the University of Ottawa Heart Institute (UOHI) and the Royal Institute of Mental Health Research (IMHR) – by imaging staff. Blood was transported from the clinic to the wet lab by me, Jason Zelt (MD/PhD Candidate), Kirabo Nekesa (BSc Candidate), Myriam Adi (BSc Candidate) and Dr. Benjamin Rotstein for UOHI samples, and by me and Katie Dinelle (MSc) for IMHR. I performed blood handling, as well as HPLC and SPE method development and separations, with assistance from Dr. Benjamin Rotstein. Plasma protein binding was determined by me, Jason Zelt, Kirabo Nekesa, Myriam Adi and Dr. Benjamin Rotstein. Parallel imaging studies were performed by Jason Zelt, Zacharie Saint-Georges (MD/PhD Candidate), Katie Dinelle, Dr. Lisa M. Mielniczuk (MD), Dr. Jakov Shlik (MD, PhD), Dr. Rob Beanlands (MD) and Dr. Robert DeKemp (PhD). Images were analyzed by me, Zacharie Saint-Georges and Dr. Robert DeKemp. Data analysis and input function derivatization was performed by me, Dr. Robert DeKemp and Dr. Benjamin Rotstein. [$^{18}$F]Flubrobenguane was developed by Lantheus Medical Imaging, represented by Dr. Simon Robinson (PhD). I wrote the manuscript with assistance from Dr. Robert DeKemp and Dr. Benjamin Rotstein. All authors approved the final version.

### 5.2.2. Abstract

**Background:** Cardiac sympathetic nervous system molecular imaging has demonstrated prognostic value. Compared with *meta*-[$^{11}$C]hydroxyephedrine, [$^{18}$F]flubrobenguane (FBBG) facilitates reliable estimation of SNS innervation using similar analytical methods and possesses a more convenient physical half-life. The aim of this study was to evaluate pharmacokinetic and metabolic properties of FBBG in target clinical cohorts.

**Methods:** Blood sampling was performed on 20 participants concurrent to FBBG PET imaging (healthy = NORM, non-ischemic cardiomyopathy = NICM, ischemic cardiomyopathy = ICM, post-traumatic stress disorder = PTSD). Image-derived blood time-activity curves were transformed to plasma input functions using cohort-specific corrections for plasma protein binding, plasma-to-whole blood distribution, and metabolism.

**Results:** The plasma-to-whole blood ratio was 0.78 ± 0.06 for NORM, 0.64 ± 0.06 for PTSD and 0.60 ± 0.14 for (N)ICM after 20 minutes. 22 ± 4% of FBBG was bound to plasma proteins. Metabolism of FBBG in (N)ICM was delayed, with a parent fraction of 0.71 ± 0.05 at 10 minutes post-injection compared to 0.53 ± 0.03 for PTSD/NORM. While there were variations in metabolic rate, metabolite-corrected plasma input functions were similar across all cohorts.

**Conclusions:** Rapid plasma clearance of FBBG limits the impact of disease-specific corrections of the blood input function for tracer kinetic modeling.

**Key Words:** flubrobenguane, PET, fluorine-18, metabolism, sympathetic nervous system

**Abbreviations:**

FBBG [$^{18}$F]Flubrobenguane

HED *Meta*-[$^{11}$C]hydroxyephedrine

HF Heart failure

ICM Ischemic cardiomyopathy

NET Norepinephrine transporter

NICM Non-ischemic cardiomyopathy

PET Positron emission tomography

PPB Plasma protein binding

PTSD Post-traumatic stress disorder

SNS Sympathetic nervous system

### 5.2.3. Introduction

[$^{18}$F]Flubrobenguane, or *N*-[3-bromo-4-(3-[$^{18}$F]fluoropropoxy)benzyl]guanidine (FBBG, also known as LMI1195),[1] is a recently developed radiotracer designed for imaging of the cardiac sympathetic nervous system (SNS) using positron emission tomography (PET). Its uptake into myocardium, mediated by the norepinephrine transporter (NET), is diminished in patients with ICM as a result of progressive denervation.[2] The two most prominent SNS molecular imaging agents are *meta*-[$^{123}$I]iodobenzylguanidine (mIBG) used in gamma scintigraphy and single-photon emission computed tomography (SPECT), and *meta*-[$^{11}$C]hydroxyephedrine (HED) used in PET. These radiotracers have shown utility in cardiac imaging clinical trials, assisting in mortality prognostication, evaluation of arrhythmias and in identifying highest risk for sudden cardiac death in patients suffering from cardiomyopathies.[3–5] Non-invasive SNS imaging offers considerable potential for cardiac care, although limitations exist with the current methods.

Despite the availability of mIBG, suboptimal image quality and semi-quantification[6] have limited its utility in cardiac SNS imaging. Furthermore, while PET offers superior image quality over SPECT,[5] the short half-life of carbon-11 (20.4 min) in HED limits clinical access and wider distribution. FBBG is a benzylguanidine similar to mIBG but carries a fluorine-18 nuclide for PET imaging with a convenient 110-minute half-life that can support wider availability, multi-site clinical trials, and quantitative imaging protocols. FBBG shares similar biodistribution profiles to mIBG in preclinical models.[1,7,8] We explored a similar comparison with HED, and demonstrated that FBBG and HED provide equivalent regional quantitative distribution in patient cohorts with and without ischemic cardiomyopathy.[2,9] Additionally, a first-in-human study reported on dosimetry, biodistribution and safety in 12 healthy subjects.[10]

Accurate quantification of NET distribution using kinetic modeling requires a set of corrections, including for blood metabolites, to obtain accurate parent plasma input functions. Sinusas *et al.* reported such measurements in healthy volunteers,[10] which we applied in our initial analysis of FBBG imaging in cardiomyopathy patients.[2] However, these corrections may not be applicable to all patients, particularly those with dysfunctional NET activity.[11] To this end, we have further investigated the blood-based distribution and metabolic profiles of FBBG in relevant clinical imaging populations.

The aims of this study were to determine the plasma metabolite and distribution profiles needed to obtain accurate input functions for FBBG in patients with non-ischemic cardiomyopathy

(NICM), ischemic cardiomyopathy (ICM), and in healthy volunteers (NORM). Additionally, we included patients with post-traumatic stress disorder (PTSD) as part of ongoing research into a group at elevated risk of heart failure.[12] Beginning with an image-derived blood input function of the radiotracer, we determined the amount of freely available parent fraction (non-metabolized FBBG) in plasma throughout our PET data acquisition. To access this function, we observed the ratio of activity in the plasma compared to whole blood, the binding of FBBG to plasma proteins, and the metabolism of the parent compound in plasma over time.

### 5.2.4. Methods

#### Patient Population

We previously reported FBBG cardiac imaging in ischemic and nonischemic cardiomyopathy patients and healthy volunteers.[2] Data reported herein were collected both from a subsample of the previously reported cohort as well as additional subjects recruited using the same criteria. Recruitment methodology for patients with PTSD can be found in the Supplemental Information. Characteristics of imaging subjects can be found in Table S1. The study was approved by the Ottawa Health Science Network Research Ethics Board. All patients provided informed consent.

#### PET Imaging and Blood Collection

Patients underwent 40-minute or 60-minute dynamic FBBG PET imaging in a supine position while awake in a GE Discovery 690 PET-CT scanner (Waukesha, WI) or Siemens mMR PET-MR scanner (Knoxville, TN). The radiosynthesis of FBBG was performed as previously described.[1,10,13] A bolus of 3 MBq/kg FBBG (followed by a 10 mL saline push) was administered intravenously. Venous blood (>2 mL) was collected into heparinized tubes through a cannula placed in a vein in the antecubital fossa of the opposite arm to injection at a series of nominal timepoints (0.5, 1, 2, 5, 10, 20, 30, 40, 60 min).

#### Plasma Protein Binding

Tracer binding to plasma proteins is assumed to occur instantaneously following injection and to remain stable over the course of imaging. The free fraction in plasma ($f_P$) was determined

using ultracentrifugation. $f_P$ was calculated by subtracting the bound fraction from 1. More details on the methodology can be found in the Supplemental Information.

**Plasma-to-Whole Blood Ratio**

Tracer uptake into red blood cells follows a biexponential time-course and affects concentration in plasma available for exchange with target tissues.[14] To account for this time-dependent effect, activity in aliquots of plasma and whole blood were compared to derive a plasma-to-whole blood concentration ratio (PBR). The methodology is further described in the Supplemental Information.

A curve describing the cohort-specific plasma-to-whole blood ratio over time was determined by fitting to the function shown in **Equation 1**:

$$PBR(t) = Ae^{-mt^2} + B(1 - e^{-nt}) \quad (1)$$

where t is the blood sample time in minutes, and *A*, *B*, *m*, and *n* are function parameters derived for each cohort. Area under the curve (AUC) was calculated using GraphPad Prism 9.0 (La Jolla, CA), following the trapezoid rule.

**Plasma Metabolites**

Samples were prepared similarly to the HPLC protocol described elsewhere[10,15] and in the Supplemental Information. A solid-phase extraction method to separate FBBG from metabolites was validated against patient samples also analyzed by HPLC. The results were equivalent by both methods. Protein-free plasma samples were loaded onto a Sep-Pak Light C18 cartridge and washed with increasing concentrations of acetonitrile in water (0%, 10%, 20%, 20%, 30%, 70%, 100%, 100%). Each sample and residual activity on the cartridge was then assayed on a γ-counter. Polar metabolites were eluted with ≤30% acetonitrile, whereas the parent compound was eluted with ≥70%. The resulting collected activity was summed to determine the fraction of parent compound in plasma.

A curve describing the cohort-specific unaltered parent FBBG fraction (PF) over time was determined by fitting to **Equation 2**:

$$PF(t) = 1 - e^{-\frac{\tau}{t}} \quad (2)$$

where t is the blood sample time in minutes, and τ is a time constant describing the rate of conversion to metabolites in each cohort.

**Metabolite-Corrected Image-Derived Plasma Input Function**

Dynamic PET images were analyzed with Hybrid Viewer PDR 6.1.2 software (Hermes Medical Solutions). Spherical regions of interest were drawn in the left atrial cavity and the resulting whole-blood time-activity curves, $C_{WB}(t)$, were recorded (Figure 1). To account for small variations in tracer arrival time, a gamma variate function was fit to the bolus first-pass data (0–2 min), and the $C_{WB}(t)$ curves were resampled to unit area with the peak centered at 1 minute post-scan start.

For each scan, a final image-derived input function was then calculated according to **Equation 3**, representing the concentration of unaltered parent FBBG in arterial plasma:

$$C_{FP}(t) = C_{WB}(t) \times PBR(t) \times PF(t) \times f_P \quad (3)$$

where t is the dynamic image sampling time in minutes. Area under the curve (AUC) was then calculated as the time frame-weighted activity.

**Statistics**

Data are reported as a mean with standard deviation or mean with 95% confidence interval. Metabolic time constants, PBR(t) constants and AUC values were compared between groups using one-way ANOVA. Curve fitting, statistical analysis and graphical representation were performed using GraphPad Prism.

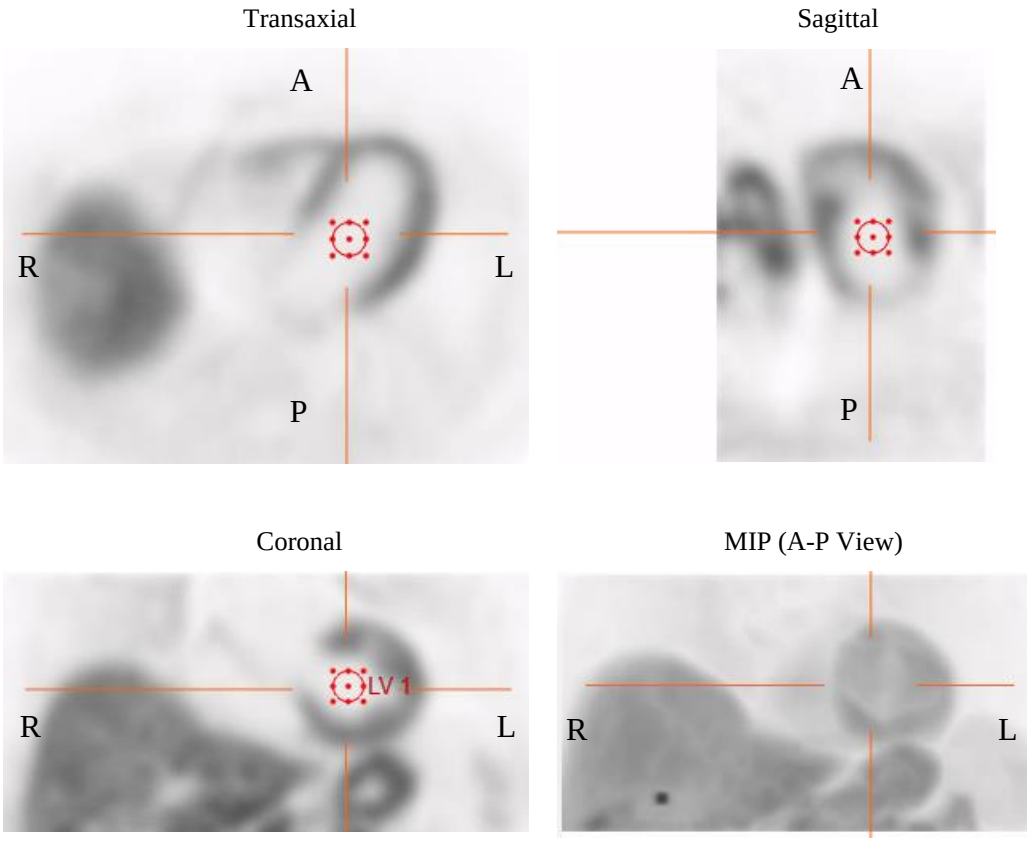


**Figure 5.1.** Cardiac PET imaging with [$^{18}$F]flubrobenguane. FBBG PET images showing tracer uptake at 30-60 minutes post-injection in a 70-year-old man with ischemic cardiomyopathy. Placement of a spherical volume-of-interest in the left ventricle (LV) cavity is illustrated in red for acquisition of the whole-blood time activity data.

### 5.2.5. Results

**Plasma Protein Binding**

Among patient cohorts (NICM = 5, ICM = 5, NORM = 5, PTSD = 5), there were 4 NICM, 4 ICM, 2 NORM and 2 PTSD data sets available. The remaining participants were not included due to missing blood sampling prior to radiotracer administration. The bound fraction was found to be 23 ± 4% in NICM, 22 ± 1% in ICM, 17 ± 5% in NORM, and 27 ± 5% in PTSD. The overall mean value was 22 ± 4%, with no significant difference between patient groups (ANOVA, $p > 0.05$) as shown in **Figure 2A**.

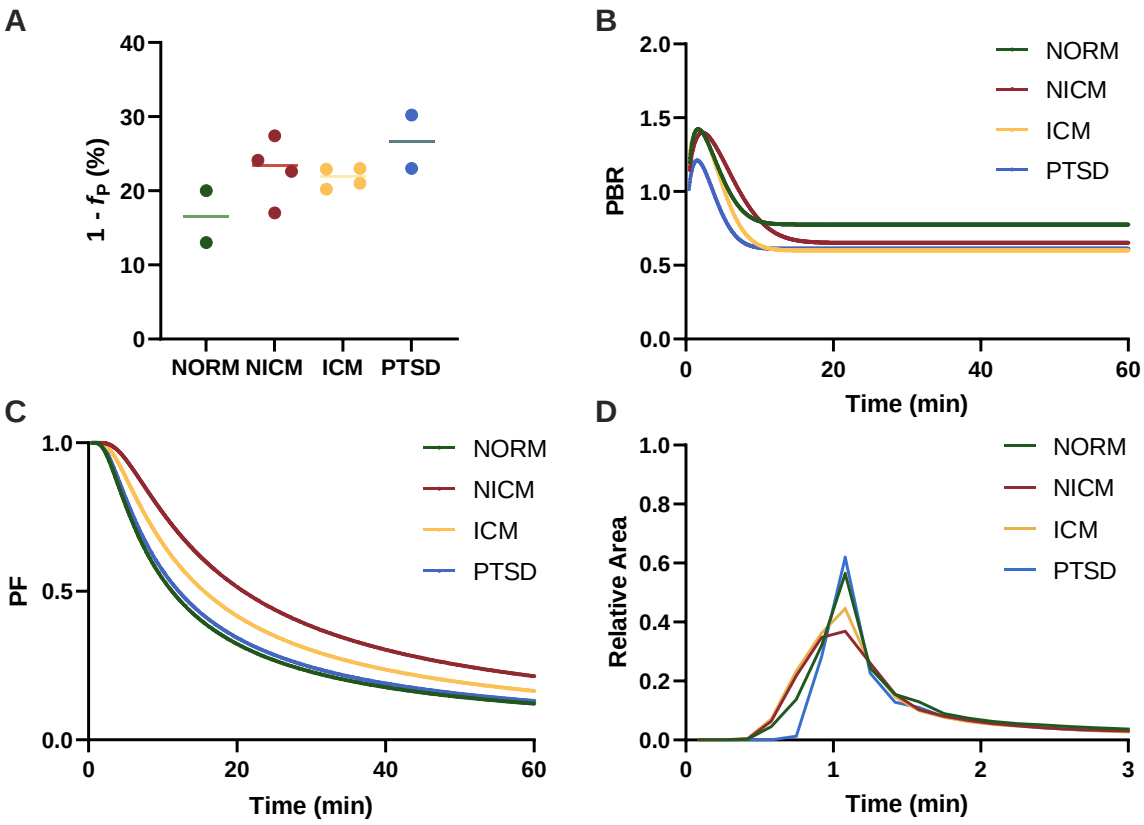


**Figure 5.2.** Metabolic and pharmacokinetic measurements of [$^{18}$F]flubrobenguane. (**A**) Fraction of FBBG bound to plasma proteins ($n$ = 2–4/group), (**B**) plasma-to-whole blood ratio of radioactivity following i.v. administration of FBBG ($n$ = 5/group), (**C**) fraction of parent FBBG, 0–60 minutes ($n$ = 5/group), (**D**) parent plasma input function time activity curves, 0–3 minutes ($n$ = 5/group).

### Plasma-to-Whole Blood Ratio

The plasma-to-whole blood ratio reached a maximum of 1.4 ± 0.1 early after injection before settling to 0.78 ± 0.1 for NORM, 0.64 ± 0.1 for PTSD and 0.60 ± 0.1 for the cardiomyopathy cohorts ((N)ICM) at 20 minutes post-injection (**Figure 2B**). There was no significant difference in AUC between cohorts (ANOVA, $p > 0.05$). Fits were derived according to the formula described by **Equation 1** and plotted (**Figure S1**). Parameters *A*, *B*, *m*, and *n* were compared; significant differences were found in parameter *n* between ICM and other cohorts (**Table 1**, $p = 0.038$ vs NORM, $p = 0.002$ vs NICM, $p = 0.010$ vs PTSD).

**Figure 5.3.** Fitted parameters for plasma-to-blood ratio (PBR) and parent fraction (PF).

| | PBR | | | | PF |
|---|---|---|---|---|---|
| | ***A*** | ***B*** | ***m* (min$^{-2}$)** | ***n* (min$^{-1}$)** | **τ (min)** |
| **NORM** | 0.86 ± 0.13 | 0.75 ± 0.10 | 0.06 ± 0.06 | 1.71 ± 1.30 | 7.99 ± 1.57 |
| **NICM** | 0.92 ± 0.04 | 0.63 ± 0.20 | 0.02 ± 0.01 | 1.06 ± 0.40 | 15.87 ± 8.42 |
| **ICM** | 0.90 ± 0.09 | 0.61 ± 0.05 | 0.03 ± 0.01 | 1.92 ± 1.63* | 10.81 ± 1.95 |
| **PTSD** | 0.85 ± 0.16 | 0.69 ± 0.04 | 0.12 ± 0.16 | 1.37 ± 0.87 | 8.80 ± 2.70 |
| **ANOVA** | p = .762 | p = .275 | p = .281 | p = .278 | p = .063 |

Values are mean ± standard deviation; * p < .05 vs. NORM

**Plasma Metabolites**

The parent fraction was determined for each of the cohorts (**Figure 2C**). After 10 minutes, the parent fraction was 0.71 ± 0.05 and 0.53 ± 0.03 in the (N)ICM and healthy/PTSD cohorts respectively. After 30 minutes, 0.32 ± 0.06 and 0.24 ± 0.02 unaltered parent fraction remained for (N)ICM and for healthy/PTSD groups. Parent fraction for all groups was 0.20 ± 0.03 by 60 minutes. Fits were prepared to describe the parent fraction of FBBG over time (**Figure S2**). Metabolic rate constants were derived according to **Equation 2** for each cohort (**Table 1**, $\tau = 7.80$ in NORM, 8.43 in PTSD, 14.47 in NICM and 10.80 in ICM). No significant difference was found, although a trend towards significance between NORM and NICM was present ($p = 0.066$). AUCs were calculated, with significant differences between NORM and NICM revealed following an overall significant ANOVA (**Table 2**, $p = 0.048$).

**Metabolite-Corrected Image-Derived Plasma Input Function**

Whole blood time activity curves were sampled from regions of interest drawn in the left atrium in dynamic PET images. Subsequent data normalization, followed by corrections using **Equation 3** provided plasma input functions (**Figure 2D**). Calculations of AUC were used to compare cohorts; no significant difference existed between cardiomyopathic patients and healthy volunteers (**Table 2**).

**Figure 5.4.** Area under the curve analyses of PBR, PF, and $C_{FP}$.

| | $AUC_{PBR(t)}$ | $AUC_{PF(t)}$ | $AUC_{C_{FP}(t)}$ |
|---|---|---|---|
| **NORM** | 48.66 ± 3.12 | 19.41 ± 2.36 | 0.62 ± 0.08 |
| **NICM** | 42.53 ± 10.98 | 28.06 ± 7.78* | 0.61 ± 0.04 |
| **ICM** | 40.36 ± 3.31 | 23.43 ± 2.60 | 0.56 ± 0.06 |
| **PTSD** | 42.33 ± 3.91 | 20.52 ± 4.19 | 0.55 ± 0.09 |
| **ANOVA** | p = .217 | p = .048 | p = .333 |

Values calculated 0–60 min, mean ± standard deviation;

* $p < .05$ vs NORM

### 5.2.6. Discussion

Pharmacokinetic metrics such as plasma protein binding, metabolism and activity distribution between plasma and whole blood were determined for the radiotracer FBBG to improve accuracy of imaging quantification. From these data it can be observed that, while there are variations in metabolic profiles for clinical imaging populations, the plasma input functions of FBBG are similar among sampled cohorts. Delayed metabolism in cardiomyopathy patients may be related to reduced cardiac output and hence reduced passage through metabolic organs. Ultimately, the similarity of the parent input functions suggests a universal metabolite correction may be appropriate.

The data for the NORM cohort were subsequently compared to the first-in-human study done by Sinusas *et al.*[10] There were no significant differences found between the two groups of healthy volunteers, with a peak mean plasma concentration at 1–2 min, and clearance to 0.00078 ± 0.00083 percent of injected dose per millilitre (%ID/mL) within 5 minutes (in comparison to 0.00046 ± 0.00007 %ID/mL). Furthermore, the metabolism resembled that of the prior cohort, with parent fractions of 0.49 ± 0.11, and 0.23 ± 0.05 at 10- and 30-minutes post-injection respectively in comparison to previously reported 0.37 ± 0.19 at 15 min, and 0.19 ± 0.13 at 30 min.

This study has some limitations, namely in the collection of venous samples. Kinetic analysis of PET imaging data ideally proceeds from arterial blood activity distribution to reflect parent tracer in plasma as input to compartmental or graphical tracer kinetic models. This, however, presents a clinical obstacle due to the invasiveness of arterial blood sampling. Image-derived input functions can be deployed to arrive at similar quantification without invasive blood

sampling, but lacks corrections for PBR, PF, and $f_p$. As demonstrated by Harms *et al.*,[14] venous blood samples can be used in quantification of HED cardiac SNS imaging, but requires an empirically derived venous-to-arterial transformation. Additionally, our study was completed across two sites with minor differences in tracer administration and blood collection protocols resulting in small timing inconsistencies in the data. These are unlikely to affect the quantitative results presented.

Finally, the limited sample size of this study may obscure additional meaningful differences in metabolism or pharmacokinetics between cohorts. The observed differences appear to be offset and minimized by rapid clearance of activity from whole blood. The resulting input functions suggest the validity of a single set of corrections for cardiomyopathy and control imaging subjects.

### 5.2.7. New Knowledge Gained and Conclusion

Cardiomyopathy patients metabolize the sympathetic nervous system radiotracer [$^{18}$F]flubrobenguane more slowly than healthy control subjects. This could lead to increased radiotracer concentrations in circulating blood available for uptake into tissue and adrenergic neurons. However, [$^{18}$F]flubrobenguane is rapidly cleared from blood in cardiomyopathy patients, PTSD patients, and healthy subjects and therefore no statistical differences were observed in total radiotracer availability in plasma over the course of imaging. Accurate quantification of sympathetic innervation using [$^{18}$F]flubrobenguane is unlikely to be confounded by metabolic differences in cardiomyopathy patients.

We assessed the pharmacokinetic and metabolic parameters of the cardiac SNS tracer [$^{18}$F]flubrobenguane (LMI1195) in target imaging populations. Slower tracer metabolism was observed in cardiomyopathy patients compared to healthy volunteers. FBBG clears rapidly from circulation and therefore disease-specific metabolite blood input corrections may be unnecessary given comparable distribution in plasma.

### 5.2.8. Funding and Disclosures

This study was supported by the Heart and Stroke Foundation of Canada, the Cardiovascular Network of Canada (CANet), and an Ontario Early Researcher Award to B.H.R. This project was also funded by a university-industry partnership grant (RE07-021) from the

Ontario Research Fund, Lantheus Medical Imaging, Inc, the University Medical Research Fund, and a Faculty of Medicine Translational Research Grant. B.A.M. is supported by the Natural Science and Engineering Research Council of Canada (NSERC PGS-D). J.G.E.Z. and Z.S. are supported by the Vanier Canada Graduate Scholarship Program. R.S.B. is supported in part by a University of Ottawa Distinguished Chair in Cardiac Imaging Research.

R.D.K. receives royalties from Rubidium PET technologies licenses to Jubilant Radiopharma and INVIA Medical Solutions; and received unrestricted research grant funding or honoraria from Siemens Molecular Imaging, IONETIX and Jubilant Radiopharma. R.S.B. has received honoraria and grants from GE HealthCare, Lantheus Medical Imaging, Inc, and Jubilant Draximage not related to this work. The other authors report no disclosures.

### 5.2.9. References


(1) Yu, M.; Bozek, J.; Lamoy, M.; Guaraldi, M.; Silva, P.; Kagan, M.; Yalamanchili, P.; Onthank, D.; Mistry, M.; Lazewatsky, J.; Broekema, M.; Radeke, H.; Purohit, A.; Cdebaca, M.; Azure, M.; Cesati, R.; Casebier, D.; Robinson, S. P. Evaluation of LMI1195, a Novel $^{18}$F-Labeled Cardiac Neuronal PET Imaging Agent, in Cells and Animal Models. *Circ. Cardiovasc. Imaging* **2011**, *4* (4), 435–443. https://doi.org/10.1161/circimaging.110.962126.

(2) Zelt, J. G. E.; Britt, D.; Mair, B. A.; Rotstein, B. H.; Quigley, S.; Walter, O.; Garrard, L.; Robinson, S.; Mielniczuk, L. M.; deKemp, R. A.; Beanlands, R. S. Regional Distribution of Fluorine-18-Flubrobenguane and Carbon-11-Hydroxyephedrine for Cardiac PET Imaging of Sympathetic Innervation. *JACC Cardiovasc. Imaging* **2021**, *14* (7), 1425–1436. https://doi.org/10.1016/j.jcmg.2020.09.026.

(3) Hartmann, F.; Ziegler, S.; Nekolla, S.; Hadamitzky, M.; Seyfarth, M.; Richardt, G.; Schwaiger, M. Regional Patterns of Myocardial Sympathetic Denervation in Dilated Cardiomyopathy: An Analysis Using Carbon-11 Hydroxyephedrine and Positron Emission Tomography. *Heart* **1999**, *81* (3), 262–270. https://doi.org/10.1136/hrt.81.3.262.

(4) Jacobson, A. F.; Senior, R.; Cerqueira, M. D.; Wong, N. D.; Thomas, G. S.; Lopez, V. A.; Agostini, D.; Weiland, F.; Chandna, H.; Narula, J. Myocardial Iodine-123 Meta-Iodobenzylguanidine Imaging and Cardiac Events in Heart Failure: Results of the Prospective ADMIRE-HF (AdreView Myocardial Imaging for Risk Evaluation in Heart Failure) Study. *J. Am. Coll. Cardiol.* **2010**, *55* (20), 2212–2221. https://doi.org/10.1016/j.jacc.2010.01.014.

(5) Fallavollita, J. A.; Heavey, B. M.; Luisi, A. J.; Michalek, S. M.; Baldwa, S.; Mashtare, T. L.; Hutson, A. D.; deKemp, R. A.; Haka, M. S.; Sajjad, M.; Cimato, T. R.; Curtis, A. B.; Cain, M. E.; Canty, J. M. Regional Myocardial Sympathetic Denervation Predicts the Risk of Sudden Cardiac Arrest in Ischemic Cardiomyopathy. *J. Am. Coll. Cardiol.* **2014**, *63* (2), 141–149. https://doi.org/10.1016/j.jacc.2013.07.096.

(6) Dobbeleir, A. A.; Hambÿe, A.-S. E.; Franken, P. R. Influence of High-Energy Photons on the Spectrum of Iodine-123 with Low- and Medium-Energy Collimators: Consequences for Imaging with $^{123}$I-Labelled Compounds in Clinical Practice. *Eur. J. Nucl. Med.* **1999**, *26* (6), 655–658. https://doi.org/10.1007/s002590050434.

(7) Yu, M.; Bozek, J.; Lamoy, M.; Kagan, M.; Benites, P.; Onthank, D.; Robinson, S. P. LMI1195 PET Imaging in Evaluation of Regional Cardiac Sympathetic Denervation and Its Potential Role in Antiarrhythmic Drug Treatment. *Eur. J. Nucl. Med. Mol. Imaging* **2012**, *39* (12), 1910–1919. https://doi.org/10.1007/s00259-012-2204-y.

(8) Werner, R. A.; Rischpler, C.; Onthank, D.; Lapa, C.; Robinson, S.; Samnick, S.; Javadi, M.; Schwaiger, M.; Nekolla, S. G.; Higuchi, T. Retention Kinetics of the $^{18}$F-Labeled Sympathetic Nerve PET Tracer LMI1195: Comparison with $^{11}$C-Hydroxyephedrine and $^{123}$I-MIBG. *J. Nucl. Med.* **2015**, *56* (9), 1429–1433. https://doi.org/10.2967/jnumed.115.158493.

(9) Zelt, J. G. E.; Mielniczuk, L. M.; Orlandi, C.; Robinson, S.; Hadizad, T.; Walter, O.; Garrard, L.; Beanlands, R. S. B.; deKemp, R. A. PET Imaging of Sympathetic Innervation with [$^{18}$F]Flurobenguan vs [$^{11}$C]MHED in a Patient with Ischemic Cardiomyopathy. *J. Nucl. Cardiol.* **2019**, *26* (6), 2151–2153. https://doi.org/10.1007/s12350-018-01527-5.

(10) Sinusas, A. J.; Lazewatsky, J.; Brunetti, J.; Heller, G.; Srivastava, A.; Liu, Y.-H.; Sparks, R.; Puretskiy, A.; Lin, S.; Crane, P.; Carson, R. E.; Lee, L. V. Biodistribution and Radiation Dosimetry of LMI1195: First-in-Human Study of a Novel $^{18}$F-Labeled Tracer for Imaging Myocardial Innervation. *J. Nucl. Med.* **2014**, *55* (9), 1445–1451. https://doi.org/10.2967/jnumed.114.140137.

(11) Sinusas, A. J.; Liu, C. Multi-Tracer Positron Emission Tomography Quantification of Sympathetic Innervation: Tracer Similarity But Not Equivalence. *JACC Cardiovasc. Imaging* **2021**, *14* (7), 1437–1439. https://doi.org/10.1016/j.jcmg.2020.10.007.

(12) Roy, S. S.; Foraker, R. E.; Girton, R. A.; Mansfield, A. J. Posttraumatic Stress Disorder and Incident Heart Failure Among a Community-Based Sample of US Veterans. *Am. J. Public Health* **2015**, *105* (4), 757–763. https://doi.org/10.2105/ajph.2014.302342.

(13) Yu, M.; Bozek, J.; Kagan, M.; Guaraldi, M.; Silva, P.; Azure, M.; Onthank, D.; Robinson, S. P. Cardiac Retention of PET Neuronal Imaging Agent LMI1195 in Different Species: Impact of Norepinephrine Uptake-1 and -2 Transporters. *Nucl. Med. Biol.* **2013**, *40* (5), 682–688. https://doi.org/10.1016/j.nucmedbio.2013.03.003.

(14) Harms, H. J.; Huisman, M. C.; Rijnierse, M. T.; Greuter, H.; Hsieh, Y.-L.; Haan, S. de; Schuit, R. C.; Knaapen, P.; Lubberink, M.; Lammertsma, A. A. Noninvasive Quantification of Myocardial $^{11}$C-*Meta*-Hydroxyephedrine Kinetics. *J. Nucl. Med.* **2016**, *57* (9), 1376–1381. https://doi.org/10.2967/jnumed.115.167437.

(15) Hilton, J.; Yokoi, F.; Dannals, R. F.; Ravert, H. T.; Szabo, Z.; Wong, D. F. Column-Switching HPLC for the Analysis of Plasma in PET Imaging Studies. *Nucl. Med. Biol.* **2000**, *27* (6), 627–630. https://doi.org/10.1016/s0969-8051(00)00125-6.

### 5.3. Supplementary Information

#### 5.3.1. General Information

**PTSD Recruitment:**

Individuals with PTSD are veterans or members of the Canadian Armed Forces with a history of military-related trauma recruited from the Operational Stress Injury clinic at the Royal Ottawa Mental Health Centre. The Mini International Neuropsychiatric Interview as well as the Clinician Administered PTSD Scale and the Life Events Checklist for DSM-5 were administered by a trained psychiatrist to confirm a PTSD diagnosis.[16] This study was approved by the Royal Ottawa Health Care Group Research Ethics Board (#2018035).

**Plasma Protein Binding:**

Patient plasma was obtained through centrifugation (3200 RPM at 4 °C for 7 minutes) of a blood sample collected prior to tracer administration. Around 750 kBq of FBBG was added to a 500 μL aliquot of plasma, which was then incubated for 10 minutes at 37 °C. Approximately 400 μL of the spiked plasma was loaded into the upper level of a Millipore ultrafiltration tube (Centrifree®) with a 30,000 Da molecular weight cut-off. The remaining 100 μL was used to aliquot precisely measured volumes (20 μL) into 3 counting tubes. The filtration devices were then centrifuged for 10 minutes at 3200 RPM. Once complete, the filtrate was aliquoted (20 μL) into 3 additional counting tubes. The counting tubes were placed into a rack and activity was measured on a Hidex AMG gamma counter. Triplicates were then averaged to determine the plasma protein binding for each imaging subject.

**Plasma-to-Whole Blood Ratio:**

500 μL of whole blood was sampled from each timepoint. The blood vials were then centrifuged to isolate plasma, from which 500 μL was collected. The aliquots were then placed on the γ-counter to determine their counts. At each timepoint, the ratio of activity in the plasma was then compared to the whole blood to determine PBR.

**HPLC Metabolites:**

Whole blood samples drawn during PET were centrifuged to isolate plasma. Plasma samples were mixed with urea (1 g) and then diluted to 2 mL with water. They were then co-injected with unlabeled FBBG on to a column-switching radio-HPLC[15] equipped with a Waters OASIS HLB capture column and a Luna 10 μm C18 100 Å analytic column (250 × 4.60 mm). The capture column was eluted with 1% MeCN/$H_2O$ for 4 minutes prior to valve-switching, at which point the capture column was eluted in reverse direction and in line with the analytical column using 27.5% MeCN/0.1 M ammonium formate buffer. Flow rates were 1 mL/min. The compound retention was ~16 min and was confirmed by monitoring the UV chromatogram. A fraction collector was used to gather the eluate with 2 min resolution, then assayed for activity on a γ-counter. Polar metabolites were summed and compared to the parent compound to determine the fraction of FBBG.

### 5.3.2. Supplemental Figures

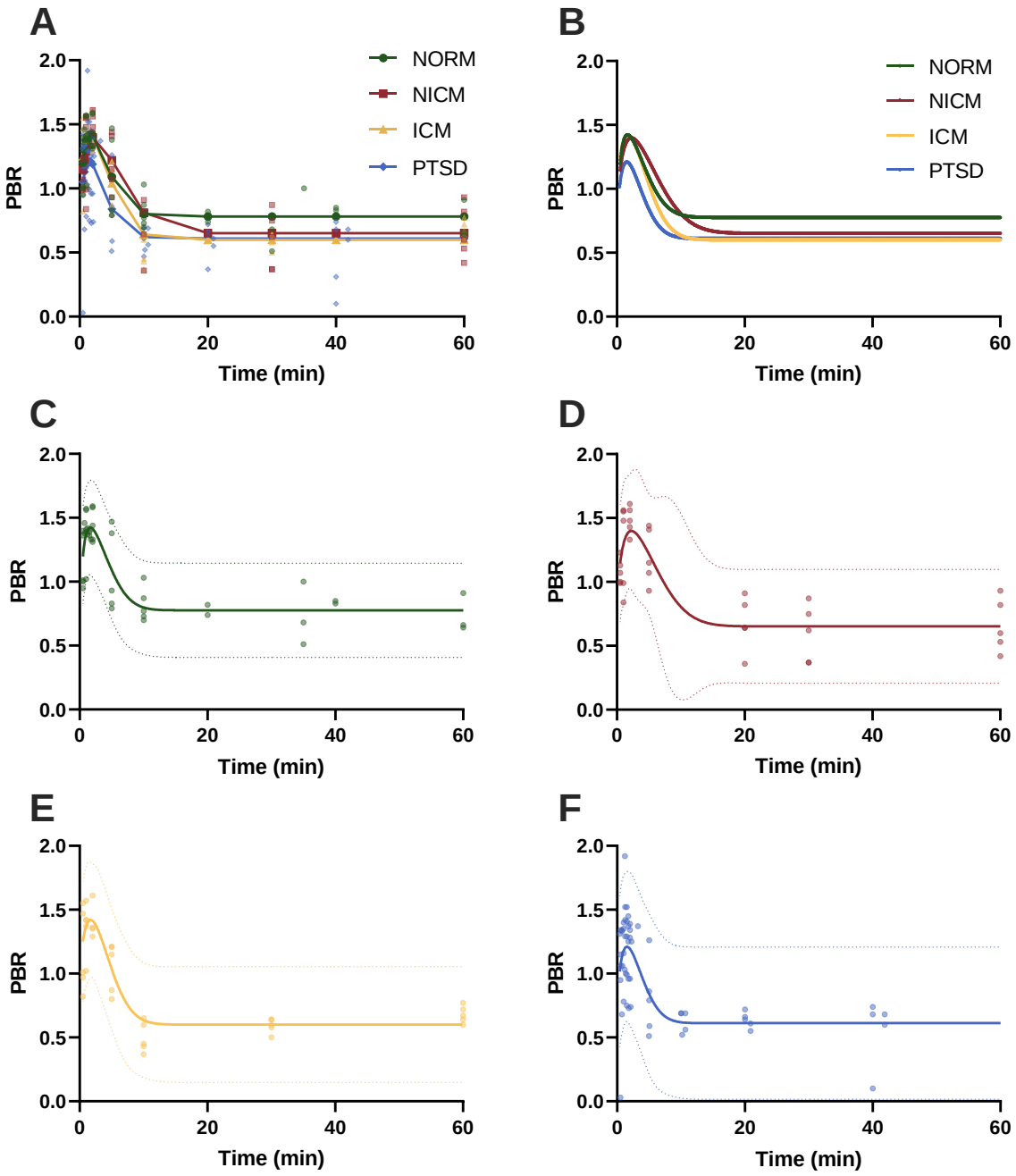


**Figure S5.1.** Plasma-to-whole blood ratio, mean and 95% CI. (A) Measured PBR data, (B) PBR fitted functions, (C) NORM, (D) NICM, (E) ICM, (F) PTSD.

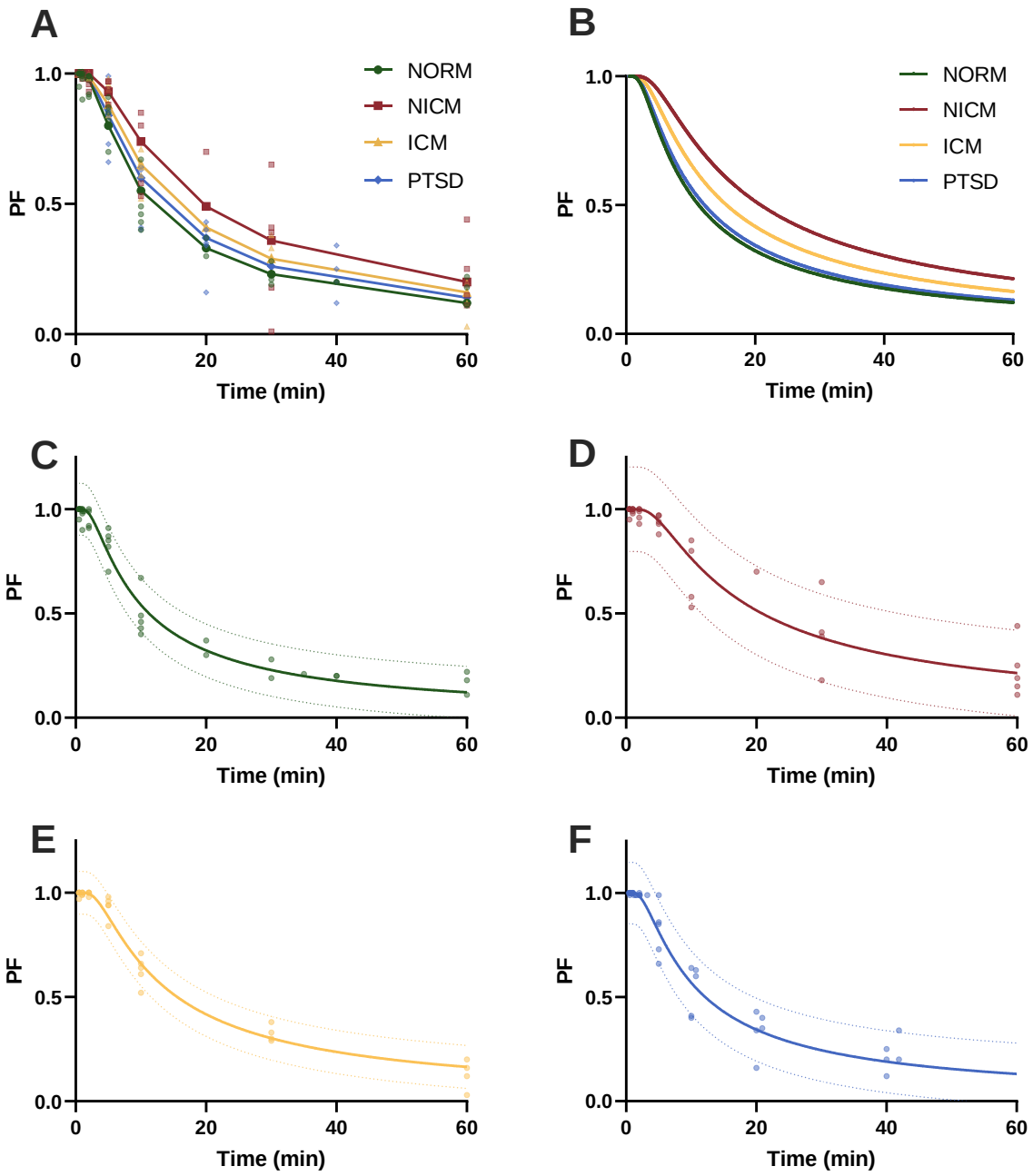


**Figure S5.2.** Parent fraction, mean and 95% CI. (A) Measured PF data, (B) PF fitted functions, (C) NORM, (D) NICM, (E) ICM, (F) PTSD.

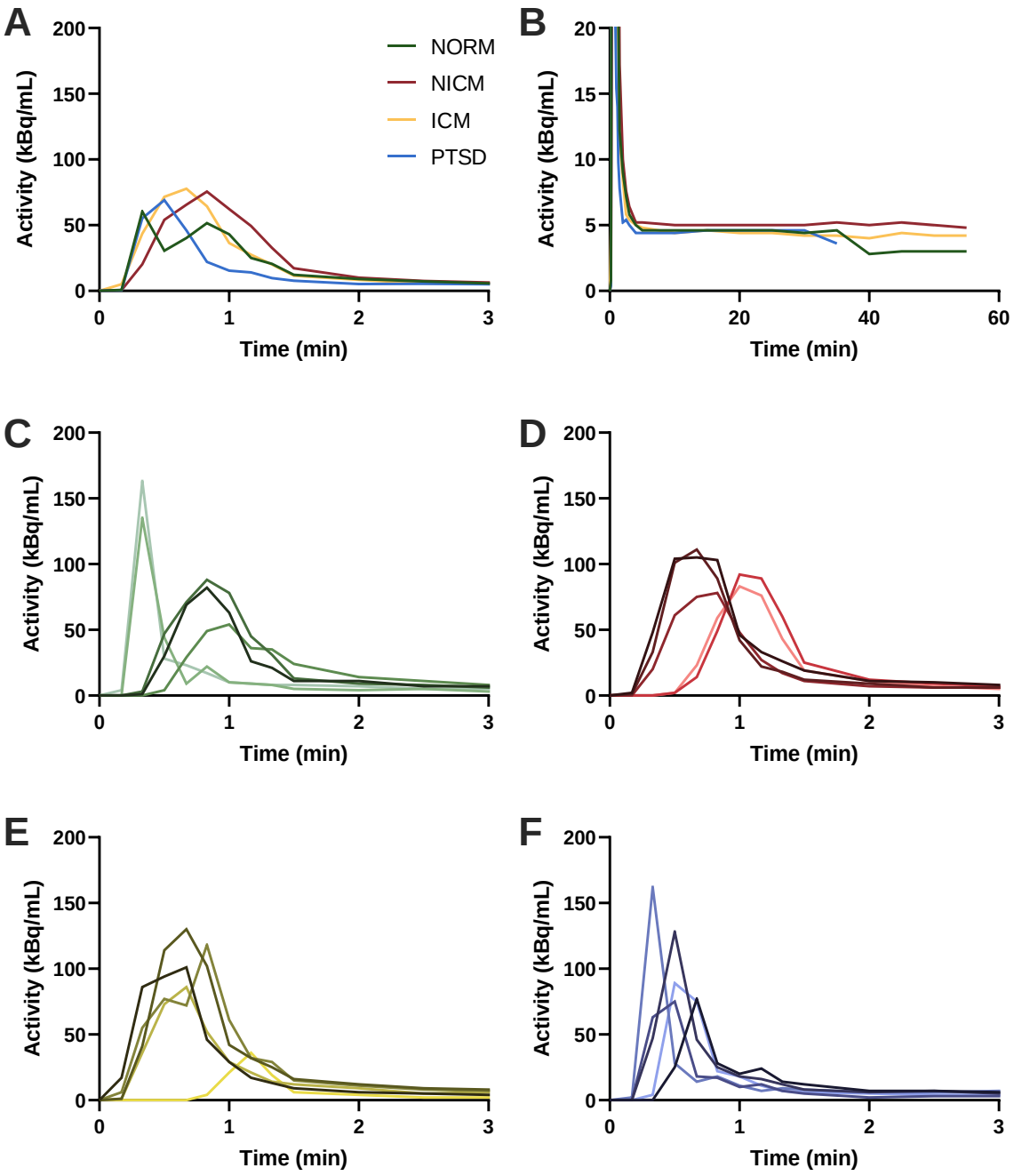


**Figure S5.3.** Left atrial time-activity curves. Full cohort (A) 0–3 minutes; (B) 0–60 minutes. (C) NORM, (D) NICM, (E) ICM, (F) PTSD.

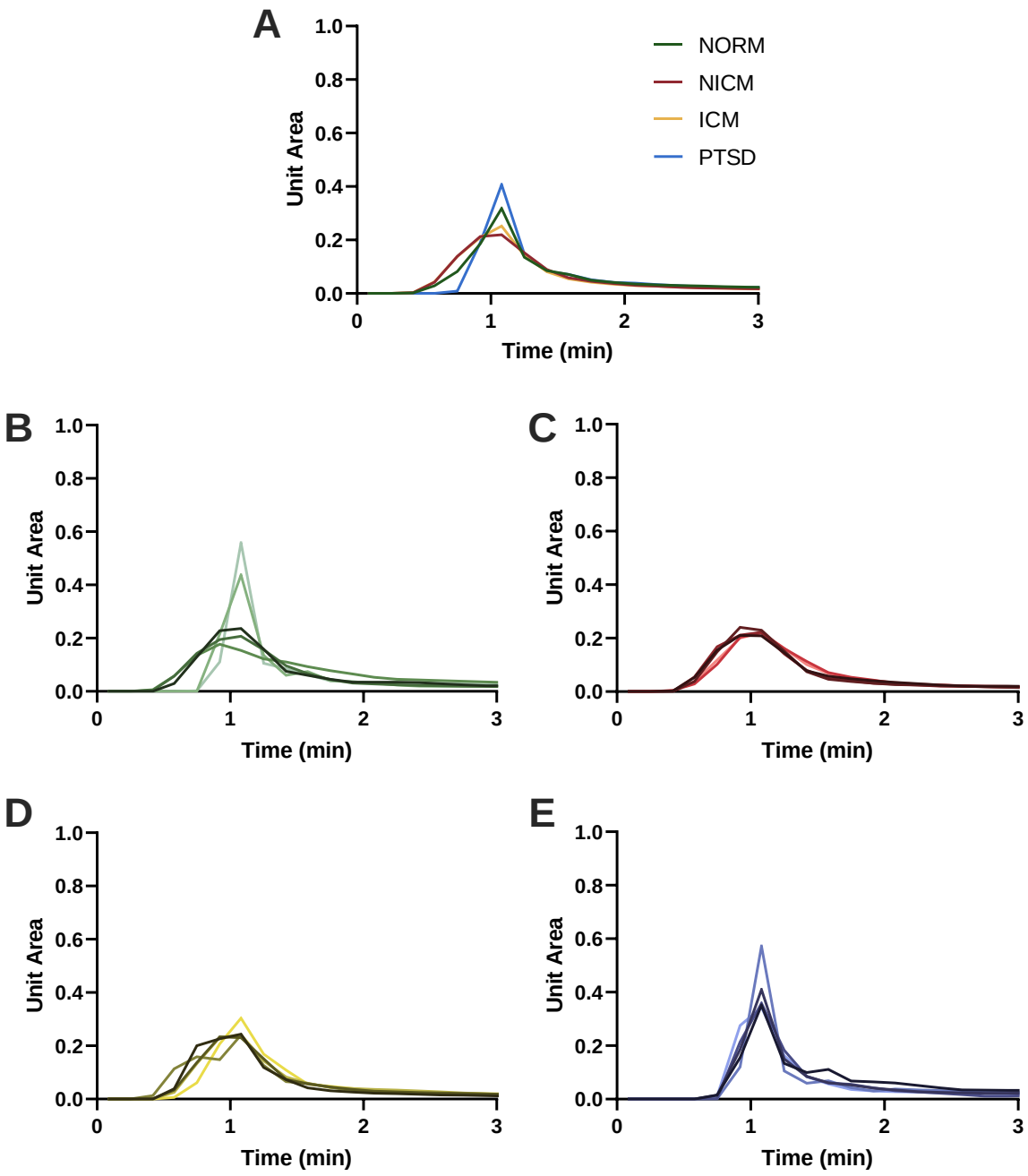


**Figure S5.4.** Left atrial cavity time-activity curves normalized by gamma variate. (A) Full cohort, (B) NORM, (C) NICM, (D) ICM, (E) PTSD.

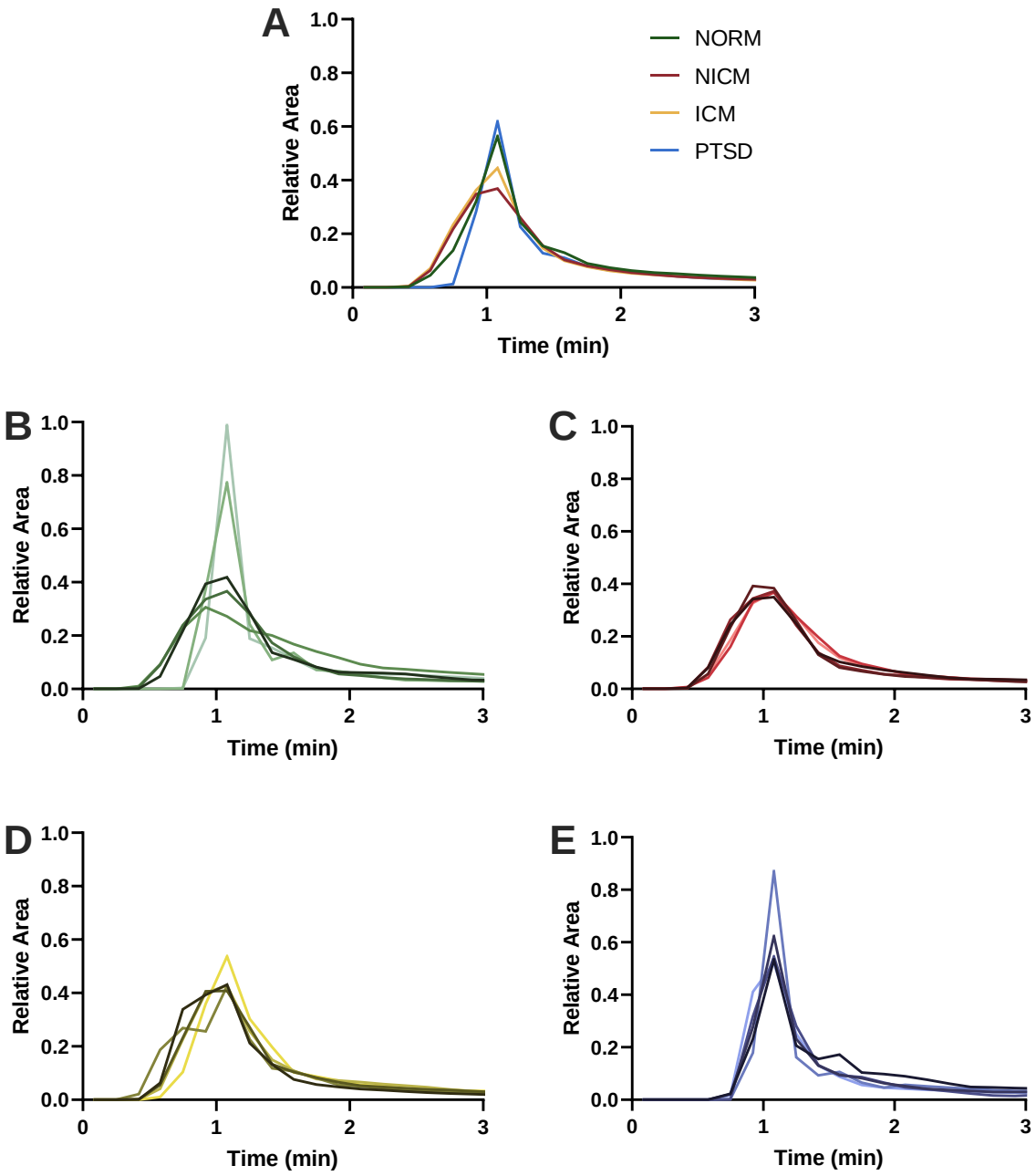


**Figure S5.5.** Parent plasma input function time-activity curves. After data normalization and formula correction. (A) Full cohort, (B) NORM, (C) NICM, (D) ICM, (E) PTSD.

### 5.3.3. Supplemental Tables

**Figure S5.6.** Characteristics of imaging subjects

| | **NORM** *n* = 5 | **NICM** *n* = 5 | **ICM** *n* = 5 | **PTSD** *n* = 5 |
|---|---|---|---|---|
| **Clinical Data** | | | | |
| Male | 5 (100) | 3 (60) | 5 (100) | 3 (60) |
| Age (yrs) | 51.0 ± 7.8 | 62.4 ± 4.3 | 68.0 ± 6.5 | 46.4 ± 5.6 |
| Caucasian | 2 (40) | 2 (40) | 5 (100) | - |
| BMI ($kg/m^2$) | 27.2 ± 3.5 | 28.8 ± 5.4 | 30.6 ± 3.3 | 28.8 ± 3.1 |
| NYHA class (I/II/III/IV) | 0/0/0/0 | 1/3/0/0 | 2/2/0/0 | 0/0/0/0 |
| Heart rate ($min^{-1}$) | 62.6 ± 8.3 | 65.8 ± 13.5 | 58.2 ± 3.5 | 70.0 ± 11.1 |
| Systolic blood pressure (mmHg) | 131.6 ± 11.1 | 131.2 ± 22.6 | 133.6 ± 16.3 | 124.4 ± 14.6 |
| **Imaging data** | | | | |
| FFBG Dose (MBq) | 257.9 ± 37.9 | 276.4 ± 51.8 | 293.6 ± 19.6 | 257.6 ± 28.7 |
| LVEF (%) | 60.2 ± 5.6 | 39.8 ± 6.9 | 33.5 ± 8.0 | 62.4 ± 7.0 |
| **Laboratory data** | | | | |
| NT-proBNP (pg/mL) | <50 | 392.6 ± 443.8 | 428.6 ± 319.2 | 67.3 ± 5.1 |
| Creatinine (μM) | 88.3 ± 15.0 | 80.2 ± 22.5 | 106.6 ± 48.1 | 80.5 ± 22.6 |
| **Medications** | | | | |
| β-blockers | 0 (0) | 5 (100) | 5 (100) | 0 (0) |
| ACE/ARB | 0 (0) | 2 (40) | 1 (20) | 0 (0) |
| Diuretics | 0 (0) | 1 (20) | 3 (60) | 0 (0) |
| Lipid lowering agents | 1 (20) | 4 (80) | 5 (100) | 1 (20) |

Values are *n* (%) or mean ± standard deviation

### 5.3.4. Supplemental References

16. Sheehan DV, Lecrubier Y, Sheehan KH, et al. The Mini-International Neuropsychiatric Interview (M.I.N.I.): The Development and Validation of a Structured Diagnostic Psychiatric Interview for DSM-IV and ICD-10. *J Clin Psychiatry* **1998**;*59*(S20):22–33.

## 5.4. Extended Discussion

### 5.4.1. Lessons

We determined that a disease-agnostic input function may be sufficient for image analysis and quantification with [$^{18}$F]flubrobenguane, likely due to its rapid clearance from circulation. While our data was derived from venous sampling as opposed to the preferred albeit invasive arterial sampling, the findings could be sufficient in indicating the pharmacokinetic and metabolic profile of [$^{18}$F]FBBG. A study comparing venous sampling to arterial blood draws could further demonstrate the validity of the method.

Additionally, we developed and corroborated a solid-phase extraction methodology to separate flubrobenguane from its metabolites for determination of the parent compound fraction. While HPLC is a reliable approach, not all facilities are outfitted with an instrument capable of performing chromatographic separations; SPE on the other hand is more universally applicable and requires very little that isn't already present in most radiochemistry laboratories.

### 5.4.2. Perspectives

#### *5.4.2.1. Conclusions*

Flubrobenguane is a novel radiotracer undergoing investigation for imaging cardiac sympathetic innervation. Studies indicate its potential as an imaging agent as well as its comparability to [$^{11}$C]HED. In our analysis, we assessed the pharmacokinetic properties of the radiotracer as well as its metabolic outcomes in order to develop an input function for image quantification. This was completed in multiple disease cohorts and healthy volunteers to determine the potential differences across groups. We determined that a generalized input function would be acceptable for [$^{18}$F]flubrobenguane image analysis.

#### *5.4.2.2. Future Directions*

The PAREPET II study (NCT03493516, Prediction of ARrhythmic Events with Positron Emission Tomography) is currently underway and is anticipated to be completed in 2025. Its findings will inform on the potential for [$^{18}$F]flubrobenguane imaging of cardiac sympathetic innervation to evaluate risks for sudden cardiac death. Given the current determinations on the radiotracer, it shows great promise in acting as a stronger alternative to the gold standard [$^{11}$C]HED due to its $^{18}$F label and the ability to be widely distributed.

# Chapter 6: Final Discussion

## 6.1. Afterword

PET imaging has become an invaluable tool for both clinical use in diagnosis and patient stratification, and in improving understanding of biochemical pathways in the body. The development of PET radiotracers is a considerable process, often beginning with radiochemistry and the synthesis of new target ligands. Many traditional organic syntheses are incompatible with radiochemistry-specific considerations, primarily half-life management and the very low concentrations of radioactive synthon produced, and so novel methodologies need to be prepared. Following method development, radiotracers can be labelled and isolated for imaging studies, whether it be for animal models or clinical patient evaluations. After image collection, proper analysis of images is important to ensure accurate quantification and interpretation of the data.

In this thesis, radiochemistry using [$^{11}$C]$CO_2$ was discussed in depth. Chapter 2 and chapter 4 detail the development of two methodologies to access $^{11}$C-amides and $^{11}$C-amino acids respectively, using both fixation chemistry and isotopic exchange. Chapter 3 focuses on the development of a $^{11}$C-carbonyl-labelled radiotracer intended to be used for cardiac imaging. Additionally, this thesis describes the validation of radiotracers *via* image analysis in clinical patient cohorts; chapter 5 elaborates on the process of compartmental modeling and properly interpreting collected images following PET studies.

### 6.1.1. Chapter 2

Traditional syntheses for amides prove ineffective or inefficient when translated to radiochemistry. Many radiochemistry-specific approaches to $^{11}$C-amides are limited in their scope, either requiring longer multistep syntheses to prepare sufficiently reactive intermediates or lacking both reactivity and reaction control to access pharmaceutically relevant products. Seeing a need for a general method, we sought to develop the synthesis of $^{11}$C-amides using tuneable reactivity and $^{11}$C-isocyanates prepared *in situ*.

In chapter 2, our work in *Organic Letters* with the rhodium-catalyzed coupling of organozinc iodides and $^{11}$C-isocyanates is described. Extensive investigation of the chemistry informed translation to radiosynthesis, followed by the preparation of a scope demonstrating the capacity of the reaction. The modular nature of the method, being able to rapidly evaluate a series of organozinc iodide nucleophiles alongside various isocyanate electrophiles, suggests potential value in radiochemical compound library evaluations. Additionally, a derivatized $^{11}$C-amino acid,

[$^{11}$C]*N*-acetyl glutamic acid, was prepared in line with our interest in amino acid biochemistry and could be used for imaging studies.

Desiring improved reactivity and product diversity inspired additional investigation into alternative organometallics, methods to prepare $^{11}$C-isocyanates, and targeting general synthesis of $^{11}$C-carbonyls; our work in *Chemical Communications*, *Chemistry – A European Journal*, and additional unpublished data is briefly discussed.

Access to $^{11}$C-amides remains a challenge with current carbon-11-labelling methodologies, largely due to the need to form both the $^{11}$C–N bond and the $^{11}$C–C bond during radiosynthesis. While Grignard reagents can be used to derivatize $^{11}$C-isocyanates, their excessive reactivity limits their functionality. Organozinc iodides offer more versatility, especially given reactivity mediated by rhodium catalysis, but they lack sufficient compatibility to access heteroatoms common in drug-like molecules. Alternative organometallics have yet to solve this need; organostannanes do not show a significant improvement in functional group tolerance, and while boronic acids have shown promise in coupling with isocyanates to produce amides, the required catalytic systems remain problematic with reagents for $^{11}$C-isocyanate synthesis *in situ*. No significant advances in $^{11}$C-amide synthesis have been published since, and so $^{11}$C-amides remain an important target for radiosynthetic method development.

However, given the potential compatibility of boronic acids and/or esters with heteroaromatic moieties that we observed in our robustness assays, alternative means of accessing $^{11}$C-isocyanates that avoid the use of problematic phosphine ligands would be an area for additional research. This could possibly be resolved using iminophosphoranes, as they undergo purification prior to use in radiolabelling, eliminating problematic reagents; this opposes the current Mitsunobu reaction that occurs *in situ*. Iminophosphoranes have been demonstrated to be a promising means of access to $^{11}$C-carbonyl compounds, especially in their ability to build out sequential libraries with modular syntheses; our lab's investigation into urea pharmacophores consisting of amino acid building blocks demonstrates the ease-of-radiosynthesis of this approach. Additional targets have also been accessed since with $^{11}$C-isocyanates, such as in the targeting of additional $^{11}$C-carbonyl compounds like $^{11}$C-benzimidazolones and $^{11}$C-formamides.[1,2]

### 6.1.2. Chapter 3

Rev-erb is a key regulator of circadian biology, imparting significant control over inflammatory processes in the body. The circadian clock has been demonstrated to play a vital role in instigating cardiac inflammation following myocardial infarction and the strong inflammatory response to its standard treatment – reperfusion. Pharmacological treatment of Rev-erb using (±)-SR9009 shows promise in the management of cardiac inflammation, lowering activation of the NLRP3 inflammasome. However, translation to human studies requires investigation into the biochemical implications, as SR9009 has been found to also act independently of Rev-erb.

In chapter 3, (*R*)- and (*S*)-[$^{11}$C]SR9009 were prepared to evaluate Rev-erb distribution and dynamics. An enantiopure synthesis to conserve the stereocenter was developed so as to evaluate variations in isomer imaging behaviour. Radiochemical optimization of reaction conditions provided [$^{11}$C]SR9009 in suitable yields for additional projects concerned with imaging.

Circadian effects on cardiovascular health have continued to be investigated in recent years, regardless of the mechanism of action (i.e. whether it be through Rev-erb or downstream effects from alternative effectors like LXRα). The circadian clock therefore remains a vital target for pharmacological intervention to improve outcomes post ischemia and subsequent reperfusion, or in a progressive and declining condition like heart failure. Regardless of the pharmacodynamics of SR9009 treatment, the phenotypic response of its dosing results in improved cardiac outcomes and function, and so it still offers great value in clinical care.

Nonetheless, our successful labelling of SR9009 with carbon-11 allows for investigation into the behaviours of the drug once in the body. We can decipher additional information on its distribution throughout the body with measurable uptake in tissues and organs of interest and can evaluate the differences depending on the method of administration into the body. Further analysis of its metabolism and method of excretion from the body could provide useful pharmacological information for clinical trials in cardiovascular care.

Additional targets of Rev-erb could be worthy of investigation for both clinical care and in radiotracer design, like SR9011 and the antagonist of Rev-erb, SR8278.[3] Differences in affinity for Rev-erb and for potential off-targets like LXRα may suggest a superior drug or imaging agent depending on the results of the imaging studies and the conclusions on the source of cardioprotective effects.

### 6.1.3. Chapter 4

$^{11}$C-Amino acids are often either made with specific radiosyntheses tailored to each individual target, or using the general Strecker synthesis with the scarcely available $^{11}$C-synthon, [$^{11}$C]HCN. With this in mind, a general synthesis for labelled amino acids would allow for more widespread methodological adaptation, providing valuable biochemical studies and potential for diagnostic purposes. In particular, variations in oxidative metabolism and higher concentrations of circulating branched chain amino acids like leucine have been connected to cardiovascular diseases and their prognosis.

Additional work from our lab, described in our work in the *Journal of Labelled Compounds and Radiopharmaceuticals*, targeted the synthesis of $^{11}$C-phenylacetic acids using photochemical methods. The preparation of $^{11}$C-carboxylic acids has long been explored by the field, although more reliable and improved methods are still in demand. Carbon isotope exchange (CIE) is a growing focus for radiochemists and others preparing carbon-labelled products given the simplicity of the reaction approach. The potential to label $^{11}$C-carboxylic acids like in $^{11}$C-amino acids could be addressed with CIE.

In chapter 4, our work in *Nature Chemistry*, *Nature Protocols*, and an additional upcoming submission describes the carboxylation/decarboxylation reaction scaffold that allows for the labelling of α-amino acids. Using aldehyde catalysts, stable isotope-containing amino acids are condensed into Schiff bases which can then undergo carboxylation by *$CO_2$, followed by decarboxylation to provide the desired *C-amino acid. Seeking improvements to the $^{11}$C-labelling methodology and wishing to simplify the process, we evaluated alternative catalysts and conditions and demonstrated the reaction tolerance. Additionally, methods to derive L- and D-$^{11}$C-amino acids were tested, with enantiomeric resolution providing enantiopure [$^{11}$C]leucine for imaging.

Having already completed substantial optimization for the $^{11}$C-labelling methodology, continued investigation into asymmetric syntheses for L- and D-$^{11}$C-amino acids would be a preferred next step. While evaluation of a chiral catalyst to promote protonation on one face of the substrate yielded poor $^{11}$C-labelling results, the method worked successfully under different conditions with alternative carbon isotopes. Identifying an aldehyde with more rapid reaction rates capable of enriching the enantiomer prepared could provide simpler means of achieving enantiopure $^{11}$C-amino acids. Alternative catalytic additions such as a chiral Lewis acid might also contribute to enantioenrichment such that resolution of the two enantiomers becomes easier.

Given the interest in applying photocatalysis to carbon isotope exchange methodologies discussed in chapter 4, there may yet be compatibility with the labelling of α-amino acids. Recent work has employed photodecarboxylation in a very similar manner to yield amines from amino acids; the potential for recarboxylation may be worth investigating.[4]

The branched chain amino acids – leucine, isoleucine and valine – have become increasingly more relevant in the context of cardiovascular health in recent years. Imaging with [$^{11}$C]leucine can provide vital information on the rates of oxidative metabolism within the heart, and potentially offer diagnostic or evaluative insight into several cardiac pathologies.

### 6.1.4. Chapter 5

[$^{18}$F]Flubrobenguane is a fluorine-18-labelled radiotracer for imaging the norepinephrine transporter; its potential in the evaluation of cardiac denervation and comparisons to [$^{11}$C]HED were investigated by our team. Pharmacokinetic parameters required to construct an input function are an important part of evaluating and analysing the derived images. However, previous studies of [$^{18}$F]FBBG employ a function derived from healthy volunteers and not the clinically-relevant cohorts that would be undergoing imaging for disease diagnosis and prognosis.

In chapter 5, our work in the *Journal of Nuclear Cardiology* and the *Journal of the American College of Cardiology's Cardiovascular Imaging* details the evaluation of [$^{18}$F]flubrobenguane in clinical imaging populations. In parallel to imaging studies conducted at two clinical sites, we collected blood samples that were treated and analysed to determine pharmacological and metabolic parameters. These were then used to develop disease-specific input functions to evaluate the significance and any potential differences in biochemistry between cohorts. Our findings determined that while there may be underlying differences in biochemical behaviour amongst groups, a universal input function would be sufficient due to rapid clearance rates. While more metabolically stable alternatives to [$^{18}$F]FBBG exist, like [$^{18}$F]*m*FBG and other novel targets in the literature, our findings determined we can still collect high contrast images in spite of these rates of metabolism.

In addition to the development of disease-specific input functions for image analysis, I also translated metabolite analysis from dual-column HPLC to a more practical SPE method that can be much more easily adapted at imaging facilities. Not only could this be used for [$^{18}$F]FBBG

blood analysis, the success in translating the method demonstrates the capability for other tracers to also be analysed by this approach.

### 6.1.5. General

This thesis details significant advances in methodologies for both radiosynthesis and tracer evaluation, intending to be adaptable and efficient for production facilities around the world. Translational radiochemistry is an important concept to ensure that radiotracers and their synthetic means of preparation are easily reproducible and practical; implementing radiochemical methodologies depends on their simplicity and the ease in their syntheses, and so developing methods that can be automated and adapted is paramount.

In chapter 2, milder organometallics than the literature standard of Grignard reagents were used to prepare $^{11}$C-amides. The rhodium-catalyzed coupling of organozinc iodides with isocyanates was completely automated on a radiosynthesis unit and included rapid *in situ* preparation of $^{11}$C-isocyanates and their subsequent derivatization. Isolation of these compounds proceeded with ease, also demonstrating the modularity of these $^{11}$C-carbonyl compounds to build out SAR libraries. Additional methods to simplify current literature methods for $^{11}$C-carbonyl compounds was completed.

In chapter 3, an enantiopure synthesis for SR9009 was developed. This is important as the (*R*)- and (*S*)- enantiomers of a drug may exhibit differences in pharmacological effect and in imaging characteristics. Our approach is simple and involves only one additional step to retain stereochemistry and provide enantiopure product at the end as opposed to the industrial method for the racemate. This was then used for radiolabelling to prepare [$^{11}$C]SR9009 for imaging studies to provide additional information on the context of its mechanism of action. The synthesis was automated and includes reformulation of the radiopharmaceutical for imaging studies.

In chapter 4, a novel approach to $^{11}$C-amino acids was developed. This method is very easy to reproduce, requiring the purchase of easily-accessible amino acids and simple aldehyde catalysts. The automated carbon isotope exchange is compatible with chiral resolution techniques to isolate pure L- or D-$^{11}$C-amino acids for imaging. This method is far simpler than current literature as it can be generalized to all amino acids, and doesn't require secondary synthons of carbon-11 that might be difficult to prepare. Direct carboxylation with [$^{11}$C]$CO_2$ remains one of the most efficient means of introducing carbon-11 into molecules.

Finally, in chapter 5, image-derived input functions simplify the PET technician's workflow in image analysis. With our data suggesting the use of a universal input function being sufficient, we obviate the need to develop disease-specific metrics requiring constant blood sampling from imaging subjects. [$^{18}$F]FBBG has been demonstrated to be a similar tracer to the current standard in [$^{11}$C]HED, allowing for an increase to its distribution potential with the longer-living fluorine-18 radioisotope.

### 6.1.6. References


(1) Horkka, K.; Dahl, K.; Bergare, J.; Elmore, C. S.; Halldin, C.; Schou, M. Rapid and Efficient Synthesis of 11C-Labeled Benzimidazolones Using [$^{11}$C]Carbon Dioxide. *ChemistrySelect* **2019**, *4* (6), 1846–1849. https://doi.org/10.1002/slct.201803561.

(2) Luzi, F.; Gee, A. D.; Bongarzone, S. Rapid One-Pot Radiosynthesis of [Carbonyl-$^{11}$C]Formamides from Primary Amines and [$^{11}$C]$CO_2$. *EJNMMI radiopharm. chem.* **2020**, *5* (1), 20. https://doi.org/10.1186/s41181-020-00103-y.

(3) Kojetin, D. J.; Burris, T. P. REV-ERB and ROR Nuclear Receptors as Drug Targets. *Nat Rev Drug Discov* **2014**, *13* (3), 197–216. https://doi.org/10.1038/nrd4100.

(4) Tan, D.-H.; Das, A.; Huang, V.; Schoch, T. D.; Mohammed, A. L.; Lipshultz, J. M. Pyridoxal-Inspired Photo-Decarboxylase Catalysis: Photochemical Decarboxylation of Unprotected Amino Acids. *Angewandte Chemie International Edition n/a* (n/a), e202424843. https://doi.org/10.1002/anie.202424843.